Restoring airway function in muco-obstructive diseases by modulating TMEM16A and SLC26A9

DISSERTATION ZUR ERLANGUNG DES DOKTORGRADES
DER NATURWISSENSCHAFTEN (DR.RER.NAT.)
DER FAKULTÄT FÜR BIOLOGIE UND VORKLINISCHE MEDIZIN
DER UNIVERSITÄT REGENSBURG

vorgelegt von
Raquel Martins Centeio
aus
Lisboa, Portugal

im Jahr
2022

DAS PROMOTIONSGESUCH WURDE EINGEREICHT AM:
26.10.2022

DIE ARBEIT WURDE ANGELEITET VON:
PROF. DR. MED. KARL KUNZELMANN

UNTERSCHRIFT:

DIE ARBEIT WURDE ANGELEITET VON: PROF. DR. MED. KARL KUNZELMANN

PRÜFUNGSAUSSCHUSS:

VORSITZENDER: PROF. DR. JOACHIM GRIESENBECK

1.GUTACHTER: PROF. DR. MED. KARL KUNZELMANN

2.GUTACHTER: PROF. DR. MICHAEL GRAY

3. PRÜFER: PROF. DR. MED. FRANK SCHWEDA

ERSATZPERSON: DR. PD JAN MEDENBACH

Real knowledge is to know the extent of one's ignorance.

– Confucius

SUMMARY

Human airways are permanently exposed to the external environment, which contains a myriad of noxious agents such as pathogens, sterile irritants, and allergens. The airway epithelium and its barrier properties constitute the first-line defence against these inhaled insults, preventing them from invading the airway mucosa and coordinating, when necessary, the recruitment of the immune system to assist in airway clearance. Alterations or congenital abnormalities of the airway epithelial barrier can lead to chronic airway diseases and compromise respiratory homeostasis. Chronic respiratory diseases are leading causes of death worldwide, with chronic obstructive pulmonary disease (COPD) and asthma accounting for nearly 3.7 million yearly passings. In parallel, cystic fibrosis (CF), caused by defective cystic fibrosis transmembrane conductance regulator (CFTR) protein expression and/or function in epithelia, is the leading cause of genetic disease-related death amongst Caucasians. CFTR is a Cl^- and HCO_3^- channel expressed at the apical membrane of airway epithelial cells, involved in the regulation of airway surface liquid (ASL) hydration and pH. Despite presenting distinct underlying pathophysiological mechanisms, these diseases share common features such as excessive airway mucus production, airway remodelling, and bronchoconstriction, that contribute to the development of chronic airway inflammation. Current therapeutical strategies are disease- or patient-specific, and several patients remain untreated due to therapy unresponsiveness or acquired resistance. Alternative therapies un der development for chronic inflammatory airway diseases approach the modulation of non-CFTR epithelial ion channels and transporters that are also involved in the regulation of airway homeostasis. Two other putative Cl^- secretory proteins, transmembrane protein 16A (TMEM16A) and solute carrier family 26 member 9 (SLC26A9), are highly expressed in the airways and represent promising candidates for modulation.

TMEM16A is a Ca^{2+}-activated Cl^- channel that has in parallel been shown to be involved in the regulation of intracellular Ca^{2+} signals, relevant for airway mucus secretion, bronchoconstriction, and inflammatory mediator release. Its expression in the airway epithelium has been localized to the apical membranes of fluid-secretory ciliated cells but to a much larger extent mucus-producing goblet cells. Expression of TMEM16A is also evident in airway smooth muscle cells, involved in airway contraction. In this work, we evaluated the function of TMEM16A under pathological conditions in mouse airways and human airway models and concluded that TMEM16A plays a more relevant role in supporting airway mucus production and release, as well as bronchoconstriction, than Cl^--induced fluid secretion. In agreement with this, inhibition of TMEM16A by niclosamide, an FDA/EMA-approved drug, ameliorates the pathologic phenotype by dampening airway mucus production and secretion, relaxing airways, and inhibiting the release of inflammatory mediators. This may support repurposing of

niclosamide for the treatment of chronic airway inflammatory diseases. We assessed the direct administration of niclosamide to airways while encapsulated in slow-releasing micro- and nanoparticle formulations to circumvent potential systemic side effects of the drug as well as the need for repetitive applications. We propose this strategy to be further modified to target niclosamide specifically to mucus-secretory airway goblet cells. Our results suggest TMEM16A-inhibitors to be assessed in clinical trials.

SLC26A9 has been shown to work as an uncoupled Cl^- transporter as well as a coupled Cl^-/HCO_3^- exchanger. Its immunolocalization in the airway epithelium, however, was unresolved. We demonstrated apical expression in ciliated epithelial cells of human, mouse, and piglet airways, consistent with a role in luminal transport. Furthermore, we made use of the herein described, novel, highly potent and selective, SLC26A9-inhibitor, S9-A13, to further explore the function of SLC26A9 in airways. Our data suggest that ion transport by SLC26A9 depends on expression of CFTR. In the presence of CFTR, SLC26A9 does not mediate Cl^- secretion and therefore may not contribute to basal or stimulated airway Cl^- conductance. It rather operates as an exchanger, potentially recycling CFTR-secreted Cl^- and exchanging it for HCO_3^- ions. Thereby, it is likely to contribute to the regulation of ASL pH. Stimulation of SLC26A9 in CF, and in COPD caused by acquired dysfunction of CFTR, may provide the luminal HCO_3^- efflux necessary for proper mucus expansion and thus formation of the airway epithelial barrier, as well as for innate antimicrobial immunity. On the other hand, in the absence of CFTR, SLC26A9 appears to operate as an uncoupled Cl^- transporter. Pharmacological potentiation of SLC26A9 may then compensate for the lack of CFTR-mediated Cl^- efflux and subsequent fluid secretion. However, in most people with CF, biosynthesis of both CFTR and SLC26A9 is compromised. Here, rescue and potentiation of both proteins should be the strategy of choice.

In summary, inhibiting TMEM16A and enhancing expression and function of SLC26A9 in chronically inflamed airways may support lung function and respiratory homeostasis.

ZUSAMMENFASSUNG

Die menschlichen Atemwege sind ständig einer Vielzahl von schädlichen Stoffen wie Krankheitserregern, sterilen Reizstoffen und Allergenen ausgesetzt. Das Epithel der Atemwege und seine Eigenschaft als mechanische Barriere bildet die erste Verteidigungslinie gegen diese inhalierten Schadstoffe. Sie verhindert, dass diese Schadstoffe in die Schleimhaut der Atemwege eindringen können. Zusätzlich wird das Immunsystem rekrutiert, um die Abwehr zu unterstützen. Veränderungen oder angeborene Anomalien der Barriere-Funktion können zu chronischen Atemwegserkrankungen führen und die Homöostase der Atemwege beeinträchtigen. Chronische Atemwegserkrankungen sind weltweit eine der Haupttodesursachen. Chronisch obstruktive Lungenerkrankungen (COPD) und Asthma verursachen jährlich fast 3,7 Millionen Todesfälle. Daneben ist die Mukoviszidose (zystische Fibrose, CF), die durch eine fehlerhafte Expression oder Funktion des Cystic Fibrosis Transmembrane Conductance Regulator (CFTR)-Proteins in Epithelien verursacht wird, die Hauptursache für genetisch bedingte Todesfälle in der kaukasischen Bevölkerung. CFTR ist ein Ionenkanal für Cl^- und HCO_3^- und wird an apikalen Membranen von Epithelzellen der Atemwege exprimiert. CFTR ist wesentlich an der Regulierung der Hydratation und des pH-Werts der Atemwegsoberflächenflüssigkeit (ASL) beteiligt. Obwohl diese Krankheiten unterschiedliche pathophysiologische Mechanismen unterliegen, haben sie Gemeinsamkeiten, die zur Entwicklung einer chronischen Atemwegsentzündung beitragen: übermäßige Schleimproduktion, Umbau der Atemwege und Bronchokonstriktion. Gegenwärtige therapeutische Strategien sind krankheits- oder patientenspezifisch, wobei aber viele Patienten aufgrund von Therapieversagen oder erworbener Resistenzen nicht therapiert werden können. Alternative Therapien für diese Patienten, die derzeit entwickelt werden, zielen auf epitheliale Nicht-CFTR-Ionenkanälen und Transportern ab, die auch an der Regulierung der Homöostase der Atemwege beteiligt sind. Zwei mutmaßliche Cl^- sekretorische Proteine, das Transmembrane Protein 16A (TMEM16A) und der Transporter Solute Carrier Family 26 member 9 (SLC26A9), werden in den Atemwegen stark exprimiert und stellen vielversprechende Kandidaten für pharmakologische Angriffspunkte dar.

TMEM16A ist ein Ca^{2+}-aktivierter Cl^- Kanal, der auch zusätzlich intrazelluläre Ca^{2+}-Signale moduliert. TMEM16A ist für die Schleimsekretion, die Bronchokonstriktion und die Freisetzung von Entzündungsmediatoren in den Atemwegen relevant. TMEM16A wird in apikalen Membranen von sekretorischen Flimmerepithelzellen exprimiert, aber in einem viel größeren Ausmaß auch in den schleimproduzierenden Becherzellen. Die Expression von TMEM16A in Becherzellen ist bei Atemwegsentzündungen deutlich erhöht. Hier unterliegen Becherzellen einer akuten Proliferation und/oder Transdifferenzierung. Die Expression von TMEM16A ist auch in glatten Atemwegsmuskelzellen, die an der Atemwegskontraktion

während entzündlicher Atemwegserkrankungen beteiligt sind, nachgewiesen. In dieser Arbeit wurde die Funktion von TMEM16A unter pathologischen Bedingungen in den Atemwegen der Maus und in humanen Atemwegsmodellen untersucht. Aus den erhobenen Daten lässt sich schließen, dass TMEM16A eine wichtige Rolle bei der Unterstützung der Produktion und Freisetzung von Atemwegsschleim und der Bronchokonstriktion hat, aber weniger für die Cl^- induzierten Flüssigkeitssekretion zuständig ist. In Übereinstimmung mit diesen Daten verbessert die Hemmung von TMEM16A durch Niclosamid, ein von der FDA/EMA zugelassenes Medikament, den pathologischen Phänotyp, indem es die Schleimproduktion und -sekretion der Atemwege dämpft, die Atemwege entspannt und die Freisetzung von Entzündungsmediatoren hemmt. Niclosamid könnte deswegen als Medikament für die Behandlung chronisch entzündlicher Atemwegserkrankungen eingesetzt werden. Wir untersuchten weiterhin die Effekte von Niclosamid welches in Mikro- und Nanopartikeln mit langsamer Freisetzung eingekapselt war. Eine solche Formulierung reduziert die Gefahr potenzieller systemischer Nebenwirkungen. Diese Strategie sollte weiter untersucht und verbessert werden, um die Wirkung von Niclosamid auf schleimsekretorischen Zellen zu erhöhen. Diese vielversprechenden sollten in klinischen Studien validiert werden.

SLC26A9 arbeitet als Cl^--Transporter und als gekoppelter Cl^-/HCO_3^--Austauscher. Seine Immunlokalisierung im Epithel der Atemwege war bislang unklar. Wir konnten SLC26A9 in den Atemwegen von Menschen, Maus und Schweinen eindeutig in der apikalen Membran von Flimmerepithelzellen nachweisen. Diese Lokalisation deutet auf eine apikale Transportfunktion von SLC26A9 hin. Mit Hilfe des neuen, hochwirksamen und selektiven SLC26A9-Inhibitor S9-A13 konnte die Funktion von SLC26A9 in den Atemwegen genauer untersuchen werden. Die erhobenen Daten deuten darauf hin, dass die Funktionsweise von SLC26A9 von der CFTR-Expression abhängig ist. In Anwesenheit von CFTR vermittelt SLC26A9 keine Cl^--Sekretion und kann daher auch nicht zur basalen oder stimulierten Cl^--Sekretion in den Atemwegen beitragen. Vielmehr fungiert SLC26A9 als Cl^-/HCO_3^--Austauscher, der die über CFTR sezernierten Cl^- Ionen recycelt und gegen HCO_3^- austauscht und somit zur Regulierung des pH-Werts der ASL beiträgt. Möglicherweise könnte die eingeschränkte CFTR Funktion bei Mukoviszidose durch die Stimulierung von SLC26A9 kompensiert werden. Aktivierung von SLC29A9 könnte den HCO_3^--Efflux aufrechterhalten, der für die Schleimbildung und Schutzfunktion des Atemwegsepithels notwendig ist. In Abwesenheit von CFTR funktioniert SLC26A9 als entkoppelter Cl^--Transporter. Deswegen könnte die Aktivierung von SLC26A9 das völlige Fehlen der CFTR-vermittelten Flüssigkeitssekretion, bei einigen Fällen von Mukoviszidose, kompensieren. In den häufigsten Fällen von Mukoviszidose ist jedoch die gemeinsame Insertion von CFTR und SLC26A9 in die Plasmamembran beeinträchtigt. Angesichts der gekoppelten Biogenese beider Proteine sollte hier eine Kombination einer SLC26A9-Potenzierungstherapie mit Medikamenten, die die Protein-Protein-Interaktionen bei intrazellulärer Retention beeinflussen, die Strategie der Wahl sein.

Zusammenfassend lässt sich sagen, dass die Hemmung von TMEM16A und die Verstärkung der SLC26A9-Expression und/oder -Funktion in chronisch entzündeten Atemwegen zur Wiederherstellung der Lungenfunktion und der Homöostase der Atemwege beitragen kann.

PREFACE

This work is the result of the combination of published papers under the form of book chapters. Therefore, the reader may encounter variations (e.g., mouse nomenclature), accordingly to the guidelines of the different journals. The chapters consist of the following manuscripts:

Chapter 2: **Centeio R.**, Ousingsawat J., Cabrita I., Schreiber R., Talbi K., Benedetto R., Doušová T., Verbeken, E. K., De Boeck, K., Cohen I., Kunzelmann K. Mucus Release and Airway Constriction by TMEM16A May Worsen Pathology in Inflammatory Lung Disease. *International Journal of Molecular Sciences*. 2021 July; 22(15): 7852.

Chapter 3: **Centeio R.**, Ousingsawat J., Talbi K., Schreiber R., Kunzelmann K. CLCA1 Regulates Airway Mucus Production and Ion Secretion Through TMEM16A. *International Journal of Molecular Sciences*. 2021 May; 22(10): 5133.

Chapter 4: Ousingsawat J., **Centeio R.**, Cabrita I., Talbi K., Zimmer O., Graf M., Göpferich A., Schreiber R., Kunzelmann K. Airway Delivery of Hydrogel-Encapsulated Niclosamide for the Treatment of Inflammatory Airway Disease. *International Journal of Molecular Sciences*. 2022 Jan; 23(3): 1085.

Chapter 5: Ousingsawat J., **Centeio R.**, Schreiber R., Kunzelmann K. Expression of SLC26A9 in Airways and Its Potential Role in Asthma. *International Journal of Molecular Sciences*. 2022 Mar; 23(6): 2998.

Chapter 6: Jo S., **Centeio R.**, Park J., Ousingsawat J., Jeon D., Talbi K., Schreiber R., Ryu K., Kahlenberg K., Somoza V., Delpiano L., Gray M. A., Amaral M. D., Railean V., Beekman J. M., Rodenburg L. W., Namkung W., Kunzelmann K. The SLC26A9 inhibitor S9-A13 provides no evidence for a role of SLC26A9 in airway chloride secretion but suggests a contribution to regulation of ASL pH and gastric proton secretion. *The FASEB Journal*. 2022 Nov; 36(11): e22534.

INDEX

LIST OF ABBREVIATIONS

Abbreviation	Definition/Nomenclature
+/+,	Wild-type/ normal
-/-, KO	Homozygous knockout/ gene deletion
β-AR	β-adrenergic receptor
6CFSMEo-	Cystic fibrosis bronchial submucosal epithelium
AC*X*	Adenylate cyclase type *X*
ACE2	Angiotensin-converting enzyme 2
ACh	Acetylcholine
AHR	Airway hyperresponsiveness
AMP	Antimicrobial peptide/protein
ASL	Airway surface liquid
ASM	Airway smooth muscle
AT1R	Angiotensin-II type 1 receptor
ATII	Angiotensin-II
ATP	Adenosine triphosphate
BAL	Bronchoalveolar lavage
BCi-NS1	Immortalized non-smoker airway basal cells clone 1
C-ter	Carboxyl-terminus
Ca^{2+}	Calcium ion
CaCC	Calcium-activated chloride channel
CAL	CFTR associated ligand
CaM	Calmodulin = calcium-modulated protein
CaMKII	Calcium/calmodulin-dependent protein kinase II
cAMP	Cyclic adenosine monophosphate
CBF	Ciliary beating frequency
CF	Cystic fibrosis
CFBE	Cystic fibrosis bronchial epithelium
CFinh/CFTRinh-172	CFTR inhibitor 172
CFTR	Cystic fibrosis transmembrane conductance regulator
CICR	Calcium-induced calcium release
Cl^-	Chloride ion
CDX	Cluster of differentiation X
CLCA*X*	Calcium-activated chloride channel regulator *X*
COPD	Chronic obstructive pulmonary disease
COVID-19	Coronavirus disease
CPI-17	C-kinase potentiated protein phosphatase-1 inhibitor of 17 kDa

CSE	Cigarette smoke exposure
cSNP	Coding single nucleotide polymorphism
DAG	Diacylglycerol
DAMP	Damage-associated molecular pattern
DIDS	4,4'-diisothiocyanatostilbene-2,2'-disulfonic acid
DNA	Deoxyribonucleic acid
ECM	Extracellular matrix
EM	Electron microscopy
EMA	European Medicines Agency
ENaC	Epithelial sodium channel
ER	Endoplasmic reticulum
ERK*X*	Extracellular signal-regulated kinase *X*
F508del	Phenylalanine deletion at position 508
FDA	Food and Drug Administration (USA)
FOXA2	Forkhead box protein A2
FRT	Fisher rat thyroid
GC(M)	Goblet cell (metaplasia)
GEF	Guanine nucleotide exchange factor
GDP	Guanine diphosphate
GTP	Guanine triphosphate
GPCR	G protein-coupled receptor
h	Human
H^+	Hydrogen ion/ proton
H*X*R	Histamine receptor type X
HA	Hyaluronic acid
HCO_3^-	Bicarbonate ion
HEK	Human embryonic kidney epithelium
HGT-1	Human gastric cancer
I^-	Iodide ion
IBMX	3-isobutyl-1-methylxanthine
IC_{50}	Half maximal inhibitory concentration
IF	IBMX+forskolin
Ig*X*	Immunoglobulin *X*
IL-*X*	Interleukin *X*
ILC2	Group 2 innate lymphoid cells
IP_3(R)	Inositol triphosphate (receptor)
(I)PH	Idiopathic pulmonary hypertension
Isc/ I'sc	Short-circuit current / Equivalent short-circuit current

I.T.	Intratracheal
JAG-1	Jagged Canonical Notch Ligand 1
K^+	Potassium ion
KCNE3	Potassium voltage-gated channel subfamily E regulatory subunit 3
KCNN4/SK4	Potassium calcium-activated channel subfamily N member 4
KCNQ1	Potassium voltage-gated channel subfamily Q member 1
M3	Muscarinic receptor 3
MAPK*X*	Mitogen-activated protein kinase *X*
MCC	Mucociliary clearance
MLC(K/P)	Myosin light-chain (kinase/phosphatase)
MMP	Matrix metalloproteinase
m	Murine
mRNA	Messenger ribonucleic acid
MUC	Mucin
NBD	Nucleotide-binding domain
N-CLCA1	Amino-terminal portion of CLCA1
NF-kB	Nuclear factor kappa-light-chain-enhancer of activated B cells
NKCC1	Sodium-potassium-chloride cotransporter 1
N-ter	Amino-terminus
Na^+	Sodium ion
NaCl	Sodium chloride (salt)
NE	Neutrophilic elastase
NHERF1	Na^+/H^+ exchanger regulatory factor 1
OVA	Ovalbumin
P1	Purinoreceptor 1
$P2Y_2$	Purinoreceptor 2Y2
PA	Pulmonary artery
PAMP	Pathogen-associated molecular pattern
PCL	Periciliary layer
RT-PCR	Reverse transcription-polymerase chain reaction
PDZ	Post synaptic density protein (PSD95), Drosophila disc large tumour suppressor (Dlg1), and zonula occludens-1 protein (zo-1)
PEG	Polyethylene-glycol
PIP_2	Phosphatidylinositol 4,5-bisphosphate
PK(A/C)	Protein kinase (A/C)
PLC	Phospholipase C
PM	Plasma membrane
PPX	Protein phosphatase X

PRR	Pathogen-recognition receptor
R	Regulatory (domain)
ROCK	Rho-kinase
RyR	Ryanodine receptor
TEER	Transepithelial electrical resistance
TGF	Transforming growth factor
T_H*X*/Th*X*	T helper cells type *X*
TM	Transmembrane domain
TMEM16*X*	Transmembrane protein 16*X*
TNF	Tumour necrosis factor
TRAM34/T34	Triarylmethane-34
TRP*X*	Transient receptor potential *X*
TSLP	Thymic stromal lymphopoietin
SARS-CoV-2	Severe acute respiratory syndrome coronavirus type 2
SERCA	Sarcoplasmic/endoplasmic reticulum calcium-ATPase
SCN^-	Thiocyanate ion
shRNA	Small hairpin RNA
siRNA	Small interfering RNA
SLC26A*X*	Solute carrier family 26 member *X*
SMG	Submucosal gland
SNARE	Soluble N-ethylmaleimide–sensitive factor attachment protein receptor
SNAP-23	Synaptosomal-associated protein 23
SOCE	Store-operated calcium entry
SPDEF	SAM-pointed domain-containing Ets-like factor
SPLUNC1	Short palate lung and nasal epithelial clone 1
SR	Sarcoplasmic reticulum
STAS	Sulphate transporter and anti-sigma factor antagonist
STAT*X*	Signal transducer and activator of transcription *X*
STIM1	Stromal interaction molecule 1
UTP	Uridine-5’-triphosphate
VAMP	Vesicle-associated membrane protein
VGCC	Voltage-gated calcium channels
VRAC	Volume-regulated anion channel
VWA	von Willebrand factor type A
WNK	With-no-lysine (K)
YFP	Yellow fluorescent protein

LIST OF FIGURES

LIST OF TABLES

CHAPTER 1 | INTRODUCTION

Physiological properties of the airway epithelium

The vital act of breathing requires the airways to be permanently exposed to the external environment, which contains a myriad of noxious agents such as pathogens, sterile irritants, and allergens. Hence, the airway epithelium constitutes the first-line defence against these inhaled insults, preventing them from invading the airway mucosa. The airway epithelium comprises four main properties[1]:

Barrier function

The airway epithelium constitutes a physical barrier to invasion, consisting of a monolayer of polarized cells which maintain their cohesion by intercellular junctional complexes. These regulate the paracellular permeability of the epithelium to restrict the entry of harmful substances, yet allow when necessary the movement of ions, macromolecules, fluids, and immune cells through the paracellular space[2]. Nevertheless, the first obstacle to overcome when facing the airway epithelium is its protective mucus layer.

Mucociliary clearance

The secreted airway mucus and the airway cilia work together with the mechanical action of cough to trap, move and clear inhaled noxious agents out of the lungs. For efficient clearance, the airway surface liquid (ASL) layer, which comprises both the mucus layer and the underlying periciliary liquid (PCL) layer that bathes the airway cilia, must be kept at an appropriate state of hydration. This is regulated mainly through the coordinated actions of the epithelial sodium (Na^+) channel (ENaC) that mediates Na^+ absorption, and the cystic fibrosis transmembrane conductance regulator channel (CFTR) that mediates chloride (Cl^-) secretion in the airways. Water absorption or secretion passively follows the net flux of these electrolytes, to maintain ASL homeostasis[3]. The ASL pH has also been shown to play a crucial role in the diffusivity of gel-forming mucin proteins and subsequent transportability of mucus[4], and CFTR-dependent bicarbonate (HCO_3^-) secretion, debated whether directly through the CFTR channel and/or via other transporters regulated by CFTR, has been proposed as critical for ASL pH regulation[5-10].

Environment sensing

Airway epithelial cells express pattern-recognition receptors (PRRs) capable of recognizing pathogen- and damage-associated molecular patterns (PAMPs/DAMPs), that sense local invading pathogens and host-derived tissue damage indicators and generate pro-

inflammatory signals that recruit and activate immune cells at the site of threat[11,12]. Particular cells in the airway epithelium, namely neuroendocrine cells, are also capable of secreting bioactive neuropeptides in response to fluctuations in oxygen levels, and these can affect the pulmonary blood flow and the airway calibre[13].

Innate immunity

Airway epithelial cells are the main manufacturers of antimicrobial peptides and proteins (AMPs) present in the ASL, and these are key effector molecules in host defence. While some of these molecules are present constitutively, others are induced in response to pathogen-recognition by PRRs. AMPs can directly act as microbicides in the ASL, efficiently neutralize toxins, and attract and activate immune cells[14]. The airway epithelium also maintains a tightly regulated protease/antiprotease secretory balance, which plays a pivotal role in processes such as mucin production, degradation of microbial peptides, activation of immune cells and inflammatory mediators, control of viral infection, control of tissue damage upon inflammation, and tissue regeneration/repair[15-17].

The airway epithelium ultimately coordinates its physical, mechanical, biochemical, and cellular properties to protect the airways from harmful invading agents and toxic insults that constantly challenge the airway epithelial barrier, and that can otherwise strongly compromise the respiratory homeostasis (Figure 1.1).

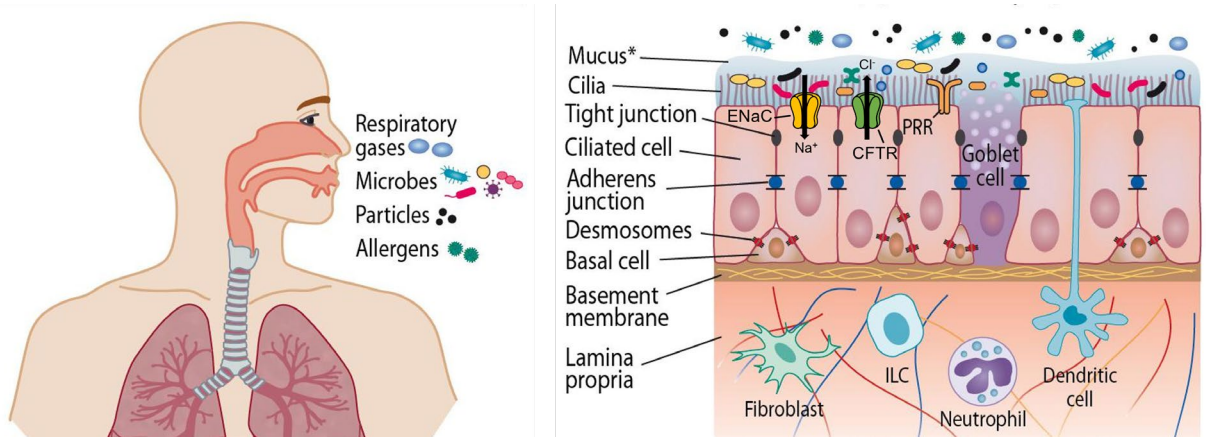

Figure 1.1 | *Airway epithelial dynamics.*
Generic, non-comprehensive representation of the normal airway epithelial dynamics. Adapted from[18].

Two key physiological mechanisms are pertinent to follow this thesis and will therefore be described in more detail: 1) airway mucus production and secretion; and 2) airway constriction and dilation. Thereafter, it will be further elucidated and exemplified how alterations or congenital abnormalities of the airway epithelial barrier can lead to chronic respiratory diseases.

Airway mucus production and secretion

The surface airway epithelium comprises multiple cell types, of which ciliated and goblet cells represent the two main groups. Ciliated cells, through the synchronized beating of their cilia, ensure an effective mucociliary clearance in cooperation with goblet cells, the main mucus producing cells of the airways[19]. In proximal, larger airways (diameter > 2 mm), submucosal glands (SMG) are the main contributors to mucus and fluid secretion. These structures consist of serous terminations (acini) contiguous to mucous tubules, that culminate in a single collecting duct. This duct then narrows into a ciliated duct which is continuous with the airway surface, and which propels the glandular secretions into the airway lumen[20,21] (Figure 1.2A).

The airway mucus is ultimately composed by a variety of products secreted by airway epithelial and glandular cells, namely fluid, electrolytes, metabolites, antimicrobial molecules, immunomodulatory molecules, and mucins[22]. While water constitutes 97% of normal mucus, mucins, heavily glycosylated polymeric proteins (up to 90% carbohydrate by mass), are its main structural components, that confer airway mucus its viscoelastic gel-forming properties[22]. Airway mucins can be subdivided into cell surface-associated mucins, secreted non-polymerizing mucins, and secreted polymerizing gel-forming mucins[23]. Belonging to the latter group, mucins MUC5AC and MUC5B are the most abundantly expressed in the airways. MUC5AC is the main gel-forming mucin secreted by goblet cells of the surface airway epithelium, while MUC5B originates mainly, but not exclusively, from the mucous cells of the airway submucosal glands[24]. MUC5B is the main mucin expressed at baseline conditions in the small airways and is thought to perform most of the homeostatic clearance functions, while MUC5AC is the main mucin upregulated under inflammation and is under negative control by the transcription factor forkhead box protein A2 (FOXA2)[25,26]. The transcription factor SAM-pointed domain-containing Ets-like factor (SPDEF) is thought to be central in regulating a transcriptional network inducing airway goblet cell differentiation and mucus production. This includes mucin genes, but also genes involved in mucin glycosylation and secretion[27,28]. Nevertheless, signal transduction pathways not involving SPDEF have also been proposed as critical for mucin gene expression[29]. After synthesis and post-translational modification, gel-forming mucins are stored within intracellular secretory granules, tightly packed at low pH (6.2), high concentration of calcium (Ca^{2+}) ions, and highly dehydrated, where they remain until stimulated for release by exocytosis[30].

The airway mucus is continuously being cleared, which requires replenishing via a constitutive release of newly synthesized mucins, in order to maintain a normal healthy protective barrier. This is achieved given the continuous presence in the ASL of low levels of adenosine triphosphate (ATP), the most important mucin secretion stimulant (secretagogue) for the surface epithelium, which binds and activates apical membrane purinergic $P2Y_2$ receptors. This induces a low, steady-state activity of the secretory machinery[22]. In healthy

airways, the basal rate of secretion matches the basal rate of mucin synthesis, which leads to low intracellular mucin accumulation[31]. While in resting state, each mucin-containing secretory granule is thought to be tethered to the plasma membrane by Rab proteins, known for regulating several steps of vesicle formation and trafficking, and membrane fusion. These Rab proteins are attached to effector proteins which dock the scaffold protein Munc18, which in turn binds the Munc13-dependent closed-conformation of the membrane-anchored, one α-helix Syntaxin protein. When ATP binds the G protein-coupled receptor (GPCR) $P2Y_2$, a G_q-coupled purinergic receptor, phospholipase C (PLC) is activated, which cleaves membrane phospholipid phosphatidylinositol 4,5-bisphosphate (PIP_2) and generates the intracellular second messengers diacylglycerol (DAG) and inositol triphosphate (IP_3)[31,32]. DAG activates Munc13, which opens Syntaxin and allows the formation of a four-α-helix SNARE (soluble N-ethylmaleimide–sensitive factor attachment protein receptor) complex, with two additional α-helices from membrane-bound SNAP-23 (synaptosomal-associated protein 23) and one from VAMP (vesicle-associated membrane protein), which draws together the secretory granule and the plasma membrane. Concurrently, IP_3 migrates and binds its Ca^{2+}-channel receptor (IP_3R) at the endoplasmic reticulum (ER) membrane, inducing the release of Ca^{2+} from ER stores. This in turn activates vesicle-bound Synaptotagmin to induce final twisting of the SNARE complex and consequent fusion of the secretory granule and plasma membranes, which results in mucin release to the extracellular space[31,32] (Figure 1.2B). During secretion, unfolding of the condensed mucins requires an increase in pH as well as Ca^{2+}-ion sequestration, which are both achieved by CFTR-dependent HCO_3^- secretion. This allows the mucins to adsorb more than 100-fold their mass in water and expand up to 1000-fold their dehydrated volume, to form a normal healthy mucus layer, with the appropriate viscoelasticity for ciliary clearance[31,33].

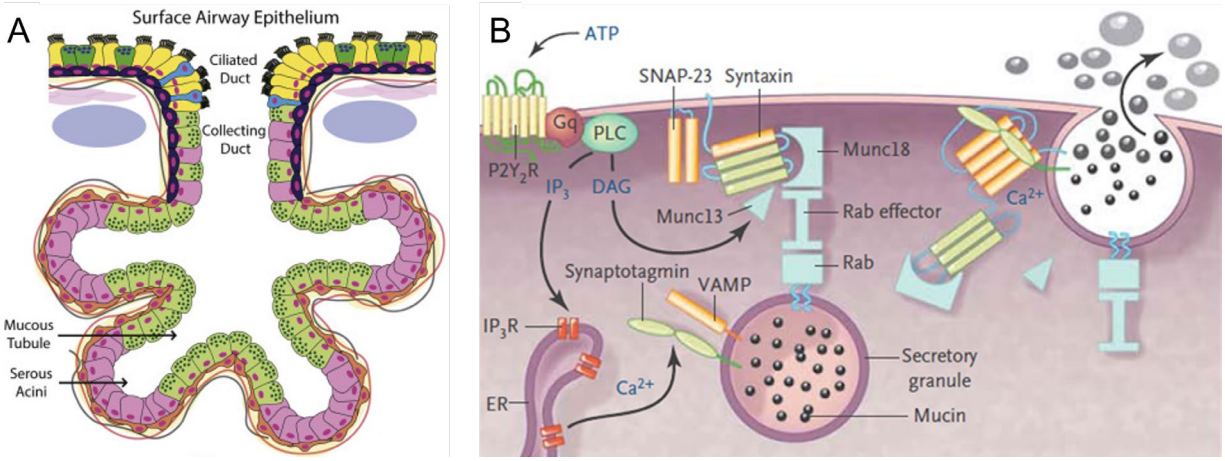

Figure 1.2 | *Airway submucosal glands and goblet/mucous cell secretory granule exocytosis.* Schematic representation of (A) an airway submucosal gland, adapted from[34]; and (B) the mechanism of mucin-containing secretory granule exocytosis in airway goblet/mucous cells, adapted from[22].

Airway constriction and dilation

In the posterior region of upper airways, neighbouring cartilage, a layer of airway smooth muscle (ASM) is organized as muscle bands, and these become thinner and circumferentially arranged around smaller, distal airways[35]. ASM cells are mechanically active and express several receptors for physiological stimuli that mediate contractile mechanisms[36]. The ASM has an intrinsic tone (a sustained tension) maintained by a feedback loop between the muscle and other sensory and regulatory tissues, and further acute contraction can be induced. Ultimately, the ASM is responsible for controlling the airway calibre, regulating the airflow to optimize ventilation, and mechanical reflexes such as cough[35,37].

In the adult lung, endogenous mediators that regulate both tonic and acute ASM contraction can originate from nerve terminals, structural airway cells or inflammatory cells, and the large majority of these act on GPCRs expressed at the surface of ASM cells, and drive changes in intracellular Ca^{2+} levels through several mechanisms[35]. A pivotal example of this is acetylcholine (ACh), the predominant neurotransmitter released by parasympathetic cholinergic nerves in the airways, but which can also be secreted by non-neuronal cells, such as airway epithelial and inflammatory cells[38]. Binding of ACh to $G_{\alpha q}$-coupled M3 muscarinic receptors on ASM cells activates phospholipase C-*β* (PLC*β*), which, as described previously, generates the secondary messengers IP_3 and DAG[39]. Muscle cells have a specialized type of smooth ER, that is referred to as sarcoplasmic reticulum (SR). IP_3R activation at the SR membrane leads to release of SR-stored Ca^{2+}. This can be further stimulated by subsequent activation of Ca^{2+}-induced Ca^{2+} release (CICR) by SR membrane-localized ryanodine receptors (RyR)[39]. Cytoplasmic Ca^{2+} oscillations in ASM cells primarily occur as the Ca^{2+} released by IP_3Rs and RyRs is re-taken up into SR stores by the sarcoplasmic/endoplasmic reticulum Ca^{2+}-ATPase (SERCA) pump, and are responsible for maintaining the intrinsic ASM tone, as well as for further contraction upon effective ACh concentrations that increase their frequency[35]. These oscillations are also finely tuned by other mechanisms of Ca^{2+} extrusion and uptake from extracellular sources[40]. The elevated cytoplasmic Ca^{2+} binds to the regulatory protein calmodulin (CaM), and the Ca^{2+}-CaM complex binds and activates myosin light-chain kinase (MLCK), which then phosphorylates myosin light chain (MLC), the regulatory subunit of myosin. This phosphorylation is essential for the ATPase function of myosin, which, by hydrolysing ATP, triggers the sliding movement of myosin filament “heads” along actin filaments, creating a cross-bridge of actomyosin filaments in the cytoskeleton of the ASM, that generates the contraction[39] (Figure 1.3).

In parallel, ACh also mediates Ca^{2+}-sensitization of the ASM. ACh binding to M3 receptors activates guanine-exchange protein RhoGEF, which converts inactive RhoA-GDP into active RhoA-GTP, then able to activate Rho-kinase (ROCK). ROCK phosphorylates the regulatory subunit of MLC phosphatase (MLCP), inhibiting its enzymatic activity. Additionally,

DAG-induced activation of protein kinase C (PKC) phosphorylates and activates CPI-17, an inhibitory protein of MLCP. This results in sustained myosin phosphorylation, and consequently, sustained ASM contraction and airway constriction[39]. Emptied SR Ca^{2+} stores are replenished by the SERCA pump and by the STIM1 Ca^{2+}-sensor protein located at the SR, that complexes with the Ca^{2+}-selective ion pore Orai at the plasma membrane and mediates store-operated Ca^{2+} entry (SOCE) from the extracellular space. The decrease in cytoplasmic Ca^{2+} levels leads to MLC dephosphorylation and muscle relaxation[35,39] (Figure 1.3).

Stimulation of ASM relaxation is predominantly mediated by the circulating hormone adrenaline, released by the adrenal glands[35]. Adrenaline binds G_s-coupled β_2-adrenergic receptors on ASM cells, activating adenylate cyclase (AC). AC generates cAMP from intracellular ATP, which leads to activation of the cAMP-dependent protein kinase A (PKA). PKA phosphorylates several targets involved in the ASM contractile machinery such as the IP_3R, leading to its decreased sensitivity to IP_3, and reduced Ca^{2+} oscillations[41]. PKA also interferes with the Ca^{2+}-sensitivity of the ASM by phosphorylating MLCK, inhibiting its activity and the formation of the actomyosin cross-bridges, thereby inducing ASM relaxation and airway dilation[42].

Besides its relevance for regulating the airway tone, the ASM also carries additional proliferative and immunomodulatory functions that play a role in airway homeostasis[43].

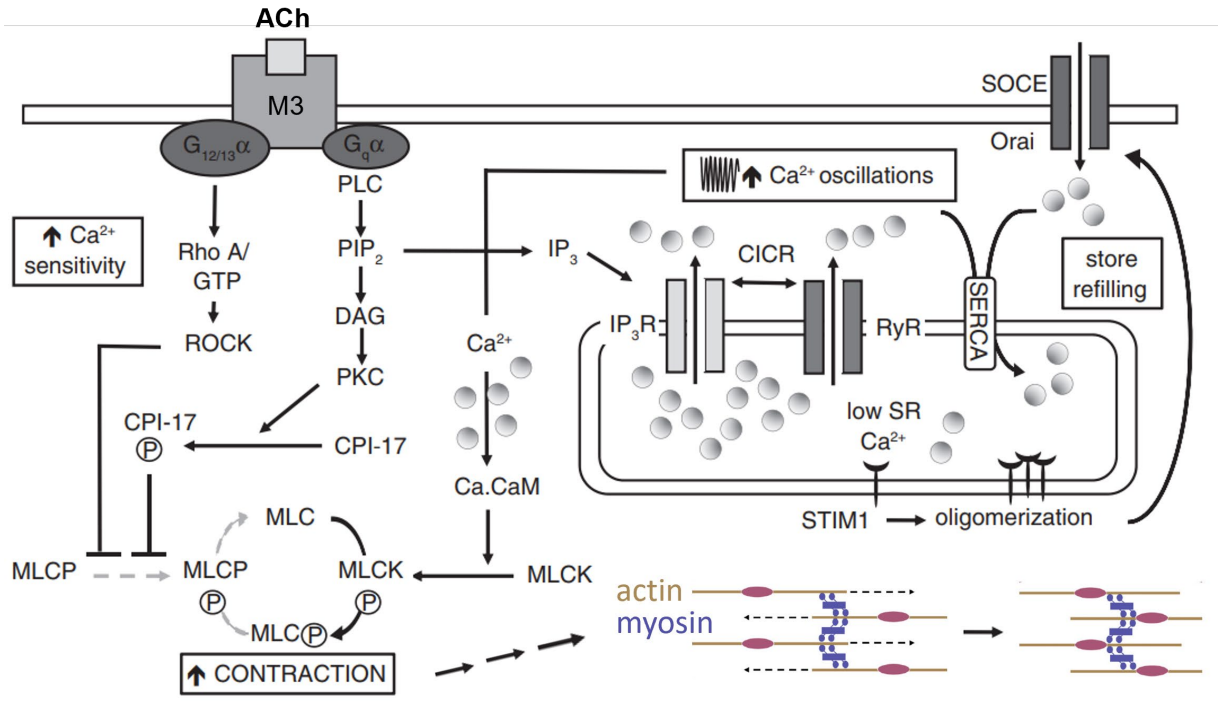

Figure 1.3 | *Airway smooth muscle contraction.*
Schematic illustration of contractile mechanisms in airway smooth muscle cells. Adapted from[35,44].

Chronic inflammatory airway disease

Acute inflammation of the lungs is a physiological response against invading threats and overall damaged cells, and is crucial to eradicate the stimuli, initiate the healing process and restore airway integrity. Contrarily, chronic inflammation prevents the natural arrest of the inflammatory response and leads to disruption of otherwise healthy tissues, provoking a continuous cycle of amplification of the inflammation and progressive damage to the airways[45]. Concurrently, the growing impairment of the front-line defense against inhaled noxious agents can further facilitate infectious and inflammatory exacerbations[46].

Chronic respiratory diseases are leading causes of death worldwide, with chronic obstructive pulmonary disease (COPD) alone ranking third with 3.23 million deaths in 2019, and asthma accounting for 455 000 deaths in the same period (latest statistics[47,48]). While these can result from long-term environmental exposure to harmful gases and airborne particles, e.g., tobacco smoke and occupational dusts, genetic predisposition factors can expedite the disease onset and/or aggravate its outcome[49]. Cystic fibrosis (CF) is a genetic disease caused by mutations in the CFTR gene and is the leading cause of genetic disease-related death amongst the Caucasian population, which is frequently due to respiratory failure caused by recurrent cycles of infection and inflammation of CFTR-dysfunctional airways[50,51].

Overproduction of airway mucus with altered physical properties is a major common factor contributing to the morbidity and mortality of chronic inflammatory airway diseases. While goblet cells are not abundant in the surface epithelium of airways distal to the trachea, goblet cell hyperplasia (proliferation) and/or metaplasia (transdifferentiation) can be induced during airway inflammation, particularly in the context of chronic disease[32,52]. Paradoxically, while an insufficient mucus barrier would leave the airways more vulnerable to injury, production of excessive/altered mucus contributes to impaired mucociliary clearance as well as airway obstruction, both triggering inflammation[24]. Despite the ultimate presentation of similar symptoms, such as shortness of breath, coughing, wheezing and expectoration, chronic inflammatory airway diseases can have very distinct underlying pathophysiological mechanisms[53].

Cystic fibrosis

To this date, more than 2000 variants in the CFTR gene have been reported, many associated with the autosomal recessive disease cystic fibrosis (CF)[54,55]. These mutations have been grouped in several categories, according to the defect they cause on the CFTR protein expression and function, a cyclic AMP (cAMP)-dependent and phosphorylation-regulated Cl^-/HCO_3^- channel, that sits on the apical membrane of epithelial ciliated cells, and is also expressed in immune cells[56-58]. These defects can range from no mRNA production due to large

deletions in the gene, no protein expression due to nonsense-mediated decay of transcripts resulting from premature stop codons, and milder defects leading to impaired gating, decreased conductance, or less stability of the protein at the plasma membrane (PM)[59]. The levels of functional CFTR expression strongly correlate with the clinical phenotype of disease severity observed in patients[60,61]. The by far most common CFTR defect, affecting about 90% of patients worldwide on at least one allele, is a phenylalanine (F) deletion at position 508 (F508del) that causes misfolding of the CFTR protein and impairs its proper traffic to the PM[62,63].

Lack of CFTR activity at the PM leads to a dysregulation of ion and fluid homeostasis across several epithelia, the major cause of morbidity and mortality in CF being, however, pulmonary disease[64]. This is thought to be triggered mainly by two CFTR-related secretory defects in the airway epithelium of CF patients: 1) a defective Cl^- and consequently fluid secretion that causes a dehydration of the ASL, impairing the movement of the airway cilia responsible for mucociliary clearance (MCC)[65,66]; 2) a defective CFTR-dependent HCO_3^- secretion that leads to acidification of the ASL, making it suboptimal for the activity of antimicrobial peptides and proteins, and impairing proper mucin unpacking and expansion, leading to the tethering of mucus to the airway surface and obstruction of submucosal gland ducts[33,67,68]. Both factors establish a predisposition towards persistent bacterial infections, keeping trapped pathogens close to the airway surface[69].

This provides constant stimuli for inflammation, and CFTR-deficient airway epithelial and immune cells have also been shown to suffer from a constitutive abnormality in the regulation of cytokine production, namely, showing an increased production of pro-inflammatory cytokines, particularly IL-8, and decreased production of anti-inflammatory cytokines[57,70]. IL-8 is a potent neutrophil chemoattractant, and CF patients have a characteristic chronic neutrophilic infiltration of the airways, leading to an excessive release of neutrophilic elastase (NE) and other neutrophil-derived proteases, such as matrix metalloproteinases 8 and 9 (MMP-8,9)[71,72]. NE digests elastin fibres and other extracellular matrix (ECM) proteins, causing damage to the airway wall and a permanent enlargement of parts of the airways (bronchiectasis)[73]. This is, however, accompanied by thickening of the airway wall to due remodelling processes that lead to deposition of fibrotic tissue, which is associated with end-stage small airway narrowing in CF[1,74]. In addition, excess proteolytic activity of NE (that exceeds antiprotease capacity in CF) also promotes goblet cell metaplasia and mucus hypersecretion; impairs ciliary beating, the activity of antimicrobial peptides and proteins, phagocytic events, and neutrophil-mediated bacterial killing; and further stimulates the release of pro-inflammatory cytokines, perpetuating the cycle of inflammation, injury and repair[75,76]. Some studies have even demonstrated a NE-mediated proteolytic activation of ENaC[77,78], and NE-induced CFTR degradation[79], further contributing to ASL dehydration and mucus stasis. Moreover, the defective phagocytic clearance of apoptotic neutrophils leads to their necrosis in the airways, resulting in the release of intracellular contents such as DNA, that greatly

contribute to mucus viscosity and adherence[76,80]. Ultimately, CF is characterized by chronic mucus plugging of the airways, airflow obstruction, bacterial colonization and inflammation, and progressive airway damage, culminating in respiratory failure.

Chronic obstructive pulmonary disease

Chronic exposure to external toxic agents, most commonly cigarette smoke, is the major risk factor for the development of chronic obstructive pulmonary disease (COPD)[81]. These inhaled insults can directly trigger PRRs on the surface of airway cells, and pollutant-damaged cells can indirectly release DAMPs, to initiate pattern recognition and the inflammatory response[82]. Chemotactic (cell-recruiting) factors such as TNF-α and IL-8, are then released to mobilize immune cells to the injured region, mainly neutrophils and monocytes that later differentiate into macrophages *in situ*. Epithelial and immune airway cells release proteases such as NE and MMPs-8,9, which, at the level of terminal airways, cause degradation of the alveolar wall attachments composed by elastin fibers that are held tight around the small airways, leading to alveolar collapse (emphysema) and an increase in small airway/overall lung compliance[45,82]. Subsequently, airway cells secrete the cytokine TGF-β, which triggers fibroblast proliferation and activation, and small airway wall remodeling via deposition of fibrotic tissue[83]. Given chronic exposure to the environmental insult, a cycle of inflammation, injury and repair is established, which leads to progressive thickening of small airway walls and airway narrowing, growing airflow obstruction, and a compromise of gas exchanges at the alveolar level, ultimately causing significant declines in lung function[84].

Alveolar macrophages (M1/M2 phenotypes) are particularly affected by cigarette smoke exposure (CSE), which impairs their phagocytic clearance activity of apoptotic cells (efferocytosis; M1), and favors an imbalanced differentiation into a wound-healing phenotype (M2), sustaining inflammation[85]. This and other alterations of the airway inflammatory microenvironment, together with genetic and epigenetic susceptibility factors, have been implicated in the persistence of the inflammatory response in CSE-mediated COPD, despite smoking cessation[82]. Of relevance is that chronic CSE has been shown to induce an acquired CFTR dysfunction in the small airways of patients with normal CFTR alleles[86,87]. This results in permanent ASL dehydration and defective mucociliary transport[88,89], and further affects innate immunity, as outlined previously. CSE has also been shown to independently induce goblet cell metaplasia/hyperplasia and MUC5AC overproduction, which further exacerbates the mucus abnormality and leads to plugging in COPD airways[90,91]. Consequently, air trapping is worsened, and retention of harmful agents at the epithelial surface is favored, fueling a new cycle of infection-mediated inflammation. Ultimately, the pathophysiology of COPD may share several phenotypical features with CF, particularly upon acquired CFTR-deficiency[1].

Asthma

Asthma is a multifactorial chronic respiratory disease that comprises several endotypes and phenotypes, characterized by distinct pathophysiological molecular mechanisms, biomarkers, onset, symptoms, severity grades and treatment strategies[92]. Several genetic susceptibility and environmental risk factors have been identified to correlate with an increased likelihood of developing asthma[93].

Chronic exposure of the immune system to mostly harmless agents, such as house dust mite allergens, may cause it to develop a hypersensitivity that leads to the generation of exaggerated immune reactions, in response to an ordinary exposure to the given agent (allergy)[94]. On that note, a relevant and well-characterized subtype of asthma is allergic asthma, defined as an allergy-induced chronic inflammation and hyperreactivity of the bronchi and bronchioli[95]. Exposure to inhaled allergens stimulates the airway epithelium to release pro-inflammatory cytokines such as IL-33, IL-25, and TSLP, which ultimately activate innate and adaptive immune cells to secrete another set of cytokines, primarily IL-4, IL-5, and IL-13[96]. Importantly, TSLP is responsible for dendritic cell migration into lymph nodes, necessary for priming naïve $CD4^+$ T lymphocytes into IL-4-competent T cells. These then migrate into B lymphocyte zones within the lymph node and prime them to an immunoglobulin type E (IgE)-secreting phenotype. T cells later move into the circulation and complete their maturation into type 2 T helper cells (T_H2), being later recruited to the airway epithelium and the subepithelial mucosa, where they secrete IL-5 and IL-13[96,97]. Inflammation in allergic asthma, as well as other subtypes, is often referred to as T_H2-mediated inflammation. In parallel, airway epithelium-resident mast cells, group 2 innate lymphoid cells (ILC2), and chemoattracted basophils, are activated by IL-33 and IL-25, and secrete in response IL-4, IL-5, IL-6 and IL-13, that help support B and T cell maturation and recruitment, inhibit the function of regulatory T cells responsible for suppressing the immune response, and lead to macrophage activation and eosinophil attraction[96,97]. Eosinophilic infiltration of the airways is regarded as a defining feature of allergic asthma, and degranulation of eosinophils is thought to release immunomodulatory cytokines, chemokines involved in the recruitment of effector T_H2 cells, mediators of bronchoconstriction and mucus production, and also tissue-destructive proteins, MMPs, and TGF-β, that elicit airway remodeling events and fibrosis[98]. Additionally, in a positive feedback loop that helps to perpetuate inflammation, IgE secreted by B cells binds mast cells and basophils, extending their survival and hence sustaining their activation given chronic exposure to the allergen[96]. Activated mast cell and basophil degranulation leads to the release of several stimuli for bronchoconstriction, such as histamine and prostaglandin D2[92]. In asthma, besides progressive airway wall fibrosis and thickening, airway narrowing, and other airway remodeling features typical of chronic inflammatory airway diseases, an increase in ASM mass is characteristic, due to ASM cell hyperplasia and hypertrophy[99]. Not only do these ASM cells

mediate further inflammatory processes, but they also cause airway hyperresponsiveness (AHR), generating excessive bronchoconstriction in response to common airway irritants, causing acute but reversible airflow limitation. This is thought to be led by the increase in total ASM mass, as well as by the overproduction of contractile mediators by sustained enlarged pools of mast cells, basophils, and eosinophils in the airways[99,100].

Other contributing factors such as cytokine-potentiated increases in intracellular free Ca^{2+}, have also been described to enhance ASM contractility in asthma[100]. IL-13, particularly, has been reported to augment agonist-induced contractions of the ASM via several mechanisms[101,102]. IL-13 has also been extensively characterized as a mediator of mucus overproduction. In a proposed sequence of events, binding of IL-13 to its receptor in mucous cell progenitors (e.g. club cells), leads to phosphorylation of the STAT6 transcription factor and its translocation to the nucleus, where it induces expression of STAT6-responsive genes, one of these being the master regulator SPDEF[103]. SPDEF may directly induce the expression of several mucous cell genes, but also indirectly cause this by inhibition of the repressor FOXA2, driving goblet cell metaplasia[27,103]. One of the genes induced by SPDEF is the calcium-activated chloride channel regulator 1 (CLCA1) gene, which encodes a protein with a metalloproteinase domain, that suffers intracellular self-cleavage and is secreted as a soluble complex of C-terminal and N-terminal fragments[27,104]. Proteomic and transcriptomic analyses have identified CLCA1 as the most increased protein in the bronchoalveolar lavage (BAL) fluid[105], and the most upregulated gene transcript in lung tissue[106], of particular mouse models of asthma. CLCA1 expression has also been shown to be strongly upregulated in bronchial tissues from asthmatic individuals[107]. The next proposed step is the binding of secreted N-CLCA1, in an autocrine or paracrine fashion, to a putative receptor that initiates a mitogen-activated protein kinase 13 (MAPK13)-dependent signaling pathway, that culminates in the upregulation of MUC5AC, and mucus overproduction[108,109]. The chronic airway inflammation in asthma is ultimately characterized by progressive airway narrowing, mucus plugging, and AHR, that cause airflow obstruction. Continuing damaging changes to the airway mucosa in asthma, eventually confer susceptibility to other types of inflammation, namely, pathogen-mediated, and predispose an individual to asthmatic exacerbations[110].

Current therapies for chronic inflammatory airway diseases

Several therapeutical strategies are already available or under development for the treatment of chronic airway inflammatory diseases, with the aim of improving overall lung function and preventing exacerbations. These target different pathophysiological aspects, namely, they are aimed at decreasing mucus production, decreasing mucus secretion, promoting mucus clearance, overcoming bronchoconstriction, attenuating or reversing airway

remodeling, downregulating inflammation, and/or treating airway infection[22,42,111,112]. Inhaled or intranasal medications, although not always achievable, are the ultimate goal, as they allow higher drug deposition into the airways and circumvent to a large extent the related adverse effects brought about by oral/systemic administration[113].

Amongst the most common medications for asthma are glucocorticoids and bronchodilators. Glucocorticoids bind intracellular glucocorticoid receptors and trigger enhanced expression of anti-inflammatory genes and suppression of pro-inflammatory genes, controlling airway inflammation[114]. Bronchodilators are most often β-adrenergic receptor (β-AR) agonists, or muscarinic acetylcholine receptor antagonists, that lead to ASM relaxation and an enlarged airway luminal diameter, improving airflow and mucus clearance[115]. β-agonists can also increase ciliary beating frequency, while antimuscarinic drugs may decrease airway mucin secretion, promoting MCC[22]. Nevertheless, long-term systemic adverse effects of glucocorticoid therapy have been described[116], as well as mechanisms of glucocorticoid resistance or insensitivity in asthmatic patients[117]. Additionally, β-AR desensitization and defective re-sensitization due to chronic overstimulation by β-agonists has been described to contribute to morbidity in asthma, with impaired bronchodilation and heightened bronchoconstriction[118,119].

For the treatment of cystic fibrosis, besides inhaled muco-active drugs that help thin the CF-typical thick, sticky airway mucus, and make it easier to cough out of the lungs, as well as inhaled antibiotic therapies to treat airway bacterial infection[120], a lot of effort has been put in the last two decades into developing so-called “CFTR modulators”, i.e., drugs targeted at restoring or enhancing the expression, function, and/or stability of CFTR in the airways[121]. These aim at normalizing fluid, mucus, and inflammatory mediator homeostasis, by correcting the underlying CFTR defect that triggers those secretory irregularities. However, a small percentage of CF patients carry CFTR mutations that have low to no chance of rescue through current or future pharmacological strategies, such as large genomic deletions[59]. Other subsets of patients may simply be unresponsive to approved therapies[62].

Regarding COPD, although therapies targeting the prevention or reversal of emphysema are still under development[122,123], oxygen may be administered when blood levels are low, and the chronic bronchial inflammation phenotype is often treated with the same drugs available for asthma, although glucocorticoids have been shown to be much less effective in treating non-eosinophilic inflammation[124]. In COPD cases where CFTR dysfunction has been acquired, CF therapies and CFTR modulator drugs may be of relevance, given smoking persistence[125,126].

Alternative therapies for chronic inflammatory airway diseases

So-called CFTR mutation-bypassing treatments arose in the context of CF, with the goal of achieving an effective therapeutical solution for all CF patients, independently of their basic CFTR defect. One proposal was to target alternative non-CFTR epithelial Cl^- and/or HCO_3^- channels and transporters in the airways, that may also contribute to fluid and mucus homeostasis[59]. Given that a shared feature of all chronic airway inflammatory diseases is an imbalance of the airway fluid:mucus ratio, primarily due to mucus overproduction, which results in impaired clearance and airway obstruction[22], these therapies can ultimately be extended beyond cases of CFTR dysfunction (e.g. asthma, COPD). Two other major Cl^-/HCO_3^--secretory proteins are present in the human airway epithelium, and thus represent promising drug targets. These are transmembrane protein 16A (TMEM16A) and solute carrier family 26 member 9 (SLC26A9).

TMEM16A modulation

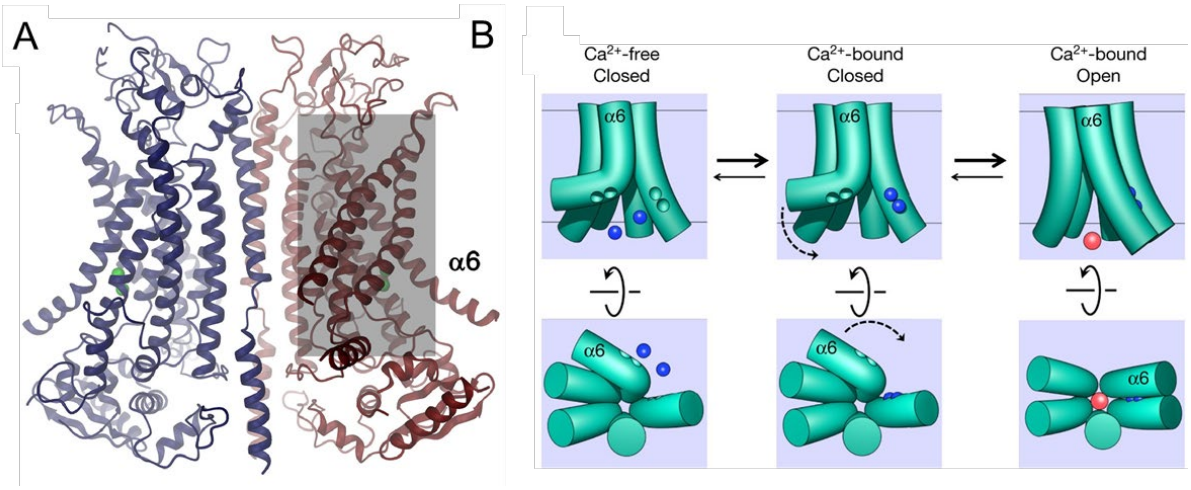

Figure 1.4 | *Structure of the mouse TMEM16A homodimer.*
(A) Ribbon representation of the mouse TMEM16A homodimer viewed from within the membrane. The region containing the ion conduction pore is highlighted as a grey box in one of the subunits. (B) Schematic, non-comprehensive depiction of the mechanisms leading to activation of TMEM16A. Green cylinders represent pore-lining helices; blue spheres, Ca^{2+}; red sphere, Cl^-. α-helix 6 (α6) is involved in the gating mechanism and undergoes conformational changes upon Ca^{2+}-binding. Adapted from[127,128].

TMEM16A belongs to the 10-member TMEM16 family of paralogous proteins that function as Ca^{2+}-activated Cl^- channels (CaCC; TMEM16A, B), high Ca^{2+}-activated phospholipid scramblases (TMEM16C-E, G-K), or phospholipid scramblases that also conduct Cl^- and other ions upon strong increases in intracellular Ca^{2+} (TMEM16F)[129]. These proteins used to be called anoctamins (ANO1-10). TMEM16A in particular (Figure 1.4), has been found to mediate CaCC currents in several cell types, such as airway and intestinal epithelial cells,

acinar cells of salivary and pancreatic glands, airway smooth muscle cells, interstitial cells of Cajal, and dorsal root ganglion neurons[130]. There, various physiological roles for TMEM16A have been demonstrated, namely, transepithelial ion transport, smooth muscle contraction, gastrointestinal mobility, transmission of nociceptive (pain-sensing) signals, control of neuronal excitability, among others[129,130].

In the airway epithelium, TMEM16A is expressed at the apical membrane of cells, particularly in mucus-secretory goblet cells, and to a lesser extent in fluid secretion-driving ciliated cells. This is further evident under airway inflammation, characterized by mucous cell hyper- or metaplasia, where expression levels of TMEM16A have been consistently shown to be strongly upregulated[131-135]. This aspect has generated a lot of controversy regarding the direction in which to modulate TMEM16A in the airways, for the amelioration of chronic inflammatory disease. While the primary idea put forward by the CF field was to find activator drugs for TMEM16A, promoting its Cl^- secretory activity and thereby compensating for the lack of CFTR-mediated fluid secretion, the contribution of TMEM16A for airway fluid secretion, and the overall contribution of fluid secretion to the pathological phenotype in CF has been recently put into question.

Lack of CF-like airway disease in CFTR-/- mice that showed no cAMP-mediated (CFTR-dependent) Cl^- secretion, was firstly explained by a potential compensation via an apical CFTR-independent, Ca^{2+}-regulated Cl^- conductance, detected in airway epithelial cultures from these mice[136]. However, recent studies involving ciliated cell-TMEM16A-/- mice[137], and human patients carrying a truncating, non-functional variant of TMEM16A[138], have shown that a strongly compromised airway CaCC does not translate into CF-like lung disease. Of relevance is the fact that these studies also detected a secondary impairment of airway cAMP-mediated CFTR currents, which was explained by a described TMEM16A-CFTR co-localization and molecular interaction in a functional compartment, tethered via PDZ scaffold-interacting motifs expressed on both proteins[137]. Seemingly, CFTR requires TMEM16A for insertion and full activation at the plasma membrane[137,139].

Moreover, a parallel role for TMEM16A in mediating compartmentalized intracellular Ca^{2+} signals has been described, via its demonstrated physical interaction with IP_3Rs at the ER membrane. This tethers the ER close to plasma membrane domains where TMEM16A and GPCRs are co-localized and enhances ER Ca^{2+} store release upon GPCR stimulation[140,141]. Notably, TMEM16A is preferentially activated by this specific, localized Ca^{2+} elevation, whereas extracellular Ca^{2+} influx through PM-localized voltage-gated Ca^{2+} channels (VGCC), for e.g., is mostly ineffective[140,141]. Mediation of Ca^{2+} signals by TMEM16A is thought to contribute to its recently emphasized role in airway goblet cells in supporting mucus secretion, while Cl^- efflux subsequent to TMEM16A activation by contractile mediator-induced Ca^{2+} release has been shown to support depolarization of ASM cells, stimulate VGCC activation and Ca^{2+} influx, and enhance bronchoconstriction[132,133,142-145]. This is of particular relevance under inflammation,

where TMEM16A has also been shown to be upregulated in ASM cells[143]. Cl^- efflux-mediated depolarization of mucous and ASM cells can also induce activation of voltage-dependent ryanodine receptors (RyRs), further contributing to ER Ca^{2+}-release[146]. Therefore, an antagonistic idea of inhibiting TMEM16A in airway inflammatory diseases was put forward, aiming primarily to decrease mucus hypersecretion, and lessen airway hyperresponsiveness.

To date, several molecules that are TMEM16A inhibitors have been identified – mainly through high-throughput screening strategies –, including niclosamide[147], benzbromarone[132], and many others[135]. The downregulating effects of these on mucus and ASM contractility have been demonstrated extensively[132,147-150]. Noteworthy to mention is that niclosamide is a well-tolerated FDA- and EMA-approved drug for the treatment of intestinal helminthic infestations, and repurposing of this compound for the treatment of airway inflammatory disease has been recently proposed[147,150].

SLC26A9 modulation

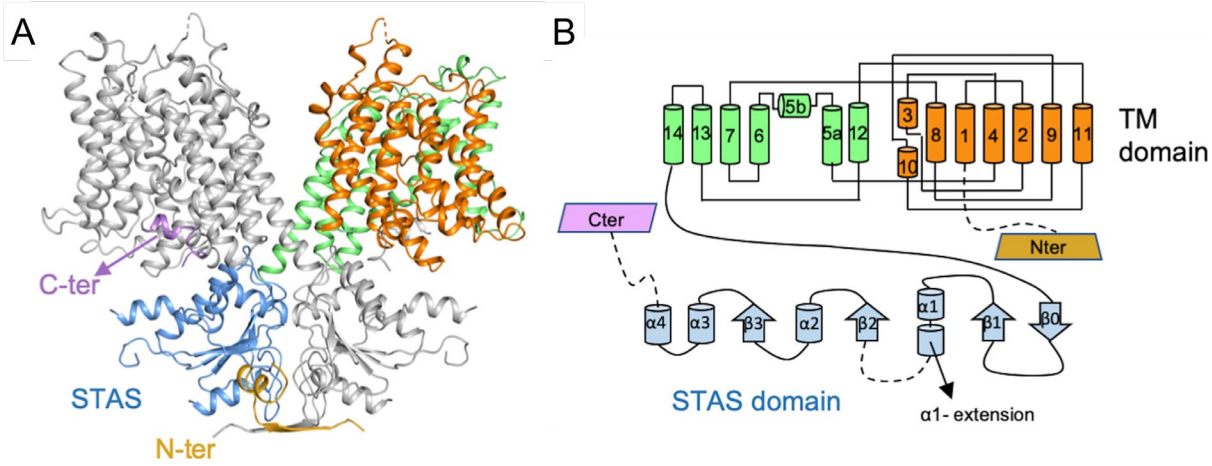

Figure 1.5 | *Structure of the human SLC26A9 homodimer.*
(A) Ribbon representation of the human SLC26A9 homodimer viewed from within the membrane and colored according to the different domains represented in (B). TM, transmembrane; N-ter, N-terminus; C-term, C-terminus. Adapted from[151].

SLC26A9 is a member of the SLC26 family of 10 functional paralogous anion exchangers and channels (SLC26A1-9,11), that can transport a broad range of substrates including Cl^-, HCO_3^-, I^-, and thiocyanate (SCN^-), with anion selectivities, modes of transport and stoichiometries characteristic of each member[152]. Most SLC26 proteins have been localized to the luminal membrane of epithelial cells, where they are thought to play a physiological role in epithelial Cl^- and HCO_3^- transport, relevant for regulating the content and pH of epithelial fluids, which is of vital importance for the integrity and function of several organs (e.g., the lungs and the stomach)[153,154]. While this transport was shown to be tightly dependent on CFTR, a demonstrated physical interaction between the regulatory (R) domain of CFTR and the sulphate

transporter and anti-sigma factor antagonist (STAS) domain common to all SLC26 proteins, in a functional complex tethered by PDZ motif-binding scaffold proteins, as well as a described CFTR/SLC26 reciprocal regulatory interaction, proposed SLC26 as a family of CFTR "accessor" proteins that contribute to its function in several epithelia[155-157].

Amongst all the SLC26 family members, SLC26A9 (Figure 1.5) is particularly expressed in the lungs[158], yet its role there is not very well-characterized. SLC26A9 has been shown to operate as a constitutively active, uncoupled Cl^- transporter, but also as a Cl^-/HCO_3^- exchanger, although the literature is controversial on its HCO_3^- permeability[159-163]. Evidence for mixed uncoupled and coupled exchange properties has been demonstrated for other members of the SLC26 family, which might rely on the individual cellular context, namely, the transporter isoform, the particular ion being transported, the luminal membrane potential, and the different anionic gradients at a given state[154,164]. Notably, SLC26A9 has been shown to operate as a fast transporter, with channel-like transport properties[165].

SLC26A9 has long been thought to mediate the basal transepithelial Cl^- conductance in the airways, besides contributing together with CFTR to cAMP-activated Cl^- currents[159,166], which, together with its potential ability to conduct HCO_3^-, proposed SLC26A9 as a target to compensate for the CFTR dysfunction in CF epithelia. Indeed, SLC26A9 has recently been reported as a gene modifier of lung function in CF, and also of the response to CFTR-modulator therapies, in patients carrying a specific CFTR mutation that does not affect its traffic to the membrane, but does so its gating properties[167]. In parallel, patients carrying the most common mutation in CF, the F508del-CFTR trafficking mutant, were not affected by SLC26A9 genetic variants[167]. This is likely due to the demonstrated aberrant traffic and intracellular retention and degradation of SLC26A9 in the presence of F508del-CFTR, which was explained by SLC26A9/CFTR co-localization and reciprocal regulation in a functional complex[166]. Inevitably, this implies co-compromised functional expression of CFTR and SLC26A9 in most CF cases. Nevertheless, many CF patients carrying a plethora of other mutations could still benefit from SLC26A9-modulating drugs. Furthermore, SLC26A9 has also been associated with other airway inflammatory diseases. Namely, a genetic study demonstrated an association between a SLC26A9 genetic variant that results in decreased protein expression *in vitro*, and an increased risk for asthma[168]. The same study also analysed SLC26A9-/- mice and reported that while SLC26A9 seems to not contribute to airway Cl^- secretion and overall lung health/morphology under physiological conditions, it plays a role in Cl^- conductance during T_H2-mediated, allergic asthma-like airway inflammation, and, while not affecting mucus overproduction, it supports mucus clearance, with asthmatic SLC26A9-/- mice showing evident airway mucus obstruction[168]. Hence, SLC26A9 constitutes a promising therapeutic target for muco-obstructive airway diseases.

AIM OF THE STUDY

This research focused on exploring the role of TMEM16A and SLC26A9 as targets to be pharmacologically modulated for the amelioration of airway inflammatory muco-obstructive diseases. Given recent controversial findings and the ongoing debate in the field regarding the direction in which to modulate TMEM16A – activation or inhibition –, we first aimed at addressing the dynamic expression pattern of TMEM16A in healthy vs. inflamed airways, as well as the effect of TMEM16A activators/potentiators and inhibitors on mucus production and secretion, and on bronchoconstriction. This is highlighted in Chapter 1. Chapter 2 unravels a novel role for TMEM16A in mediating mucus production and secretion induced by CLCA1 in the airways, which is of particular relevance under T_H2-mediated inflammation, when levels of CLCA1 are extraordinarily upregulated. Here, we also aimed at assessing whether CLCA1-mediated stabilization of TMEM16A could contribute to enhanced Ca^{2+}-activated Cl^-, and hence fluid, secretion in the airways. In Chapter 3, we aimed at further exploring the repurpose of niclosamide, an FDA/EMA-approved TMEM16A-inhibitor, for the treatment of airway inflammation and muco-obstruction. Here, we tested new approaches for direct niclosamide application to the airways, with the goal of circumventing systemic side effects and enhancing tissue-targeting, local drug deposition levels and long-term bioavailability. In Chapter 4, we addressed the lack of consensus on the expression pattern of SLC26A9 in the airways under normal or inflammatory conditions. In Chapter 5, we aimed at decisively discriminating between CFTR- and SLC26A9-mediated airway Cl^- secretion under basal and stimulated conditions, as well as assessing other potential functions for SLC26A9 in the airway epithelium. For that, we made use of a herein described novel highly potent and selective SLC26A9-inhibitor, S9-A13.

CHAPTER 2 | MUCUS RELEASE AND AIRWAY CONSTRICTION BY TMEM16A MAY WORSEN PATHOLOGY IN INFLAMMATORY LUNG DISEASE

Abstract

Activation of the Ca^{2+} activated Cl^- channel TMEM16A is proposed as a treatment in inflammatory airway disease. It is assumed that activation of TMEM16A will induce electrolyte secretion, and thus reduce airway mucus plugging and improve mucociliary clearance. A benefit of activation of TMEM16A was shown *in vitro* and in studies in sheep, but others reported an increase in mucus production and airway contraction by activation of TMEM16A. We analysed expression of TMEM16A in healthy and inflamed human and mouse airways and examined the consequences of activation or inhibition of TMEM16A in asthmatic mice. TMEM16A was found to be upregulated in the lungs of patients with asthma or cystic fibrosis, as well as in the airways of asthmatic mice. Activation or potentiation of TMEM16A by the compounds Eact or brevenal, respectively, induced acute mucus release from airway goblet cells, and induced bronchoconstriction in mice *in vivo*. In contrast, niclosamide, an inhibitor of TMEM16A, blocked mucus production and mucus secretion *in vivo* and *in vitro*. Treatment of airway epithelial cells with niclosamide strongly inhibited expression of the essential transcription factor of Th2-dependent inflammation and goblet cell differentiation, SAM pointed domain-containing ETS-like factor (SPDEF). Activation of TMEM16A in people with inflammatory airway diseases is likely to induce mucus secretion along with airway constriction. In contrast, inhibitors of TMEM16A may suppress pulmonary Th2 inflammation, goblet cell metaplasia, mucus production, and bronchoconstriction, partially by inhibiting expression of SPDEF.

Keywords: TMEM16A; ETX001; Eact; brevenal; asthma; cystic fibrosis; airways
Published as: Centeio R., Ousingsawat J., Cabrita I., Schreiber R., Talbi K., Benedetto R., Doušová T., Verbeken, E. K., De Boeck, K., Cohen I., Kunzelmann K. Mucus Release and Airway Constriction by TMEM16A May Worsen Pathology in Inflammatory Lung Disease. *International Journal of Molecular Sciences*. 2021 July; 22(15): 7852.
Own experimental contribution: Ovalbumin-sensitization of animals; intratracheal instillation of drugs; mouse lungs isolation, paraffin-embedding and slicing; mucus stainings by Alcian blue; airway cross-sectional area analysis; Western blot.
Own written contribution: Original draft preparation, review and editing.
Other contributions: Designed experiments and analysed data.

Introduction

Recent work has proposed activation or potentiation of Ca^{2+} activated TMEM16A (anoctamin 1) chloride ion channels as a mutation-agnostic treatment for people with cystic fibrosis (CF) and other inflammatory airway diseases[169]. This strategy is based on early data showing nucleotide stimulation of nasal Cl^- transport[170], and numerous subsequent *in vitro* and *ex vivo* studies[171-173]. It is assumed that activation of TMEM16A will induce airway electrolyte secretion and lead to reduced airway mucus plugging with an improvement in mucociliary clearance. However, purinergic stimulation of Ca^{2+}-dependent Cl^- secretion by denufosol or direct Ca^{2+}-dependent stimulation by lancovutide (Moli1901) failed to show a benefit for lung function in CF patients[174,175]. Recently, the novel TMEM16A potentiator ETX001 was shown to enhance the activity of TMEM16A and increase fluid secretion *in vitro*, and to improve mucociliary clearance in noninflamed ovine airways *in vivo*[169]. The related compound ETD002 is currently being evaluated in a phase 1 clinical trial (www.clinicaltrials.gov).

Available data suggest that TMEM16A is hardly expressed in the airways and airway smooth muscle (ASM) of noninflamed lungs, but is upregulated in CF and asthma in humans, piglets, mice, and guinea pigs[134,137,147,149,176]. Nucleotides such as ATP or UTP are released at higher levels during goblet cell metaplasia, causing enhanced airway mucin secretion[32,177#]. Aerosolized UTP was shown to increase mucociliary clearance in CF patients, when applied alone or when co-administrated together with amiloride, the inhibitor of epithelial Na^+ channels[178,179]. However, the lack of beneficial effects of the TMEM16A-activators denufosol and lancovutide on lung function in CF may be due to enhanced mucus secretion.

Danahay et al. reported no effects of the TMEM16A potentiator ETX001 on airway mucus, bronchoconstriction, or pulmonary arterial contraction[180]. This is surprising, as many studies suggest a role of TMEM16A in the upregulation of mucus production as well as mucus release[132,133,145,149,181]. Moreover, upregulation of TMEM16A expression in ASM was shown to strongly correlate with airway hyperresponsiveness and airway contraction[143,147,148,182]. Notably, asthmatic conditions are frequently found in patients with CF[183]. Finally, TMEM16A is reported to contribute to pulmonary artery contraction, leading to pulmonary arterial hypertension[184-187], a condition that is prevalent in adults with asthma or cystic fibrosis[188,189]. We therefore analysed the expression and function of TMEM16A in human lungs, in mouse lungs *in vivo*, and airway epithelial cells *in vitro*. We found an enhanced expression of TMEM16A in submucosal glands, ASM, and pulmonary blood vessels in CF and asthmatic lungs. The data support a role of TMEM16A in mucus production. Activation or potentiation of TMEM16A induced acute mucus secretion with airway contraction in OVA-challenged mice, while the TMEM16A inhibitor niclosamide antagonized mucus production and secretion. Thus, activation of TMEM16A in inflammatory airway diseases could worsen clinical symptoms.

Materials and Methods

Animals and treatments: Allergen challenge of mice has been described in Schreiber et al.[190]. In brief, mice were sensitized to ovalbumin (OVA; Sigma-Aldrich, St. Louis, MO, USA) by intraperitoneal (I.P.) injection of 100 µg OVA in 100 µL aluminium hydroxide gel adjuvant (InvivoGen, San Diego, CA, USA) on days 0 and 14. From days 21 to 23, mice were anesthetized and challenged to OVA by intratracheal (I.T.) instillation of 50 µg OVA in 100 µL saline. Control mice were sham sensitized with the adjuvant aluminium hydroxide gel and challenged to saline by I.T. instillation. TMEM16A activator Eact (4.8 µg/100 µL saline) was administered by I.T. instillation 4 h before animal sacrifice on day 26. TMEM16A inhibitor niclosamide (30 µM in 100 µL saline) was administered by I.T. instillation from days 21 to 25, and animals were sacrificed on day 26. The TMEM16A potentiator brevenal (3.2 µg/100 µL saline) was administered to non-sensitized/challenged control mice by I.T. instillation 10 min before animal sacrifice. Control I.T. instillation was performed with saline alone. All animal experiments complied with the general guidelines for animal research, in accordance with the United Kingdom Animals Act, 1986, and associated guidelines, and EU Directive 2010/63/EU for animal experiments. All animal experiments were approved by the local Ethics Committee of the Government of Unterfranken/Wurzburg/Germany (AZ: 55.2-2532-2-677) and were conducted according to the guidelines of the American Physiologic Society and German Law for the Welfare of Animals.

Cell culture and treatments: All cells were grown at 37 °C in a humidified atmosphere with 5% (v/v) CO2. Culture conditions of Calu-3 and CFBE cells have been de-scribed earlier [191]. In brief, airway epithelial cells were grown in DMEM/Ham's F-12 with L-Glutamine medium supplemented with 10% (v/v) foetal bovine serum (FBS), 1% (v/v) L-glutamine 200 mM and 1% (v/v) HEPES 1M (all from Capricorn Scientific, Ebsdorfergrund, Germany). CFBE parental cells were grown in MEM with Earle's Salts with L-Glutamine medium (Capricorn Scientific, Ebsdorfergrund, Germany) supplemented with 10% FBS. Cells were treated with IL-13 (20 ng/mL; Enzo Life Sciences, Lörrach, Germany) for 72 h in Opti-MEM Reduced Serum Medium (Gibco/Thermo Fisher Scientific, Waltham, MA, USA); treatment was refreshed every day. Niclosamide (ethanolamine salt, 1 µM) was applied simultaneously with IL-13 for MUC5AC staining/ western blot/ PCR experiments or 1 h before measurements for patch clamp experiments. Cells were pre-incubated with brevenal (500 nM) for 15 min for patch clamp experiments or 5 h for Ca2+ measurements.

Knockdown of TMEM16A in CFBE parental cells was performed by transfecting siTMEM16A (5-CCUGUACGAAGAGUGGGCACGCUAU-3, Invitrogen, Carlsbad, CA, USA) using standard protocols for Lipofectamine 3000 (Invitrogen, Carlsbad, CA, USA). Scrambled siRNA

(Silencer® Select Negative Control siRNA #1, Ambion, Austin, TX, USA) was transfected as negative control. All experiments were performed 72 h after transfection.

RT-PCR: For semi-quantitative RT-PCR, total RNA from Calu-3 airway epithelial cells was isolated using NucleoSpin RNA II columns (Macherey-Nagel, Düren, Germany). Reverse transcription of RNA and polymerase chain reaction (PCR) were described in an earlier report [191]. Total RNA (0.5 µg / 25 µL reaction) was reverse-transcribed using random primer (Promega, Mannheim, Germany) and M-MLV Reverse Transcriptase RNase H Minus (Promega, Mannheim, Germany). Each RT-PCR reaction contained sense and antisense primers (0.5 µM) (Table 2.1), 0.5 µL cDNA, and GoTaq Polymerase (Promega, Mannheim, Germany). After 2 min at 95 °C, cDNA was amplified (20–30 cycles) for 30 s at 95 °C, 30 s at 57 °C, and 1 min at 72 °C. PCR products were visualized by loading on peqGREEN (Peqlab, Düsseldorf, Germany) containing agarose gels and analysed using ImageJ.

Table 2.1 | *RT-PCR primers.*

Target	Primers	Size (bp)
TMEM16A	forward: 5′-CGACTACGTGTACATTTTCCG reverse: 5′-GATTCCGATGTCTTTGGCTC	445
MUC5AC	forward: 5′-GCTCAGCTGTTCTCTGGACG reverse: 5′-GTCACATTCCTCAGCGAGGTC	279
SPDEF	forward: 5′-GTGCTCAAGGACATCGAGAC reverse: 5′-CCTAATGAAGCGGCCATAGC	423
GAPDH	forward: 5′-GTATTGGGCGCCTGGTCAC reverse: 5′-CTCCTGGAAGATGGTGATGG	200

Western blotting: Protein was isolated from cells using a lysis buffer containing 25 mM Tris-HCl pH 7.4, 150 mM NaCl, 1 mM EDTA, 5% glycerol, 0.43% Nonidet P-40, 100 mM dithiothreitol (both from PanReac AppliChem, Barcelona, Spain), and 1× pro-tease inhibitor mixture (Roche, Basel, Switzerland). Protein separation and blotting were performed as described in an earlier report [191]. Proteins were separated by 8.5% SDS-PAGE and transferred to a PVDF membrane (GE Healthcare, Munich, Germany). Membranes were incubated with primary rabbit monoclonal [SP31] anti-TMEM16A antibody (#ab64085; Abcam, Cambridge, UK; 1:500 in 1% (w/v) NFM/TBS-T) overnight at 4 °C. A rabbit polyclonal anti-β-actin antibody (#A2066; Sigma-Aldrich, St. Louis, MO, USA; 1:10 000 in 5% (w/v) NFM/TBS-T) was used for loading control. Afterwards, membranes were incubated with horseradish peroxidase (HRP)-conjugated goat polyclonal anti-rabbit secondary antibody (#31460; Invitrogen, Carlsbad, CA, USA) at room temperature for 2 h, and immunoreactive signals were visualized using a SuperSignal HRP Chemiluminescence Substrate detection kit (#34577; Thermo Fisher Scientific, Waltham, MA, USA).

Immunohistochemistry, immunocytochemistry, airway cross sections, and stitching microscopy: Staining and analysis of human lung tissue slides were approved by the ethics committee of the University Hospital Motol, Charles University in Prague, Prague, Czech Republic (approval number EK-853//18, date of approval 18 July 2018). Paraffin embedded human lung sections (5 µm) were deparaffinized with xylene and rehydrated through a series of ethanol. Antigen retrieval was performed in pre-heated Tris-EDTA buffer (pH 9.0) for 15 min, using a microwave. After cooling down to room temperature and appropriate washing, sections were blocked with 5% IgG-free bovine serum albumin (BSA) and 0.05% Triton X-100 in PBS with 0.05% Tween-20 (PBS-T) for 1 h at room temperature. Primary antibodies were diluted in 1% IgG-free BSA in PBS-T and incubated overnight at 4 °C. Rabbit polyclonal anti-human TMEM16A antibody (1:100; raised against YLKLKQQSPPDHEECVKRKQR, aa 688-708; Davids Biotechnology, Regensburg, Germany) was used for immunofluorescence staining. After washing steps, sections were incubated in Alexa Fluor 488-labeled donkey anti-rabbit IgG (1:400; Invivogen Europe, Toulouse, France) and counterstained with Hoe33342 (1 mM, 1:200; AppliChem, Darmstadt, Germany) for 1 h at room temperature. After washing, coverslips were then mounted in fluorescence mounting medium (Dako, Hamburg, Germany). For 3,3-diaminobenzidine (DAB) staining, quenching of endogenous peroxidase was performed before blocking step with 1% hydrogen peroxide in ethanol for 15 min. The primary antibody, anti-DOG1/TMEM16A (SP31, Novus Biologicals, USA) was incubated overnight at 4 °C. After washing, biotinylated donkey anti-rabbit IgG (Santa Cruz, Heidelberg, Germany) at 1:500 dilution was applied for 1 h at room temperature. Sections were washed in PBS-T and were then incubated with avidin-peroxidase complex (Vectastain kit, Vector laboratories) for 1 h at room temperature. The peroxidase was then developed by DAB (Sigma, Taufkirchen, Germany). Slides were counterstained with haematoxylin. Immunofluorescence and immuno-histochemistry were detected with an Axio Observer microscope equipped with Axiocams 503 mono and 305 colour, ApoTome.2, and ZEN 3.0 (blue edition) software (Zeiss, Oberkochen, Germany). Cross sectional areas were determined by automatic marking and analysis of airway lumens using Zen software and Axio Observer microscope equipped with AxioCam and ApoTome2. Stitching microscopy was performed using motorized Axio Observer and Zen software.

For MUC5AC stainings, Calu-3 airway cells seeded onto glass coverslips were fixed with 4% PFA/PBS for 10 min at room temperature, washed in PBS with Ca^{2+} and Mg^{2+} (PBS^{++}), incubated in 0.5% Triton X-100/PBS^{++} for 10 min at room temperature, washed, blocked with 1% BSA/PBS^{++} for 40 min at room temperature, incubated with mouse monoclonal anti-MUC5AC antibody (1:300 in 1%BSA/PBS^{++}; ab3649; Abcam, Cambridge, UK) for 1 h at 37 °C, washed, incubated with Alexa Fluor 488-labeled donkey anti-mouse IgG (1:300 in 1%

BSA/PBS^{++}; Invitrogen, Carlsbad, CA, USA) and counterstained with Hoe33342 (1:200) for 1 h at room temperature. Cells were then washed and mounted in fluorescence mounting medium. MUC5AC staining was quantified using ImageJ. Additional details are provided in an online data supplement.

Mucus staining and analysis of mucus release and airway contraction: Mouse airways were fixed by transcardial perfusion and lung perfusion by tracheal instillation via tracheostomy of fixative solution containing 4% PFA in PBS. Tissues were left in fixative solution overnight and embedded in paraffin the next day. 5 µm cuts were deparaffinized, stained with standard Alcian blue solution, and counterstained with Nuclear Fast Red solution (Sigma-Aldrich, St. Louis, MO, USA). After the dehydration and clearing steps, whole mouse lungs or sections were mounted in DePeX mounting medium (SERVA Electrophoresis, Heidelberg, Germany). Stainings were assessed by light microscopy. Stitching microscopy was used to analyse whole mouse lungs. Mucus-stained and cross-sectional areas were determined using ImageJ.

Patch clamp: Calu-3 and CFBE cells were patch clamped after growing on coated glass coverslips for 2–3 days. Whole-cell patch clamp techniques and data analysis have been described earlier [192]. In brief, patch pipettes were filled with a cytosolic-like solution containing (in mM): KCl 30, K-Gluconate 95, NaH_2PO_4 1.2, Na_2HPO_4 4.8, EGTA 1, Ca-Gluconate 0.758, $MgCl_2$ 1.03, D-Glucose 5, ATP 3; pH 7.2. The intracellular (pipette) Ca^{2+} activity was 0.1 µM. Fast whole-cell current recordings were performed as described recently[193]. The bath was perfused continuously with standard bicarbonate-free Ringer's solution (in mM: NaCl 145, KH_2PO_4 0.4, K_2HPO_4 • 3 H_20 1.6, Glucose 5, $MgCl_2$ • 6 H_20 1, Ca-Gluconate • 1 H_20 1.3) at a rate of 8 mL/min. Patch pipettes had an input resistance of 2–4 MΩ and whole-cell currents were corrected for serial resistance. Currents were recorded using a patch clamp amplifier (EPC 7; List Medical Electronics, Darmstadt, Germany), the LIH1600 interface, and PULSE software (HEKA, Lambrecht, Germany), as well as Chart software (AD Instruments, Spechbach, Germany). Cells were stimulated with 1, 10 or 100 µM ATP in standard bicarbonate-free Ringer's solution. Cells were current clamped for most of the time. In regular intervals, membrane voltage (Vc) was clamped in steps of 20 mV from −100 to +100 mV. The inhibitor of Ca^{2+}-activated KCNN4 K^+ channels, TRAM-34 (100 nM), was present in all patch clamp experiments to avoid potential activation of Ca^{2+}-activated K^+ channels.

Measurement of $[Ca^{2+}]_i$: Cells were seeded on coated glass coverslips and loaded with 2 µM Fura-2, AM Ester (Biotium, Hayward, CA, USA) and 0.02% Pluronic F-127 (Invitrogen, Carlsbad, CA, USA) in standard bicarbonate-free Ringer's solution for 1 h at room temperature. Measurement of intracellular Ca^{2+} concentrations has been described earlier[192]. Cells were then mounted in a thermostatically controlled imaging chamber adapted to an inverted

microscope (Axiovert S100, Zeiss, Oberkochen, Germany), maintained at 37 °C and perfused at a rate of 5 mL/min. Fura-2 was excited at 340/380 nm using a high-speed polychromatic illumination system for microscopic fluorescence measurements (Visitron Systems, Puchheim, Ger-many), and emission was recorded between 470 and 550 nm using a CoolSnap HQ CCD camera (Roper Scientific, Planegg, Germany/Visitron Systems, Puchheim, Germany). Cells were stimulated with 1, 10 and 100 µM ATP in standard bicarbonate-free Ringer's solution. Intracellular calcium ($[Ca^{2+}]_i$) was calculated from the 340/380 nm fluorescence ratio after background subtraction using the formula $[Ca^{2+}]_i = Kd \times (R-Rmin)/(Rmax-R) \times (Sf2/Sb2)$, where R is the observed fluorescence ratio. The values Rmax and Rmin (maximum and minimum ratios) and the constant Sf2/Sb2 (ratio between the fluorescence of free and Ca^{2+}-bound Fura-2 at 380 nm) were determined using 2 µM ionomycin (Calbiochem, San Diego, CA, USA), 5 µM nigericin (Sigma-Aldrich, St. Louis, MO, USA), 10 µM monensin (Sigma-Aldrich, St. Louis, MO, USA) and 5 mM EGTA (Carl Roth, Karlsruhe, Germany) to equilibrate intracellular and extracellular Ca^{2+} in intact Fura-2-loaded cells. The dissociation constant (Kd) for the Fura-2•Ca^{2+} complex was taken as 224 nM[194]. Control of experiment, imaging acquisition, and data analysis were done with the software package MetaFluor (Universal Imaging, Bedford Hills, NY, USA).

Mucociliary clearance analysis: Freshly excised tracheas from non-sensitized mice were cut open and mounted onto glass coverslips in a humidified chamber. 1 µm fluorescent beads (FluoSpheres™ #F8823; Invitrogen, Carlsbad, CA, USA) were added to the apical side of the isolated tracheas in standard bicarbonate-free Ringer's solution. Niclosamide (1 µM) was applied acutely to the tracheal surface in Ringer's solution. Video imaging of the tracheal surface (Axio Observer, Zeiss, Oberkochen, Germany) allowed for the tracking of fluorescent particle trajectories and speed (analysis by Image J), and assessment of ciliary beating properties such as stroke amplitude and frequency (analysis by ZEN 3.0 (blue edition) software, Zeiss, Oberkochen, Germany). As experimental control, ciliary movement and thus particle clearance were inhibited by cooling tracheas down to 4 °C.

Materials and statistical analysis: All compounds used were of the highest available grade of purity and were bought from Sigma-Aldrich (St. Louis, MO, USA), unless indicated otherwise. Brevenal was kindly provided by Dr. Daniel Baden, PhD (UNC, Wilmington, North Carolina, USA). Data are shown as individual trac-es/representative images and/or as summaries with mean values ± SEM, with the respective number of experiments given in each figure's legend. For statistical analysis, paired or unpaired Student's t-test or ANOVA were used where appropriate. A p-value of <0.05 was accepted as a statistically significant difference.

Results

Expression of TMEM16A in healthy, asthmatic, and CF lungs

In noninflamed human lungs, TMEM16A was either only sparsely or not at all expressed in both surface epithelium and submucosal glands. In contrast, expression of TMEM16A was detected in submucosal glands of asthma patients and people with CF (Figure 2.1). CF submucosal glands were often found to be hypertrophic. Expression of TMEM16A is also enhanced in ASM of asthma patients and in people with CF and appears to be enhanced in the endothelium of pulmonary blood vessels (Supplementary Figures 2.1 and 2.2).

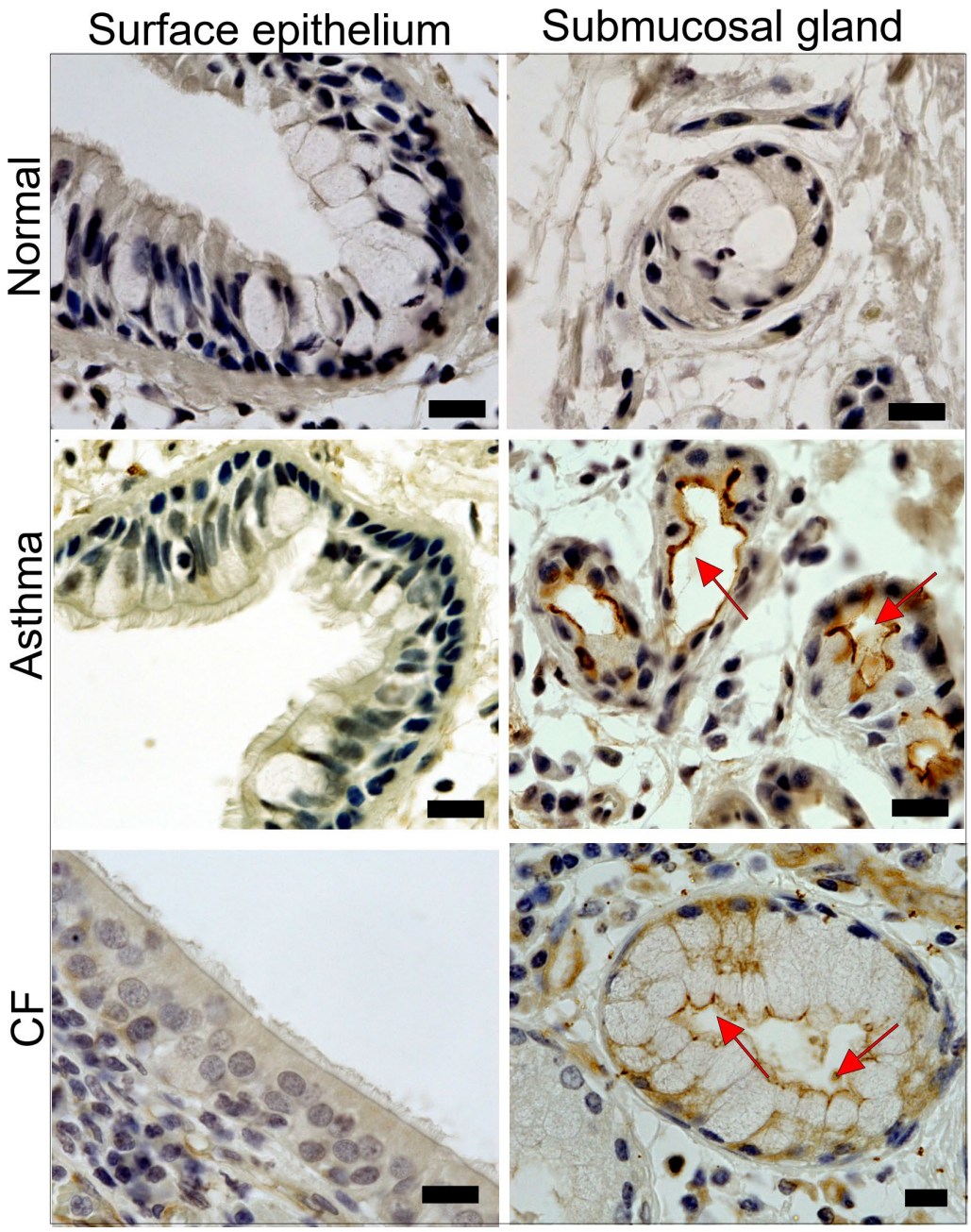

Figure 2.1 | *Expression of TMEM16A in human healthy, asthmatic, and CF lungs.*
Lung slices of normal airways indicate little expression of TMEM16A in both surface airway epithelium and airway submucosal glands. Pronounced expression of TMEM16A in apical membranes of surface epithelial cells and airway submucosal glands of patients with asthma and CF (brown precipitation, DAP staining). Submucosal glands were often found to be hypertrophic. Representative stainings of four patients each. Bars indicate 20 µm.

Acute activation of TMEM16A by Eact induces mucus release and airway constriction

Eact is an activator of TMEM16A that may also activate other ion channels such as TRPV4[195-197]. We found earlier that Eact potently activates TMEM16A overexpressed in HEK293 cells, with only a slight increase in intracellular Ca^{2+} levels[196]. Eact was applied to ovalbumin (OVA)-sensitized asthmatic mice, which present pronounced goblet cell metaplasia (Figure 2.2A, left panel). Acute application of Eact by intratracheal instillation induced the release of mucus from goblet cells, which caused accumulation of mucus in airways (Figure 2.2A, right panel, Figure 2.2B). Moreover, by analyzing airway cross sections, we detected a pronounced narrowing of the airways due to Eact-induced airway contraction (Figures 2.2A, C).

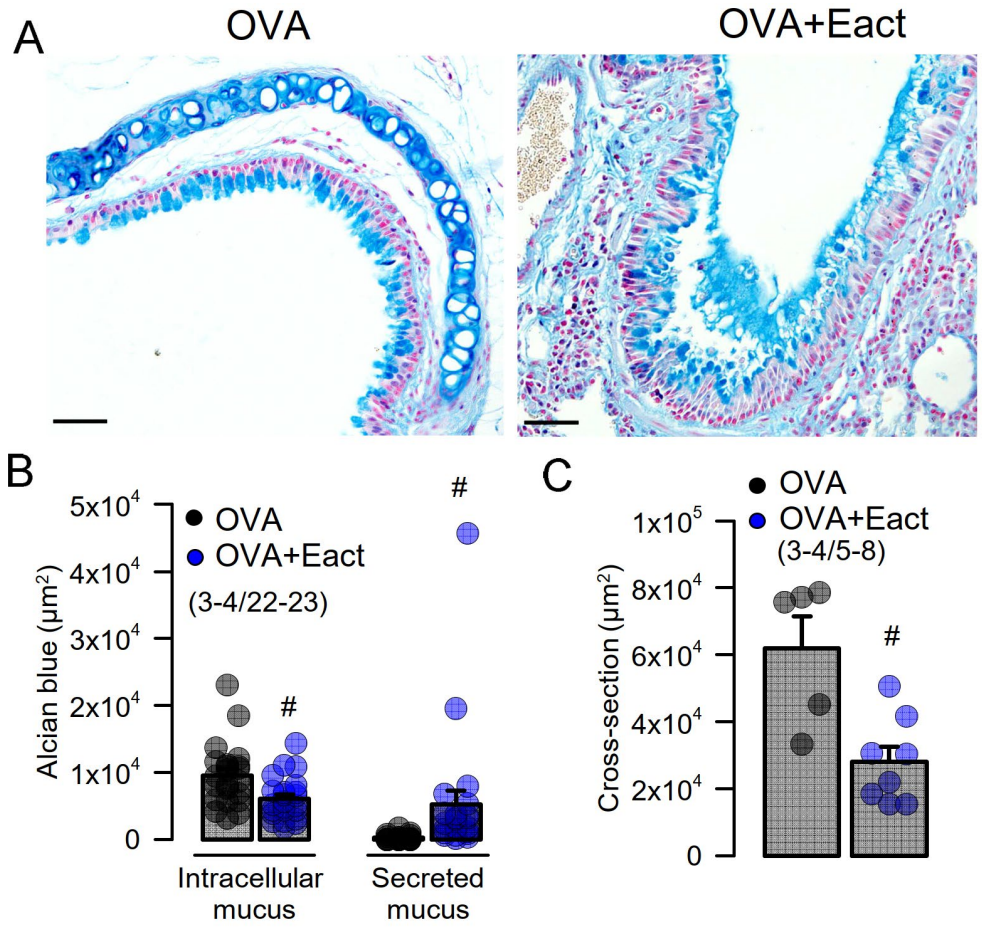

Figure 2.2 | *Activation of TMEM16A by Eact induces mucus release and airway contraction.*
(A) Mucus staining by Alcian blue in OVA-treated asthmatic mice. Acute application of the activator of TMEM16A, Eact (4.8 µg/mL intratracheal), induced acute release of mucus from goblet cells and increased intraluminal mucus. Bars indicate 50 µm. (B) Summary of intracellular and intraluminal mucus. (C) Summary of cross-sectional area indicating airway contraction by Eact. Mean ± SEM (number of animals/number of measurements). #significant difference when compared to control ($p < 0.05$, unpaired t-test).

Mucus production and mucus secretion is strongly inhibited by niclosamide

We performed in-depth analysis of mouse lungs using stitching microscopy. The data show a low number of mucus producing cells in control airways (Figure 2.3, upper panel, Figure 2.4). In contrast, OVA-sensitized mice demonstrated massive goblet cell metaplasia and accumulation of intraluminal mucus (Figure 2.3, middle panel, Figure 2.4). Application of the TMEM16A inhibitor niclosamide for 4 days strongly reduced goblet cell metaplasia, mucus production, and accumulation of mucus in the airways of OVA-sensitized mice (Figure 2.3, lower panel, Figure 2.4). The present results suggest beneficial effects of niclosamide, i.e., inhibition of TMEM16A in inflammatory airway diseases, comparable to the results in earlier reports[147,150]. Previous reports also demonstrated relaxation of airways by niclosamide, along with reduced cytokine release[147,150]. It is therefore likely that niclosamide will be beneficial for the treatment of inflammatory airway diseases, including Covid-19[198]. Additional work will be required to analyze in more detail the effects of niclosamide on the release of other Th1, Th2, and Th17 cytokines. Although niclosamide was shown to dampen intracellular Ca^{2+} signals, we did not find evidence for reduced ciliary stroke amplitude or attenuated mucociliary clearance by niclosamide[150,196] (Supplementary Figure 2.3).

Expression of MUC5AC and activation of TMEM16A in Calu-3 cells are inhibited by niclosamide

We further analyzed expression of MUC5AC induced by the Th2-cytokine IL-13 in Calu-3 human submucosal epithelial cells (Figure 2.5). Similar to the findings in mice *in vivo*, niclosamide potently inhibited MUC5AC expression[191] (Figures 2.5A, B). Attenuation of mucus production was paralleled by inhibition of TMEM16A whole-cell currents (Figures 2.5C, D). It should be noted that Calu-3 cells express significant amounts of TMEM16A, particularly after exposure to IL-13[191]. Treatment with niclosamide not only inhibited TMEM16A currents, but also attenuated TMEM16A expression (Figure 2.6A). These results obtained in airway cells correspond well to the inhibition of TMEM16A expression by niclosamide and other TMEM16A

blockers, such as Ani9 or benzbromarone, in mouse kidneys[199]. Thus, TMEM16A inhibitors not only block Cl^- currents, but also inhibit expression of TMEM16A in long-term treatment[199].

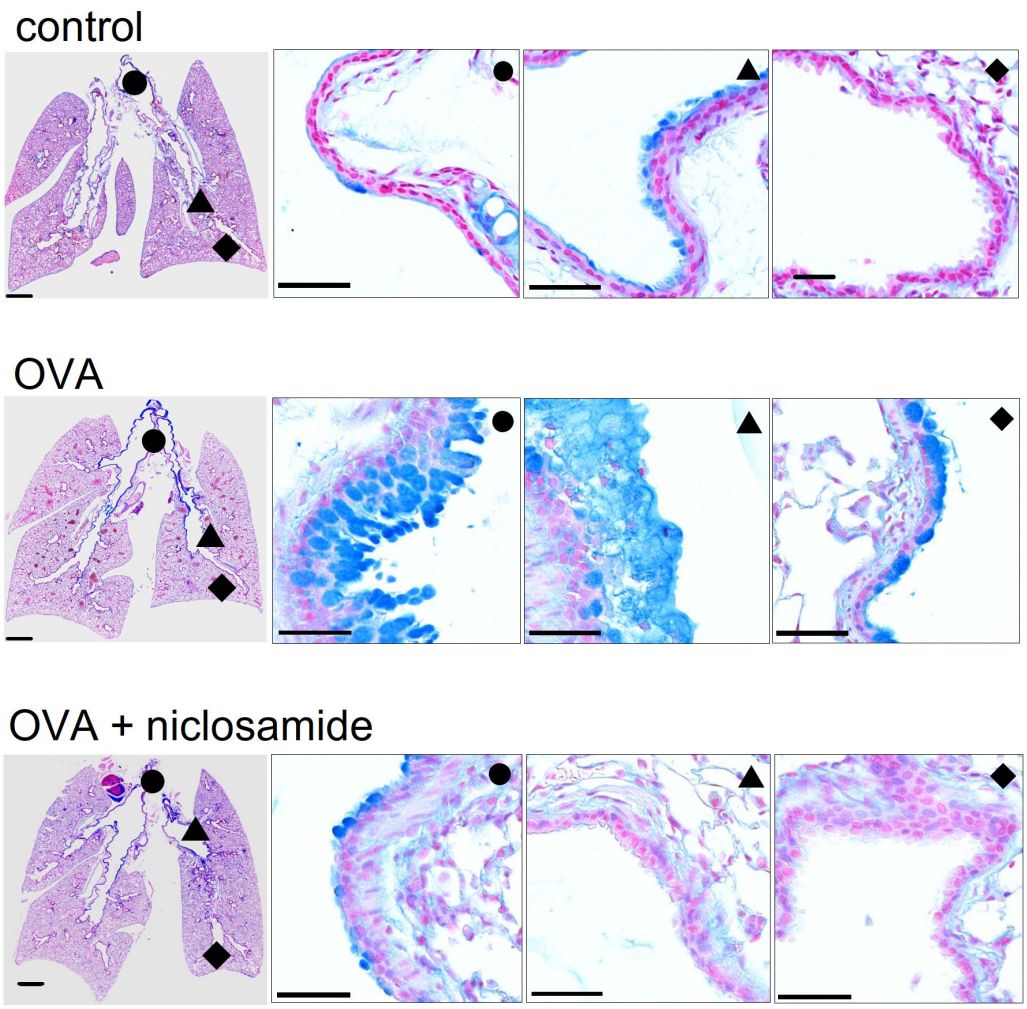

Figure 2.3 | *Mucus production and mucus secretion is inhibited by niclosamide.*
Whole mouse lung analysis by stitching microscopy. Low level mucus production and mucus secretion in proximal (●), central (▲), and peripheral (◆) airways of control mice. Bars = 1000 (very left panels) and 50 µm (higher resolution panels), respectively. Pronounced upregulation of mucus production and intraluminal mucus accumulation in lungs of OVA-treated (asthmatic) mice. Mucus production and mucus secretion is strongly suppressed in asthmatic mice treated with niclosamide (13 µg/mL, 4 days).

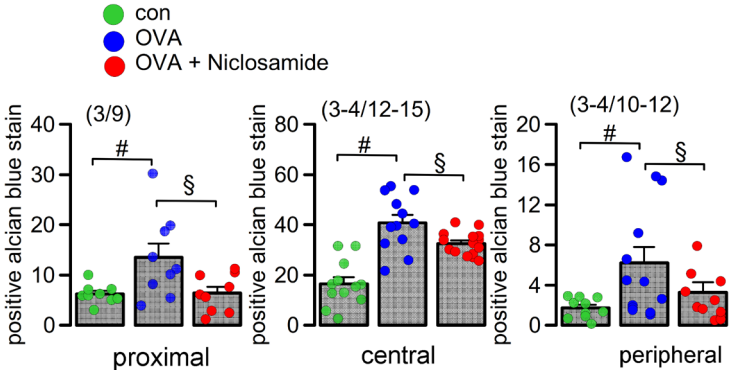

Figure 2.4 | *Quantification of airway mucus.*

Quantification of mucus in proximal, central, and peripheral airways. Mean ± SEM (number of mice/number of airways analyzed). #significant difference when compared to control ($p < 0.05$, ANOVA). §significant difference when compared to OVA ($p < 0.05$, ANOVA).

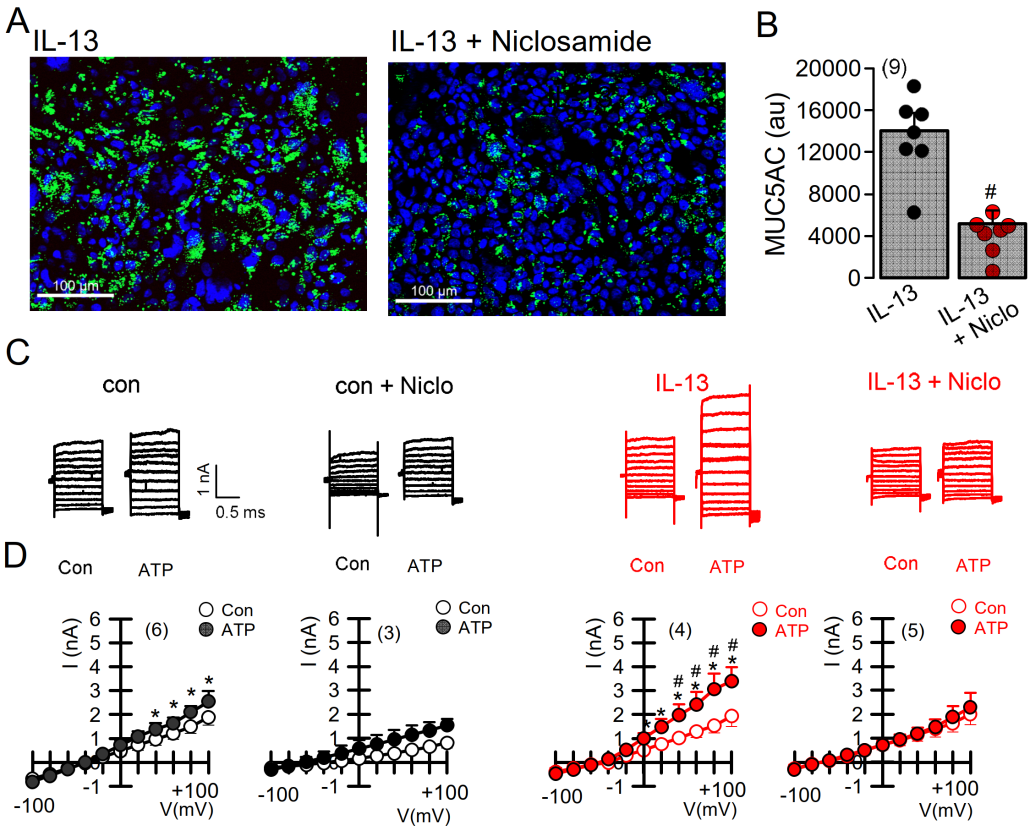

Figure 2.5 | *Expression of MUC5AC and activation of TMEM16A in Calu-3 airway epithelial cells is inhibited by niclosamide.*

(A) Expression of MUC5AC induced by IL-13 (20 ng/mL; 72 h) in Calu-3 airway epithelial cells was inhibited by simultaneous incubation with niclosamide (1 µM). Bar = 100 µm. (B) Quantification of MUC5AC expression indicating inhibition by niclosamide (Niclo). (C) Current overlays from whole-cell patch clamp experiments before and after induction of MUC5AC expression by IL-13. Activation of whole-cell currents by purinergic stimulation (ATP, 100 µM) was enhanced by IL-13, which was completely inhibited by acute application of niclosamide (1 µM). (D) Corresponding current/voltage relationships. The inhibitor of Ca2+-activated KCNN4 K+ channels, TRAM-34 (100 nM), was present in all patch clamp experiments to avoid potential activation of Ca2+-activated K+ channels. Mean ± SEM (number of cells). *significant activation by ATP ($p < 0.05$, paired t-test). #significant difference when compared to the absence of IL-13 ($p < 0.05$, unpaired t-test).

Niclosamide inhibits expression of TMEM16A, MUC5AC, and SPDEF in Calu-3 cells

Because long-term treatment with TMEM16A inhibitors suppresses expression of TMEM16A, we asked whether niclosamide affects the transcription of proteins relevant to

airway inflammation. In fact, in IL-13-treated Calu-3 cells, transcription of MUC5AC and TMEM16A were clearly blocked by niclosamide (Figures 2.6B, C). SAM pointed domain-containing ETS transcription factor (SPDEF) is the central integrator of goblet cell differentiation and pulmonary Th2 inflammation[27,200,201]. We also found a pronounced inhibition of SPDEF-mRNA expression by treatment with niclosamide (Figure 2.6C). Inhibition of SPDEF expression may therefore be a crucial mechanism for the anti-inflammatory effects observed from niclosamide.

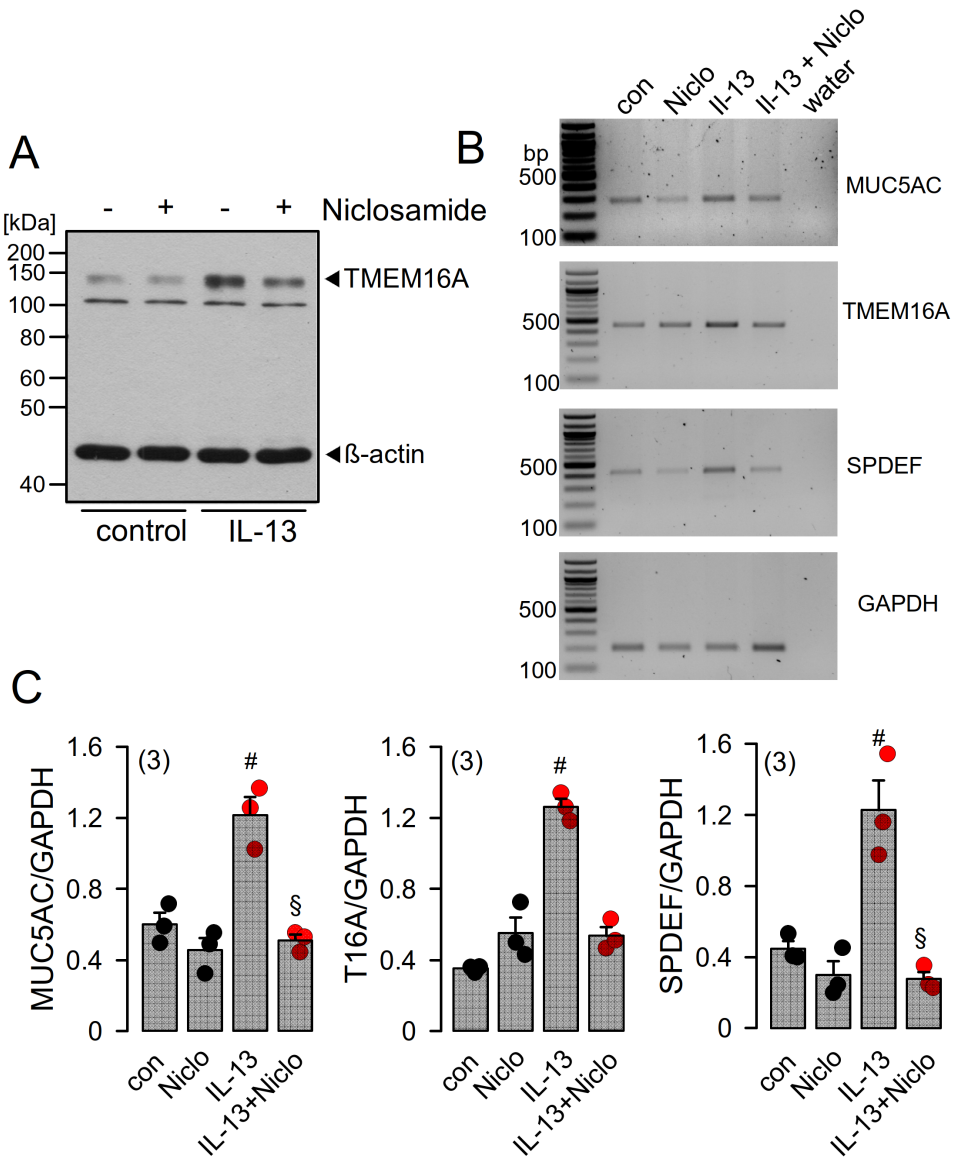

Figure 2.6 | *Niclosamide inhibits expression of MUC5AC and SPDEF in Calu-3 cells.*
(A) Western blot indicating upregulation of TMEM16A in Calu-3 cells by IL-13 (20 ng/mL, 72 h) and inhibition of expression by niclosamide (1 µM). Blots were performed in triplicates. (B) RT-PCR analysis of the expression of MUC5AC, TMEM16A, and SAM pointed domain-containing ETS transcription factor (SPDEF) in Calu-3 airway epithelial cells. SPDEF is an integrator of goblet cell differentiation and pulmonary Th2 inflammation. (C) Low cycle numbers (20×) were chosen for quantification of expression by relating specific signals to expression of the housekeeper protein GAPDH. IL-13 (20 ng/mL) leads to

upregulation of expression of MUC5AC, TMEM16A, and SPDEF. Niclosamide (Niclo, 1 µM, 72 h) strongly inhibits expression of MUC5AC, TMEM16A, and SPDEF. Mean ± SEM (number of assays). $^{\#,\S}$significant increase by IL-13 and inhibition by niclosamide, respectively ($p < 0.05$, ANOVA).

Potentiation of TMEM16A whole-cell currents by brevenal released airway mucus and caused bronchoconstriction

Eact has been proposed to be an activator of Ca^{2+}-permeable TRPV4 channels[197], which could suggest that the Eact-induced changes observed in the present report, such as bronchoconstriction and mucus release, are caused by a TMEM16A-independent mechanism. Although our previous study did not show a significant increase in the intracellular Ca^{2+} concentration by Eact[196], we nevertheless felt that it was important to rule out this possibility by examining the effects of another putative activator of TMEM16A.

Brevenal is a compound isolated from the marine dinoflagellate Karenia brevis[202]. It was shown to counteract bronchoconstriction induced by brevetoxin in sheep lungs. Brevenal was therefore even proposed as a potential drug to treat mucociliary dysfunctions[202]. In whole-cell patch clamp experiments, we examined the effects of brevenal on TMEM16A whole-cell currents expressed endogenously in CFBE airway epithelial cells. The experiments were performed in the presence of TRAM-34 (25 nM), to block unwanted potential activation of Ca^{2+}-activated K^+ channels. Notably, a low concentration (500 nM) of brevenal enhanced basal whole-cell currents. Concentration-dependent activation of TMEM16A Cl^- currents by stimulation of purinergic $P2Y_2$ receptors with ATP was strongly potentiated by brevenal (Figures 2.7A–D). Brevenal enhances the basal activity of TMEM16A and facilitates activation of TMEM16A through purinergic stimulation with ATP. The compound therefore may act as an activator and potentiator of TMEM16A. Brevenal appears to enhance the Ca^{2+} sensitivity of TMEM16A, as suggested by enhanced and stable time-dependent current activation at depolarized clamp voltages and enhanced activation of TMEM16A inward currents at negative clamp voltages (Figure 2.7).

To demonstrate that TMEM16A is responsible for ATP-activated currents and their potentiation by brevenal, TMEM16A expression was knocked down by siRNA (Figure 2.7, lower recordings, Supplementary Figure 2.4). Cells lacking expression of TMEM16A showed a complete absence of ATP-activated whole-cell currents, clearly indicating the exclusive activation of TMEM16A currents by ATP (Figures 2.7E, F). Moreover, brevenal was no longer able to potentiate activation of TMEM16A Cl^- currents. Taken together, these results indicate that brevenal activates basal activity and potentiates purinergic Ca^{2+}-dependent activation of TMEM16A.

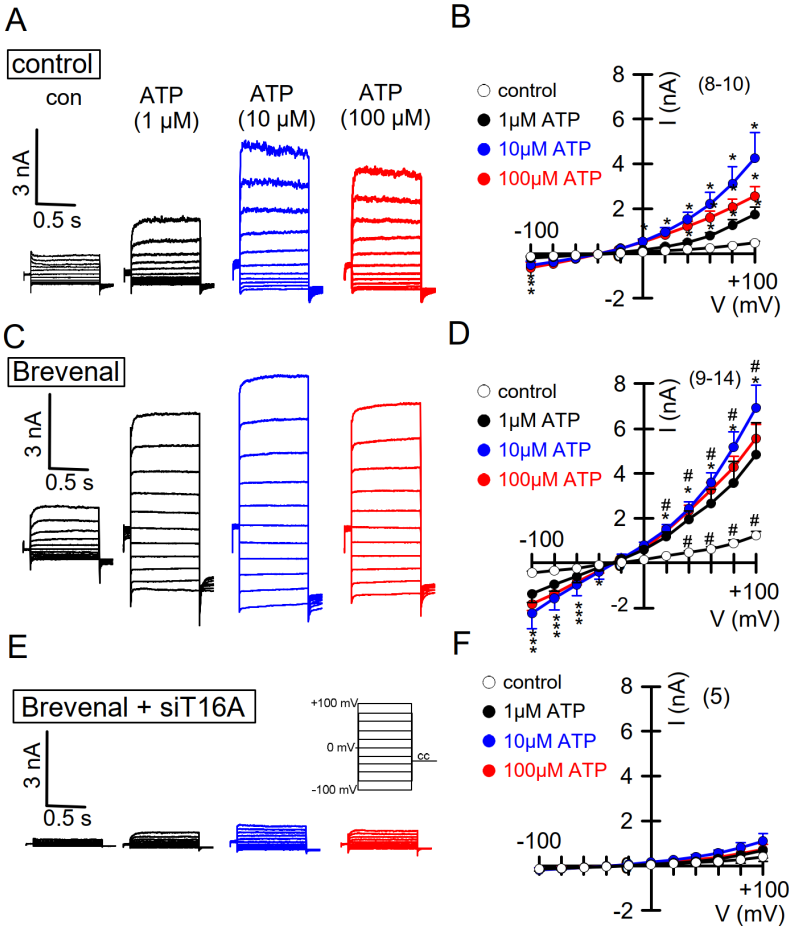

Figure 2.7 | *Activation of TMEM16A whole-cell currents is potentiated by brevenal.*
(A) Dose-dependent activation of endogenous TMEM16A whole-cell currents in CFBE airway epithelial cells, by the purinergic agonist ATP. Clamp voltages ± 100 mV in steps of 20 mV. (B) Corresponding current/voltage relationships. (C,D) Activation of whole-cell currents obtained from cells pre-incubated with brevenal (500 nM, 15 min) and corresponding current/voltage relationships. (E) Activation of whole-cell currents in brevenal-incubated cells, in which expression of TMEM16A has been knocked down by treatment with siRNA-TMEM16A (c.f. Supplementary Figure 2.2). (F) Corresponding current/voltage relationships. Mean ± SEM (number of cells). *significant activation by ATP ($p < 0.05$, ANOVA). The inhibitor of Ca^{2+}-activated KCNN4 K^+ channels, TRAM-34 (100 nM), was present in all patch clamp experiments to avoid potential activation of Ca^{2+}-activated K^+ channels. #significant difference when compared to the absence of brevenal ($p < 0.05$, ANOVA). No currents were activated in siRNA-TMEM16A-treated cells.

Brevenal could potentiate TMEM16A by releasing Ca^{2+} from endoplasmic reticulum (ER) Ca^{2+} stores or could potentiate ATP-induced Ca^{2+} store release. Alternatively, brevenal may enhance the sensitivity of TMEM16A for intracellular Ca^{2+}. We examined whether brevenal activates TMEM16A by releasing Ca^{2+} from ER stores, using the cytosolic Ca^{2+} sensor Fura-2. Brevenal neither increased basal intracellular Ca^{2+} concentrations in CFBE cells, nor augmented ATP-induced increase in intracellular Ca^{2+} (Figures 2.8A–C). We therefore

conclude that brevenal potentiates activation of TMEM16A, probably by enhancing its Ca^{2+} sensitivity.

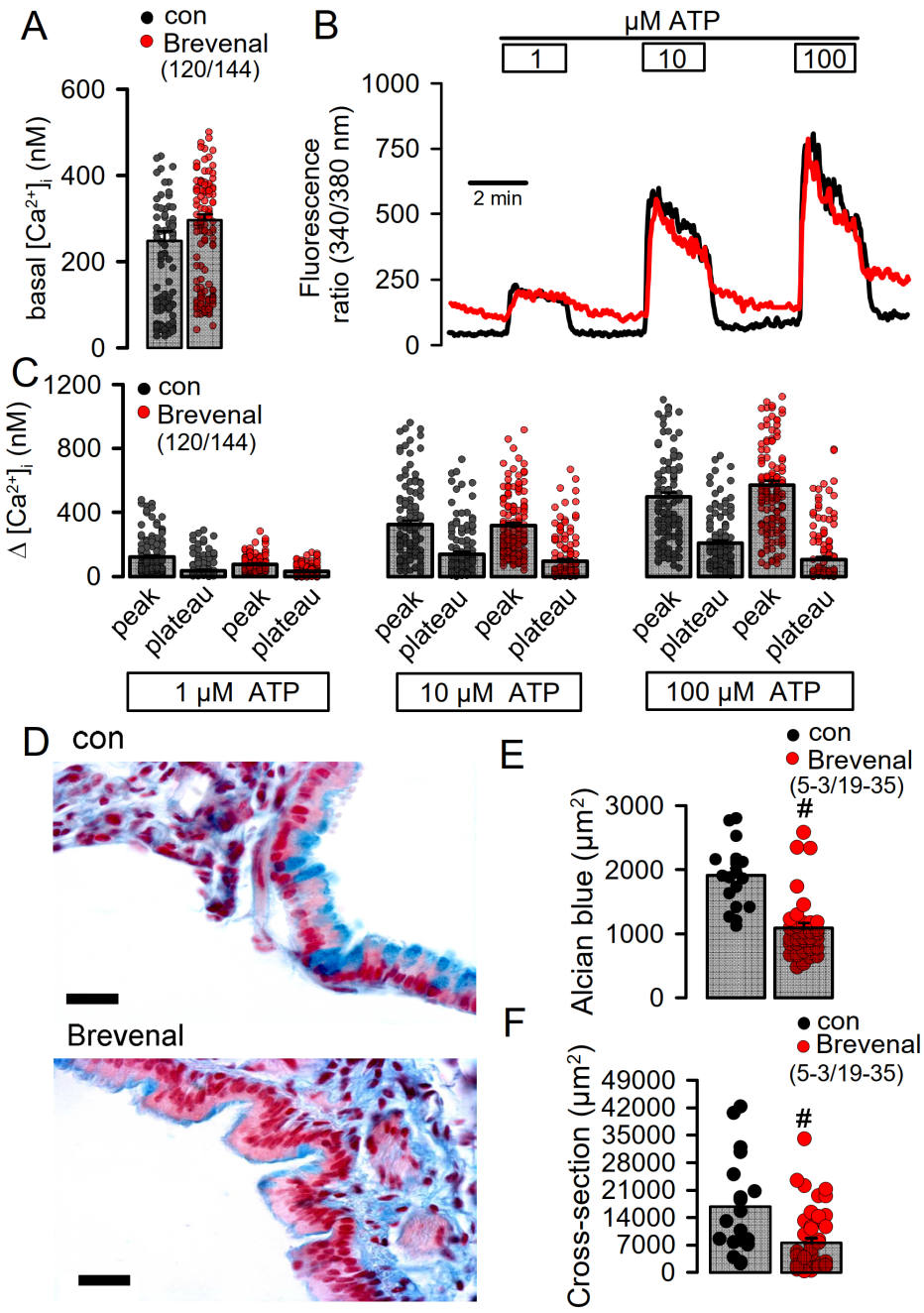

Figure 2.8 | *Brevenal does not increase intracellular Ca^{2+} but releases mucus from goblet cells and induces airway contraction.*

(A) Comparable basal intracellular Ca^{2+} levels in airway epithelial cells in the absence or presence of brevenal (500 nM, 15 min preincubation), as measured by the Ca^{2+} sensor Fura-2. (B) Concentration-dependent rise in intracellular Ca^{2+} by ATP in the absence or presence of brevenal. (C) Concentration-dependent increase in peak and plateau Ca^{2+} by ATP in the absence or presence of brevenal. (D) Effects of acute application of brevenal (3.2 µg/100 µL, 10 min) in mouse airways by tracheal instillation. Alcian blue staining of mucus indicated reduced intracellular mucus in airways treated with brevenal. Brevenal-

exposed airways appeared contracted. Bars = 15 µm. (E) Summary of Alcian blue staining in airway epithelial cells reflecting the amount of intracellular mucus, which is significantly reduced upon exposure to brevenal. (F) Summary of airway cross-sectional area obtained in airways of control mice and mice treated with brevenal, suggesting airway contraction by brevenal. Mean ± SEM; (number of animals/number of measurements). #significant difference when compared to control mice ($p < 0.05$, ANOVA).

In order to examine how the TMEM16A potentiator brevenal affects airway function, we applied brevenal acutely to mouse airways by tracheal instillation. During the application of brevenal, we observed that some animals developed severe breathing problems. Briefly after the application of brevenal, the mice were sacrificed, and their lungs were stained for mucus. Alcian blue staining revealed reduced intracellular mucus in airway goblet cells after treatment with brevenal, suggesting acute release of mucus (Figures 2.8D, E). Moreover, brevenal-exposed airways appeared to be contracted. Analysis of airway cross sections indicated reduced airway diameters, which suggests airway contraction induced by brevenal (Figures 2.8D, F). Additional *in vivo* studies are therefore warranted before TMEM16A activators or potentiators are considered for the treatment of inflammatory airway diseases.

Discussion

In the present study, we examined the role of the Ca^{2+}-activated Cl^- channel TMEM16A in mouse airways and human airway epithelial cells. TMEM16A is regarded as a secretory Cl^- channel that might compensate for the absence of CFTR-mediated Cl^- secretion in the airways of people with cystic fibrosis. While TMEM16A is almost undetectable in normal human airways using a highly specific diagnostic antibody[203], it was clearly detectable in asthmatic lungs and the lungs of CF patients. The surface (or superficial) airway epithelium showed very little expression of TMEM16A in contrast to the apical membrane of submucosal glands. A TMEM16A-based therapeutic strategy should therefore probably target TMEM16A in the submucosal glands, rather than in the surface epithelium. Secretion of both fluid and mucus takes place in submucosal glands[134,204,205]. TMEM16A was detected all along the tubular submucosal glands, suggesting that it may contribute to both CFTR-dependent fluid secretion and mucus secretion. However, because ATP-induced steady fluid secretion is essentially due to CFTR and not by TMEM16A[192], activation of TMEM16A to induce fluid secretion in CF may be ineffective. In contrast, mucus secretion is induced due to upregulation of TMEM16A in goblet cells, which supports mucus secretion[145]. Thus, TMEM16A-mediated mucus production[191] and mucus release[145] dominate in inflamed airways. Pharmacologic activation of TMEM16A to induce Cl^- secretion in CF lungs could therefore be problematic. Additional work

in vivo in CF animal models or in biopsies *ex vivo* is required to quantify the contribution of TMEM16A to mucus and fluid secretion. Exclusive *in vitro* experiments with cultured airway cells will not provide definitive answers as *in vitro* monolayers do not maintain the complexity of naïve airways and do not form submucosal glands.

We have shown the expression of TMEM16A in airway smooth muscle in lung sections of patients with asthma or CF. Together with numerous previous studies, there is clear evidence that TMEM16A contributes essentially to airway hyperresponsiveness[132,143,147,150,182]. Rather surprisingly, the TMEM16A potentiator ETX001 apparently did not contract isolated bronchi or arteries of human donors without asthma, CF, or pulmonary hypertension[180]. However, given the fact that expression of TMEM16A in noninflamed human lungs is very low, but upregulated in the lungs of patients with asthma, CF, or pulmonary hypertension, the effects of potentiators or activators should be examined in the lungs of affected patients or in corresponding animal models[145,150,206,207]. Along this line, expression of TMEM16A was upregulated in arterial endothelial cells of CF and asthma lungs, probably due to local hypoxia. TMEM16A overexpression in pulmonary arterial endothelial cells contributes to idiopathic pulmonary hypertension[186,187], and upregulation of TMEM16A in CF lungs is very likely to contribute to PH and decreased survival in severe CF[189].

The present data indicate that application of Eact, the activator of TMEM16A[195], acutely releases airway mucus and contracts airways *in vivo*. We observed that some of the animals presented with severe breathing problems after the application of Eact. Although we did not observe much of an increase in intracellular Ca^{2+} by Eact in an earlier study[196], Eact may be able to directly increase intracellular Ca^{2+}, e.g., by activating transient receptor potential (TRP) channels[197], and may therefore cause pulmonary effects independent of activation of TMEM16A. However, inhibition of TMEM16A by niclosamide completely blocked Eact-induced activation of TMEM16A (Supplementary Figure 2.5). We also examined the effects of brevenal, another putative activator of TMEM16A[135]. In the present study, we found that brevenal indeed enhances basal activity of TMEM16A and facilitates activation of TMEM16A through purinergic stimulation with ATP. Moreover, we found no evidence for a direct or indirect rise in intracellular Ca^{2+} by brevenal. Nevertheless, it could still be that brevenal enhances Ca^{2+} very locally and only in close proximity to TMEM16A, because we used Fura-2 to measure global intracellular Ca^{2+} levels. This interesting compound may therefore act as an activator and potentiator of TMEM16A expressed endogenously in human airway epithelial cells (Figures 2.7 and 2.8). Brevenal appears to enhance the Ca^{2+} sensitivity of TMEM16A, which is reflected by enhanced time-dependent current activation and enhanced activation of TMEM16A inward currents[208] (Figure 2.7). Similarly to Eact, brevenal also caused acute mucus release and bronchoconstriction *in vivo*, which caused severe breathing problems in several animals. The present results therefore strongly contraindicate the use of brevenal in inflammatory airway

diseases, unlike two recent reports which promote brevenal as a treatment in chronic respiratory disease[202,209]. In contrast to these reports, our study was done in animals with induced asthma, which leads to goblet cell metaplasia and upregulation of TMEM16A and a number of proinflammatory proteins, including SPDEF. Moreover, and as shown in Figure 2.1, noninflamed lung tissue and macrophages[210] express very little or no TMEM16A.

Niclosamide, in contrast, strongly attenuated goblet cell metaplasia in the present and previous reports[150]. The TMEM16A blocker niflumic acid removed airway mucus excess and improved survival in a rat pneumonia model[211]. As TMEM16A is upregulated in ASM and in the arterial endothelium, niclosamide-induced inhibition of TMEM16A is a promising new treatment in CF, IPH, and asthma[150,185,187]. Moreover, niclosamide is currently being investigated as a drug for the treatment of the viral inflammatory lung disease COVID-19[212]. We have shown that niclosamide inhibits expression of SPDEF, a central integrator in inflammatory lung diseases[200]. Although activation/potentiation of TMEM16A may induce airway Cl^- secretion in submucosal glands, parallel increase in mucus production/secretion, ASM contraction and pulmonary arterial blood pressure may compromise lung function in people with inflammatory airway diseases. Taken together, acute activation or potentiation of TMEM16A is likely to induce adverse effects in inflamed airways. Therefore, additional studies *in vivo* should be performed before these drugs are further evaluated in humans.

Acknowledgements

This research was funded by the UK Cystic Fibrosis Trust SRC013, German Research Foundation (DFG) KU756/14-1, and Gilead Foundation. We thank Daniel Baden (University of North Carolina, NC, USA) for providing the brevenal. The technical assistance by Helena Lowack and Patricia Seeberger is greatly appreciated.

Supplementary material

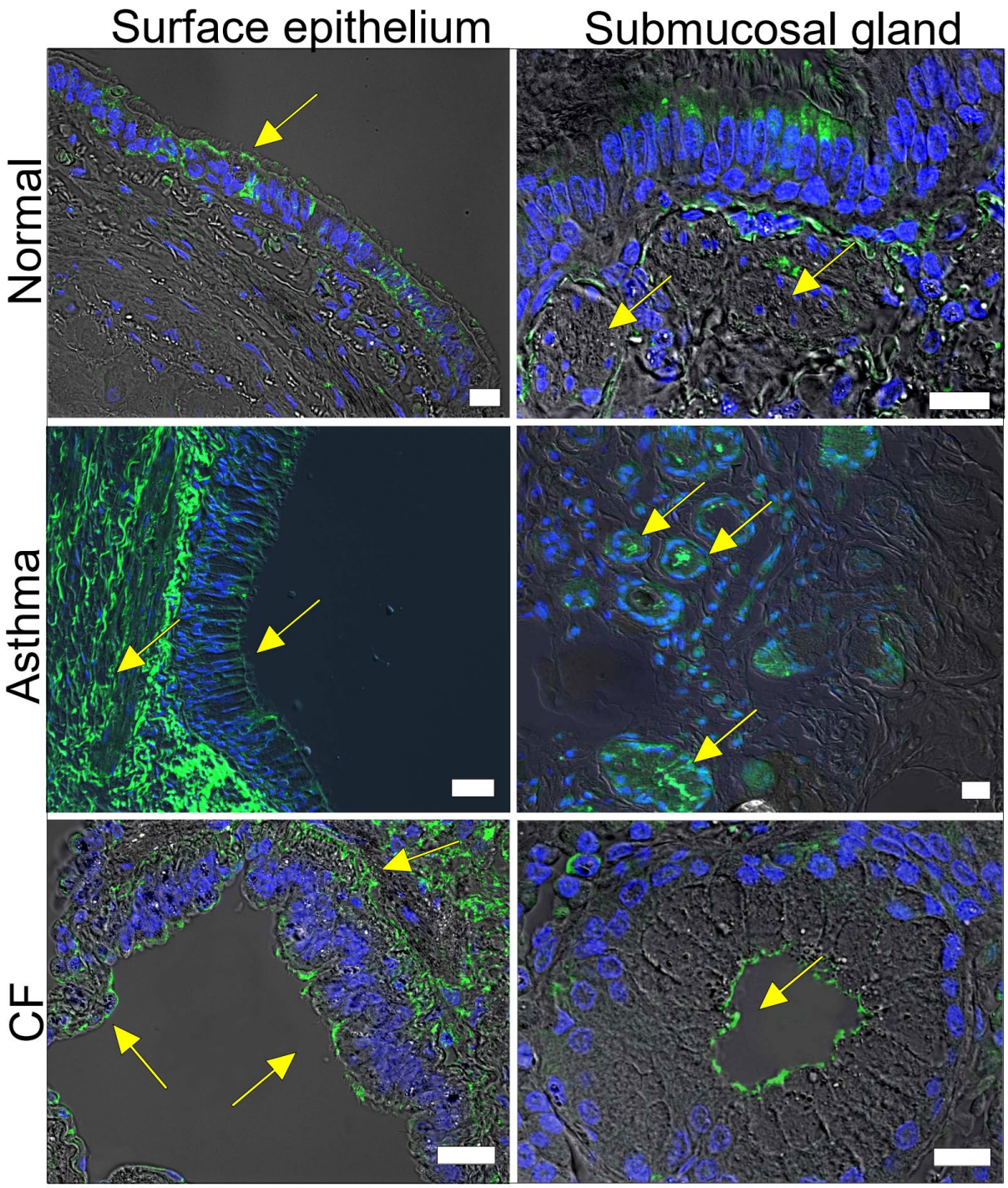

Supplementary Figure 2.1 | *TMEM16A is expressed in submucosal cells of human airways.* Immunofluorescence of TMEM16A in human airways. Little or no expression is found in surface epithelium, airway smooth muscle and submucosal glands of normal airways. Asthmatic airways show some expression in the surface epithelium, but clear expression in airway smooth muscle. Expression is also regularly detected in submucosal glands. CF airways show expression in surface epithelium and airway smooth muscle with higher levels of expression in submucosal glands. Bar = 20 µm. Yellow arrows indicate expression of TMEM16A (green fluorescence).

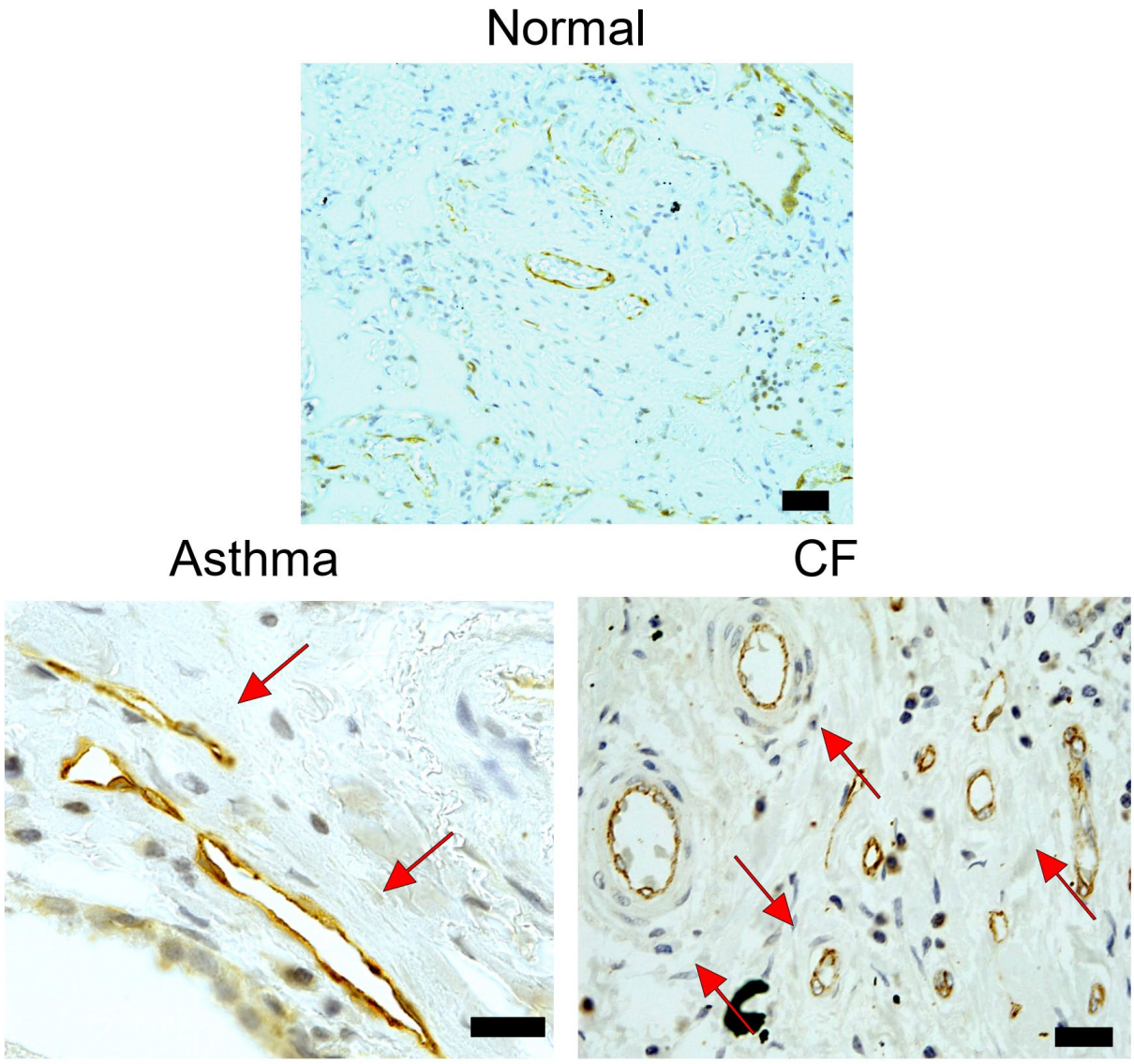

Supplementary Figure 2.2 | *TMEM16A is expressed in pulmonary blood vessels.*
Using 3,3'-diaminobenzidine (DAB) staining, TMEM16A is found predominantly in the endothelium of pulmonary blood vessels. Pronounced staining (brown precipitation) is found in vessels of asthmatic lungs and lungs of people with CF. Bar = 20 µm. Red arrows indicate expression of TMEM16A (brown precipitation).

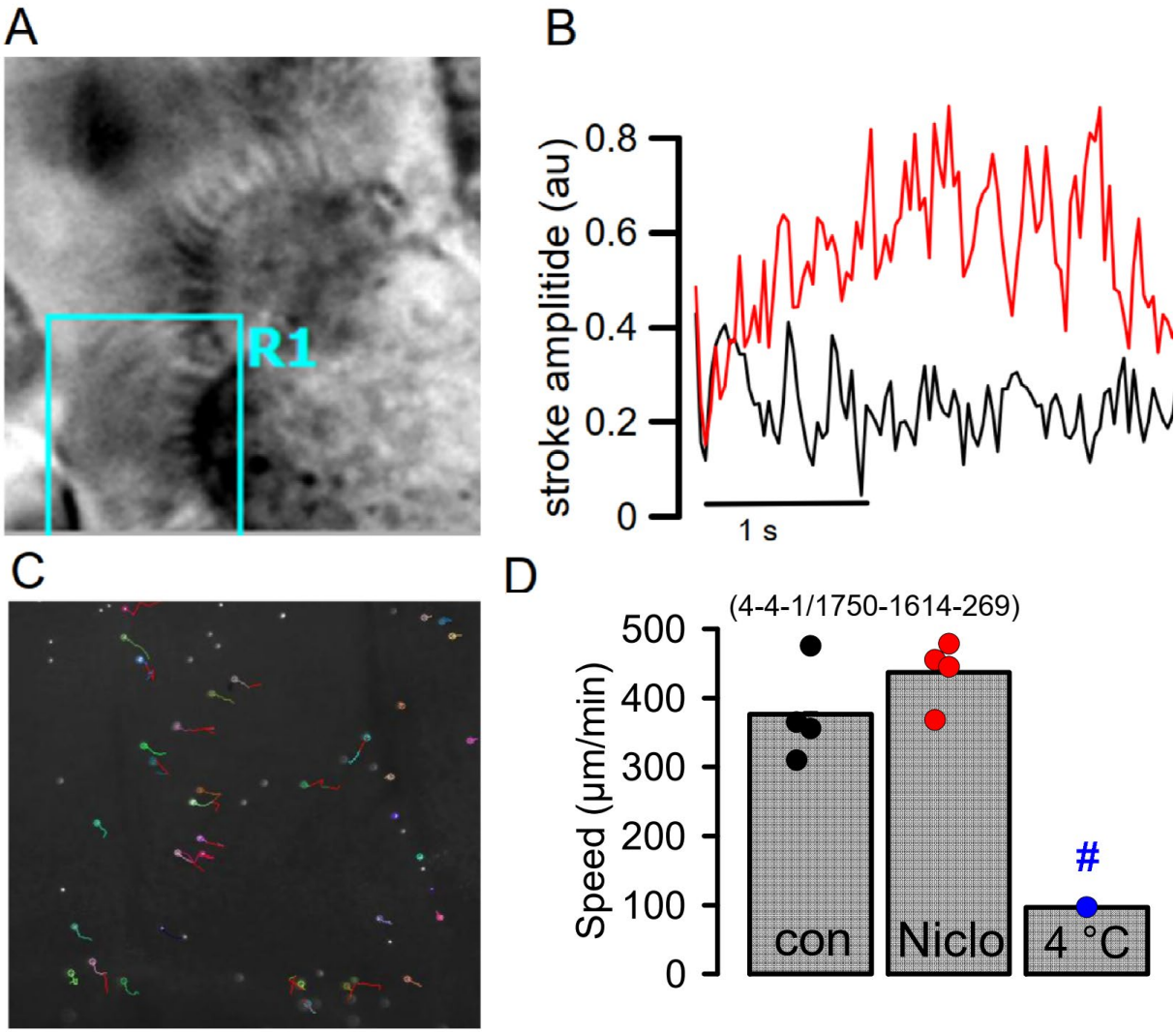

Supplementary Figure 2.3 | *Niclosamide does not inhibit mucociliary clearance.*
A,B) Ciliary stroke amplitude and frequency measured and analyzed by video imaging of isolated mouse tracheas (Zeiss Axiovision, Munich). Acute application of 1 µM niclosamide does not affect stroke amplitude or frequency (n=3 mice/37-89 events). C,D) Particle tracking and trajectories assessed by video imaging of moving fluorescent beads on isolated tracheas. Experiments were performed in a humidified chamber. Niclosamide did not inhibit basal particle movement. In contrast, cooling of the tissue strongly reduced particle clearance. Mean ± SEM (n=4 mice/269-1750 particles tracked). $^{\#}$significant inhibition by low temperature ($p < 0.05$, ANOVA).

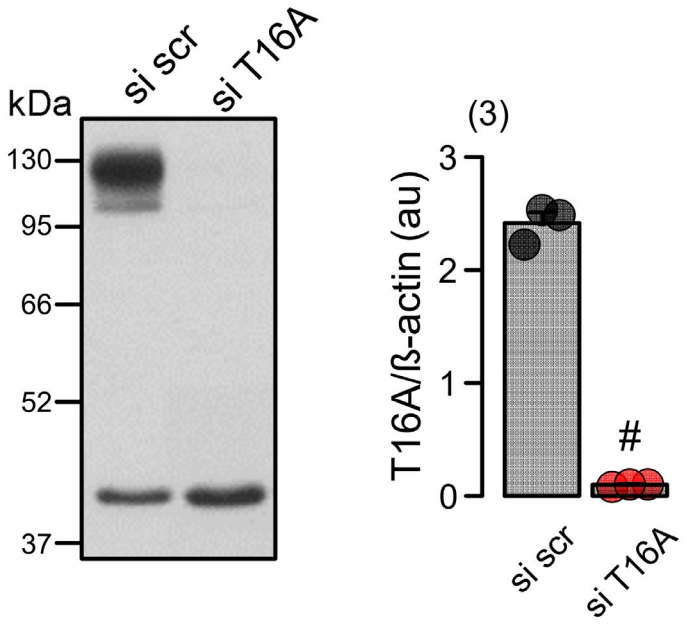

Supplementary Figure 2.4 | *siRNA-knockdown of TMEM16A in CFBE airway epithelial cells.*
Western blot of TMEM16A expressed in CFBE airway epithelial cells treated with scrambled RNA or with TMEM16A-siRNA, which successfully knocked-down expression of TMEM16A (left panel). Blots were performed in 3 replicates (right panel). Mean ± SEM (number of replicates). #significant difference ($p<0.05$; unpaired t-test).

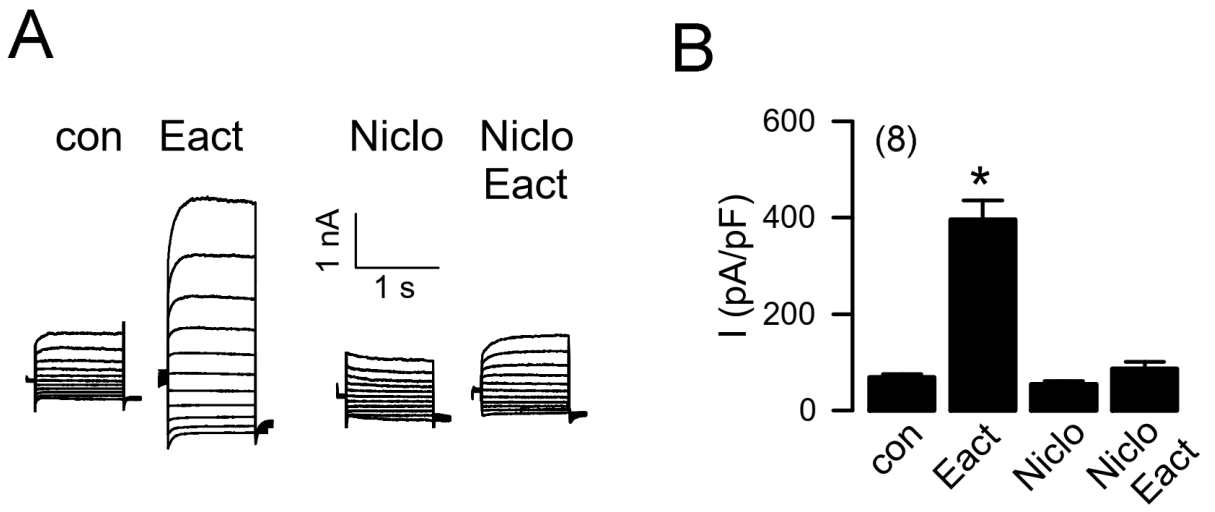

Supplementary Figure 2.5 | *Niclosamide inhibits activation of TMEM16A by Eact. Expression of TMEM16A in HEK293 cells.*

TMEM16A whole cell currents were activated by the activator of TMEM16A, Eact (1 µM). Niclosamide (Niclo; 1 µM) completely inhibited activation of TMEM16A. Mean ± SEM (number of experiments). *significant activation by Eact ($p<0.05$; paired t-test).

CHAPTER 3 | CLCA1 REGULATES AIRWAY MUCUS PRODUCTION AND ION SECRETION THROUGH TMEM16A

Abstract

TMEM16A, a Ca^{2+}-activated chloride channel (CaCC), and its regulator, CLCA1, are associated with inflammatory airway disease and goblet cell metaplasia. CLCA1 is a secreted protein with protease activity that was demonstrated to enhance membrane expression of TMEM16A. Expression of CLCA1 is particularly enhanced in goblet cell metaplasia and is associated with various lung diseases. However, mice lacking expression of CLCA1 showed the same degree of mucous cell metaplasia and airway hyperreactivity as asthmatic wild-type mice. To gain more insight into the role of CLCA1, we applied secreted N-CLCA1, produced *in vitro*, to mice *in vivo* using intratracheal instillation. We observed no obvious upregulation of TMEM16A membrane expression by CLCA1 and no differences in ATP-induced short circuit currents (I_{SC}). However, intraluminal mucus accumulation was observed by treatment with N-CLCA1 that was not seen in control animals. The effects of N-CLCA1 were augmented in ovalbumin-sensitized mice. Mucus production induced by N-CLCA1 in polarized BCi-NS1 human airway epithelial cells was dependent on TMEM16A expression. IL-13 upregulated expression of CLCA1 and enhanced mucus production, however, without enhancing purinergic activation of I_{SC}. In contrast to polarized airway epithelial cells and mouse airways, which express very low levels of TMEM16A, nonpolarized airway cells express large amounts of TMEM16A protein and show strong CaCC. The present data show an only limited contribution of TMEM16A to airway ion secretion but suggest a significant role of both CLCA1 and TMEM16A for airway mucus secretion.

Keywords: CLCA1; TMEM16A; anoctamin 1; airway epithelium; mucus; MUC5AC; KCNN4

Published as: Centeio R., Ousingsawat J., Talbi K., Schreiber R., Kunzelmann K. CLCA1 Regulates Airway Mucus Production and Ion Secretion Through TMEM16A. *International Journal of Molecular Sciences*. 2021 May; 22(10): 5133.

Own experimental contribution: Ovalbumin-sensitization of animals; conditioned-media preparation and intratracheal instillation; mouse trachea and lungs isolations; Ussing chamber experiments; Western blots; immunocytochemistry; growth, paraffin-embedding and slicing of polarized cells; mucus stainings by Alcian blue.

Own written contribution: Original draft preparation, review and editing.

Other contributions: Designed experiments and analysed data.

Introduction

TMEM16A is a Ca^{2+}-activated chloride (Cl^-) channel (CaCC) that belongs to a family of 10 proteins, operating as phospholipid scramblases and Cl^- channels[129]. In the lungs, TMEM16A is expressed at low levels in airway epithelial cells and airway and pulmonary arterial smooth muscle cells and is upregulated during inflammatory airway diseases such as asthma and cystic fibrosis (CF)[132,145,149,213]. However, it remains unclear whether TMEM16A is particularly relevant for mucus production and mucus secretion or for secretion of electrolytes covering the airways[135,145,214]. Earlier reports describe that TMEM16A is essential for the function of CFTR by providing local Ca^{2+} levels required for insertion of CFTR into the plasma membrane, and for full activation of CFTR through Ca^{2+}-sensitive adenylate cyclase 1[137-139,192,215,216].

Many studies associate expression of TMEM16A and the regulator of Ca^{2+}-activated Cl^- channels, CLCA1, with goblet cell metaplasia and mucus production/secretion [132,145,147,149,181,191,217]. Inflammatory airway disease is associated with enhanced expression of CLCA1 in airway epithelial cells and high levels in the bronchoalveolar lavage (BAL) fluid[218,219]. It should be mentioned that different than previously thought, CLCA1 is a secreted protein and a regulator of TMEM16A membrane expression[220]. The so called von Willebrand factor type A (VWA) domain in secreted N-terminal CLCA1 was shown to serve as the minimal requirement for interaction and activation of TMEM16A[221,222]. Interestingly, the microtubular inhibitor nocodazole also augmented TMEM16A currents within minutes after exposure.

Expression of CLCA1 is enhanced in goblet cell metaplasia and associated with various lung diseases[217]. However, mice lacking expression of CLCA1 (mClca3 according to the earlier nomenclature) showed the same degree of mucous cell metaplasia and airway hyperreactivity as wild-type mice when challenged with viruses or allergens[223]. As CLCA1 is not essential for the development of mucous cell metaplasia, expression of other CLCA paralogs was proposed as a mechanism for functional redundancy. Using CLCA1-knockout mice, Mundhenk et al. found that CLCA1 does not contribute to basal, cAMP and Ca^{2+}-regulated short circuit currents in mouse trachea. Notably, tracheal instillation of IL-13 in *wt* mice produced a strong upregulation of CLCA1, along with goblet cell metaplasia and mucin expression, but did not increase Ca^{2+}-activated short circuit currents (I_{sc})[224]. In $CLCA1^{-/-}$ tracheas, goblet cell metaplasia, mucin expression and Ca^{2+}-activated I_{sc} were similar, and no compensatory upregulation of CLCA5 was observed.

The controversies regarding the cellular function of CLCA1 triggered the present study, in which we examined the effects of secreted CLCA1 (N-CLCA1) in mouse airways *in vivo* and in airway epithelial cells *in vitro*. We found that CLCA1 augments intraluminal mucus, possibly by enhanced mucus production/secretion or by inducing mucus expansion. However, no clear increase in TMEM16A-dependent Cl^- transport could be identified.

Materials and Methods

Animals and treatments: Allergen challenge of mice has been described previously[190]. In brief, mice were sensitized to ovalbumin (OVA; Sigma-Aldrich, St. Louis, Missouri, USA) by intraperitoneal (I.P.) injection of 100 µg OVA in 100 µL Aluminium Hydroxide Gel Adjuvant (InvivoGen, San Diego, California, USA) on days 0 and 14. At days 21 to 23, mice were anesthetized (ketamine 90–120 mg/kg and xylazine 6–8 mg/kg) and challenged to OVA by intratracheal (I.T.) instillation of 50 µg OVA in 100 µL saline. Control mice were sham sensitized with aluminium hydroxide gel and challenged to saline by I.T. instillation. Allergen reaction was allowed to develop for 72h. CLCA1-conditioned media (N-CLCA1; 100 µL; preparation described below) was administered to control or OVA-challenged animals by I.T. instillation 24 hrs before sacrificing the animals. Control I.T. instillation was performed with mock-conditioned media. All animal experiments complied with the reporting of *in vivo* experiments guidelines and were carried out in accordance with the United Kingdom Animals Act, 1986, and associated guidelines, and EU Directive 2010/ 63/EU for animal experiments. All animal experiments were approved by the local Ethics Committee of the Government of Unterfranken/Wurzburg (AZ: 55.2-2532-2-1359-15) and were conducted according to the guidelines of the American Physiologic Society and German Law for the Welfare of Animals.

Cell culture and treatments: All cells were grown at 37°C in a humidified atmosphere with 5% CO2. Calu3 human airway epithelial cells were grown in DMEM/Ham's F-12 with L-Glutamine medium supplemented with 10% (v/v) foetal bovine serum (FBS), 1% (v/v) L-glutamine 200mM and 1% (v/v) HEPES 1M (all from Capricorn Scientific, Ebsdorfergrund, Germany). Human embryonic kidney HEK293T cells were grown in DMEM low glucose medium supplemented with 10% (v/v) FBS and 1% (v/v) L-glutamine 200mM (all from Capricorn Scientific, Ebsdorfergrund, Germany).

Construction of expression plasmids has been described previously[225]. In brief, CLCA1 was cloned from human colon and ligated into a pcDNA3.1 vector. For conditioned media preparation, HEK293T cells were seeded at 500.000 cells per 6well and next day transfected with empty pcDNA3.1 (mock) or hCLCA1 plasmids using standard protocols for Lipofectamine 3000 (Invitrogen, Carlsbad, California, USA). After 6h, the medium was changed to serum-free media (Opti-MEM Reduced Serum Medium (Gibco/Thermo Fisher Scientific, Waltham, Massachusetts, USA)) and 24h later the supernatants – control or enriched in secreted CLCA1 protein (N-CLCA1) were collected.

BCi-NS1 cells (kindly provided by Prof. R. Crystal, Weill Cornell Medical College, New York, USA) were cultured in supplemented Bronchial Epithelial Cell Growth Medium (Lonza, Basel,

Switzerland). For polarization, BCi-NS1 cells were seeded onto permeable supports (Snapwell #3801, Corning, New York, USA) in an air-liquid interface by seeding 300.000 cells on human type IV collagen- (Sigma-Aldrich, St. Louis, Missouri, USA) -coated inserts. Cells were maintained in a media consisting of 1:1 DMEM:Ham's F12 supplemented with 10% (v/v) FBS, 1% (v/v) P/S, 0.5% (v/v) Amphotericin B and 0.1% (v/v) Gentamycin (all from Capricorn Scientific, Ebsdorfergrund, Germany). On the following day, the serum was replaced with 2% (v/v) of serum-substitute Ultroser G (Pall Life Sciences, New York, USA). On the second day after seeding, the media was removed from the upper compartment to expose the apical surface to air and to establish an air-liquid interface (ALI). Cells were grown for 28 days on filters, and transepithelial resistances (TEER) were measured regularly, which was in the range as described earlier[191].

Cells were treated with IL-13 (20 ng/mL; Enzo Life Sciences, Lörrach, Germany) for 72h in Opti-MEM, and treatment was refreshed every day in the absence or presence of the inhibitors Ani9 and Niclosamide-ethanolamine (both 1 µM; Sigma-Aldrich, St. Louis, Missouri, USA). Treatment with mock- or CLCA1-conditioned media was applied for 24-48 hrs. Treatment of polarized BCi cells was performed both in the basolateral media and by adding 100 µL to the apical compartment. Knockdown of TMEM16A was performed by transfection of siRNA against TMEM16A (5-GGUUCCCAGC CUACCUCACUAACUU-3; Invitrogen, Carlsbad, California, USA) using standard protocols for Lipofectamine 3000. Scrambled siRNA (Silencer® Select Negative Control siRNA #1, Ambion, Austin, Texas, USA) was transfected as negative control. Knockdown of TMEM16A was validated as reported earlier [191]. All experiments were performed 48-72h after transfection.

RT-PCR: For semi-quantitative RT-PCR total RNA from tracheal epithelial cells, lung tissue, Calu3 or 6CFSMEo- cells was isolated using NucleoSpin RNA II columns (Macherey-Nagel, Düren, Germany). Total RNA (0.5 µg / 25 µl reaction) was reverse-transcribed using random primers (Promega, Mannheim, Germany) and M-MLV Reverse Transcriptase RNase H Minus (Promega, Mannheim, Germany). Each RT-PCR reaction contained sense (0.5 µM) and antisense primers (0.5 µM) (Table 3.1), 0.5 µl cDNA and GoTaq Polymerase (Promega, Mannheim, Germany). After 2 min at 95°C, cDNA was amplified (targets 30-35 cycles, reference Gapdh 25 cycles) for 30 s at 95°C, 30 s at 56°C and 1 min at 72°C. PCR products were visualized by loading on Midori Green Xtra (Nippon Genetics Europe) containing agarose gels and analysed using Image J 1.52r (NIH, USA).

Table 3.1 | *RT-PCR primers.*

Gene accession number	Primers	Size (bp)
Mouse Tmem16a NM_001242349.2	s: 5´-GTGACAAGACCTGCAGCTAC as: 5´-GCTGCAGCTGTGGAGATTC	406
Human TMEM16A NM_018043.7	s: 5´-CGACTACGTGTACATTTTCCG as: 5´-GATTCCGATGTCTTTGGCTC	445
Mouse Cftr NM_021050.2	s: 5´-GAATCCCCAGCTTATCCACG as: 5´-CTTCACCATCATCTTCCCTAG	544
Human CFTR NM_000492.4	s: 5´-CGACTACGTGTACATTTTCCG as: 5´-GCTCTTGTGGACAGTAATATATCG	568
Human CLCA1 NM_001285.4	s: 5´-GGGGCCATTTAAGAGTTCTG as: 5´-CTCTCCACAGTTGCCCATC	379
Mouse Slc26a9 NM_177243.4	s: 5´-CATTTGCTGCGCTCTCTCAG as: 5´-CCTCTTCTCCTGCTTCCGG	568
Mouse Kcnn4 NM_008433.4	s: 5´-GAATCAGCCACAGTGTGTC as: 5´-CCTCCTTTGTCTTATTGTGG	515
Human KCNN4 NM_002250.3	s: 5´-GATTTAGGGGCGCCGCTGAC as: 5´-CTTGCCCCACATGGTGCCC	405
Human KCNQ1 NM_000218.3	s: 5´-CCACGGGGACTCTCTTCTG as: 5´-GGCACCTTGTCCCCATAG	505
Mouse Muc5ac NM_010844.3	s: 5´-CACCAAAGACAGCAGATCATC as: 5´-GTTCTGAGGACTCTGCATGG	295
Human SPDEF NM_012391.3	s: 5´-GTGCTCAAGGACATCGAGAC as: 5´-CCTAATGAAGCGGCCATAGC	423
Human Mouse Gapdh NM_001289726	s: 5´-GTATTGGGCGCCTGGTCAC as: 5´-CTCCTGGAAGATGGTGATGG	200

Transepithelial Ussing chamber recordings: Animals were sacrificed by cervical dislocation and isolated tracheas were cleaned, sectioned and kept in ice-cold standard bicarbonate-free Ringer's solution (in mM: NaCl 145, KH_2PO_4 0.4, K_2HPO_4 • 3 H_20 1.6, Glucose 5, $MgCl_2$ • 6 H_20 1, Ca-Gluconate • 1 H_20 1.3; pH 7.4). Tissues were mounted into Ussing chambers in supports with a circular aperture of 0.177 cm^2. Polarized cell inserts were mounted onto supports with a circular aperture of 1.13 cm^2. Luminal and basolateral sides of the epithelia were perfused continuously at a rate of 5 mL/min with standard bicarbonate-free Ringer's solution ± compounds (Amiloride 10 µM, apical; Tram34 100 or 300 nM, basolateral; Ani9 10 µM, apical; ATP 100 µM, apical; all from Sigma-Aldrich, St. Louis, Missouri, USA). Luminal and basolateral solutions were heated to 37 °C using a water jacket. Experiments were carried out under open-circuit conditions. Data were continuously collected using PowerLab software (AD Instruments, Spechbach, Germany). Values for transepithelial voltages (Vte) were referred to the serosal side of the epithelia. Transepithelial resistances (Rte) were determined by applying short (1s) current pulses ($\Delta I = 0.5$ µA). Rte and equivalent short circuit currents (I'_{sc}) were calculated according to Ohm's law ($Rte = \Delta Vte/\Delta I$, $I_{sc} = Vte/Rte$).

Western blotting: Protein was isolated from cells using a lysis buffer containing 25 mM Tris-HCl pH 7.4, 150 mM NaCl, 1 mM EDTA, 5% glycerol, 0.43% Nonidet P-40, 100 mM dithiothreitol (both from PanReac AppliChem, Barcelona, Spain) and 1X protease inhibitor mixture (Roche, Basel, Switzerland). For supernatant protein precipitation the trichloroacetic acid (TCA) method was used. Proteins were then separated by 8.5% SDS-PAGE and transferred to a PVDF membrane (GE Healthcare, Munich, Germany). Membranes were incubated overnight at 4 °C with primary antibodies: rabbit anti-TMEM16A (ab64085, Abcam, Cambridge, UK; 1:500 in 1% (w/v) NFM/TBS-T), rabbit anti-CLCA1 (ab180851, Abcam; 1:1000 in 3% (w/v) NFM/TBST-T), mouse anti-(S)PDEF(G10) (sc-166846, Santa Cruz Biotechnology; 1:250 in 3% (w/v) NFM/TBST-T) and rabbit anti-KCNN4 (APC-064, Alomone Labs, Jerusalem, Israel; 1:500 in 3% (w/v) NFM/TBST-T). The antibodies rabbit anti-Actin (A2066; Sigma-Aldrich, St. Louis, Missouri, USA; 1:10 000 in 5% (w/v) NFM/TBS-T), rabbit anti-Lamin A/C (#c-20681, Santa Cruz Biotechnology, Dallas, Texas, USA; 1:60 000 in 3% (w/v) NFM/TBST-T) and rabbit anti-Na+/K+-ATPase (sc-28800, Santa Cruz Biotechnology; 1:1500 in 5% (w/v) NFM/TBST-T) were used as loading controls. Membranes were then incubated with horseradish peroxidase (HRP)-conjugated goat anti-rabbit or sheep anti-mouse secondary antibodies at room temperature for 2 hrs and immunoreactive signals were visualized using a SuperSignal HRP Chemiluminescence Substrate detection kit (34577; Thermo Fisher Scientific, Waltham, Massachusetts, USA).

Immunocytochemistry: For TMEM16A stainings in Calu3 airway cells, cells seeded onto glass coverslips were fixed with a pre-cooled 3:1 mix of methanol:acetone for 10 min at -20 °C, washed in PBS with Ca^{2+} and Mg^{2+} (PBS^{++}), blocked with 5% BSA/PBS^{++} for 30 min at room temperature, incubated with rabbit anti-TMEM16A antibody (1:100 in 1%BSA/PBS^{++}; ab64085, Abcam, Cambridge, UK) for 1h at 37 °C, washed, incubated with Alexa Fluor 488-labeled donkey anti-mouse IgG (1:400 in 1%BSA/PBS^{++}, Invitrogen, Carlsbad, California, USA) and counterstained with Hoe33342 (1:200) for 1h at room temperature. Cells were then washed and mounted in fluorescence mounting medium. Plasma membrane (PM)-staining was quantified using ImageJ.

Mucus staining in polarized cells: BCi cells polarized in permeable supports were fixed in 4% PFA/PBS for 20 min at room temperature and embedded in paraffin. 5 µm paraffin cuts were deparaffinized, stained with standard Alcian blue solution and counterstained with Nuclear Fast Red solution (Sigma-Aldrich, St. Louis, Missouri, USA). After dehydration & clearing steps, sections were mounted in DePeX mounting medium (SERVA Electrophoresis, Heidelberg, Germany). Stainings were assessed by light microscopy. Mucus-stained (blue) areas were determined using ImageJ.

Mucus staining in lungs: Mouse lungs and tracheas were fixed by transcardial perfusion and lung perfusion with 4% paraformaldehyde in PBS. Tissues were incubated overnight in fixative solution and then embedded in paraffin. Paraffin embedding sections of 5 µm were deparaffinized, stained with standard Alcian blue solution and counterstained with Nuclear Fast Red solution (Sigma-Aldrich, Darmstadt, Germany). After dehydration & clearing steps, whole mouse lungs sections were mounted in DePeX mounting medium (SERVA Electrophoresis, Heidelberg, Germany). Stainings were assessed by light microscopy. and determined using ImageJ.

Patch clamp: Cells were patch clamped when grown on coated glass coverslips. Coverslips were mounted in a perfused bath chamber on the stage of an inverted microscope (IM35, Zeiss) and kept at 37 °C. Patch pipettes were filled with a cytosolic-like solution containing (in mM): KCl 30, K-Gluconate 95, NaH_2PO_4 1.2, Na_2HPO_4 4.8, EGTA 1, Ca-Gluconate 0.758, $MgCl_2$ 1.03, D-Glucose 5, ATP 3; pH 7.2. The intracellular (pipette) Ca^{2+} activity was 0.1 µM. The bath was perfused continuously with standard bicarbonate-free Ringer's solution (in mM: NaCl 145, KH_2PO_4 0.4, K_2HPO_4 1.6, Glucose 5, $MgCl_2$ 1, Ca-Gluconate 1.3) at a rate of 8 ml/min. Patch pipettes had an input resistance of 2–5 MΩ and whole cell currents were corrected for serial resistance. Currents were recorded using a patch clamp amplifier EPC9, and PULSE software (HEKA, Lambrecht, Germany) as well as Chart software (AD Instruments, Spechbach, Germany). Cells were stimulated with 1 µM ATP in the absence and presence of TRAM34. In regular intervals, membrane voltage (Vc) was clamped in steps of 20 mV from -100 to +100 mV from a holding voltage of -100 mV. Current density was calculated by dividing whole cell currents by cell capacitance.

Materials and statistical analysis: All compounds used were of highest available grade of purity and were bought from Sigma-Aldrich (St. Louis, Missouri, USA), unless indicated otherwise. Data are shown as individual traces/representative images and/or as summaries with mean values ± SEM, with the respective number of experiments given in each figure legend. For statistical analysis, paired or unpaired Student's t-test or ANOVA were used as appropriate. A p-value of < 0.05 was accepted as a statistically significant difference.

Results

Asthmatic conditions but not CLCA1 enhanced expression of TMEM16A

CLCA1 has been proposed to augment mucus production and to increase membrane expression of TMEM16A. However, available data are controversial and data from naïve airways are scarce. We therefore exposed mice *in vivo* to secreted N-terminal CLCA1 protein,

which was produced by expression of CLCA1 in HEK293 cells and harvesting of N-CLCA1 from the supernatant (Supplementary Figure 3.1). N-CLCA1 or control buffer were applied to mouse airways by intratracheal instillation and animals were sacrificed 24 h later. Airway epithelial cells were harvested from isolated tracheas and expression of secretory ion channels and transporters such as Tmem16A, Cftr, Slc26a9, Kcnn4, as well as Muc5ac was analysed. Except for Cftr, mRNA expression was not affected by N-CLCA1 (Figure 3.1A). Our data correspond to a previous report on excised human airway tissue stimulated with inflammatory cytokines *in vitro*[219]. Moreover, expression of TMEM16A was not detected in mock treated mouse trachea and only occasionally found in mucus producing epithelial cells by immunohistochemistry of N-CLCA1 tracheas (data not shown). Analysis of different airway sections demonstrated an impressive accumulation of mucus in the airways of N-CLCA1 treated animals, suggesting induction of mucus secretion by N-CLCA1 (Figure 3.1B). In contrast to N-CLCA1-induced secretion of mucus (lower panels), mucus was not detected in airways of mice treated with control supernatant (upper panels).

We also analysed smaller airways from asthmatic mice sensitized *in vivo* towards ovalbumin. In contrast to treatment with N-CLCA1, transcriptional upregulation was observed of Tmem16a, Cftr and Muc5ac in airway epithelial cells of asthmatic airways, along with a small but significant increase in Kcnn4 expression (Figure 3.2A,B). Alcian blue staining indicated pronounced goblet cell metaplasia in airways of asthmatic mice[135] (Figure 3.2C, OVA, lower panel). Additional intratracheal application of N-CLCA1 in OVA-sensitized asthmatic mice further augmented goblet cell metaplasia and induced mucus secretion with intraluminal accumulation in the airways. These effects of N-CLCA1 may be related to the mucus expanding properties of CLCA1 described earlier[226]. However, as previous studies demonstrated a role of TMEM16A for mucus secretion, N-CLCA1 may also induce mucus secretion through an increase in TMEM16A-function[145,191,221].

KCNN4 is upregulated in asthma which counteracts activation of TMEM16A

Ion transport was assessed under open circuit conditions in tracheas of control mice and mice treated with N-CLCA1. No differences were found in basal amiloride-sensitive Na^+ absorption (Figure 3.3A,B). Moreover, ATP-activated ion transport was not different in N-CLCA1-treated mice when compared to control mice (Figure 3.3C,D). In the presence of the TMEM16A-blocker Ani9 or the KCNN4 inhibitor TRAM-34, both basal and ATP-activated transport were similar in CLCA1 and control treated airways (Figure 3.3E–H). Interestingly, we detected an upregulation of KCNN4 in tracheas and other airway sections of asthmatic (OVA-treated) mice (Figure 3.2A, Supplementary Figure 3.2A-C). Moreover, KCNN4 was also upregulated by IL-13 in Calu3 airway epithelial cells (Supplementary Figure 3.2D,E). We examined whether both Ca^{2+}-activated KCNN4 K^+ channels and TMEM16A Cl^- channels are

activated by increase in intracellular Ca^{2+} with ATP using patch clamp experiments, as this question cannot be clearly examined in Ussing chamber recordings. In fact, the data demonstrate that KCNN4 is activated by increase in intracellular Ca^{2+}, which corresponds to earlier observations by Lee and Fosket.

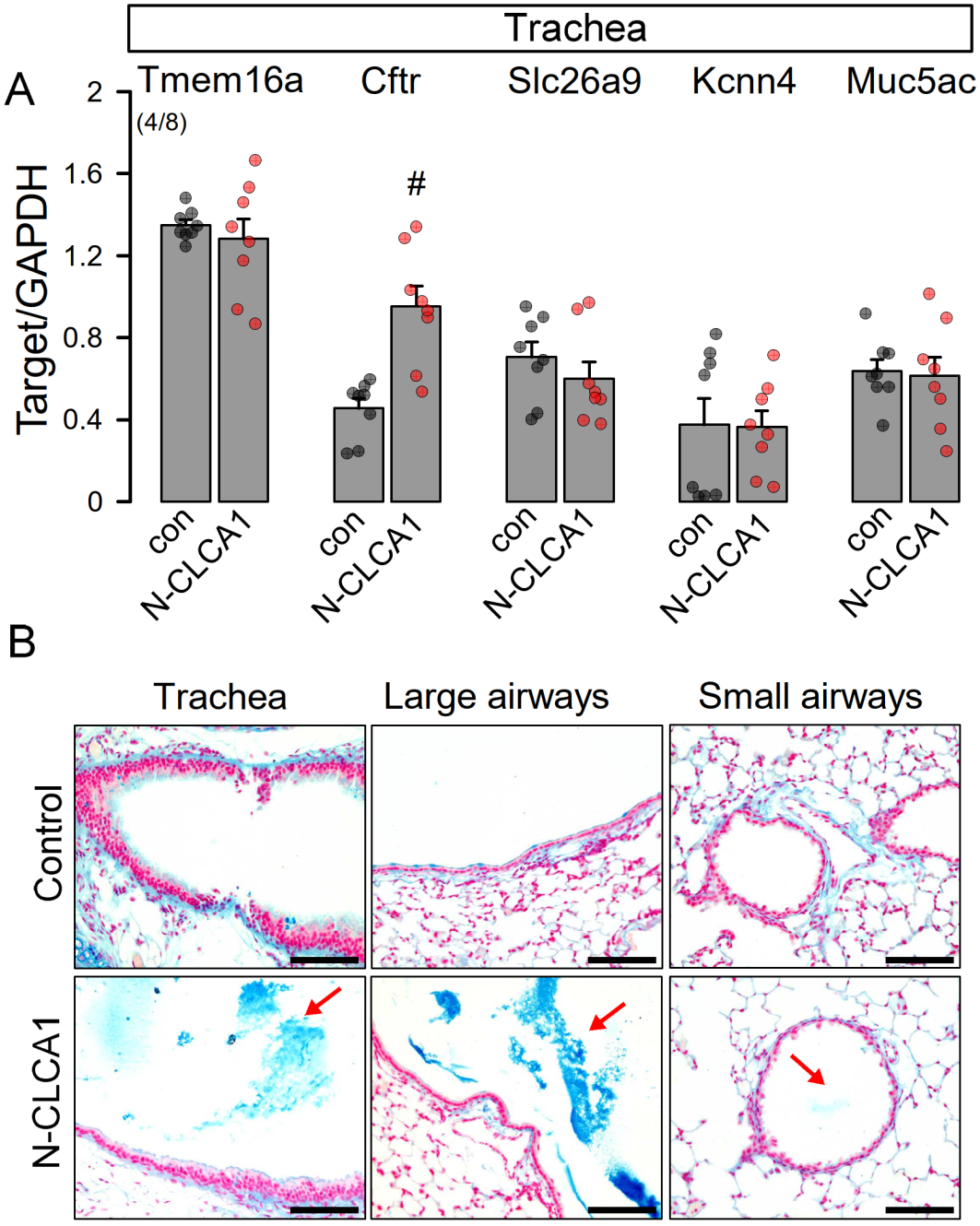

Figure 3.1 | *N-CLCA1 increases mucus production in vivo.*

(A) Semiquantitative RT-PCR analysis of the expression of MUC5AC, TMEM16A, CFTR, SLC26A9 and KCNN4 in isolated tracheal epithelial cells from control mice and mice treated for 24 h with N-CLCA1. Mean ± SEM (number of animals/number of reactions). #significant difference when compared to control or mock ($p < 0.05$; unpaired t-test). (B) Alcian blue staining indicating enhanced mucus secretion in airways exposed to N-CLCA1. Bar = 100 µm.

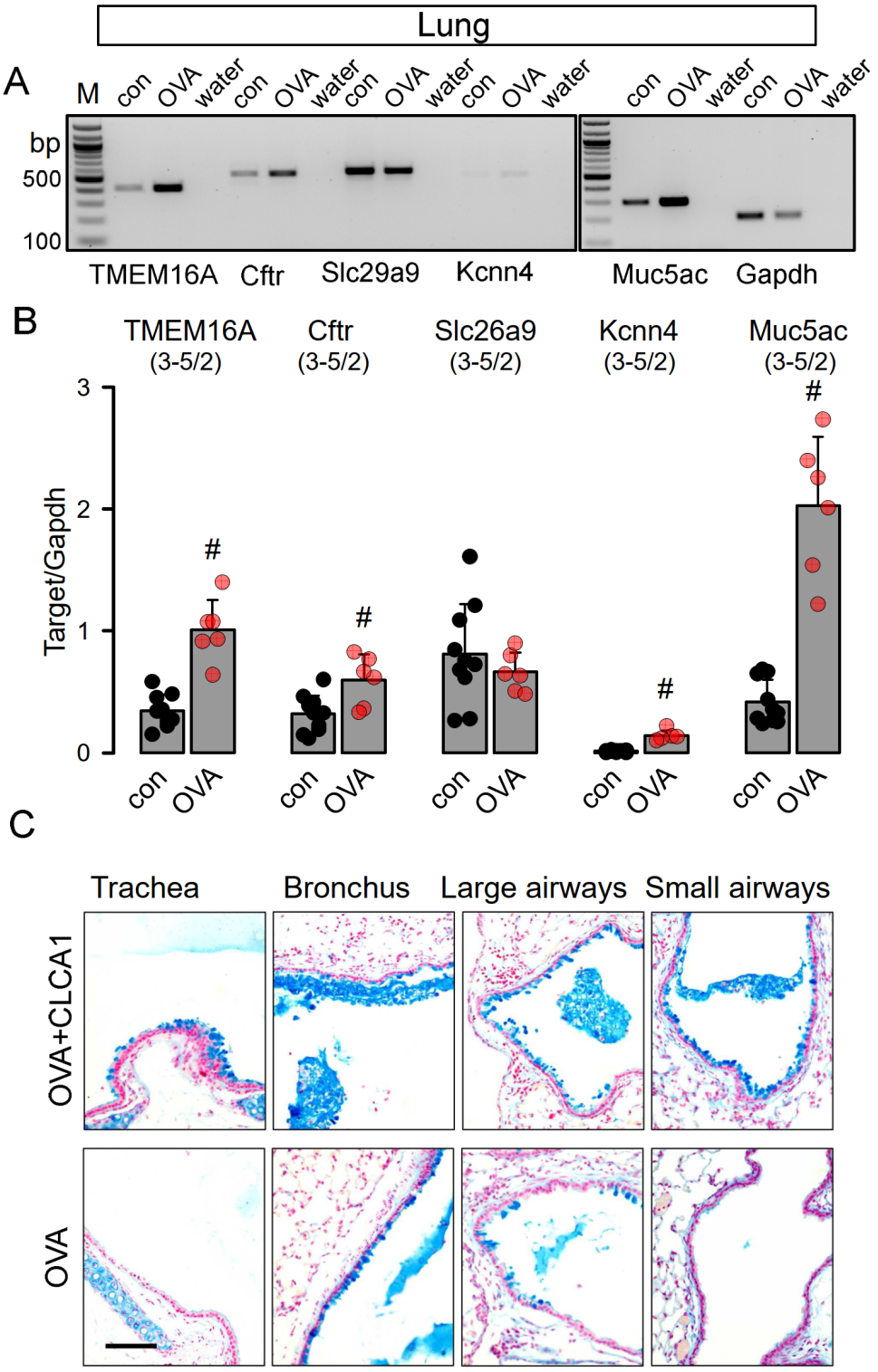

Figure 3.2 | *N-CLCA1 enhances mucus secretion in asthmatic mouse lungs in vivo.*
(A,B) Semiquantitative RT-PCR analysis of the expression of Tmem16a, Cftr, Slc26a9 and Kcnn4, and Muc5ac in lungs from control mice and OVA-treated mice. Expression of Tmem16a, Cftr, Kcnn4, and Muc5ac is enhanced in asthmatic (OVA) mice. Mean ± SEM (number of animals/number of experiments). #significant difference when compared to control ($p < 0.05$; unpaired t-test). (C) Alcian blue staining of airways from OVA-sensitized mice treated with N-CLCA1 (upper panel) and OVA-sensitized mice without additional treatment with N-CLCA1 (lower panel). N-CLCA1 induced additional secretion of mucus with enhanced accumulation of the mucus in central and peripheral airways. Bar = 100 µm.

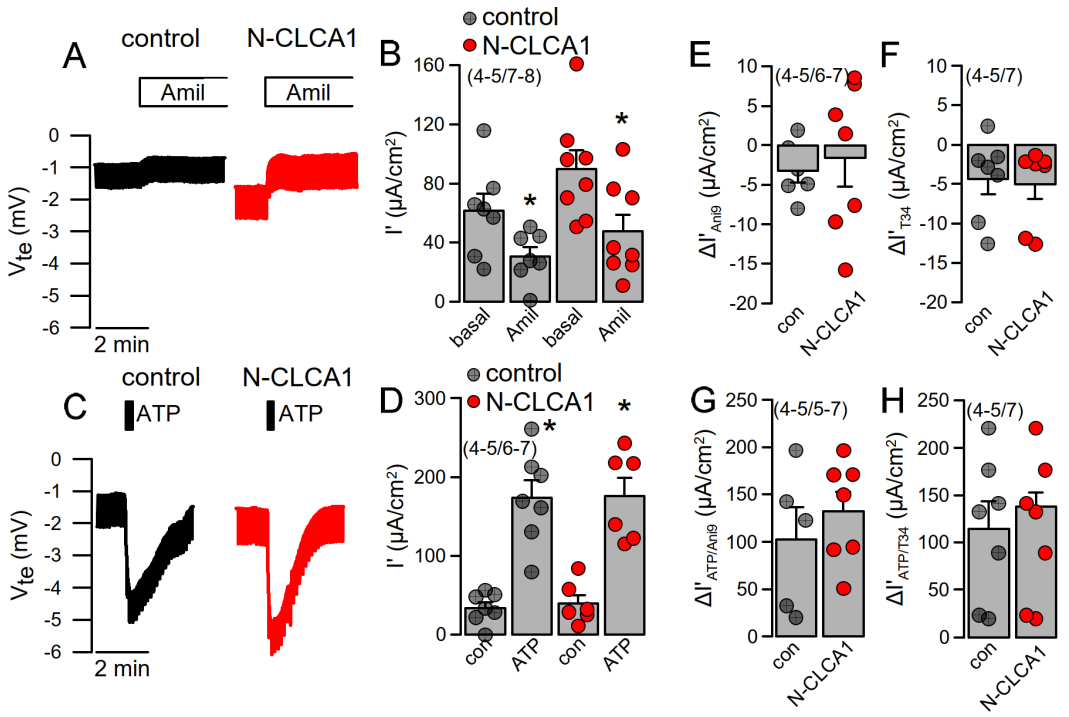

Figure 3.3 | *N-CLCA1 does not induce additional Ca^{2+}-activated Cl^- secretion in mouse tracheas.* A,B) Original Ussing chamber recording of the transepithelial voltages measured in mouse trachea under open circuit conditions and summary of the calculated equivalent short circuit current (I'). No significant changes in amiloride-sensitive (10 µM) Na^+ absorption was detected by 24 h exposure to N-CLCA1. C,D) No significant changes in ATP (luminal; 100 µM)—induced negative voltage deflection and ATP-activated I' was detected by N-CLCA1. E,F) N-CLCA1 did not induce an effect of Ani9 (10 µM) or TRAM-34 (100 nM) on basal currents. G,H) Effects of ATP in the presence of luminal Ani9 or basolateral TRAM-34 (T34) were independent of N-CLCA1. Mean ± SEM (number of animals/number of experiments). *significant effect of amiloride and ATP ($p < 0.05$; paired t-test).

Under control conditions, ATP activated only small ion currents in Calu3 cells. In contrast, ATP hyperpolarized the membrane voltage and clearly activated a whole cell K^+ current in cells exposed to IL-13 (Supplementary Figure 3.2F,G). Inhibition of KCNN4 by TRAM-34 abolished the ATP-induced hyperpolarization and induced a strong outward rectification Supplementary Figure 3.2F–H). Peak currents measured at the clamp voltage of +100 mV were similar in the absence or presence of TRAM-34. In the absence of TRAM-34, whole cell currents were dominated by KCNN4, while TMEM16A currents dominated in the presence of TRAM-34—i.e., in the absence of KCNN4 currents. In the absence of KCNN4 currents cells are depolarized which facilitates activation of voltage-dependent TMEM16A channels by increase in intracellular Ca^{2+}. In contrast, in the absence of TRAM-34, Ca^{2+}-dependent activation and hyperpolarization by KCNN4 inhibits activation of TMEM16A[227]. This is further supported in the human CF submucosal airway epithelial cell line 6CFSMEo-. This cell line demonstrates pronounced expression of both TMEM16A and KCNN4, but no or little expression of CFTR, CLCA1, and the potassium channel KCNQ1 (Supplementary Figure 3.3A). Stimulation by ATP

activated a whole cell K^+ current and hyperpolarized the membrane voltage, which was more pronounced than in Calu3 cells. The KCNN4 inhibitor TRAM-34 abolished hyperpolarization by ATP-dependent activation of KCNN4, but peak currents at +100 mV remained unchanged. The results demonstrate again a predominant activation of Ca^{2+}-activated K^+ currents by ATP inducing pronounced hyperpolarization, which counteracts activation of TMEM16A[227] (Supplementary Figure 3.3B,C). In contrast, TMEM16A is activated in the presence of TRAM-34 and the TMEM16A-blocker Ani9 fully inhibited ATP-activated whole cell currents (Supplementary Figure 3.3D).

Expression and plasma membrane localization of TMEM16A is enhanced by IL-13 and N-CLCA1, respectively

Above data indicate an upregulation of TMEM16A expression under asthmatic conditions and by the cytokine IL-13[191]. N-CLCA1, in contrast, did not induce expression of TMEM16A in Calu3 cells (Figure 3.4A). This is further supported by Western blotting of TMEM16A. IL-13 but not by CLCA1 enhanced expression of TMEM16A (Figure 3.4B). Immunofluorescence staining of TMEM16A demonstrated enhanced expression of TMEM16A upon treatment of Calu3 cells with the Th2-cytokine IL-13. CLCA1 did not increase the number of TMEM16A-positive cells but seemed to enhance membrane expression of TMEM16A (Figure 3.4C). Quantification of the immunofluorescence in the plasma membrane suggested an increase in plasma-membrane localization of TMEM16A by both IL-13 and N-CLCA1 (Figure 3.4D,E). We analysed whole cell currents activated by ATP in the absence and presence of N-CLCA1. In the absence of N-CLCA1 very little current was activated by ATP (Supplementary Figure 3.4). Upon exposure to N-CLCA1, cells were hyperpolarized by application of ATP, suggesting activation of KCNN4 K^+ channels. In the presence of TRAM-34 (T34), ATP no longer hyperpolarized cells and activated a more outwardly rectifying whole cell current, suggesting predominant activation of TMEM16A (Supplementary Figure 3.4). Taken together, N-CLCA1 increases KCNN4 currents, possibly by enhancing plasma membrane localization of TMEM16A, which has been shown earlier to increase intracellular Ca^{2+} signals elicited by ATP[141].

TMEM16A supports expression of SPDEF, the regulator of goblet cell metaplasia

RT-PCR analysis of SPDEF expression in Calu3 cells indicated upregulation by incubation with the cytokine IL-13 (Figure 3.5A,B). siRNA knockdown of TMEM16A inhibited upregulation of SPDEF by IL-13 suggesting a role of TMEM16A for expression of SPDEF. Moreover, densitometric quantification of SPDEF protein expression also indicated inhibition of SPDEF expression by the TMEM16A inhibitors niclosamide and Ani9 (upper and lower bands indicate glycosylated and non-glycosylated protein, respectively) (Figure 3.5C-D). Taken

together, TMEM16A expression and function controls expression of the master switch for goblet cell metaplasia, SPDEF[27,200,201].

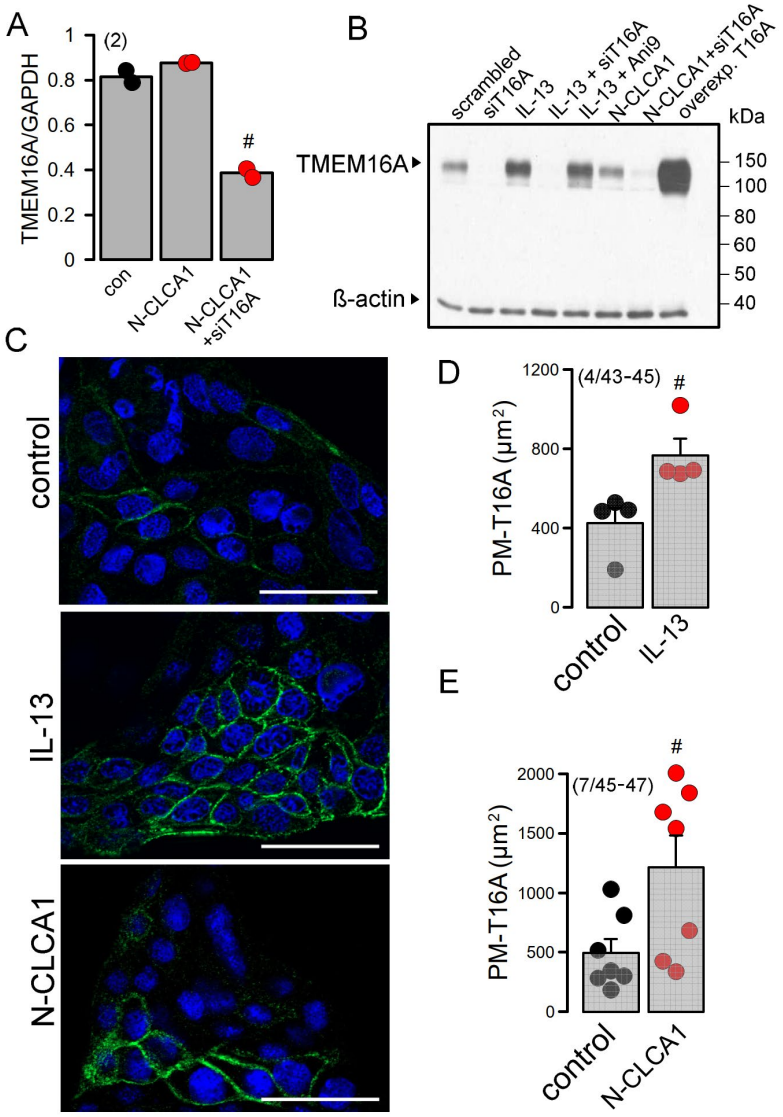

Figure 3.4 | *CLCA1 does not enhance expression of TMEM16A but stabilizes TMEM16A in the plasma membrane of Calu3 cells.*

(A) Semiquantitative RT-PCR shows no increase in TMEM16A expression by exposure to N-CLCA1. (number of measurements). (B) Western blot of TMEM16A indicates increase in expression by IL-13 but not by N-CLCA1. (C) Staining of TMEM16A in the plasma membrane indicates low expression in Calu3 cells. Exposure of Calu3 cells to IL-13 (20 ng/mL) increases expression of TMEM16A. N-CLCA1 does not increase the number of Calu3 cells expressing TMEM16A, but rather enhances membrane expression of TMEM16A in some cells. Bars = 50 µm. (D) Quantification of TMEM16A plasma membrane staining in the absence or presence of IL-13. (number of cover slips/number of cells). (E) Quantification of TMEM16A plasma membrane staining in the absence or presence of CLCA1. (number of cover slips/number of cells). Mean ± SEM #significant difference when compared to control or control ($p < 0.05$; unpaired t-test).

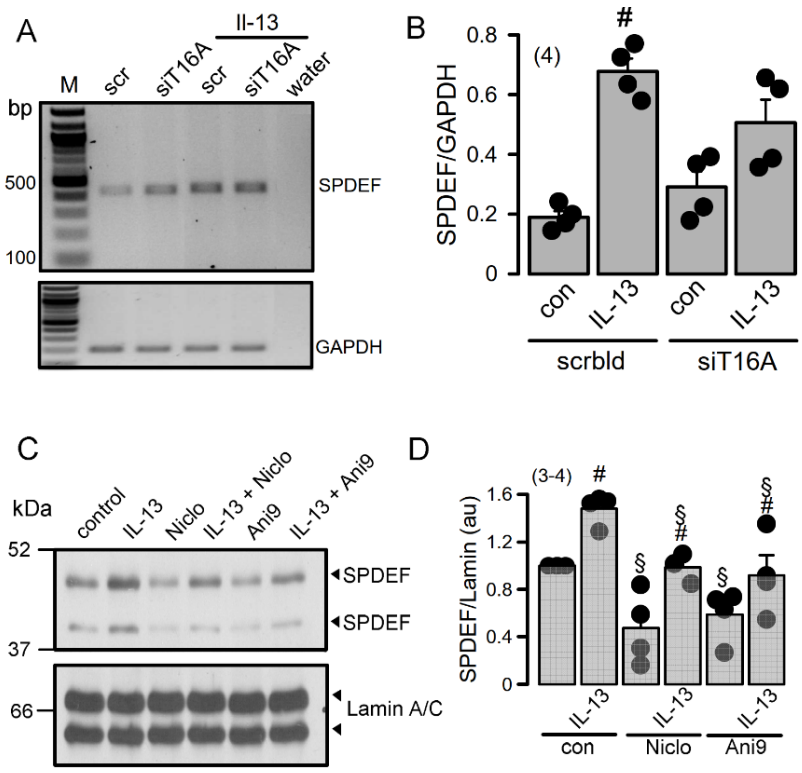

Figure 3.5 | *TMEM16A supports upregulation of the master switch for goblet cell metaplasia, SPDEF.* (A,B) RT-PCR analysis suggests inhibition of SPDEF expression by siRNA-knockdown of TMEM16A. (number of experiments). (C,D) Western blots indicating inhibition of SPDEF expression by inhibitors of TMEM16A. (number of experiments). Mean ± SEM. #significant difference when compared to scrambled, control, and IL-13, respectively ($p < 0.05$; unpaired t-test).

CLCA1-induced mucus production in polarized BCi-NS1 cells is TMEM16A-dependent

The present and previous data[191] suggest an important role of TMEM16A for IL-13 and CLCA1-induced mucus/MUC5AC production. We explored the role of TMEM16A/CLCA1 also in polarized grown BCi-NS1 human airway epithelial cells[191,228]. While expression of both TMEM16A and CLCA1 was very low in these cells, exposure of the cells to IL-13 increased expression of both proteins (Figure 3.6A). Interestingly, expression of TMEM16A was strongly reduced upon polarization of the cells, while expression of CLCA1 was upregulated (Figure 3.6B). Ussing chamber recordings under open circuit conditions demonstrated the typical negative voltage deflections upon stimulation with ATP, which were, however, not enhanced by IL-13 (Figure 3.6C,D). The basal properties of the BCi-NS1 cells were already reported in our previous study. The transepithelial resistance TEER (Rte) was >2 kΩcm^2 and was not affected by treatment with IL-13. Amiloride sensitive Isc was 9.8 µA/cm^2 for both control cells and cells stimulated with IL-13. Moreover, ATP-effects in the presence of Ani9 were similar in the absence or presence of IL-13 (Figure 3.6E). Exposure of the cells to N-CLCA1 upregulated mucus production, which was inhibited by simultaneous knockout of TMEM16A (siT16A, Figure 3.6F,G). The results obtained in these polarized airway epithelial cells confirm the important

role of TMEM16A not only for IL-13-induced goblet cell metaplasia [191], but also demonstrate an important function of TMEM16A in CLCA1-induced mucus production.

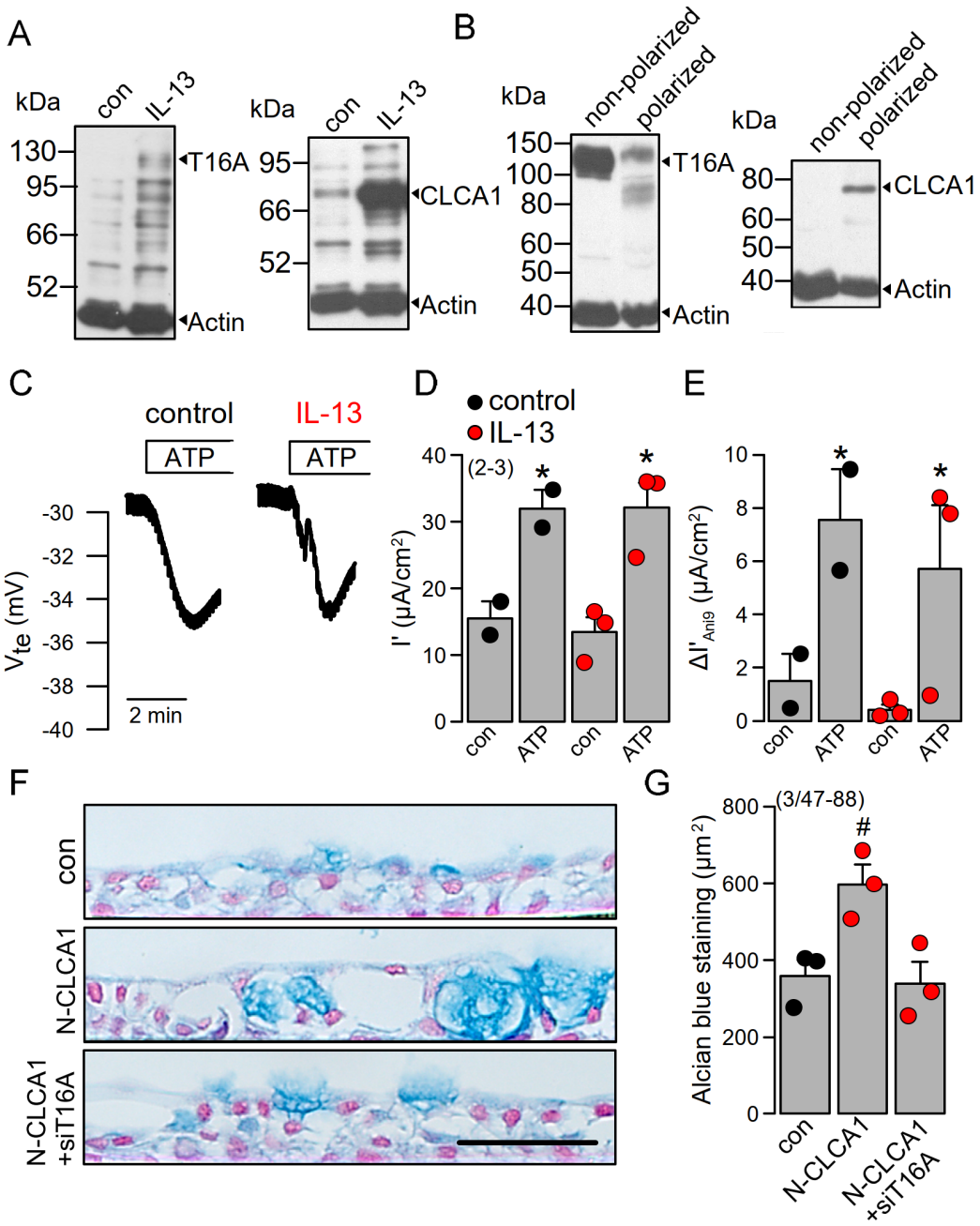

Figure 3.6 | *CLCA1-induced mucus production in polarized BCi-NS1 cells is TMEM16A-dependent.* A,B) Western blot indicating upregulation of CLCA1 expression in BCi-NS1 cells exposed to IL-13 (20 ng/mL). Expression of TMEM16A was found to be attenuated in polarized grown cells (filter-grown ALI-cultures), when compared to nonpolarized (plastic-grown) cells. In contrast, CLCA1 expression was upregulated in ALI cultures. (number of experiments). (C,D) IL-13 does not enhance ATP-induced (100 µM) negative voltage deflections and activation of short circuit currents (Isc). Activation of Isc was fully transient, i.e., the current returned to the baseline. E) The effect of the TMEM16A inhibitor Ani9 (10 µM) is not enhanced in IL-13 treated cells. (F,G) Individual examples and quantification of Alcian blue staining in polarized BCi-NS1 cells under control conditions, after exposure to N-CLCA1 or in cells treated with N-CLCA1 and siTMEM16A. Mucus expression is enhanced in N-CLCA1-treated cells, but the effect of

N-CLCA1 is blocked after knockdown of TMEM16A. (number of experiments). Scale bar = 50 µm. Mean ± SEM. #significant difference when compared to control ($p < 0.05$; unpaired t-test). *significant activation by ATP ($p < 0.05$; paired t-test).

Discussion

The calcium-activated chloride channel regulator 1 (CLCA1) was shown to be the most upregulated gene transcript (>100-fold) in a study with diisocyanate-induced asthmatic mice[106]. The ability of diisocyanate to induce CLCA1 was remarkable given the absence of Th2-type T cell cytokines IL-4 or IL-13. Because in this study the pro-asthmatic effects of diisocyanate were inhibited by crofelemer, the authors suggested a role for TMEM16A-upregulation of mucus and CLCA1. A role of TMEM16A in mucus production and mucus secretion was also suggested from our earlier studies[145,191] and a number of other reports[132,133,149,181,229,230]. Additionally, the present data suggest a role of TMEM16A in mucus production induced by CLCA1 in polarized airway epithelial cells (Figure 3.6). The expression levels of TMEM16A in mouse airways and polarized human airway epithelia are very low[137,214] and its contribution to Ca^{2+}-activated Cl^- secretion is rather limited (Figures 3.1, 3.6). Low expression of TMEM16A may not be misinterpreted as a missing role in mucus secretion[214]. A number of previous reports demonstrate TMEM16A as a membrane tether of the endoplasmic reticulum and a regulator of spatial sub-membranous Ca^{2+} signals[140,141,145]. Typically, expression of Ca^{2+}-regulating proteins such as IP_3 receptors or Ca^{2+} influx channels is scarce in terminally differentiated cells but is often enhanced when cells start proliferating. As described in our previous reports, TMEM16A expression is largely enhanced in proliferating cells[199,231,232].

The role of TMEM16A for Ca^{2+}-dependent Cl^- secretion in the airways may have been overestimated in previous studies. The reduced ATP-induced Cl^- secretion observed in the airways of TMEM16A-knockout mice[233,234] is at least in part due to the compromised function of CFTR[137-139,192,215,216]. Moreover, the use of nonspecific inhibitors of TMEM16A such as CaCCinhAO1, niclosamide, niflumic acid and others may also contribute to this overestimation. The present study also suggests that Ca^{2+}-activated KCNN4 K^+ channels are upregulated by Th2-dependent stimulation (IL-13, OVA) and are activated by purinergic stimulation, which hyperpolarizes the membrane voltage upon Ca^{2+}-dependent stimulation and disables activation of TMEM16A (Figure 3.2, Supplementary Figures 3.2-3.4). Activation of KCNN4 is essential to maintain the electrical driving force for Cl^- secretion during Ca^{2+}-dependent stimulation. Thus, we would disagree with a recent report that claims inhibition of KCNN4 to reduce Na^+ absorption and to improve mucociliary clearance in patients with cystic fibrosis[235]. In fact, airway surface liquid (ASL) in human airways relies essentially on submucosal gland secretion, which essentially need KCNN4. A number of papers indicate that basolateral Ca^{2+}-activated SK4-like potassium channels are required for chloride secretion by the airway epithelium[171,236-239].

Moreover, submucosal bicarbonate secretion also essentially requires activation of Ca^{2+}-dependent SK4 potassium channels[240,241]. Inhibition of KCNN4 is therefore likely to worsen CF-lung disease.

An important finding of the present study is the impact of TMEM16A expression and the TMEM16A inhibitors niclosamide and Ani9[147,242] on IL-13-induced expression of SPDEF. Airway epithelial SPDEF is a transcriptional regulator that integrates goblet cell differentiation and pulmonary Th2 inflammation[27,200,201]. This present observation may also help to explain why niclosamide had a clear inhibitory effect on mucus production in our previous study[150].

Accumulation of mucus in N-CLCA1-treated mice was an obvious finding of the present study (Figures 3.1, 3.2). CLCA1 may have enhanced membrane expression of TMEM16A and thereby may have increased mucus secretion. However, CLCA1 may have also contributed to unfolding and expansion of airway mucus, similar to unfolding of intestinal mucus[226,243]. Although CLCA1 was proposed to induce this effect by activating CaCC/TMEM16A *in vitro*[221,244], our present *in vivo* data do not indicate an upregulation of TMEM16A currents in mouse trachea. Thus, our data agree with other *in vivo* studies that indicate i) no contribution of CLCA1 chloride conductance in mouse airways[224] and ii) no inhibition of CLCA1-induced mucus expansion by TMEM16A channel blockers in mouse intestine[226]. Thus, results obtained *in vitro* may not necessarily reflect the situation *in vivo*. Along this line, we may refer to our previous observations that indicate a remarkable difference in functional regulation of TMEM16A, when comparing endogenous TMEM16A with overexpressed TMEM16A[196,245]. Data on the regulation of TMEM16A by CLCA1 obtained exclusively in heterologous expression systems may not necessarily apply *in vivo*. In conclusion, the regulator of TMEM16A, CLCA1, is a potent stimulus for mucus secretion and, surprisingly, for mucus production. However, CLCA1 had no measurable effect on TMEM16A-dependent Cl^- transport in naïve mouse airways and differentiated human airway epithelia, probably due to its low expression in fluid secretory cells. We speculate that activation of TMEM16A will probably not compensate for defective Cl^- secretion in cystic fibrosis.

Acknowledgements

This research was supported by the UK Cystic Fibrosis Trust SRC013, German Research Foundation (DFG) KU756/14-1, DFG SFB1350-A3, and Gilead Foundation. The technical assistance by Patricia Seeberger is greatly appreciated.

Supplementary material

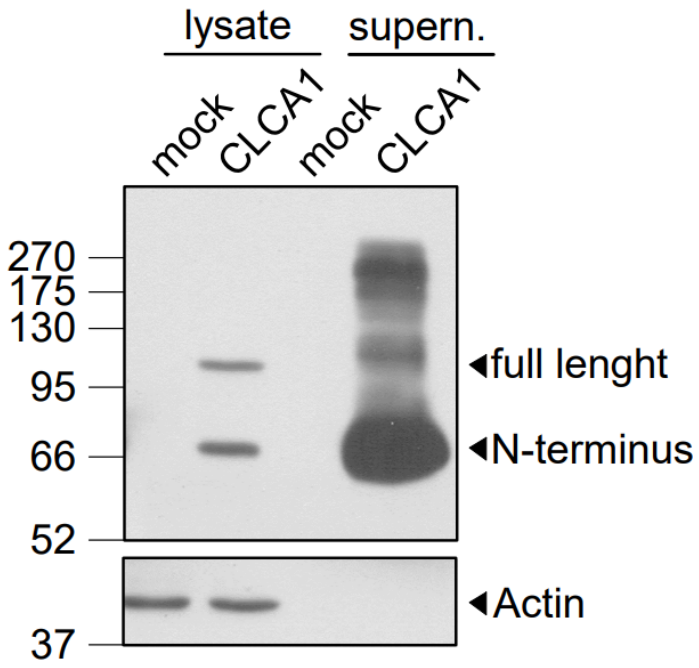

Supplementary Figure 3.1 | *CLCA1 produced in HEK293 cells.*

Cells were transfected with human CLCA1 plasmid and secreted CLCA1 was harvested in the supernatant. Western blot of full length CLCA1 and secreted CLCA1-N terminus (N-CLCA1) harvested in the supernatant.

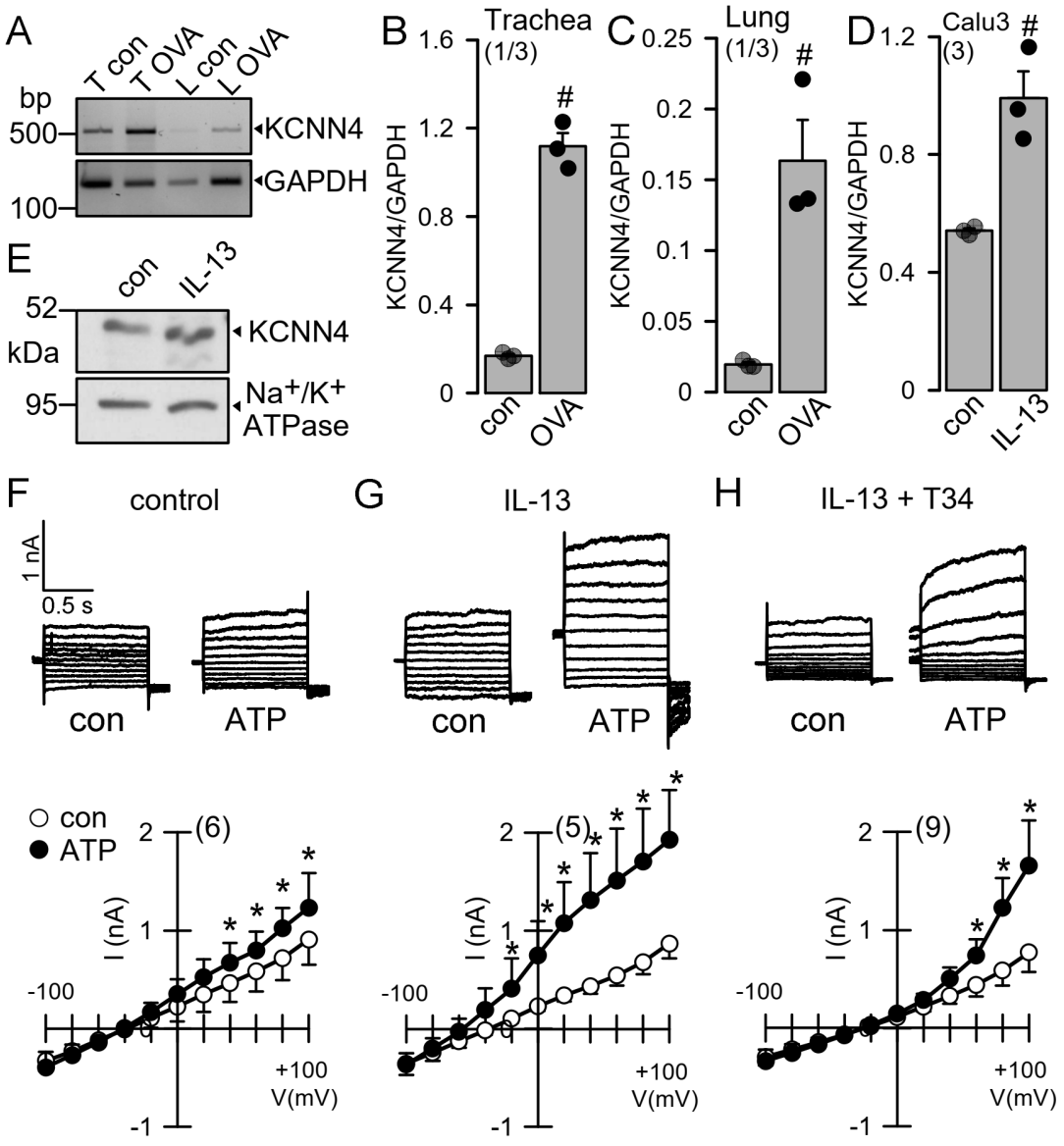

Supplementary Figure 3.2 | *Upregulation of KCNN4 channels in asthma.*

A-C) Original blot and summary for sqRT-PCR indicating upregulation of expression of the Ca^{2+}-activated K^+ channel KCNN4 in trachea (T) and lungs (L) of OVA-treated asthmatic mice. D) Summary of sqRT-PCR indicating upregulation of expression of KCNN4 in Calu3 airway epithelial cells after incubation with IL-13 (20 ng/ml). E) Western blot of KCNN4 expressed in Calu3 cells suggesting slight upregulation by IL-13. F-H) Whole cell patch clamp overlay currents and current/voltage relationships in Calu3 cells under control conditions, in the presence of IL-13, and in the presence of IL-13 and the KCNN4 blocker TRAM-34 (T34, 100 nM). ATP (100 µM) activated a whole cell current and hyperpolarized the membrane voltage in cells exposed to IL-13, suggesting predominant activation of KCNN4. In the presence of TRAM-34, whole cell currents were still activated but the membrane voltage remained depolarized. Application of ATP in the presence of the KCNN4-inhibitor Tram-34 depolarized the membrane voltage, indicating predominant activation of TMEM16A. Mean ± SEM (number of experiments). #indicates significant difference when compared to the absence of OVA or IL-13 ($p<0.05$; unpaired t-test). *indicates significant activation by ATP ($p<0.05$; paired t-test).

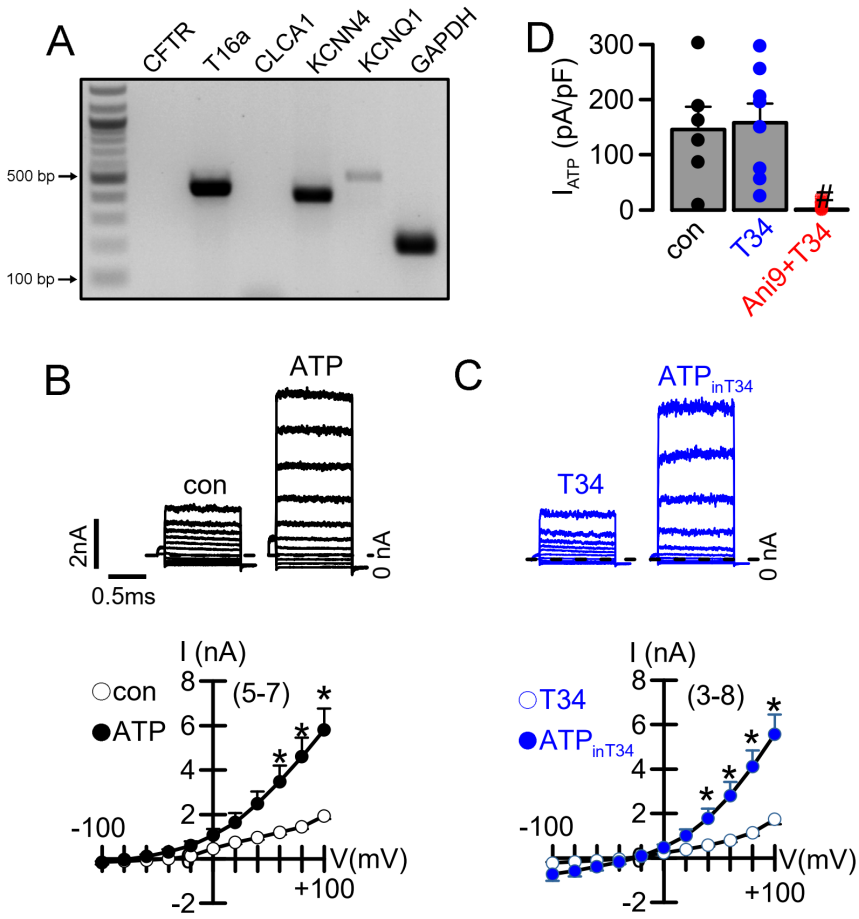

Supplementary Figure 3.3 | *Activation of TMEM16A and KCNN4 in 6CFSMEo- human submucosal glands.*

A) RT-PCR indicating pronounced expression of Ca^{2+}-dependent TMEM16A and KCNN4, with little or no expression of CFTR, CLCA1, or KCNQ1. B,C) Whole cell currents and current/voltage relationships activated by ATP (1 µM) in the absence or presence of the KCNN4-inhibitor Tram-34 (T34; 100 nM). In the absence of T34, cells were hyperpolarized by ATP, suggesting predominant activation of KCNN4 K^+ channels. In the presence of Tram-34, KCNN4 was blocked, and ATP depolarized the cells by activation of TMEM16A. D) Summary of ATP-activated whole cell currents in the absence or presence of inhibitors. Mean ± SEM (number of experiments). #indicates significant difference ($p<0.05$; unpaired t-test). *indicates significant activation by ATP ($p<0.05$; paired t-test).

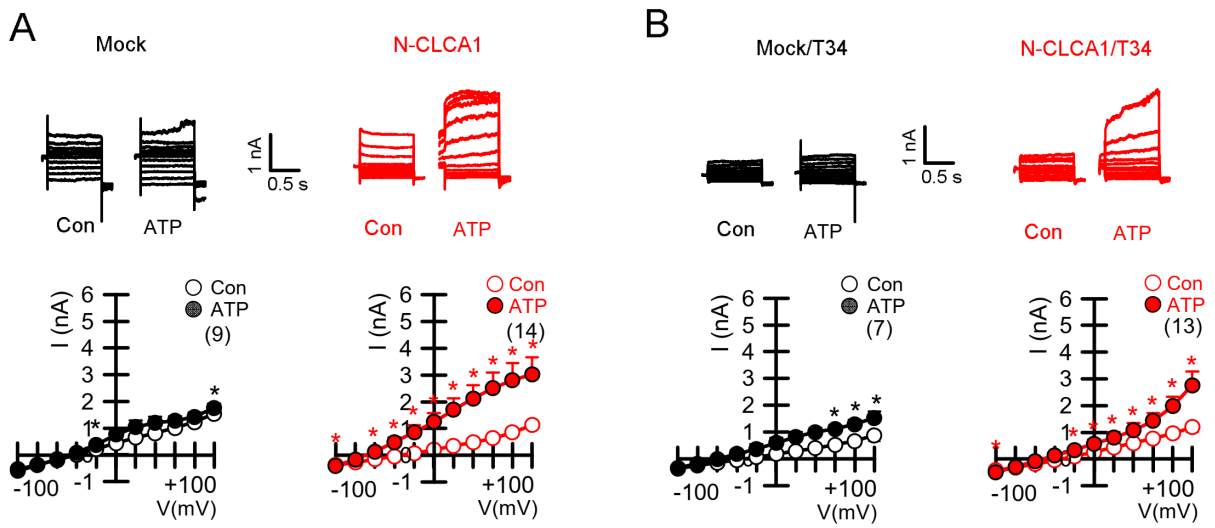

Supplementary Figure 3.4 | *Activation of whole cell currents by N-CLCA1.*
Whole cell currents and current/voltage relationships in Calu3 cells under control conditions and after exposure to CLCA1 N-terminus (N-CLCA1) in the absence (A) or presence (B) of the KCNN4-inhibitor TRAM-34 (T34; 100 nM). ATP (100 µM) activated a whole cell current and hyperpolarized the membrane voltage after incubation of the cells with N-CLCA1, suggesting predominant activation of KCNN4 K^+ channels. In the presence of TRAM-34, KCNN4 currents were inhibited, and ATP no longer hyperpolarized the cells. In the presence of TRAM-34, I/V relationships were more outwardly rectifying and peak currents at +100 mV were similar as in the absence of TRAM-34. The data indicate that upon increase in intracellular Ca^{2+}, Calu3 cells activate predominantly KCNN4 K^+ currents. Mean ± SEM (number of experiments). *indicates significant activation by ATP ($p<0.05$; paired t-test).

CHAPTER 4 | AIRWAY DELIVERY OF HYDROGEL-ENCAPSULATED NICLOSAMIDE FOR THE TREATMENT OF INFLAMMATORY AIRWAY DISEASE

Abstract

Repurposing of the anthelminthic drug niclosamide was proposed as an effective treatment for inflammatory airway diseases such as asthma, cystic fibrosis, and chronic obstructive pulmonary disease. Niclosamide may also be effective for the treatment of viral respiratory infections, such as SARS-CoV-2, respiratory syncytial virus, and influenza. While systemic application of niclosamide may lead to unwanted side effects, local administration via aerosol may circumvent these problems, particularly when the drug is encapsulated into small polyethylene glycol (PEG) hydrospheres. In the present study, we examined whether PEG-encapsulated niclosamide inhibits the production of mucus and affects the pro-inflammatory mediator CLCA1 in mouse airways *in vivo*, while effects on mucociliary clearance were assessed in excised mouse tracheas. The potential of encapsulated niclosamide to inhibit TMEM16A whole-cell Cl^- currents and intracellular Ca^{2+} signalling was assessed in airway epithelial cells *in vitro*. We achieved encapsulation of niclosamide in PEG-microspheres and PEG-nanospheres (Niclo-spheres). When applied to asthmatic mice via intratracheal instillation, Niclo-spheres strongly attenuated overproduction of mucus, inhibited secretion of the major proinflammatory mediator CLCA1, and improved mucociliary clearance in tracheas *ex vivo*. These effects were comparable for niclosamide encapsulated in PEG-nanospheres and PEG-microspheres. Niclo-spheres inhibited the Ca^{2+} activated Cl^- channel TMEM16A and attenuated mucus production in CFBE and Calu-3 human airway epithelial cells. Both inhibitory effects were explained by a pronounced inhibition of intracellular Ca^{2+} signals. The data indicate that poorly dissolvable compounds such as niclosamide can be encapsulated in PEG-microspheres/nanospheres and deposited locally on the airway epithelium as encapsulated drugs, which may be advantageous over systemic application

Keywords: TMEM16A; TMEM16F; asthma; inflammatory airway disease; Covid-19; hydrospheres; nano-spheres; niclosamide

Published as: Ousingsawat J., **Centeio R.**, Cabrita I., Talbi K., Zimmer O., Graf M., Göpferich A., Schreiber R., Kunzelmann K. Airway Delivery of Hydrogel-Encapsulated Niclosamide for the Treatment of Inflammatory Airway Disease. *International Journal of Molecular Sciences*. 2022 Jan; 23(3): 1085.

Own experimental contribution: Ovalbumin-sensitization of animals; intratracheal instillation

of Niclosamide formulations; mouse lungs isolation.

Own written contribution: Original draft preparation, review and editing.

Other contributions: Designed experiments and analysed data.

Introduction

Previous work showed that the inhibition of the Ca^{2+} activated Cl^- channel TMEM16A inhibits excessive mucus production in inflammatory airway diseases such as asthma and cystic fibrosis (reviewed in[135]). TMEM16A is upregulated in cystic fibrosis and asthma, which accompanies goblet cell metaplasia (in asthma) and goblet cell hyperplasia (in cystic fibrosis) and mucus hypersecretion[132,149]. TMEM16A is also upregulated by bacterial components[134,191,246]. Upregulation of TMEM16A is predominant in mucus-producing cells located in airway submucosal glands, and to a lesser degree in ciliated epithelial cells[132,133,246]. Moreover, TMEM16A and the related protein TMEM16F contribute to the ferroptotic death of airway epithelial cells, caused by Pseudomonas aeruginosa-induced plasma membrane lipid peroxidation[247,248]. TMEM16F was also shown to be central to syncytia formation observed in the lungs of patients with severe Covid-19[249]. The syncytia formation is triggered when SARS-CoV-2 spike (S) proteins bind to angiotensin converting enzyme type 2 (ACE2) receptors on the surface of neighbouring cells[250]. This may contribute to viral dissemination, immune evasion, and inflammatory response. Thus, TMEM16 proteins are highly relevant therapeutic targets in asthma, cystic fibrosis, and viral lung infections caused by SARS-CoV-2, respiratory syncytial virus, or influenza[249,251]. Although these predominantly airway-located diseases are of very different origin, involving distinct cytokines and patho-mechanisms, they have a participation of one (TMEM16A) or two (TMEM16A and TMEM16F) members of the TMEM16-family of proteins in common. Therefore, a drug that inhibits the activity of several TMEM16-members by means of lowering Ca^{2+}-dependent activation may be useful in the therapy of these airway diseases[196].

The anthelminthic drug niclosamide and related substances such as nitazoxanide were proposed as repurposed drugs for the treatment of asthma, cystic fibrosis, and chronic obstructive pulmonary disease[135,147,150]. Niclosamide is a potent inhibitor of TMEM16A and TMEM16F[147,150,196] and causes bronchorelaxation *in vivo* and *ex vivo*. It potently inhibited mucus production and mucus secretion, and strongly suppressed the release of the cystic fibrosis-typical interleukin IL-8[147,150,246]. Moreover, it was also shown to attenuate lung vascular remodelling in experimental pulmonary arterial hypertension[252]. During the screening of libraries containing FDA-approved drugs, niclosamide was also identified as a potent inhibitor of the replication of severe acute respiratory corona virus[253]. Niclosamide inhibits endosomal acidification, and may also act via additional mechanisms, thereby inhibiting virus uptake and virus replication[254-256]. It acts as a proton shuttle, which explains its broad antiviral activity[257].

TMEM16A and other TMEM16 family members also control intracellular Ca^{2+} levels[141,258]. As SARS-CoV-2 and other viruses hijack intracellular Ca^{2+} signalling to benefit their infection and replication, the inhibition of intracellular Ca^{2+} signalling by the TMEM16-inhibitor niclosamide may contribute to its antiviral activity[259-261]. Currently, niclosamide and the related compound nitazoxanide are under investigation in numerous clinical trials to determine their efficacy in the treatment of Covid-19 (clinicaltrials.org)[212,262-264].

Niclosamide has very low water solubility between 0.23 and 1.6 µg/mL under ambient conditions. This is the reason for poor intestinal absorption causing only low plasma levels when applied orally[265]. To enhance its bioavailability, nanoparticle formulations were developed and injected into rats intra-muscularly, which reached peak plasma concentrations of about 4.3–9.4 µM, when applied at 50–300 mg/kg[266]. The systemic application of encapsulated niclosamide might cause high systemic plasma levels, which could result in unwanted side effects. We therefore examined the effects of a local application of encapsulated niclosamide to mouse airways. In a similar approach, the successful delivery of antibiotics to airways using nanocarriers has been reported previously[267]. We found that similar to intratracheal application of the dissolved compound[150], niclosamide encapsulated in polyethylene glycol hydrogels shows potent mucus-suppressing and anti-inflammatory effects, and improves mucociliary clearance. The effects induced by intratracheal application *in vivo* could be reproduced *in vitro*. Along with these additional results, which indicate the inhibition of TMEM16A by suppression of intracellular Ca^{2+} signals, we propose niclosamide encapsulated in PEG-microspheres/nanospheres as an effective topical treatment of inflammatory airway disease.

Materials and Methods

Preparation of niclosamide-loaded PEG-spheres: For the fabrication of hydrogel microparticles, eight-armed poly(ethylene glycol) macromonomers with a molecular mass of 10,000 Da (8armPEG10k) were functionalized at its hydroxyl groups with norbornene moieties via an ester bond (8armPEG10k-e-NB), as described earlier[268]. A hydrolytically cleavable PEG-linker with thiol-groups (PEG1k-e-MPA) was prepared by end-functionalizing PEG1k in a similar manner to an esterification method described previously[268]. In brief, PEG, mercaptopropionic acid (8-fold molar excess of PEG OH-groups) and 0.4 mmol p-toluenesulfonic acid were dissolved in toluene. The reaction mixture was subsequently refluxed in a Dean–Stark apparatus under stirring for 24 h. Toluene was removed via a rotary evaporator, and the product was precipitated thrice in ice cold diethyl ether. 1H NMR showed a conversion rate of 93.3%, whereas the total yield amounted to 92.6%. A stock niclosamide suspension (Thermo Fisher Scientific, Waltham, USA) was prepared via wet-milling of 2.1 g NCL with 0.21 g Tween 20 and 4.5 mL MilliQ in a 25 mL stainless-steel milling cup with stainless-steel balls (Ø = 1 mm)[269].

Cycles (n = 5) of milling for 30 min at 600 rpm were applied with a 30 min cooling time in between. The resulting suspension was centrifuged down and the residue was resuspended in MilliQ by sonication for 30 min. The resulting Particle size distribution was determined by laser diffraction measurement (Mastersizer 2000, Malvern Panalytical Ltd, Malvern, United Kingdom) (d10 = 0.106 µm/d50 = 0.543 µm/d90 = 3.937 µm), and the NCL-content of 91.5 mg/mL was measured via UV-Vis (Kontron Uvikon 941, Goebel Instrumentelle Analytik GmbH, Au in der Hallertau, Germany) at 345 nm. A bulk hydrogel containing niclosamide particles was prepared by crosslinking a solution of 72.25 mg 8armPEG10k-e-Norb and 28.9 mg PEG1k-e-MPA in 0.739 mL MilliQ with Eosin Y (0.1 mM) and additional 110.5 µL niclosamide stock by irradiation with green light (525 nm) for 20 min[270]. Freeze drying for 125 h with a starting shelf temperature of −40 °C and 0.01 mbar and subsequently 5 h at a 10 °C shelf temperature yielded a dry gel. For the preparation of inhalable PEG-hydrogel particles, bulk freeze-dried hydrogels were cut into pieces of about 1 mm edge length and mixed with LH 70 lactose-particles (MEGGLE Group GmbH, Wasserburg am Inn, Germany) to yield 10% wt. PEG-content. The resulting mixture was pre-milled in a Retsch PM100 planetary ball mill, using a 25 mL stainless-steel milling cup with 7 stainless-steel balls (Ø = 10 mm). The powders underwent 5 cycles of 2:15 min milling at 600 rpm and 14 min cooling time. Pre-ground powders were finally milled 3 times in a McOne (Jet-pharma SA, Balerna, Switzerland) lab scale jet-mill at 12–13 bar venturi pressure and 9–10 bar grinding pressure (Linde 4.0 nitrogen). Particle size distributions of rehydrated hydrogel particles were determined as d10 = 4.332 µm, d50 = 11.310 µm, and d90 = 45.932 µm via laser diffraction (Malvern Mastersizer 2000). The refractive index of PEG-particles was chosen as 1.430 and the absorption as 0.01 based on previous investigations[268].

PEG-coated nanospheres were prepared via previously described sequential nanoprecipitation[271] of niclosamide and methoxy-terminated poly(ethylene glycol)5k-b-poly(D,L-lactide)10k (MeO-PEG5k-PLA10k). MeO-PEG5k-PLA10k synthesis was previously published [272,273]. First, we prepared a 0.01 mg/mL stock solution of niclosamide in DMSO:DMF (1:1 v/v ratio) (NIC-ss) and 0.02 mg/mL stock solutions of niclosamide and MeO-PEG5k-PLA10k in DMSO:DMF (1:1 v/v ratio), which were mixed in a 1:1 ratio (NIC/PEG-PLA-ss). To each of three 50 µL samples of NIC-ss (uncoated nanospheres) or NIC/PEG-PLA-ss (PEG-coated nanospheres), 950 µL MilliQ H2O was added and the reaction was thoroughly homogenized. The three reactions were mixed and up-concentrated using a 30 kDa cut-off Microsep advance centrifugal device (2000 rcf, 15 min). This process was repeated ten times for further up-concentration of the nanospheres. The preparation yielded approximately 300 µL of the niclosamide-nanosphere solution equivalent to 150 µM niclosamide. Nanospheres were characterized using dynamic light scattering on a ZetaSizer Nano ZS using 633 nm He-Ne laser at a backscatter angle of 173° (Malvern Instruments GmbH, Lappersdorf, Germany). The

hydrodynamic diameter (dh) and polydispersity-index (PDI) were measured for uncoated nanospheres (dh = 97.3 ± 3.8 nm, PDI = 0.09 ± 0.03; mean ± std) as well as for PEG-coated nanosphere before (dh = 91.1 ± 7.4 nm, PDI = 0.16 ± 0.04; mean ± std) and after up-concentration (dh = 125 ± 3.1 nm, PDI = 0.25 ± 0.02; mean ± std).

Animals and treatments: Allergen challenge of mice has been described previously[190]. In brief, mice were sensitized to ovalbumin (OVA; Sigma-Aldrich, St. Louis, MO, USA) by an intraperitoneal (I.P.) injection of 100 µg OVA in 100 µL aluminium hydroxide gel adjuvant (InvivoGen, San Diego, CA, USA) on days 0 and 14. At days 21 to 23, mice were anesthetized (ketamine 90–120 mg/kg and xylazine 6–8 mg/kg) and challenged to OVA by intratracheal (I.T.) instillation of 50 µg OVA in 100 µL saline with or without Niclosamide or Niclosamide-enclosing micro- and nanoparticles for a final concentration of 30 µM Niclosamide. Control mice were sham sensitized with aluminium hydroxide gel and challenged to saline by I.T. instillation. The allergen reaction was allowed to develop for 72 h, while all niclosamide instillations were maintained for days 24 and 25. Animals were sacrificed, and tissues were collected on day 26. All animal experiments complied with the guidelines for animal research and were carried out in accordance with the 'United Kingdom Animals Act, 1986' and associated guidelines, as well as EU Directive 2010/63/EU for animal experiments. All animal experiments were approved by the local Ethics Committee of the Government of Unterfranken/Wurzburg (AZ: 55.2-2532-2-55.2.2-2532-2-1359-15, approved 11.03.2021) and were conducted according to the guidelines of the American Physiologic Society and German Law for the Welfare of Animals.

Cell culture and treatments: All cells were grown at 37 °C in a humidified atmosphere with 5% CO2. Calu-3 human airway epithelial cells were grown in DMEM/Ham's F-12 with L-Glutamine medium supplemented with 10% (v/v) foetal bovine serum (FBS), 1% (v/v) L-glutamine 200 mM, and 1% (v/v) HEPES 1 M (all from Capricorn Scientific, Ebsdorfergrund, Germany). Cells were treated with IL-13 (20 ng/mL; Enzo Life Sciences, Lörrach, Germany) for 72 h in Opti-MEM, and the treatment was refreshed every day. The human airway cell line CFBE was cultured as described previously[192]. Cells were treated with niclosamide encapsulated in polyethylene glycol (PEG) hydrogel microspheres. The final concentration of niclosamide was calculated on the basis that niclosamide accounted for 1% of the microsphere's weight and the equivalent niclosamide concentration in nanospheres.

MUC5AC and Alcian blue analysis: Mouse airways were fixed by transcardial perfusion and lung perfusion by tracheal instillation via tracheostomy of a fixative solution containing 4% PFA in PBS. Tissues were left in a fixative solution overnight and embedded in paraffin the next day. Furthermore, 5 µm cuts were deparaffinized, stained with standard Alcian blue solution, and

counterstained with Nuclear Fast Red solution (Sigma-Aldrich, St. Louis, MO, USA). After dehydration and clearing steps, whole mouse lungs or sections were mounted in DePeX mounting medium (SERVA Electrophoresis, Heidelberg, Germany). Stainings were assessed by light microscopy. Mucus-stained areas were determined using ImageJ. For MUC5AC stainings, Calu-3 airway cells seeded onto glass coverslips were fixed with 4% PFA/PBS for 10 min at room temperature, washed in PBS with Ca^{2+} and Mg^{2+}, incubated in 0.5% Triton X-100/PBS for 10 min at room temperature, washed, blocked with 1% BSA/PB^{++} for 40 min at room temperature, incubated with mouse monoclonal anti-MUC5AC antibody (1:300 in 1%BSA/PBS; ab3649; Abcam, Cam-bridge, UK) for 1 h at 37 °C, washed, incubated with Alexa Fluor 488-labeled donkey anti-mouse IgG (1:300 in 1%BSA/PBS, Invitrogen, Carlsbad, California, USA), and counterstained with Hoe33342 (1:200) for 1 h at room temperature. Cells were then washed and mounted in a fluorescence mounting medium. MUC5AC-staining was quantified using ImageJ FIJI version 1.53e (National Institutes of Health, Bethesda, MD, USA)[274].

Immunocytochemistry of mCLCA1 and CD44: Mouse lungs were fixed by transcardial and lung perfusion fixation. Mouse airways were embedded in paraffin, and tissue sections (5 µm) were stained using the standard protocol for immunofluorescence. CD44 and CLCA1 were detected using rat anti-CD44 conjugated with PE-Cyanine7 (Invitrogen, Dreieich, Germany) and rabbit anti-mouse Clca3 antibody (ab46512, Abcam, Berlin, Germany), respectively. The nucleus was counterstained with 5 µM Hoe33342 (Thermo Fisher Scientific, Darmstadt, Germany). Immunofluorescence was detected with an Axio Observer microscope equipped with Axiocams 503 mono, ApoTome.2, and ZEN 3.0 (blue edition) software (Zeiss, Oberkochen, Germany). Stitching microscopy was performed using a motorized Axio Observer and Zen software[275].

Microscopic measurements of mucociliary clearance: Mucociliary clearance *ex vivo* was performed by tracking fluorescence particles' movement (modified method from[276]). Briefly, tracheas were removed and cut longitudinally down the middle of the tracheal cartilage rings. The trachea was placed in the self-made slide. Fluorescent particles (FluoSphere carboxylate, 1.0 µm, Invitrogen, Dreieich, Germany) were applied and particles' movement was tracked every 0.2 s for 5 min at room temperature using Axiocams 503 mono and ZEN 3.0 (blue edition) software (Zeiss, Oberkochen, Germany). The fluorescent bead velocity was measured by ImageJ software using the Manual tracking plugin.

Patch clamp: Cells were patch clamped when grown on coated glass coverslips. Coverslips were mounted in a perfused bath chamber on the stage of an inverted microscope (IM35, Zeiss) and kept at 37 °C. Patch pipettes were filled with a cytosolic-like solution containing (in mM): KCl 30, K-Gluconate 95, NaH_2PO_4 1.2, Na_2HPO_4 4.8, EGTA 1, Ca-Gluconate 0.758, $MgCl_2$ 1.03, D-Glucose 5, ATP 3; pH 7.2. The intracellular (pipette) Ca^{2+} activity was 0.1 µM. The bath was perfused continuously with standard bicarbonate-free Ringer's solution (in mM: NaCl 145, KH_2PO_4 0.4, K_2HPO_4 1.6, Glucose 5, $MgCl_2$ 1, Ca-Gluconate 1.3) at a rate of 8 mL/min. Patch pipettes had an input resistance of 2–5 MΩ and whole-cell currents were corrected for serial resistance. Currents were recorded using a patch clamp amplifier EPC9, and PULSE software version 8.65 (HEKA, Lambrecht, Germany) as well as Chart software version 5.5.4 (AD Instruments, Spechbach, Germany). Cells were stimulated with 1 µM ATP in the absence and presence of TRAM34. In regular intervals, membrane voltage (Vc) was clamped in steps of 20 mV from −100 to +100 mV from a holding voltage of −100 mV. The current density was calculated by dividing whole-cell currents by cell capacitance.

Measurement of $[Ca^{2+}]_i$: Cells were seeded on coated glass coverslips and loaded with 2 µM Fura-2, AM Ester (Biotium, Hayward, CA, USA) and 0.02% Pluronic F-127 (Invitrogen, Carlsbad, CA, USA) in standard bicarbonate-free Ringer's solution for 1 h at room temperature. The measurement of intracellular Ca^{2+} concentrations has been described earlier[192]. Cells were then mounted in a thermostatically controlled imaging chamber adapted to an inverted microscope (Axiovert S100, Zeiss, Oberkochen, Ger-many), maintained at 37 °C and perfused at a rate of 5 mL/min. Fura-2 was excited at 340/380 nm using a high-speed polychromatic illumination system for microscopic fluorescence measurements (Visitron Systems, Puchheim, Germany), and the emission was recorded between 470 and 550 nm using a CoolSnap HQ CCD camera (Roper Scientific, Planegg, Germany/Visitron Systems, Puchheim, Germany). Cells were stimulated with 1, 10, and 100 µM ATP in standard bicarbonate-free Ringer's solution. Intracellular calcium ($[Ca^{2+}]_i$) was calculated from the 340/380 nm fluorescence ratio after background subtraction using the formula $[Ca^{2+}]_i$ = Kd x (R-Rmin)/(Rmax-R) x (Sf2/Sb2), where R is the observed fluorescence ratio. The values Rmax and Rmin (maximum and minimum ratios) and the constant Sf2/Sb2 (ratio between the fluorescence of free and Ca^{2+}-bound Fura-2 at 380 nm) were determined using 2 µM ionomycin (Calbiochem, San Diego, CA, USA), 5 µM nigericin (Sigma-Aldrich, St. Louis, MO, USA), 10 µM monensin (Sigma-Aldrich, St. Louis, MO, USA), and 5 mM EGTA (Carl Roth, Karlsruhe, Germany) to equilibrate intracellular and extracellular Ca^{2+} in intact Fura-2-loaded cells. The dissociation constant (Kd) for the Fura-2• Ca^{2+} complex was taken as 224 nM[194]). Control of the experiment, imaging acquisition, and data analysis was conducted with the software package MetaFluor (Universal Imaging, Bedford Hills, New York, NY, USA)[194].

Materials and Statistical Analysis: All compounds used were of the highest available grade of purity and were bought from Sigma-Aldrich (St. Louis, MO, USA), unless indicated otherwise. Data are shown as individual traces/representative images and/or as summaries with mean values ± SEM, with the respective number of experiments given in each figure legend. The data have been tested for a normal distribution. As the effects have been examined in individual animals, which naturally vary with respect to their responses, outliers have not been removed. Tracings and current–voltage relationships are shown as original data and were not fitted. For statistical analysis, paired or unpaired Student's t-test or ANOVA were used as appropriate. A p-value of < 0.05 was accepted as a statistically significant difference.

Results

Niclosamide-loaded microspheres and nanospheres (niclo-spheres) inhibit mucus production in airways of asthmatic mice

Hydrogel microparticles with a molecular mass of 10,000 Da were generated with an approximate spherical particle size of the rehydrated particle between 4 and 45 µm. PEG-coated nanospheres were prepared by sequential nanoprecipitation[271], leading to particles with hydrodynamic diameters of around 97–125 nm. Ovalbumin (OVA)-sensitization was used as a common method to induce allergic asthma in rodents[190]. We detected goblet cell metaplasia and strong upregulation of mucus production in the airways of OVA-sensitized mice (Figure 4.1A). Intratracheal application of Niclo-spheres (containing 30 µM niclosamide) strongly reduced mucus production in the airways of OVA-sensitized mice (Figure 4.1A,B). The effects of niclosamide encapsulated in microspheres or nanospheres were comparable. Thus, niclosamide is efficient in suppressing mucus production when applied as a dissolved powder, as demonstrated earlier[150,246], or when deposited as Niclo-spheres. Although no direct comparison was conducted regarding the efficacy of Niclo-spheres versus dissolved niclosamide, the effect reported earlier for dissolved niclosamide[150] and the present data appear quite comparable.

Accumulation of mCLCA1 in club cells by treatment with niclo-spheres

CLCA1 (Calcium-activated chloride channel regulator 1) is upregulated in airway epithelial cells during airway inflammation[277]. CLCA1 is a secreted metalloproteinase that modulates the function of TMEM16A[221], drives mucus production[278], and shows additional pleiotropic effects during airway inflammation[279]. We analysed CLCA1 in the airways of OVA-sensitized and healthy control animals and found enhanced expression of CLCA1 in the

airways of OVA-treated animals. An in-depth analysis of CLCA1 expression was performed using stitching microscopy[275]. The release of CLCA1 from secretory cells appeared to be inhibited by Niclo-spheres (30 µM for 5 days intratracheal application) and thus accumulated in secretory (club) cells (Figure 4.2A–C). Thus, niclosamide inhibits the release of CLCA1, similar to its inhibitory effect on mucus secretion described earlier[191]. The data suggest encapsulated niclosamide as an effective anti-inflammatory treatment in asthma and other inflammatory airway diseases.

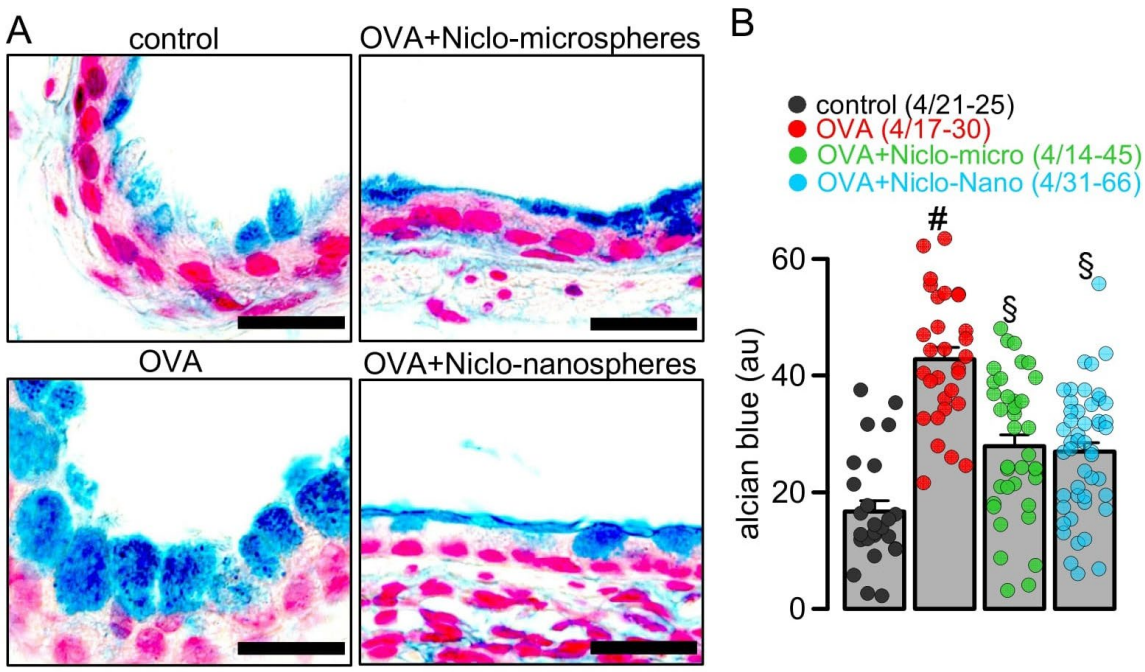

Figure 4.1 | *Inhibition of mucus production by Niclo-spheres of micrometer and nanometer size.*
(A) Airway mucus staining by Alcian blue in control mice and asthmatic mice sensitized with ovalbumin (OVA). Intratracheal instillation of niclosamide (Niclo)-loaded microspheres (0.98 mg; 30 µM niclosamide) or nanospheres (0.196 mg; 30 µM niclosamide) strongly reduced mucus production in bronchi of asthmatic mice. Bar = 50 µm. (B) Summary of experiments as shown in (A). Mean ± SEM (number of animals/number of bronchi analyzed). #significant difference from control. §significant difference from OVA ($p < 0.05$, ANOVA).

Niclo-spheres improve mucociliary clearance in asthmatic mice

Niclosamide is a potent inhibitor of the Ca^{2+} activated Cl^- channel TMEM16A[147,150,196]. TMEM16A has been claimed to contribute to Cl^- secretion by the airway epithelium and is assumed to enhance the airway surface liquid layer and to increase mucociliary clearance[169]. Thus, the inhibition of TMEM16A may counteract the inhibition of airway inflammation and mucus production. We used particle tracking in mouse tracheas *ex vivo* to measure the effect of niclosamide on mucociliary clearance (Figure 4.3A). The data show reduced mucociliary

clearance in OVA-sensitized animals, when compared to sham-treated animals (control). Treatment with microsphere-encapsulated niclosamide enhanced particle transport, almost to values found in control animals (Figure 4.3B). This result suggests that niclosamide, while possibly inhibiting the activity of TMEM16A in fluid-secreting cells[246], has no negative effects on mucus transport, but rather improves mucociliary clearance.

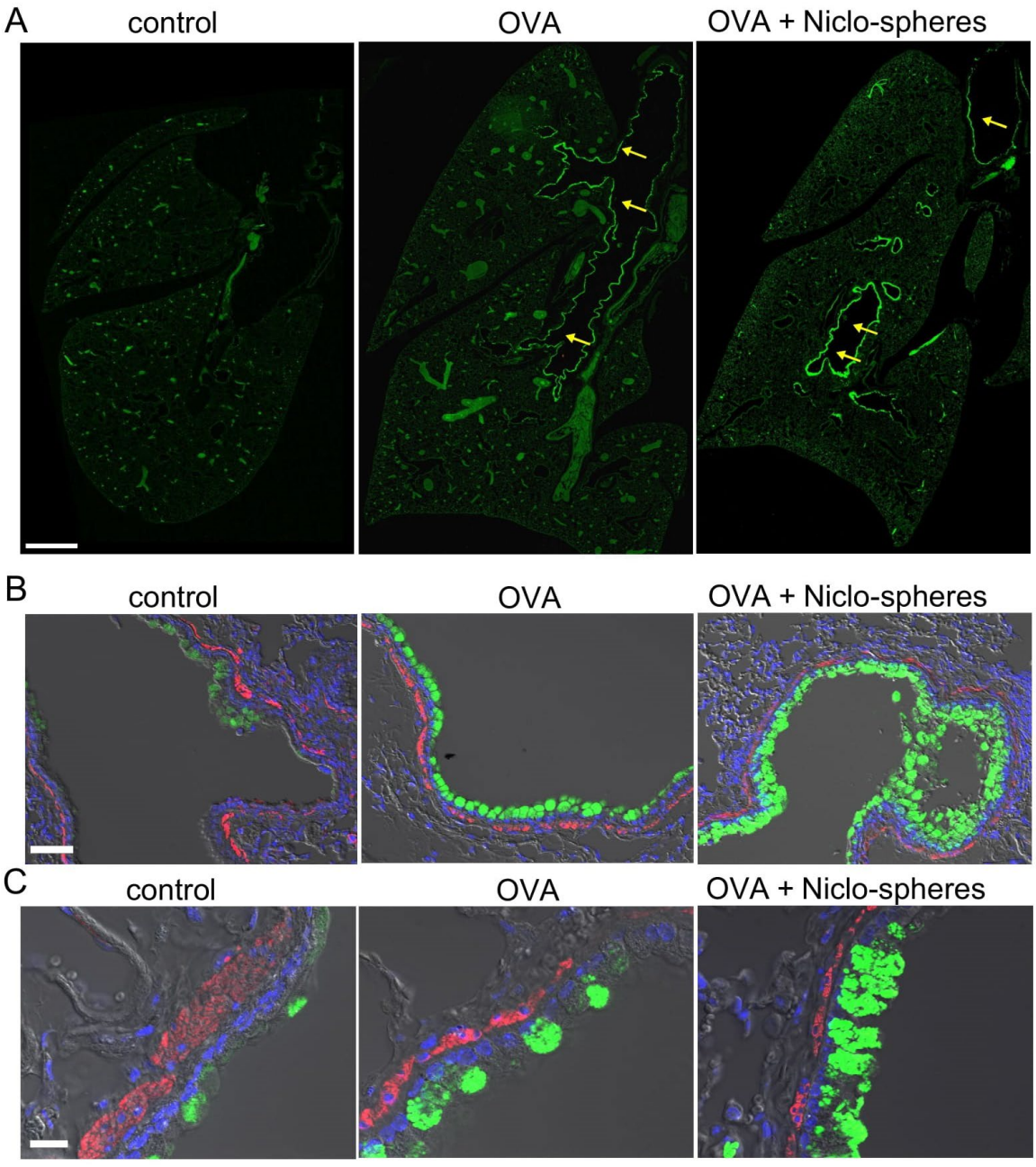

Figure 4.2 | *Accumulation of mCLCA1 in club cells by treatment with Niclo-spheres.*
(A) Whole mouse lung immunofluorescence obtained by stitching microscopy. mCLCA1 is expressed particularly in larger bronchi (yellow arrows), but not in small bronchioles and the peripheral lung tissue of asthmatic (ovalbumin (OVA)-treated) mice, and OVA-mice treated with Niclo-spheres. Intratracheal instillation of niclosamide (Niclo)-loaded spheres (Niclo-spheres; 0.196 mg; 30 µM/5 days) induced

additional accumulation of mCLCA1 in club cells. Bar = 1 mm. (B,C) mCLCA1 (green) and smooth muscle α-actin (red) at lower (B; bar = 50 µm) and higher (C; bar = 20 µm) magnification. Nuclei staining by DAPI (blue). Low expression of mCLCA1 under control conditions is upregulated in OVA-treated mice. Further accumulation of CLCA1 is observed in club cells from mice treated with Niclo-spheres; 2–3 animals for each series.

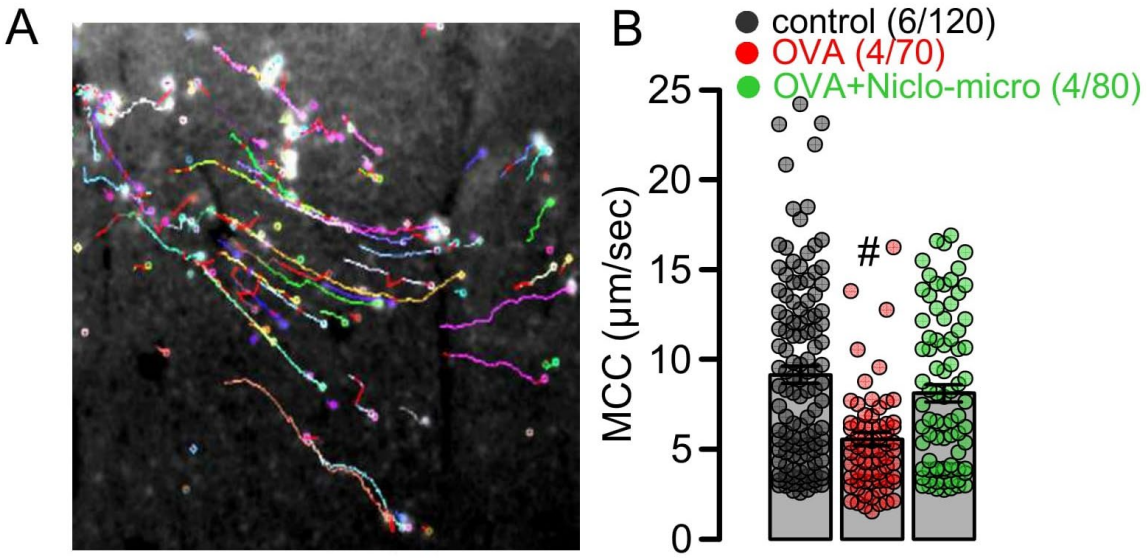

Figure 4.3 | *Effect of Niclo-spheres on mucociliary clearance.*
(A) Image from particle tracking in mouse trachea *ex vivo*, as a measure mucociliary clearance. (B) Summary for particle movement (µm/s) as a measure for mucociliary clearance (MCC) in tracheas *ex vivo* indicates that niclosamide-microspheres (0.98 mg; 30 µM) augment MCC that was reduced in tracheas of OVA-treated animals. Mean ± SEM (number of animals/number of measurements). #significant difference from control ($p < 0.05$, ANOVA).

Activation of the Ca^{2+} activated Cl^- channel TMEM16A is inhibited by niclo-spheres, but not by empty PEG spheres

Previous studies have shown that niclosamide dissolved in an aqueous solution inhibits TMEM16A ion currents[147,150,196]. We examined whether encapsulated niclosamide also inhibits TMEM16A currents, when applied acutely to CFBE human bronchial epithelial cells. To this end, cells were stimulated with ATP to activate TMEM16A. The application of empty polyethylene glycol microspheres (PEG) did not inhibit ATP-activated TMEM16A currents. In contrast, the application of niclosamide-containing microspheres potently suppressed ATP-activated TMEM16A currents (Figure 4.4). We further examined whether Ca^{2+} activated TMEM16A currents present in Calu-3 human airway submucosal cells are also inhibited by encapsulated niclosamide. To that end, the expression of TMEM16A was enhanced by the exposure of the cells to interleukin IL-13. IL-13 augmented the expression of TMEM16A mRNA (Figure 4.5A,B)

and the TMEM16A protein (Figure 4.5C). While a small whole-cell current was activated by ATP in control Calu-3 cells, the exposure to IL-13 strongly augmented the activation of TMEM16A currents. The activation of TMEM16A was not affected by empty microspheres (PEG) but was significantly inhibited by niclosamide encapsulated in microspheres or nanospheres (Figure 4.5D).

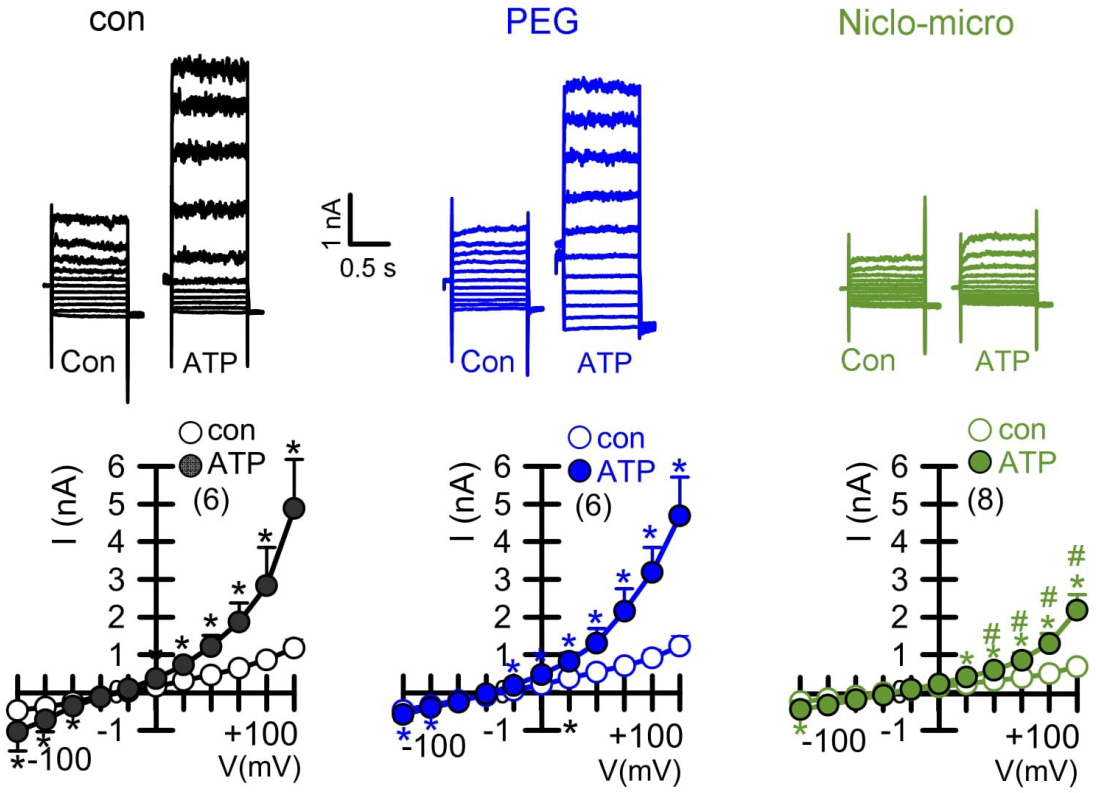

Figure 4.4 | *Activation of the Ca^{2+} activated Cl^- channel TMEM16A in CFBE human bronchial epithelial cells and inhibition by Niclo-spheres, but not by polyethylene glycol.*

Whole-cell current overlays (upper panels) and corresponding current/voltage relationships (lower panels). Activation of whole cell currents by purinergic stimulation (ATP; 100 µM) in CFBE airway epithelial cells was comparable in non-treated control cells (con) and in cells exposed to empty polyethylene glycol microspheres (PEG) but was potently inhibited by microsphere-encapsulated niclosamide (Niclo-micro, 1 µM). The inhibitor of Ca^{2+}-activated KCNN4 K^+ channels, TRAM-34 (100 nM), was present in all patch clamp experiments to avoid unwanted activation of Ca^{2+} activated K^+ channels. Mean ± SEM (number of cells). *significant activation by ATP ($p < 0.05$; paired t-test). #significant difference when compared to con or PEG ($p < 0.05$; unpaired t-test).

Niclo-spheres inhibited expression of MUC5AC in Calu-3 human airway submucosal epithelial cells

We further examined if the expression of the mucin MUC5AC, induced by the Th2-inflammatory mediator IL-13, is inhibited by Niclo-spheres. MUC5AC expression in Calu-3 cells was strongly enhanced by IL-13. (Figure 4.6A,B). The application of Niclo-spheres strongly

attenuated the expression of MUC5AC (Figure 4.6C). Notably, even concentrations of Niclo-spheres as low as 10 nM potently inhibited the expression of MUC5AC (Figure 4.6D). This is in accordance with earlier studies showing the potent inhibition of TMEM16A by dissolved niclosamide and related compounds at low nanomolar concentrations[147,150]. The data confirm the comparable effects of dissolved niclosamide[150] and encapsulated niclosamide (present data).

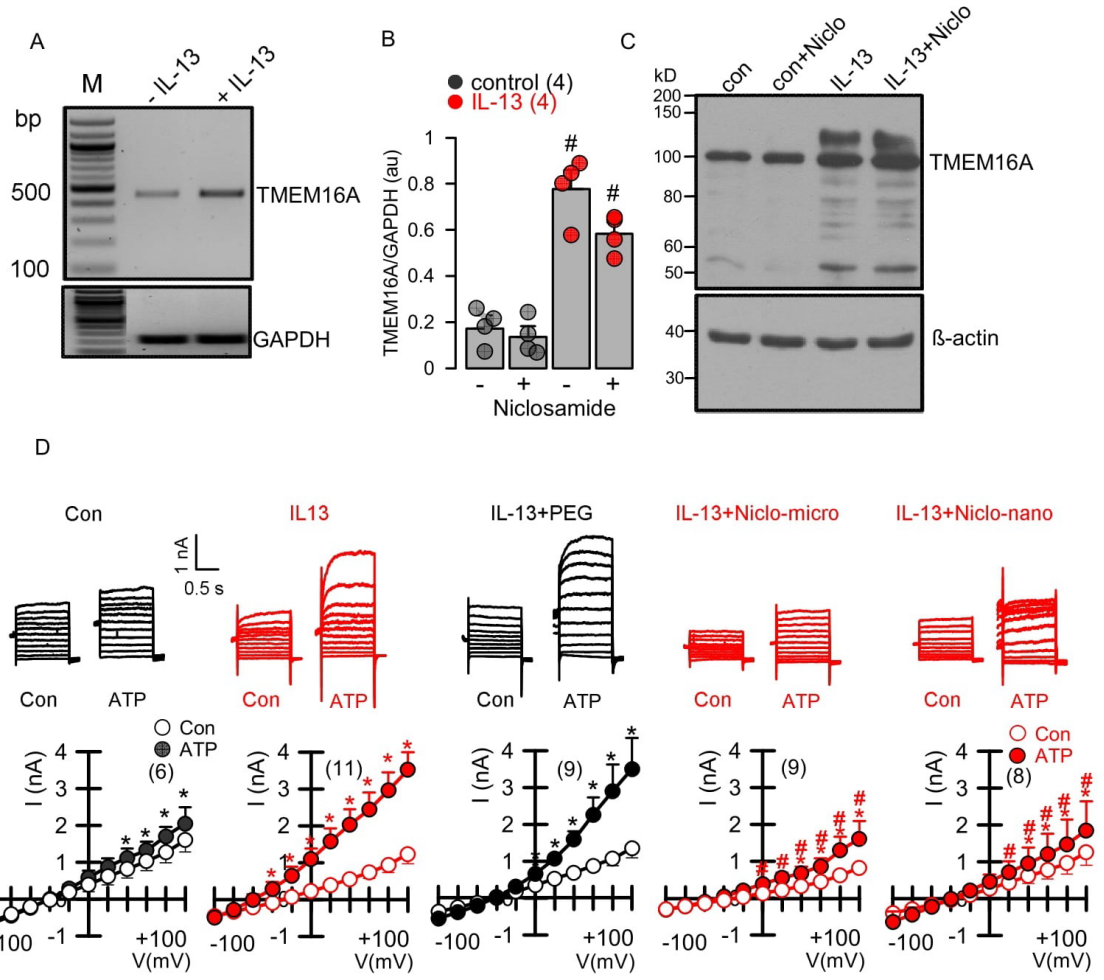

Figure 4.5 | *Enhanced expression of TMEM16A in Calu-3 human airway submucosal epithelial cells by IL-13, and inhibition of TMEM16A currents by Niclo-spheres.*

(A,B) RT-PCR analysis demonstrating enhanced expression of TMEM16A after incubation by IL-13 (20 ng/mL; 72 h) in the absence or presence of niclosamide (1 µM) (number of reactions). (C) Western blot indicating upregulation of TMEM16A-expression by IL-13 in the absence or presence of niclosamide. Note that expression of the glycosylated form of TMEM16A (upper band) is enhanced upon exposure to IL-13. Western blots were performed in triplicates. (D) Whole-cell current overlays (upper panels) and corresponding current/voltage relationships (lower panels). Activation of whole cell currents by purinergic stimulation (ATP; 100 µM) was enhanced by IL-13. Niclosamide encapsulated in microspheres (1 µM) or nanospheres (1 µM) strongly inhibited activation of TMEM16A currents by ATP. Empty spheres (PEG only) did not inhibit TMEM16A currents. The inhibitor of Ca^{2+}-activated KCNN4 K^+ channels, TRAM-34

(100 nM), was present in all patch clamp experiments, to avoid potential activation of Ca^{2+} activated K^+ channels. Mean ± SEM (number of cells). *significant activation by ATP ($p < 0.05$; paired t-test). #significant difference when compared to the absence of microspheres or nanospheres ($p < 0.05$; unpaired t-test).

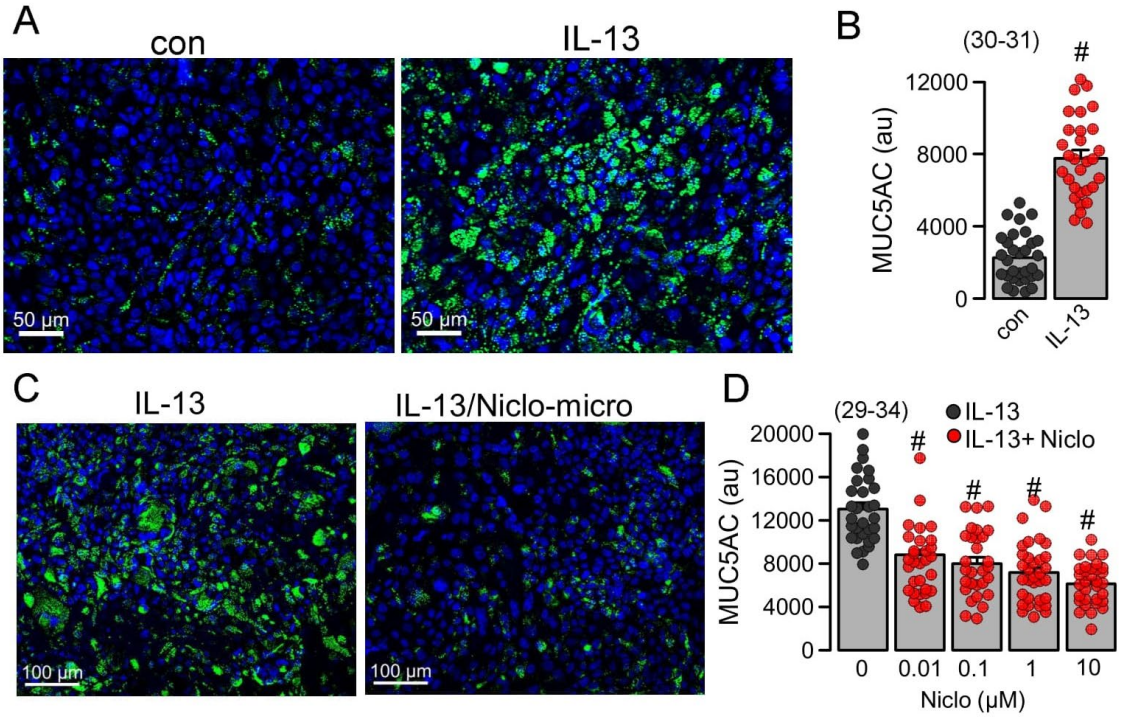

Figure 4.6 | *Inhibition of MUC5AC in Calu-3 human airway submucosal cells by Niclo-spheres.*
(A) Induction of MUC5AC expression (green fluorescence) in Calu-3 cells. Bar = 50 µm. (B) Quantitative analysis of MUC5AC expression indicates significant upregulation by IL-13 (20 ng/mL/72 h). (C) Inhibition of MUC5AC expression by niclosamide-loaded microspheres (Niclo-micro). Bar = 100 µm. (D) Concentration-dependent inhibition of MUC5AC expression by niclosamide-loaded microspheres. Mean ± SEM (number of sections analyzed). #significant difference when compared to control ($p < 0.05$; unpaired t-test) or IL-13 ($p < 0.05$; ANOVA).

Niclosamide inhibits mucus production, CLCA1-secretion and TMEM16A probably by blocking intracellular Ca^{2+} signals

Intracellular Ca^{2+} concentrations were measured in control Calu-3 cells and cells treated with IL-13, using the Ca^{2+} dye Fura2-AM. IL-13 slightly, but not significantly, augmented basal Ca^{2+} and ATP-induced Ca^{2+} increase. The acute application of niclosamide augmented basal Ca^{2+} levels and almost abolished the ATP-induced rise in intracellular Ca^{2+} (Figure 4.7). Niclosamide probably depletes endoplasmic reticulum Ca^{2+} stores, likely by the inhibition of the sarcoplasmic-endoplasmic reticulum Ca^{2+}-ATPase (SERCA) and by the inhibition of store-operated Ca^{2+} entry (SOCE)[141]. Taken together, the present data suggest that niclosamide,

encapsulated in microspheres or nanospheres, inhibits airway mucus production, attenuates airway inflammation, and inhibits the activation of TMEM16A by the suppression of intracellular Ca^{2+} signals.

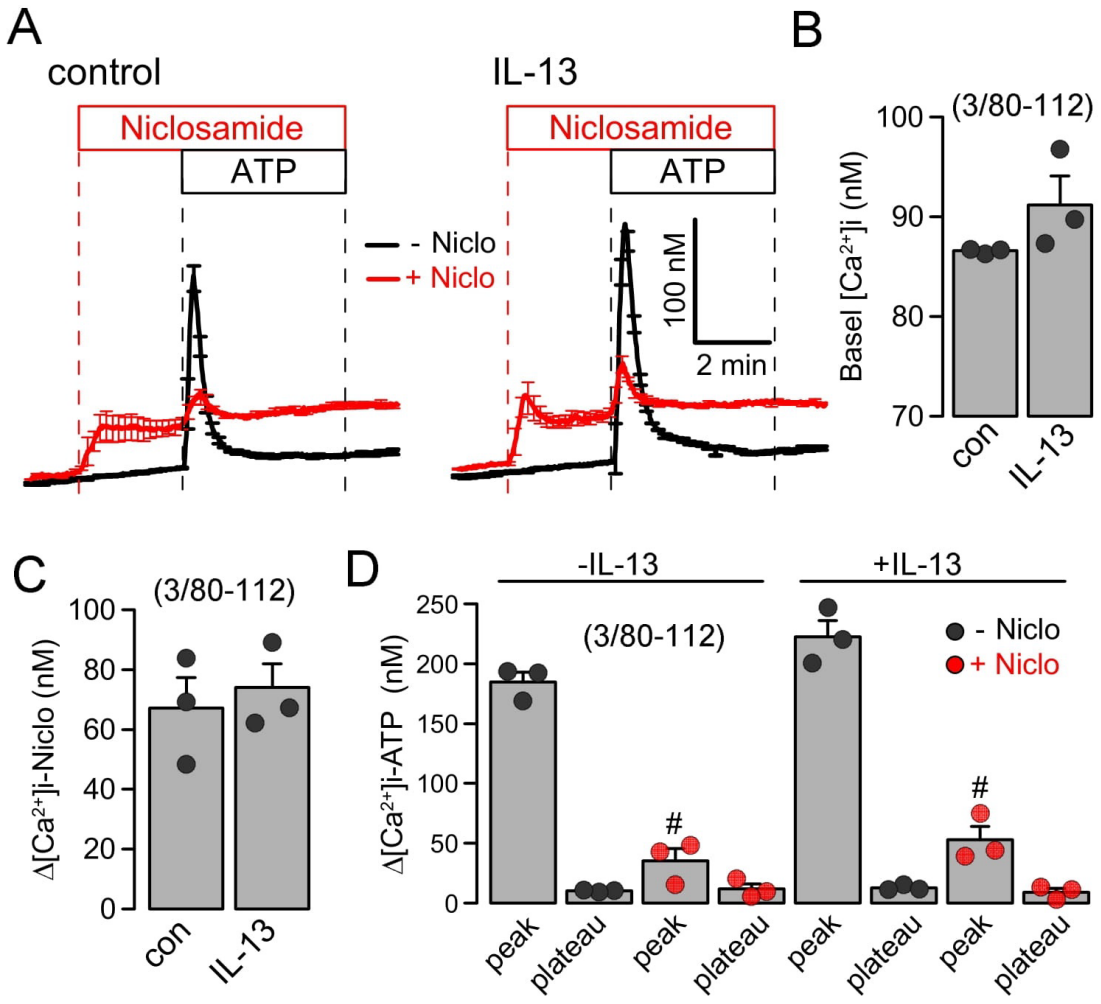

Figure 4.7 | *Inhibition of intracellular Ca^{2+} signals in Calu-3 cells by Niclo-spheres.*
(A) Summary traces for the intracellular Ca^{2+} concentration measured in control Calu-3 cells (left) and cells treated with IL-13 (20 ng/mL/72 h; right). (B) Summary of basal Ca^{2+} in treated and untreated cells. (C) Summary for the increase in intracellular Ca^{2+} by niclosamide (5 µM). (D) Summary of ATP (100 µM)-induced increase in cytosolic Ca^{2+}. IP_3-induced store release Ca^{2+} (peak) but not store operated Ca^{2+} influx (SOCE; plateau) was strongly attenuated by niclosamide. Mean ± SEM (number of independent series/number of cells analyzed). #significant difference when compared to control ($p < 0.05$; unpaired t-test) or IL-13 ($p < 0.05$; ANOVA).

Discussion

Polyethyleneimine-based non-viral gene delivery systems have been developed to target drugs efficiently[280]. Thus, niclosamide-encapsulated nanocarriers were shown to inhibit the growth of cancer cells[281]. PEG-formulations of poorly absorbable niclosamide were shown

to provide better bioavailability, which is highly relevant for its application as an anti-cancer drug and probably useful in the treatment of Covid-19[282]. It was shown that microgels unload their cargo over a 6–14-day period without showing significant cytotoxicity. Furthermore, recognition by alveolar macrophages was considerably lower than for polystyrene control particles[283]. Thus, airway deposition of encapsulated drugs appears ideal to maintain high effective local drug concentrations, without the need of repetitive applications. To that end, further chemical modification of hydrogels, by modification with ligands of mucosal surface receptors, is likely to increase tissue targeting, thereby enhancing specificity and local drug deposition[284]. Along this line, nanospheres conjugated with hyaluronic acid, a ligand of CD44, were designed to target siRNA to the airway epithelium[285]. PEG nanospheres penetrate well airway mucus. This would be an advantage particularly for the treatment of cystic fibrosis and asthma, which show the accumulation of copious amounts of mucus in the airways[286]. In fact, the PEG-formulation of drugs was shown to improve efficacy in other studies[287,288]. Because the expression of CD44, the receptor for hyaluronic acid (HA), is enhanced in the airway epithelium of asthmatic subjects, the conjugation of Niclo-spheres to HA may further enhance the targeting of airway epithelial cells [289]. We also found an upregulation of CD44 in the inflamed airways of humans and mice in the present study (Supplementary Figure 4.1). However, because the upregulation of HA was observed predominantly in the basolateral (but not apical) membrane, conjugation of Niclo-spheres with an inactive form of angiotensin II (ATII) might be more effective. This could also be useful in the treatment of Covid-19. SARS-CoV-2 binds via its spike protein to the angiotensin-converting enzyme 2 (ACE2), an enzyme receptor attached to the apical membrane of airway epithelial cells[290]. Conjugation with inactive ATII may improve the targeting of niclosamide to the site of infection and, in addition, may compete with the binding of the virus.

Niclosamide was suggested to induce a number of positive effects in asthma and cystic fibrosis lung disease by inhibiting TMEM16 proteins[147,150,246]. It was also shown to inhibit the replication of severe acute respiratory corona virus[253], and to block SARS-CoV-2 spike-protein-induced syncytia formation[249]. Covid-19 is characterized by abnormal activation of the inflammatory response and rapid deterioration of lung function due to alveolar edema[291]. Infected pneumocytes in the lungs of COVID-19 patients show abnormal morphology and frequent multinucleation. The generation of these cellular syncytia is caused by the spike protein, which, during the process of cell fusion, activates the phospholipid scramblase TMEM16F[249,292]. Activated TMEM16F disturbs the plasma membrane asymmetry, i.e., the polarized distribution of plasma membrane phospholipids, which leads to the activation of platelets, membrane shedding, and the activation of macrophages[293-295]. TMEM16A is likely to contribute to these processes because it supports the activation of TMEM16F, probably by ER-tethering to the plasma membrane and facilitating an intracellular Ca^{2+} increase[296]. Thus, TMEM16 proteins have a significant role in viral lung diseases, which should be explored in

more detail in future studies. Although the present results demonstrate a pronounced reduction of mucus production and suggest the attenuated release of CLCA1 into the airway lumen, the available data are limited to mouse airways. Moreover, the encapsulated drug has been applied by intratracheal instillation, and so far, no data are available for aerosol application, which probably would be used for topical drug application in human airways. Finally, studies on the long-term application will be required to fully assess potential unwanted effects. Taken together, the results from the present study suggest the use of Niclo-spheres in the treatment of COVID-19 and other viral respiratory infections as well as chronic inflammatory diseases such as cystic fibrosis and asthma.

Acknowledgements

This research was funded by the German Research Foundation (DFG) KU756/14-1, Gilead Foundation, and UK Cystic Fibrosis Trust SRC013.

Supplementary material

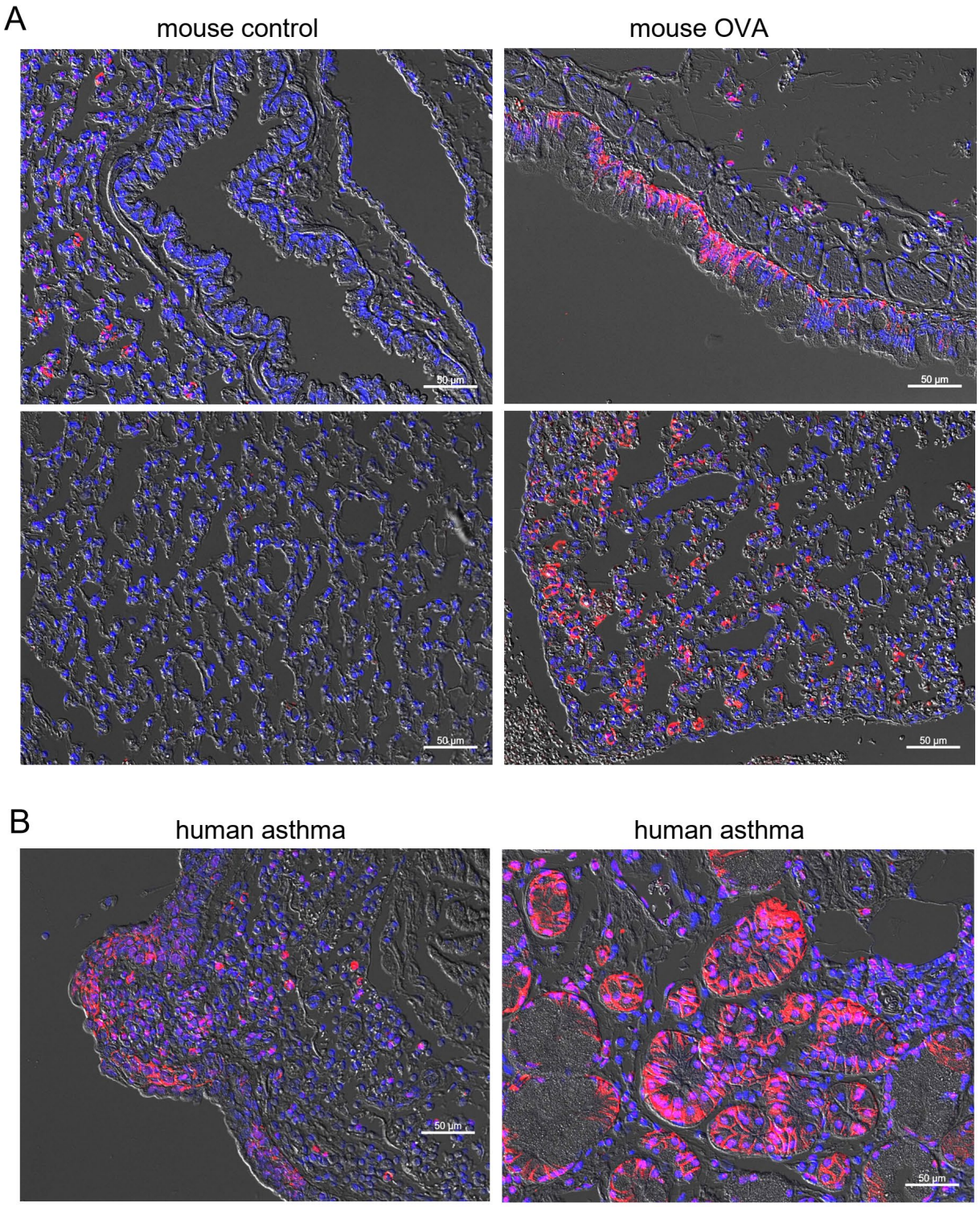

Supplementary Figure 4.1 | *Upregulation of CD44 expression in asthmatic lungs of mouse and human.* A) Upregulation of CD44 in the basolateral membrane of the airway epithelium and in alveolar epithelial cells of ovalbumin-sensitized mice. B) Pronounced expression of CD44 in submucosal glands and lung tissue of asthmatic patient. Bar = 50 µm.

CHAPTER 5 | EXPRESSION OF SLC26A9 IN AIRWAYS AND ITS POTENTIAL ROLE IN ASTHMA

Abstract

SLC26A9 is an epithelial anion transporter with a poorly defined function in airways. It is assumed to contribute to airway chloride secretion and airway surface hydration. However, immunohistochemistry showing precise localization of SLC26A9 in airways is missing. Some studies report localization near tight junctions, which is difficult to reconcile with a chloride secretory function of SLC26A9. We therefore performed immunocytochemistry of SLC26A9 in sections of human and porcine lungs. Obvious apical localization of SLC26A9 was detected in human and porcine superficial airway epithelia, whereas submucosal glands did not express SLC26A9. The anion transporter was located exclusively in ciliated epithelial cells. Highly differentiated BCi-NS1 human airway epithelial cells grown on permeable supports also expressed SLC26A9 in the apical membrane of ciliated epithelial cells. BCi-NS1 cells expressed the major Cl^- transporting proteins CFTR, TMEM16A and SLC26A9 in about equal proportions and produced short-circuit currents activated by increases in intracellular cAMP or Ca^{2+}. Both CFTR and SLC26A9 contribute to basal chloride currents in non-stimulated BCi-NS1 airway epithelia, with CFTR being the dominating Cl^- conductance. In *wt*CFTR-expressing CFBE human airway epithelial cells, SLC26A9 was partially located in the plasma membrane, whereas CFBE cells expressing F508del-CFTR showed exclusive cytosolic localization of SLC26A9. Membrane localization of SLC26A9 and basal chloride currents were augmented by interleukin 13 in *wild-type* CFTR-expressing cells, but not in cells expressing the most common disease-causing mutant F508del-CFTR. The data suggest an upregulation of SLC26A9-dependent chloride secretion in asthma, but not in the presence of F508del-CFTR.

Keywords: SLC26A9; asthma; cystic fibrosis; airways; Cl^- secretion; exocytosis; IL-13

Published as: Ousingsawat J., **Centeio R.**, Schreiber R., Kunzelmann K. Expression of SLC26A9 in Airways and Its Potential Role in Asthma. *International Journal of Molecular Sciences*. 2022 Mar; 23(6): 2998.

Own experimental contribution: Piglet lungs isolation; growth, paraffin-embedding and slicing of polarized cells; Ussing chamber experiments; Western blots.

Own written contribution: Original draft preparation.

Other contributions: Designed experiments and analysed data.

Introduction

The epithelial anion transporter SLC26A9 (solute carrier 26 family member A9) possibly contributes to airway surface hydration by operating as an uncoupled Cl^- transporter[127,165]. SLC26A9, together with the cystic fibrosis transmembrane conductance regulator (CFTR) and the Ca^{2+} activated Cl^- channel TMEM16A, is among the most important Cl^- secretory pathways in airways. SLC26A9 was suggested to have a role in inflammatory airway diseases, such as cystic fibrosis (CF) and asthma[167,168,297]. SLC26A9 belongs to a family of 10 paralogous mammalian proteins that play a role in tissue-specific ion transport, except of prestin, which mediates electromotility in inner ear outer hair cells[152,298-300]. Although operating as a chloride transporter rather than a channel, SLC26A9 nevertheless allows for high Cl^- transport rates and substantial anion currents[165]. Not entirely solved is the question of whether SLC26A9 is also able to transport bicarbonate and whether SLC26A9 or CFTR is in charge of basal anion transport in airways[159-163,165 ,301,302]. The aim of the present study was therefore to examine the contribution of SLC26A9 to airway chloride secretion.

In order to fulfil a chloride secretory function in airways, localization of SLC26A9 in the apical membrane is required. Data on the expression of SLC26A9 in human airways are still scarce. Surprisingly, immunofluorescence stainings in well-differentiated airway epithelial cells revealed expression of SLC26A9 near tight junctions[303]. A recent study in human airways also reported expression of SLC26A9 close to tight junctions[304]. However, tight junctional location of SLC26A9 is difficult to reconcile with a Cl^- secretory function. Moreover, studies in renal and gastrointestinal mucosa suggested an apical membrane location of SLC26A9[163,305,306]. Here we present a detailed analysis of the immunolocalization of SLC26A9 in normal, CF and asthmatic airways, as well as porcine airways from wild-type piglets (CFTR+/+) and from piglets lacking expression of CFTR (CFTR−/−). Apical membrane expression in ciliated epithelial cells is also demonstrated in highly differentiated BCi-NS1 human airway epithelial cells[228], which suggests a contribution of SLC26A9 to basal airway transport. BCi-NS1 airway epithelial cells form a tight epithelium typical of a native human airway epithelium. Membrane localization of SLC26A9 was enhanced in *wt*CFTR-expressing CFBE airway epithelial cells by the interleukin IL-13, which corresponds to earlier data suggesting upregulation of SLC26A9 function in mouse airways by IL-13 and possibly in asthma[168]. The present results support a role of SLC26A9 for airway chloride secretion in asthma, which may not be detectable in airways of CF-patients carrying the F508del-CFTR allele.

Materials and Methods

Tissues, cell culture and treatment: Airway sections from CFTR+/+ and CFTR−/− littermate piglets were generously provided by Prof. Dr. Nick Klymiuk (Molekulare Tierzucht und

Biotechnologie, LMU Munich)[307]. All animal procedures were performed according to the German Animal Welfare Act with permission of the local regulatory authority of LMU Munich. Piglets were euthanized within the first 24 h after birth under Ketamine (Ursotamin®, Serumwerk Bernburg, Bernburg Germany) and Azaperone (Stresnil®, Elanco Animal Health, Bad Homburg, Germany) anaesthesia by intracardiac injection of T61® (Intervet, Unterschleissheim, Germany). At least three human and piglet samples (*wt*CFTR, F508del-CFTR, CFTR+/+, CFTR−/−) were analysed. The human lung sections were kindly provided by Prof. Eric Verbeken and Prof. Kris De Boeck (University of Leuven, B-3000 Leuven, Belgium).

Human cystic fibrosis bronchial epithelial cell lines (CFBE) stably expressing *wt*CFTR or F508del-CFTR[308] were a generous gift from Dr. J.P. Clancy (University of Alabama at Birmingham, Birmingham, AL, USA). CFBE *wt*CFTR and F508del cells were cultured in MEM media supplemented with 2 mM L-glutamine and 2.5 µg/mL puromycin. Generation of CFBE cells stably expressing mCherry-Flag-*wt*CFTR and F508del-CFTR were described in a previous report[309] and were a generous gift from Prof. Dr. M.D. Amaral (University of Lisbon, Portugal). CFBE mCherry-Flag-CFTR cells were cultured in high-glucose DMEM supplemented with 2 mM L-glutamine, 1 mM pyruvate, 10 µg/mL blasticidin and 2 µg/mL puromycin. All media were supplemented with 10% heat-inactivated foetal calf serum (all culture media and supplements were from Capricorn Scientific, Ebsdorfergrund, Germany). BCi-NS1 cells (kindly provided by Prof. R. Crystal, Weill Cornell Medical College, New York, NY, USA)[228] were cultured in supplemented bronchial epithelial cell growth medium (BEGM; Lonza, Basel, Switzerland). For polarization, BCi-NS1 cells were seeded onto permeable supports for up to 30 days (Snapwell #3801, Corning, New York, USA) in an air–liquid (ALI) interface. All cells were cultured at 37 °C in a humidified atmosphere of 5% (v/v) CO2. For the IL-13 experiment, cells were treated with 20 ng/mL IL-13 (Enzo Life Sciences, Lörrach, Germany) for 72 h in OptiMEM reduced serum medium (Gibco/Thermo Fisher Scientific, Waltham, MA, USA); IL-13 was refreshed every day. SLC26A9 was detected by Western blotting using rabbit polyclonal anti-SLC26A9 (custom SCH-DRA; Davids Biotechologie, Regensburg, Germany) and HRP-conjugated goat anti-rabbit antibody.

RT-PCR: For RT-PCR, total RNA from BCi-NS1 and CFBE human airway epithelial cells was isolated using NucleoSpin RNA II columns (Macherey-Nagel, Düren, Germany). Total RNA (0.5 µg/25 µL reaction) was reverse-transcribed using random primer (Promega, Mannheim, Germany) and M-MLV reverse transcriptase RNase H minus (Promega, Mannheim, Germany). Each RT-PCR reaction contained sense (0.5 µM) and antisense primer (0.5 µM) (Table 5.1), 0.5 µL cDNA and GoTaq polymerase (Promega, Mannheim, Germany). After 2 min at 95 °C, cDNA was amplified (targets of 35 cycles, reference GAPDH 25 cycles) for 30 s at 95 °C, 30 s at 56 °C and 1 min at 72 °C. PCR products were visualized by loading on Midori Green Xtra

(Nippon Genetics Europe) containing agarose.

Table 5.1 | *RT-PCR primers.*

Gene accession number	Primers	Size (bp)
CFTR NM_000492.4	s: 5'- CTCATTAGAAGGAGATGCTCCTG as: 5´- GCTCTTGTGGACAGTAATATATCG	568
SLC26A9 NM_052934.4	s: 5´- CATTTGCTGTGCGCTTTCTG as: 5´- CCGCTTCTCCTGCTTCTTG	568
TMEM16A NM_018043.7	s: 5´- CGACTACGTGTACATTTTCCG as: 5´- GATTCCGATGTCTTTGGCTC	445
GAPDH NM_001289726	s: 5´- GTATTGGGCGCCTGGTCAC as: 5´- CTCCTGGAAGATGGTGATGG	200

Western blotting: Protein was isolated from filter-grown BCi-NS1 cells using a lysis buffer containing 25 mM Tris-HCl pH 7.4, 150 mM NaCl, 1 mM EDTA, 5% glycerol, 0.43% Nonidet P-40, 100 mM dithiothreitol (both from PanReac AppliChem, Barcelona, Spain) and 1× protease inhibitor mixture (Roche, Basel, Switzerland). Proteins were then separated by 8.5% SDS-PAGE and transferred to a PVDF membrane (GE Healthcare, Munich, Germany). Membranes were incubated overnight at 4 °C with rabbit primary antibodies against TMEM16A (ab64085, Abcam, Cambridge, UK) and α-SLC26A9 (Davids Biotechnologie, Regensburg, Germany), and a mouse primary antibody against CFTR (596, Cystic Fibrosis Foundation Therapeutics, Bethesda, MA , USA). Rabbit anti-actin (A2066; Sigma-Aldrich, St. Louis, MO, USA) was used as a loading control. Membranes were then incubated with horseradish peroxidase (HRP)-conjugated goat anti-rabbit/sheep anti-mouse secondary antibodies at room temperature for 2 h, and immunoreactive signals were visualized using a SuperSignal HRP chemiluminescence substrate-detection kit (34577; Thermo Fisher Scientific, Waltham, Massachusetts, USA).

Immunocytochemistry: For staining, cells were fixed for 10 min with methanol and acetone (5:1) mixing solution at −20 °C. Paraffin-embedded lung sections and monolayer CFBE sections (5 μm) were deparaffinized with xylene and rehydrated through a series of ethanol. The standard protocol for immunofluorescence was performed. In brief, after blocking with 5% bovine serum albumin in PBS, sections or cells were incubated in rabbit anti-SLC26A9 antibody (1:100, raised against mouse SLC26A9 aa 11–29, DRAAYSLSLFDDEFEKKDR, by Davids Biotechnologie, Regensburg, Germany; used in porcine tissues) or rabbit anti-SLC26A9 antibody (1:100, Novus Biologicals, Wiesbaden Nordenstadt, Germany; used in human tissues/cells), overnight at 4 °C. Antigen retrieval was performed in pre-heated Tris-EDTA buffer (pH 9.0) for 15 min, using a microwave before blocking (Supplementary Figure 5.1). Cells were incubated with secondary anti-rabbit antibody conjugated with Alexa Fluor 488 or Alexa Fluor 546 (1:400) for 1h at room temperature. Cilia were stained using a monoclonal antibody against acetylated tubulin produced in mouse (T7451, Sigma-Aldrich, Taufkirchen, Germany).

Nuclei were counterstained with DAPI. Airway sections or cells were mounted with fluorescence mounting medium (DAKO Cytomation, Hamburg, Germany). Immunofluorescence was examined with an Axio Observer microscope equipped with Axiocams 503 mono, ApoTome.2 and ZEN 3.0 (blue edition) software (Zeiss, Oberkochen, Germany).

Transepithelial Using chamber recordings: BCi-NS1 cells polarized on permeable supports were measured under short-circuit conditions in non-perfused chambers with bicarbonate-Ringer solution (mmol/l: NaCl 118.75; KH_2PO_4 0,4; K_2HPO_4 1,6; Glucose 5; $MgSO_4$ 1; Ca-Gluconate 1.3, $NaHCO_3$ 25; bubbled with 95% O_2/5% CO_2). Comprehensive methods have been detailed in previous reports[176,278].

Patch clamp: Cells were patch-clamped when grown on coated glass coverslips, and experiments were performed at 37 °C. Patch pipettes were filled with a cytosolic-like solution containing (in mM): KCl 30, K-Gluconate 95, NaH_2PO_4 1.2, Na_2HPO_4 4.8, EGTA 1, Ca-Gluconate 0.758, $MgCl_2$ 1.03, D-Glucose 5, ATP 3; pH 7.2. The intracellular (pipette) Ca^{2+} activity was 0.1 µM. The bath was perfused continuously at a rate of 4–6 mL/min with Ringer's solution (in mM): NaCl 145, KH_2PO_4 0.4, K_2HPO_4 1.6, Glucose 5, $MgCl_2$ 1, Ca-Gluconate 1.3. The substitution of extracellular Cl^- (5 mM) was made with gluconate. Patch pipettes had an input resistance of 2–5 MΩ, and whole-cell currents were corrected for serial resistance. The current–voltage (I–V) relationship was determined by pulsing from the holding potential of −100 mV to test potentials between −100 and +100 mV increasing in 20 mV increments. Currents were recorded using an EPC-9 computer-controlled amplifier and PULSE software (HEKA, Lambrecht, Germany), as well as Chart software (AD Instruments, Spechbach, Germany).

Results

Apical expression of SLC26A9 in human superficial airway epithelium is absent in CF

We analysed expression of SLC26A9 in human airways. Immunohistochemistry of SLC26A9 (green fluorescence) shows expression in the apical pole of the superficial epithelium in normal non-CF airways (Figure 5.1A). In contrast, airways from a CF-patient homozygous for the most common mutation, F508del-CFTR, show a lack of apical expression of SLC26A9 (Figure 5.1B).

Low levels of SLC26A9 are detected in the cytosol of CF-airways. This corresponds to several earlier studies indicating a lack of proper biosynthesis and apical expression of SLC26A9 in cultured CF airway epithelial cells[159,166,310,311]. In contrast to the superficial epithelium, expression of SLC26A9 was not detected in epithelial cells of submucosal glands in either non-CF or CF lungs (Figure 5.2).

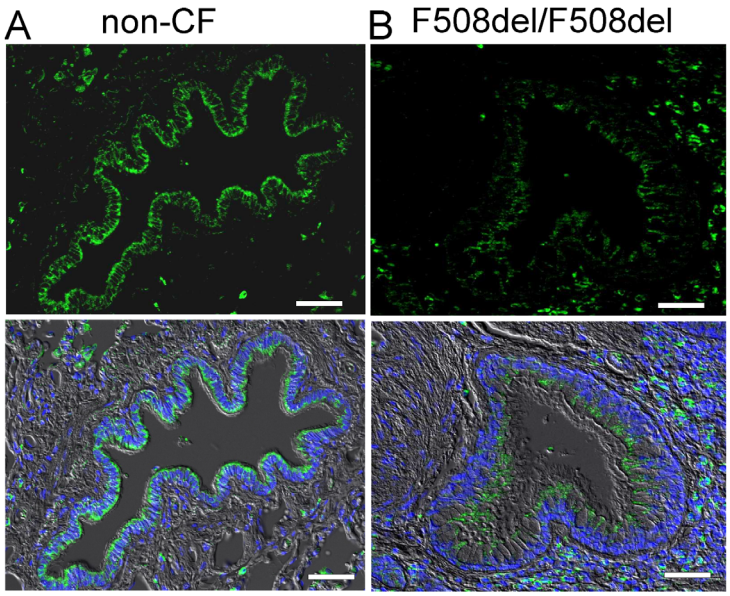

Figure 5.1 | *Apical expression of SLC26A9 in human non-CF but not CF superficial airway epithelium.* Immunohistochemistry of SLC26A9 (green fluorescence) expressed in non-CF ((A) wt-CFTR/wt-CFTR) and CF ((B) F508del-CFTR/F508del-CFTR) superficial airway epithelium. Reduced expression and intracellular localization of SLC26A9 is found in CF lungs. Bar = 50 μm. Nuclei were stained by DAPI.

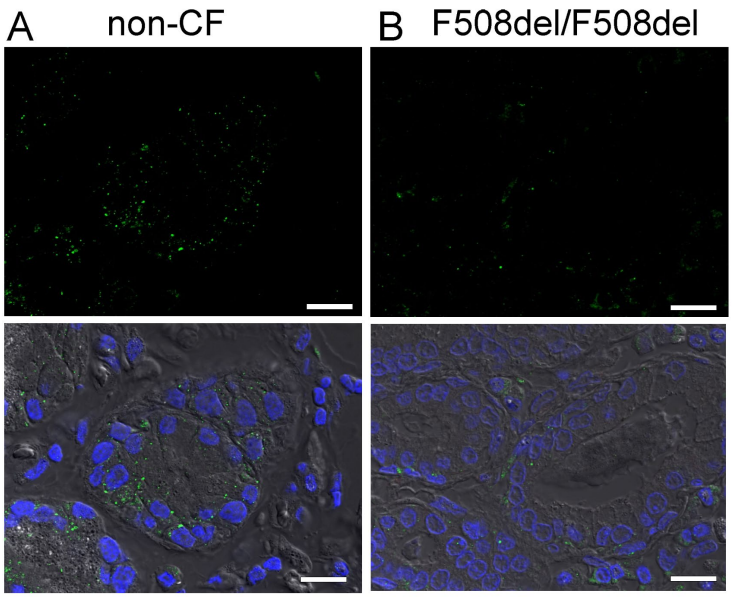

Figure 5.2 | *SLC26A9 is not expressed in human airway submucosal glands.* Immunohistochemistry of SLC26A9 (green fluorescence) in non-CF (A) and CF (B) airway sub-mucosal glands. No expression of SLC26A9 is detected in submucosal glands of either non-CF or CF lungs. Bar = 50 μm. Nuclei were stained by DAPI.

A more detailed analysis indicates expression of SLC26A9 in the apical membrane of ciliated epithelial cells. Thus, SLC26A9 is co-expressed together with CFTR in ciliated cells, whereas expression of SLC26A9 was not detected in non-ciliated cells (Figure 5.3). Notably, airways of asthma patients showed normal apical localization of SLC26A9, which even appeared somewhat stronger in some images, when compared to non-asthmatic airways. In contrast, the airways of CF patients homozygous for F508del-CFTR did not show expression of SLC26A9 (Figure 5.3).

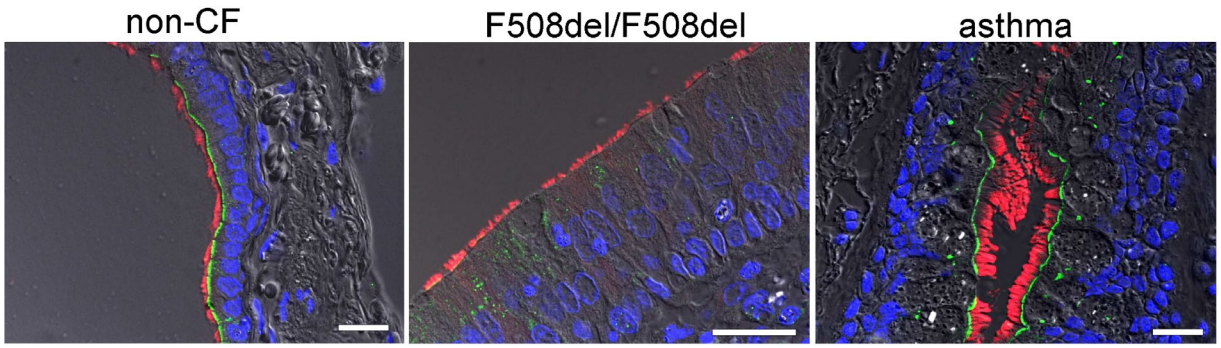

Figure 5.3 | *SLC26A9 is located in the apical membrane of ciliated airway epithelial cells.* Immunocytochemistry of SLC26A9 (green) and acetylated tubulin (red) in superficial airway epithelium from a non-CF patient, a CF patient (F508del-CFTR/F508del-CFTR) and an asthma patient. SLC26A9 is exclusively localized in the apical membrane of ciliated airway epithelial cells in non-CF and asthmatic lungs but not in CF-lungs from patients carrying the F508del-CFTR/F508del-CFTR mutation. Bar = 50 µm. Nuclei were stained by DAPI.

SLC26A9 is located in the apical membrane of ciliated airway epithelial cells of CFTR+/+ and CFTR-/- piglet lungs

In order to provide further evidence for an apical localization of SLC26A9 in airways, we analysed the expression of SLC26A9 in the porcine airway epithelium. To this end, we performed co-staining of SLC26A9 and acetylated tubulin in the superficial airway epithelium of wt-piglets (CFTR+/+) and littermate CFTR-knockout piglets (CFTR−/−). Identically to human airways, superficial airways of CFTR+/+ piglets also demonstrated clear apical expression of SLC26A9 in ciliated epithelial cells (Figure 5.4A). Remarkably, piglet airways lacking expression of CFTR also expressed SLC26A9 in the apical membrane, indicating that the absence of CFTR does not affect expression of SLC26A9. This is in sharp contrast to F508del-CFTR, which essentially abrogates SLC26A9 expression, as shown above. Like in human airways, expression SLC26A9 is not detected in airway submucosal glands of CFTR+/+ and CFTR−/− piglets (Figure 5.4B).

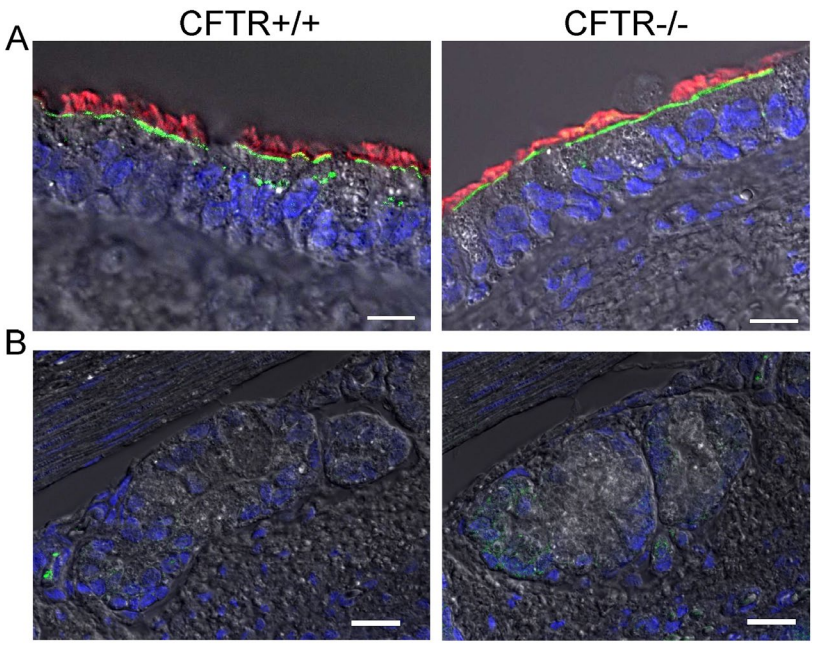

Figure 5.4 | *SLC26A9 is located in the apical membrane of ciliated airway epithelial cells of CFTR+/+ and CFTR-/- piglet lungs.*

(A) Immunocytochemistry of SLC26A9 (green) and acetylated tubulin (red) in superficial airway epithelium of wt (CFTR+/+) and CFTR-knockout (CFTR−/−) piglets. (B) Expression of SLC26A9 was not detected in airway submucosal glands of CFTR+/+ and CFTR−/− piglets. Bar = 20 µm. Nuclei were stained by DAPI.

Highly differentiated BCi-NS1 human airway epithelial cells express SLC26A9 in the apical membrane, which may contribute to basal Cl^- conductance. To further examine the role of SLC26A9 in human airway epithelial cells, we made use of the BCi-NS1 basal cell line which maintains multipotent differentiation capacity[228]. When grown on permeable supports, this cell line forms a tight airway epithelium with transport properties essentially identical to those of the original human airway epithelium. The use of chamber recordings demonstrated a basal Na^+ absorption, which is inhibited by amiloride, the inhibitor of epithelial Na^+ channels (ENaC). Steady-state and transient short-circuit currents (Isc) were activated by an increase in intracellular cAMP (using IBMX and forskolin) and by the purinergic agonist ATP, respectively (Figure 5.5A,B). Activated Cl^- secretion was inhibited by the NKCC1 inhibitor bumetanide. Polarized BCi-NS1 epithelia express similar amounts of the major Cl^- channels and transporters CFTR, TMEM16A and SLC26A9, as demonstrated by semiquantitative RT-PCR and Western blotting (Figure 5.5C–E). For TMEM16A, the bands for the glycosylated (130 kDa) and non-glycosylated (100 kDa) protein are shown. CFTR is detected as a so-called band C (180 kDa), and a band B (150 kDa). SLC26A9 shows a band at 90 kDa. The uncropped blots show a number of additional lower-molecular-weight bands for SLC26A9, which are known to be caused by several splice versions. SLC26A9 was also nicely detected in this cell line in the apical membrane of ciliated epithelial cells (Figure 5.5F). After inhibition of Na^+ absorption by

amiloride, we found that the CFTR inhibitor CFTRinh172 substantially decreased constitutive (basal) Isc, although the epithelium was not previously stimulated by IBMX/forskolin. A transient Isc was activated by stimulation with ATP (Figure 5.5G). Additional inhibition of TMEM16A by Ani9f[312] did not affect constitutive Isc, but inhibited ATP-activated Isc, suggesting that TMEM16A does not contribute to basal Cl^- secretion in human airways (Figure 5.5H). GlyH101 (GlyH) was reported to inhibit SLC26A9[159]. We applied GlyH after inhibition of CFTR with CFTRinh172 and found additional inhibition of Isc that could well be due to inhibition of SLC26A9 (Figure 5.5I). Thus, both CFTR and SLC26A9 may contribute to basal constitutive Cl^- secretion in human airways.

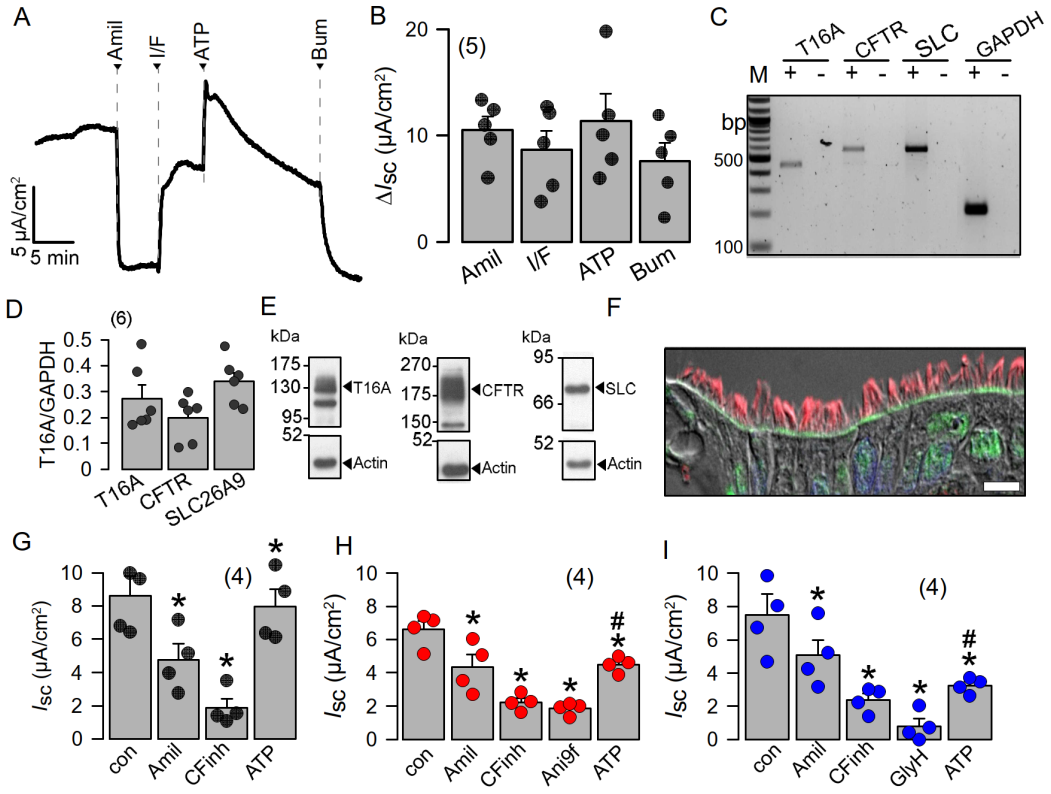

Figure 5.5 | *Highly differentiated BCi-NS1 human airway epithelial cells express SLC26A9 in the apical membrane.*

(A,B) Using chamber short-circuit current (Isc) recording from highly differentiated BCi-NS1 human airway epithelial cells. Isc is inhibited by amiloride (10 µM), indicating the expression of epithelial Na^+ channels (ENaC). IBMX (100 µM) and forskolin (2 µM) activate a non-transient CFTR-dependent Isc, which is inhibited by basolateral bumetanide (20 µM). Luminal ATP (100 µM) activates a transient Isc. (C,D) Expression of the major Cl^- secretory proteins, TMEM16A (T16A), CFTR and SLC26A9 (SLC), as detected by RT-PCR. (E) Expression of TMEM16A, CFTR and SLC26A9 detected by Western blotting. Blots were performed in duplicate. (F) Immunocytochemistry of SLC26A9 (green) and acetylated tubulin (red) in ciliated cells of highly differentiated BCi-NS1 cells grown on permeable supports. Bar = 10 µm. Nuclei were stained by DAPI. (G–I) Summaries of basal short-circuit currents in BCi-NS1 monolayers, indicating CFTR activity contributing to basal Isc, as detected by CFTRinh172 (CFinh; 10 µM). The TMEM16A-inhibitor Ani9f (10 µM) largely reduces ATP-activated TMEM16A-dependent Cl- secretion.

The inhibitor GlyH101 (GlyH; 10 µM) further inhibits basal Isc after inhibition of CFTR by CFTRinh172. Mean ± SEM (number of tissues). *significant effects by compounds ($p < 0.05$; paired t-test). #significant difference compared to G ($p < 0.05$; unpaired t-test).

IL-13 augments membrane expression of SLC26A9 and induces basal Cl^- currents in CFBE airway epithelial cells expressing wtCFTR, but not in cells expressing F508del-CFTR

We made use of the human airway epithelial cell line CFBE stably expressing wtCFTR or F508del-CFTR in order to further analyse CFTR-dependent regulation of SLC26A9. SLC26A9 might be upregulated in asthmatic airways[168]. It was proposed that SLC26A9-mediated Cl^- secretion prevents mucus obstruction in airways of IL-13 treated mice. Here, we stimulated CFBE cells with IL-13, which did not upregulate relatively low levels of SLC26A9 expressed in wt and F508del cells (Figure 5.6A). However, exposure of the cells to IL-13 enhanced membrane expression of endogenous SLC26A9 in CFBE cells expressing wtCFTR (Figure 5.6B). In contrast, F508del-CFTR-expressing cells showed exclusive intracellular localization of SLC26A9, and IL-13 was unable to translocate SLC26A9 to the plasma membrane. We analysed the corresponding whole-cell currents using patch clamp and found a constitutive Cl^- current that could be inhibited by removal of extracellular Cl^- ($5Cl^-$). Moreover, exposure to IL-13 further enhanced constitutive whole-cell currents and augmented $5Cl^-$-induced current inhibition (Figure 5.6C,D). Unlike wtCFTR-expressing cells, F508del-CFTR-expressing cells did not present constitutive currents and showed only a tiny constitutive Cl^- transport after incubation with IL-13 (Figure 5.6E,F). Taken together, the present data clearly indicate apical membrane expression of SLC26A9 in human and porcine airways, which is fully reproduced in polarized BCi-NS1 human airway epithelia. Both CFTR and SLC26A9 may contribute to constitutive chloride secretion, but CFTR clearly dominates. The Th-2 cytokine IL-13 enhances membrane expression of SLC26A9, thereby increasing constitutive Cl^- secretion.

Discussion

SLC26A9 is expressed in the apical membrane of the airway epithelium

The present data clearly show expression of SLC26A9 in the apical membrane of airways taken from original lung sections. During the course of this study, it became clear that airway epithelial cells require complete polarization and differentiation in order to express SLC26A9 apically. Thus, plastic-grown airway epithelial cells, such as BCi-NS1 or CFBE, show very little membrane expression. In additional experiments, we tried to biotinylate SLC26A9 in membranes of non-polarized (plastic-grown) BCi-NS1 and CFBE cells but found very little SLC26A9 in the biotinylated fraction (data not shown). Moreover, SLC26A9 expressed in

HEK293 cells shows almost exclusively cytosolic expression[311], similar to a stably SLC26A9-expressing FRT cell line generated recently[313]. Thus, proper analysis of the function of SLC26A9 in airways requires a polarized environment.

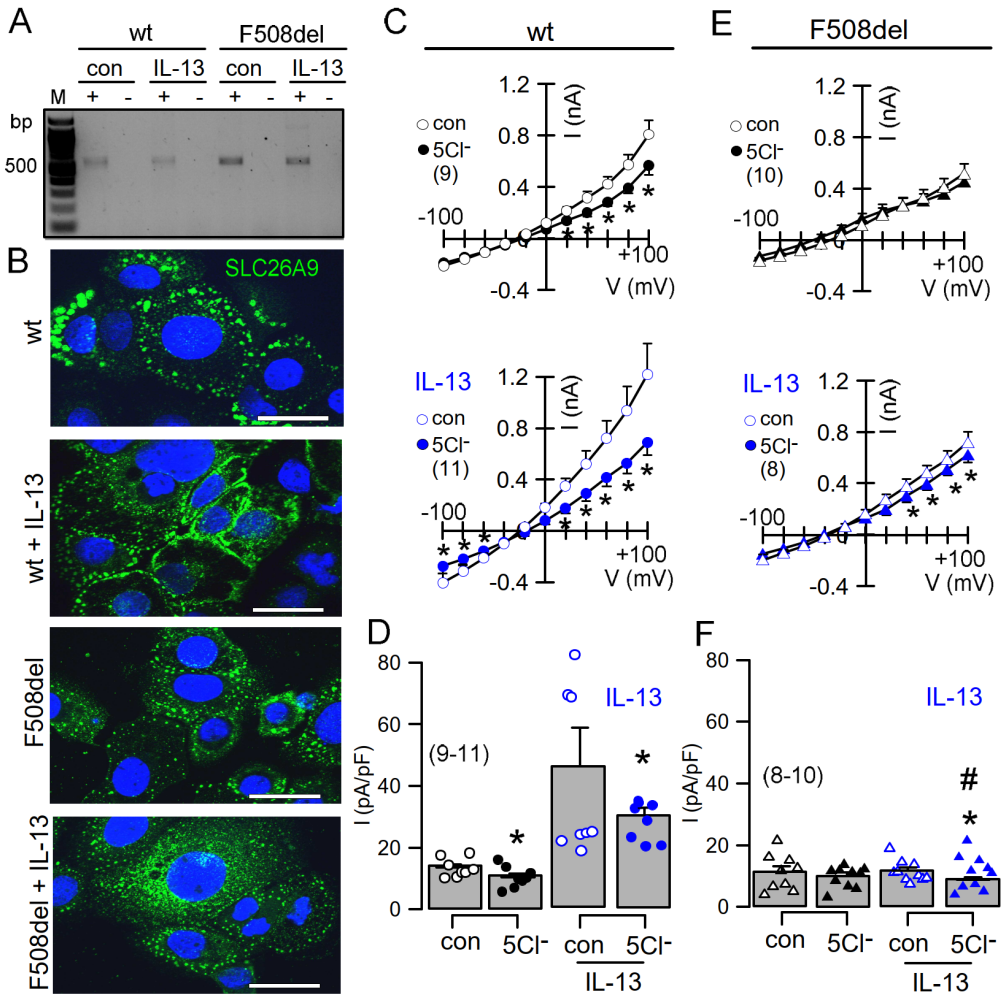

Figure 5.6 | *IL-13 augments membrane expression of SLC26A9 and induces basal currents in CFBE airway epithelial cells expressing wtCFTR but not in cells expressing F508del-CFTR.*

(A) Expression of SLC26A9 detected by RT-PCR in CFBE airway epithelial cells stably expressing wtCFTR (wt) or F508delCFTR (F508del). Cells were treated with IL-13 (20 ng/72 h), which did not enhance expression of SLC26A9. (B) Immunohistochemistry of SLC26A9 in CFBE/wtCFTR and CFBE/F508delCFTR cells. Exposure of the cells to IL-13 enhanced membrane expression of endogenous SLC26A9 in cells expressing wtCFTR, but not in cells expressing F508del-CFTR. Note that in CFBE/wtCFTR cells, some SLC26A9 is located in the plasma membrane even in the absence of IL-13, whereas CFBE/F508del cells show cytoplasmic expression of SLC26A9. Bars = 20 µm. (C–F) Current/voltage relationships showing basal currents in CFBE/wtCFTR (C,D) and CFBE/F508delCFTR (E,F) cells in the absence or presence of IL-13, as well as the effect of removal of chloride ($5Cl^-$) from the extracellular bath solution. Basal Cl^- transport detected by $5Cl^-$ replacement was larger in CFBE/wtCFTR cells when compared to CFBE/F508del cells. Mean ± SEM (number of cells). *significant inhibition by $5Cl^-$ ($p < 0.05$; paired t-test). #significant difference compared to wtCFTR ($p < 0.05$; unpaired t-test).

Localization of SLC26A9 near tight junctions was reported previously[303,304]. Although this was not a regular finding in the present study, we occasionally observed a lateral staining of SLC26A9 in native airways (not shown). We speculate that the airway epithelium in these rare lung sections was not fully differentiated, possibly due to inflammation. Importantly, SLC26A9 was only found in ciliated epithelial cells, which corresponds well to the interaction of SLC26A9 and other SLC26A solute transporters with CFTR, as described in several previous reports[155,156,159,300,314,315].

Plasma membrane expression of SLC26A9 is CFTR-dependent and is augmented by IL-13

Expression of SLC26A9 was essentially absent in human F508del-CFTR/F508del-CFTR airways. Moreover, SLC26A9 present in non-polarized CFBE cells expressing F508del-CFTR was detected exclusively in the cytosol. Both findings highlight the pronounced abrogating effect of F508del-CFTR on SLC26A9[166,310]. In contrast, SLC26A9 staining was exclusively apical in non-CF lungs and was even found in the membrane of non-polarized CFBE cells expressing wtCFTR. Notably, airways of CFTR knockout piglets demonstrated normal SLC26A9 expression in the apical plasma membrane, suggesting that SLC26A9 is able to traffic to its physiological location in the absence of CFTR, whereas co-expression with F508del-CFTR abrogates biosynthesis and trafficking of SLC26A9.

It was found that IL-13 treatment increases Cl^- secretion in airways of wild-type but not Slc26a9-deficient mice. Thus, an upregulation of SLC26A9-dependent Cl^- secretion may help to prevent mucus obstruction in asthma[168]. In airways of asthma patients, we found normal expression of SLC26A9, and in some sections, SLC26A9 staining appeared somewhat enhanced (not shown). When we treated CFBE/wtCFTR cells with IL-13, we also found an increase in SLC26A9 membrane expression, whereas SLC26A9-mRNA expression was not enhanced. Enhanced membrane expression was paralleled by enhanced constitutive Cl^- conductance, suggesting enhanced SLC26A9 conductance in asthmatic airways. It should be mentioned that IL-13 (and IL-4) also strongly upregulated airway expression of the Ca^{2+}-activated Cl^- channel TMEM16A *in vivo* and *in vitro*[191]. It was shown earlier that TMEM16A is essential for exocytosis and proper membrane protein insertion[137,138,192,216]. This is demonstrated most impressively in patients lacking expression of functional TMEM16A, as well as in TMEM16A-knockout mice[137,138,216]. Thus, Th-2 cytokines, such as IL-4 and IL-13, augment membrane expression of both CFTR and SLC26A9 because SLC26A9 and CFTR physically interact via the STAS/R domain and scaffold proteins containing PDZ domains (Figure 5.7). Such a mechanism provides enhanced constitutive Cl^- and fluid secretion and antagonizes mucus plugging, as proposed earlier[137,168,192,216].

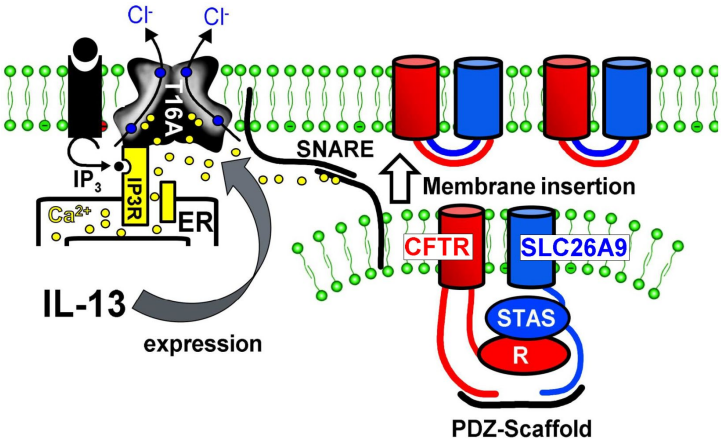

Figure 5.7 | *Enhanced membrane expression of SLC26A9 in asthma.*
Proposed mechanism for enhanced SLC26A9 expression in airways exposed to IL-13. Exposure to IL-13 leads to enhanced expression of TMEM16A. TMEM16A expressed in the apical membrane tethers the endoplasmic reticulum (ER) to the apical membrane and leads to enhanced compartmentalized Ca^{2+} signaling. Enhanced intracellular apical Ca^{2+} concentrations facilitate membrane insertion of CFTR and SLC26A9 via the Ca^{2+}-regulated SNARE (soluble N-ethylmaleimide-sensitive factor attachment protein receptor) complex.

A limitation of the present study is the limited number of available lung sections. Thus, subsequent studies should analyse expression of SLC26A9 in CF lungs from patients with different class 1–7 mutations, as well as the effect of CFTR correctors on correcting the plasma membrane location of SLC26A9. Moreover, quantitative comparison of SLC26A9 membrane expression in normal and asthmatic airways would be helpful to clarify whether asthmatic airways express more apical SLC26A9. Nevertheless, the results suggest a limited contribution of SLC26A9 to airway Cl^- secretion. This may therefore suggest an additional role of SLC26A9, maybe for bicarbonate transport. Plasma membrane location of SLC26A9 was essentially unchanged in lungs from CFTR-knockout piglets. This may explain why we did not find evidence for acidification of the airway surface liquid (ASL) in lungs of CFTR-knockout piglets in our previous study[176]. Finally, the present results support a protective function of SLC26A9 in asthmatic lungs and attach a beneficial role to IL-13, which is found to be enhanced in asthma.

Acknowledgements

This research was supported by the German Research Foundation (DFG) KU756/14-1, UK Cystic Fibrosis Trust SRC013, and Gilead Foundation. The technical assistance of Patricia Seeberger is greatly appreciated. We thank Nick Klymiuk (Ludwig Maximilian University of Munich, Germany) for providing the piglet lung tissues. The human lung sections were kindly provided by Eric Verbeken and Kris De Boeck (University of Leuven, Belgium). The authors thank R. Crystal (Weill Cornell Medical College, NY, USA) for providing the BCi-NS1 cell line.

Supplementary material

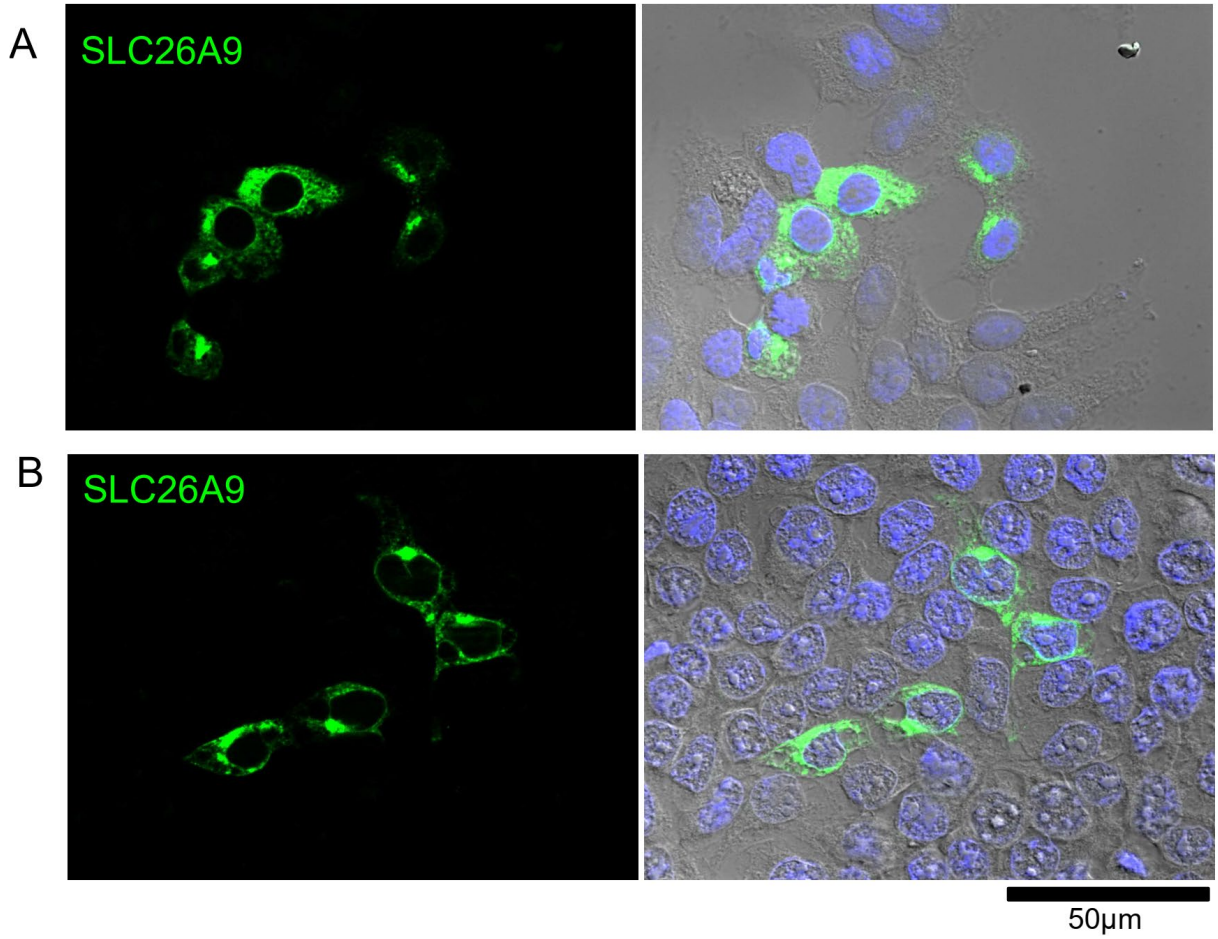

Supplementary Figure 5.1 | *Specificity of immunostaining using SLC26A9 antibodies.*
Images show SLC26A9 transfected HEK293 cells as indicated by green fluorescence of SLC26A9 expressing cells. Primary antibodies used were A) custom made AB from Davids Biotechnology, Regensburg, Germany, B) Novus Biologicals, Wiesbaden Nordenstadt, Germany). Non-transfected HEK293 cells, which do not express endogenous SLC26A9, were without fluorescence. Nuclei were stained by DAPI.

CHAPTER 6 | THE SLC26A9 INHIBITOR S9-A13 PROVIDES NO EVIDENCE FOR A ROLE OF SLC26A9 IN AIRWAY CHLORIDE SECRETION BUT SUGGESTS A CONTRIBUTION TO REGULATION OF ASL PH AND GASTRIC PROTON SECRETION

Abstract

The solute carrier 26 family member A9 (SLC26A9) is an epithelial anion transporter that is assumed to contribute to airway chloride conductance and airway surface hydration. Whether SLC26A9 or CFTR is responsible for airway Cl^- transport under basal conditions is still unclear, due to the lack of a specific inhibitor for SLC26A9. In the present study we report a novel potent and specific inhibitor for SLC26A9, identified by screening of a drug-like molecule library and subsequent chemical modifications. The most potent compound, S9-A13, inhibited SLC26A9 with an IC_{50} of 90.9 ± 13.4 nM. S9-A13 did not inhibit other members of the SLC26 family and had no effects on Cl^- channels such as CFTR, TMEM16A, or VRAC. S9-A13 inhibited SLC26A9 Cl^- currents in cells that lack expression of CFTR. It also inhibited proton secretion by HGT-1 human gastric cells. In contrast, S9-A13 had minimal effects on ion transport in human airway epithelia and mouse trachea, despite clear expression of SLC26A9 in the apical membrane of ciliated cells. In both tissues, basal and stimulated Cl^- secretion was due to CFTR, while acidification of airway surface liquid by S9-A13 suggests a role of SLC26A9 for airway bicarbonate secretion.

Keywords: airways, asthma, Cl^- secretion, cystic fibrosis, pH regulation, S9-A13, SLC26A9
Published as: Jo S., **Centeio R.**, Park J., Ousingsawat J., Jeon D., Talbi K., Schreiber R., Ryu K., Kahlenberg K., Somoza V., Delpiano L., Gray M. A., Amaral M. D., Railean V., Beekman J. M., Rodenburg L. W., Namkung W., Kunzelmann K. The SLC26A9 inhibitor S9-A13 provides no evidence for a role of SLC26A9 in airway chloride secretion but suggests a contribution to regulation of ASL pH and gastric proton secretion. *The FASEB Journal*. 2022 Nov; 36(11): e22534.
Own experimental contribution: Western blots; mouse trachea isolation; growth, paraffin-embedding and slicing of polarized cells; Ussing chamber experiments; intracellular pH measurements.
Own written contribution: Original draft preparation.
Other contributions: Designed experiments and analysed data.

Introduction

The epithelial anion transporter SLC26A9 (solute carrier 26 family member A9) is thought to contribute to hydration of the airway surface liquid (ASL) by operating as a Cl^- transporter.[159-162,301,302,316]. A recent cryo-EM structure and functional analysis revealed that SLC26A9 operates as an uncoupled chloride transporter with a high transport rate due to a rapid alternate-access mechanism[165]. Biochemical properties, trafficking, and interaction between SLC26A9 and cystic fibrosis transmembrane conductance regulator (CFTR) are well noticed, but the true contribution of SLC26A9 to airway ion transport remains unclear. Although SLC26A9 operates as a Cl^- transporter rather than a Cl^- channel, it nevertheless produces substantial Cl^- currents that may contribute to basal airway Cl^- transport, that is, Cl^- transport under resting conditions in non-stimulated airway epithelial cells.[159,311,317,318]. Notably, in gastric parietal cells, SLC26A9 was shown to be relevant for acid secretion, probably by operating as a parallel Cl^- secretory pathway[302].

CFTR and members of the SLC26A solute transporter family (SLC26A3,4,6,8,9) physically and functionally interact via R (regulatory) and STAS (Sulphate Transporter and AntiSigma factor antagonist) domains[155,156,159,300,314,315]. Transport of bicarbonate (HCO_3^-) by SLC26A9 has been proposed by some scientists[162,163,319], but was not found by other laboratories[159-161,165]. Loss of SLC26A9 was shown to alter intestinal HCO_3^- transport, acid secretion, and fluid absorption[301,302]. SLC26A9 is inhibited by nonselective chloride channel inhibitors, including 4,4'-diisothiocyanatostilbene-2,2'-disulfonic acid (DIDS), NS3623, flufenamic acid, niflumic acid, and GlyH-101. However, these compounds inhibit a large range of Cl^- channels and showed a low potency and only partial inhibition of SLC26A9[159-161]. Thus the lack of potent and selective inhibitors of SLC26A9 has hampered further investigations into the physiological function of SLC26A9.

In the present paper, we describe S9-A13, a highly potent and selective inhibitor of SLC26A9. Because we found no cross-inhibition of other SLC26 transporters or chloride channels, it was possible to analyse the contribution of SLC26A9 and CFTR to airway transport. While SLC26A9 does not contribute to airway Cl^- secretion, it controls ASL pH, probably by operating as a Cl^-/ HCO_3^- exchanger. However, in cells that do not express CFTR, SLC26A9 may operate as Cl^- transporter, and it may facilitate proton secretion in parietal cells.

Materials and Methods

Identification of SLC26A9 inhibitors by high-throughput screening: A drug-like small-molecule library including 30.000 compounds was purchased from ChemDiv. (San Diego, CA, USA). Unless indicated otherwise, other chemicals were purchased from Sigma-Aldrich (St.

Louis, MO, USA). Screening was performed in Ringer solution containing 140 NaCl, 5 KCl, 1 $MgCl_2$, 1 $CaCl_2$, 10 D-glucose, 10 HEPES (in mM; pH 7.4 with NaOH).

Animals and treatments: Allergen challenge of mice has been described previously[190]. In brief, mice were sensitized to ovalbumin (OVA; Sigma-Aldrich, St. Louis, Missouri, USA) by intraperitoneal (I.P.) injection of 100 µg OVA in 100 µL aluminium hydroxide gel adjuvant (InvivoGen, San Diego, California, USA) on days 0 and 14. At days 21 to 23, mice were anesthetized (ketamine 90–120 mg/kg and xylazine 6–8 mg/kg) and challenged to OVA by intratracheal (I.T.) instillation of 50 µg OVA in 100 µL saline. All animal experiments complied with the guidelines for animal research and were carried out in accordance with the EU Directive 2010/ 63/EU for animal experiments. All animal experiments were approved by the local Ethics Committee of the Government of Unterfranken/Wurzburg (AZ: 55.2.2-2532-2-1359-15) and were conducted according to the guidelines of the American Physiologic Society and German Law for the Welfare of Animals.

Cell culture and transfections: LN215 cells were cultured with Dulbecco's Modified Eagle Medium (Welgene, Daegu, Korea) supplemented with 10% FBS, 100 U/ml penicillin, 100 µg/ml streptomycin, 4 mM L-glutamine and 1 mM sodium pyruvate. FRT and CHO-K1 cells expressing ANO1, CFTR or SLC26A4 were cultured using methods described previously[320]. For SLC26A9 inhibitor screening and selectivity assays, LN215 cells expressing YFP-F46L/H148Q/I152L together with SLC26A3, SLC26A6 or SLC26A9 were generated by a lentiviral system containing the vectors pLenti6P.3-slc26a3, pLenti6P.3-slc26a6 and pLenti6P.3-slc26a9, respectively. Stable cell lines were selected using 1 µg/ml puromycin. Human embryonic kidney 293 (HEK293) cells were grown in DMEM media supplemented with 2 mM L-glutamine. cDNA encoding human SLC26A9 with eGFP fused to its C terminal was transfected in pcDNA3.1. Cells were transfected using standard protocols for Lipofectamine3000 (Thermo Fisher Scientific, Darmstadt, Germany). All media were supplemented with 10% heat-inactivated foetal calf serum (Capricorn Scientific, Ebsdorfergrund, Germany).

BCi-NS1 cells (kindly provided by Prof. R. Crystal, Weill Cornell Medical College, New York, USA) were cultured in supplemented Bronchial Epithelial Cell Growth Medium (BEGM; Lonza, Basel, Switzerland). BCi-NS1 cells were grown on permeable supports for up to 30 days (Snapwell #3801, Corning, New York, USA) in an air-liquid (ALI) interface. Human nasal cells were obtained from one adult donor using a cytological nasal brush and all procedures were ethically approved by the Institutional Medical Research Ethics Committee of the University

Medical Centre, Utrecht (protocol ID: 16/586). The cells were expanded and fully differentiated as previously described[321]. The human gastric tumour cell line HGT-1 was cultured as described earlier[322].

RT-PCR & plasmids: For RT-PCR total RNA from tissues or cells was isolated using NucleoSpin RNA II columns (Macherey-Nagel, Düren, Germany) and reverse-transcribed using random primer (Promega, Mannheim, Germany) and M-MLV Reverse Transcriptase RNase H Minus (Promega, Mannheim, Germany). Each RT-PCR reaction contained sense (0.5 µM) and antisense primer (0.5 µM) (Table 6.1), 0.5 µl cDNA and GoTaq Polymerase (Promega, Mannheim, Germany). After 2 min at 95°C cDNA was amplified (targets 35 cycles, reference GAPDH 25 cycles) for 30 s at 95°C, 30 s at 56°C and 1 min at 72°C. PCR products were visualized by loading on Midori Green Xtra (Nippon Genetics Europe) containing agarose.

Table 6.1 | *RT-PCR primers.*

Gene accession number	Primers	Size (bp)
human SLC26A9 NM_052934.4	s: 5´- CTACATCATTCCTGACCTGC as: 5´- CTGCATGTGATACTTTTTGGG	724
mouse Slc26a9 NM_177243.4	s: 5´- CATTTGCTGCGCTCTCTCAG as: 5´- CCTCTTCTCCTGCTTCCGG	568
GAPDH NM_001289726	s: 5´- GTATTGGGCGCCTGGTCAC as: 5´- CTCCTGGAAGATGGTGATGG	200

Cell-based high throughput screening and YFP-fluorescence quenching: LN215 cells expressing YFP-F46L/H148Q/I152L and SLC26A9 were plated at a density of 25,000 cells per well in 96-well microplates. Each well was washed two times with PBS (200 µL per well) and 50 µL of regular solution was added afterwards. Test compounds were applied to each well at 25 µM and plates were incubated for 10 min at 37 ºC. The 96-well plates were transferred to a FLUOstar Omega Microplate Reader (BMG Labtech, Ortenberg, Germany) to measure SLC26A9 activity. Baseline fluorescence was recorded for 0.8 s, then 50 µL of NaI - substituted regular solution (140 mM NaI replacing 140 mM NaCl) was injected by a syringe pump. Fluorescence was recorded for 8 s. The initial slope of YFP fluorescence was used to analyse SLC26A9-mediated I^- flux rate. YFP-fluorescence quenching assay for assessment of SLC26A4, SLC26A6, SLC26A9, CFTR, ANO1 and VRAC activity were performed accordingly, as described in a previous study[320].

Cell Viability Assay: Cell Titer 96® AQueous One Solution Assay kit (MTS) (Promega, WI, USA) was used to determine the effect of compounds on cell viability. Calu-3 cells were cultured in 96-well plates in growth medium supplemented with 10% FBS for 24 h until cell density

reached ~40%. Cells were treated with S9-A13 and cisplatin for 24 h followed by MTS analysis according to the supplier's protocol. The absorbance was measured by Infinite M200 microplate reader (Tecan, Männedorf, Switzerland) at a wavelength of 490 nm.

Western blotting: Cells were lysed with RIPA buffer (Millipore, MA, USA) containing a protease inhibitor cocktail. Each sample with equal amounts of protein was mixed with 5x SDS-sample buffer and then warmed to 37℃ for 30 min. 80 µL of protein samples were loaded to each lane, separated by 4-12% Tris Glycine Precast Gel (KOMA BIOTECH, Seoul, Korea) and then transferred to PVDF membrane. PVDF membranes were blocked with 5% non-fat skim milk in Tris-buffered saline including 0.1% Tween 20 (TBST), by incubation for 1 h at room temperature and afterwards incubating overnight at 4 ºC with the primary antibody for SLC26A9 (H00115019-A01; Abnova, Taipei City, Taiwan) and β-actin (Santa Cruz Biotechnology, Dallas, TX, USA). After incubation, the membranes were washed and incubated with HRP-conjugated anti-secondary IgG antibodies (Santa Cruz Biotechnology, Dallas, TX, USA) for 1 h at room temperature. SuperSignal™ Western Blot Substrate (Thermo Fisher Scientific, MA, USA) was used to visualize protein bands.

Immunocytochemistry: Mouse lung sections were fixed using 4% paraformaldehyde (PFA) and 3.4% sucrose in PBS. Lung sections were deparaffinized with xylene and rehydrated through a series of ethanol. Cells grown on permeable inserts were fixed with 4% PFA in PBS and embedded in paraffin. Sections or cells were incubated in rabbit anti-SCL26A9 antibody (1:100, raised against mouse SCL26A9 aa 11-29, DRAAYSLSLFDDEFEKKDR, Davids Biotechnologie, Regensburg, Germany) overnight at 4°C. Nonspecific binding of the antibody to the airway epithelium was excluded in previous publications showing lack of binding in airways from patients carrying the F508del-CFTR/F508del-CFTR mutation, which leads to a lack of apical expression of SLC26A9[323]. Antigen retrieval was performed in pre-heated Tris-EDTA buffer (pH 9.0) for 15 min, using a microwave before blocking. Cells were incubated with secondary anti-rabbit antibody conjugated with Alexa Fluor 488 or Alexa Fluor 546 (1:400) for 1h at room temperature. Nucleus was counterstained with 5 µM Hoe33342 (Thermo Fisher Scientific, Darmstadt, Germany). Section or cells were mounted with fluorescence mounting medium (DAKO Cytomation, Hamburg, Germany). Immunofluorescence was examined with an Axio Observer microscope equipped with Axiocam 503 mono, ApoTome.2 and ZEN 3.0 (blue edition) software (Zeiss, Oberkochen, Germany).

Patch clamp: Cells were patch clamped when grown on coated glass coverslips and experiments were done at 37 °C. Patch pipettes were filled with a cytosolic-like solution

containing (in mM): KCl 30, K-Gluconate 95, NaH_2PO_4 1.2, Na_2HPO_4 4.8, EGTA 1, Ca-Gluconate 0.758, $MgCl_2$ 1.03, D-Glucose 5, ATP 3; pH 7.2. The intracellular (pipette) Ca^{2+} activity was 0.1 µM. The bath was perfused continuously with Ringer's solution (in mM): NaCl 145, KH_2PO_4 0.4, K_2HPO_4 1.6, Glucose 5, $MgCl_2$ 1, Ca-Gluconate 1.3; at a rate of 5 mL/min. In some experiments extracellular chloride was substituted by equimolar concentrations of gluconate. Patch clamp experiments were performed as described previously[191].

Transepithelial Ussing chamber recordings: BCi-NS1 and primary human airway epithelial cells polarized on permeable supports were measured under short-circuit conditions in non-perfused chambers with bicarbonate-Ringer solution (mmol/l: NaCl 118.75; KH_2PO_4 0,4; K_2HPO_4 1,6; Glucose 5; $MgSO_4$ 1; Ca-Gluconate 1.3, $NaHCO_3$ 25; bubbled with 95% O_2/5% CO_2). For mouse trachea measurements, animals were sacrificed by cervical dislocation, and freshly isolated tracheas were cleaned, opened, and mounted into the same previously mentioned system, and measured under open circuit conditions. Comprehensive methods have been detailed in previous reports[176,278].

Intracellular pH measurements: For intracellular pH measurements cells were mounted and perfused with HCO_3^-/CO_2 solution (mmol/l: NaCl 118.75; KH_2PO_4 0,4; K_2HPO_4 1,6; Glucose 5; $MgSO_4$ 1; Ca-Gluconate 1.3, $NaHCO_3$ 25; bubbled with 95% O_2/5% CO_2). Cells were stimulated with Cl^- free HCO_3^-/CO_2 solution bubbled with 95% O_2/5% CO_2. ΔpH was taken as a measure of Cl^-/HCO_3^- antiport. Experimental procedures, acquisition of images and data analysis were described recently[176].

Airway surface liquid pH and assessment of proton secretory activity: Airway surface liquid pH (ASL pH) was measured using a temperature and CO_2-controlled plate reader (TECAN SPARK 10M), as previously described[324]. Briefly, the ASL was stained with 3 µL of a mixture of dextran-coupled pH-sensitive pHrodo Red (0.5 mg/mL, λex: 565 nm, λem: 585 nm, P10361, Thermo Fisher) and Alexa Fluor® 488 (0.5 mg/mL, λex: 495 nm, λem: 519 nm, D22910, Thermo Fisher) diluted in glucose-free HCO_3^- KRB, overnight at 37 °C, 5% CO_2. For experiments, all chemicals were added to the basolateral bathing solution. pHrodo and Alexa Fluor® 488 were measured every 5 minutes, data were analysed by subtracting the background values from each time point and then a ratio from pHrodo and Alexa Fluor® 488 was calculated. ASL pH standard calibration solutions were modified Ringer solution containing, in mM, 86 NaCl, 5 KCl, 1.2 $CaCl_2$, 1.2 $MgCl_2$ and either 50 MES (pH 5.5), 50 HEPES (pH 7.0) or 50 Tris (pH 8.0) at 37 ºC.

Proton secretory activity and corresponding data analysis were conducted by means of the pH-sensitive fluorescence dye 1,5 carboxy-seminaphto-rhodafluor acetoxymethylester (SNARF-1-AM; Life Technologies), as described previously[322].

Materials and statistical analysis: All compounds used were of highest available grade of purity. Data are reported as mean ± SEM. Student's t-test (for paired or unpaired samples as appropriate) or ANOVA were used for statistical analysis. A p-value < 0.05 was accepted as significant difference. For each experimental series the number of animals used, and the number of measurements/assays/reactions is provided.

Results

Identification of SLC26A9 inhibitor by high-throughput screening

For identification of novel small-molecule inhibitors for SLC26A9, a cell based high-throughput screening was conducted using LN215 astrocytoma cells that were stably expressing human SLC26A9 and halide-sensitive yellow fluorescent protein (YFP-F46L/H148Q/I152L) (Figure 6.1A). LN215-SLC26A9-YFP cells were incubated in 96-well microplates for 24 h, then treated with 25 µM of the test compounds for 10 min. Afterwards YFP fluorescence quenching by addition of iodide buffer was measured (Figure 6.1B). Representative YFP fluorescence traces and the effects of SLC26A9 inhibitors and inactive compounds are shown in Figure 6.1C,D.

Screening of 30,000 drug-like small molecules revealed three novel chemical classes of SLC26A9 inhibitors: S9-A01, S9-B01 and S9-C01. S9-A01, S9-B01 and S9-C01 potently inhibited the Cl^-/I^- exchange activity of SLC26A9 in a dose-dependent manner with IC_{50} of 2.25 ± 0.52, 16.63 ± 3.43 and 38.00 ± 1.88 µM, respectively (Figure 6.2A-D). In contrast, the CFTR-inhibitor GlyH-101 that has been reported to inhibit also SLC26A9 currents[159] did not inhibit the Cl^-/I^- exchange activity of SLC26A9, even when applied at 100 µM (Figure 6.2E). Notably, S9-A01 blocked SLC26A9 activity more potently than other inhibitors. To discover further inhibitors of SLC26A9 with even higher potency, we further evaluated the inhibitory effect of 17 additional derivatives of S9-A01 and found several compounds that were more potent than S9-A01, of which S9-A13 inhibited SLC26A9 most potently with an IC_{50} = 90.9 ± 13.4 nM (Table 6.2).

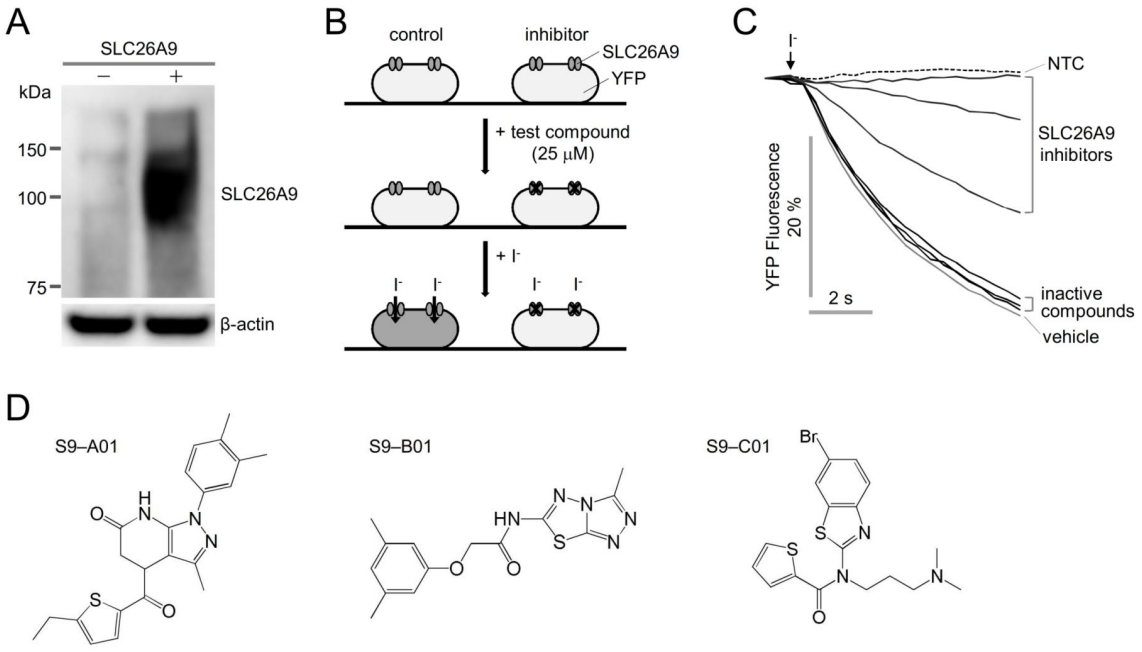

Figure 6.1 | *Identification of novel small molecule inhibitors of SLC26A9.*
A) Immunoblot of SLC26A9 in LN215 and LN215-SLC26A9-YFP cells. B) Schematic diagram showing the high-throughput screening process. C) Representative YFP fluorescence traces of SLC26A9 inhibitors and inactive compounds in LN215-SLC26A9-YFP cells. Cells were treated with test compounds at 25 µM for 10 min. D) Chemical structures of three classes of SLC26A9 inhibitors. Non-transfected cells (NTC, dashed line).

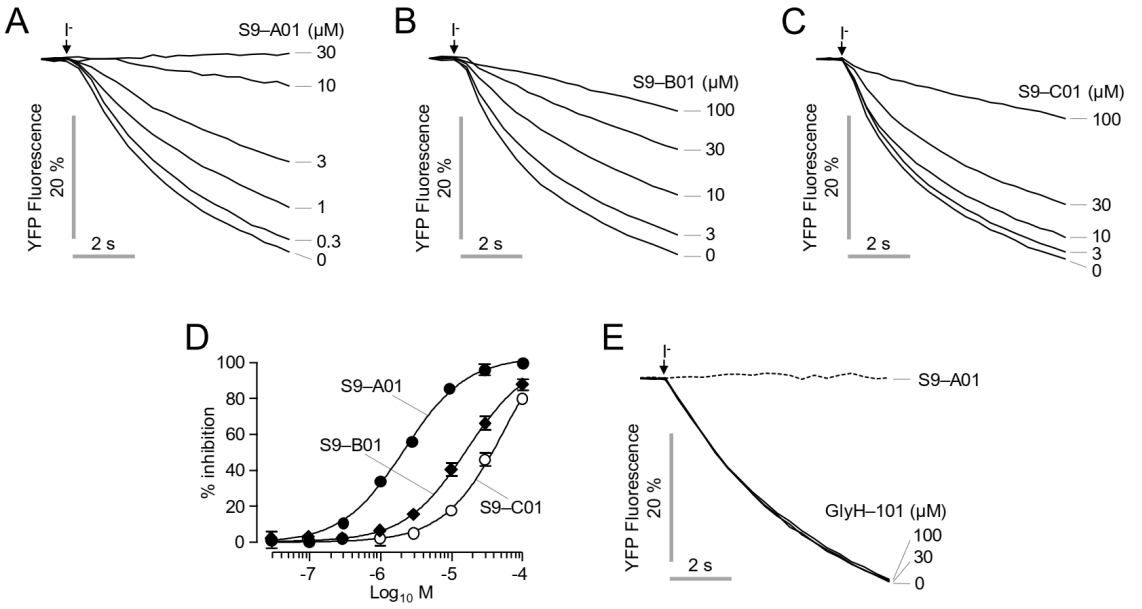

Figure 6.2 | *Effect of S9-A01, S9-B01 and S9-C01 on the Cl^-/I^- exchange activity of SLC26A9.*
A-C) Inhibitory effect of S9-A01, S9-B01 and S9-C01 on SLC26A9-mediated Cl^-/I^- exchange observed in YFP halide-quenching assays with LN215-SLC26A9-YFP cells. The indicated concentrations of S9-A01,

S9-B01 and S9-C01 were used to pretreat for 10 min prior to iodide injection. D) Dose response curves for S9-A01, S9-B01 and S9-C01. Mean ± SEM (n = 4 - 6). E) LN215-SLC26A9-YFP cells were pre-treated with the indicated concentrations of GlyH-101 and S9-A01 (30 µM) for 10 min prior to iodide injection. Mean ± SEM (n = 4 - 6).

Table 6.2 | *Effect of S9-A01 derivatives (Cmpd) on Cl^-/I^- exchange activity of SLC26A9.*
IC_{50} values were determined using YFP-fluorescence quenching assay in LN215-SLC26A9-YFP cells (mean ± S.E., n = 3).

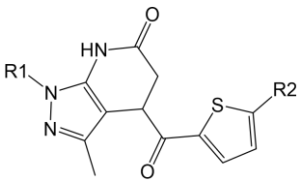

Cmpd	R1	R2	IC_{50} (µM)	Cmpd	R1	R2	IC_{50} (µM)
S9-A01	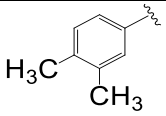	CH_2CH_3	2.25 ± 0.52	S9-A10	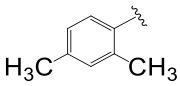	Cl	3.68 ± 0.92
S9-A02	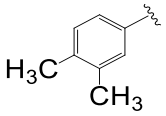	H	>30	S9-A11	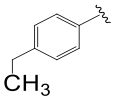	CH_2CH_3	>30
S9-A03	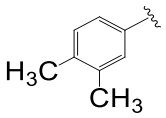	CH_3	0.28 ± 0.04	S9-A12	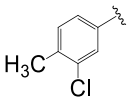	CH_2CH_3	1.08 ± 0.89
S9-A04	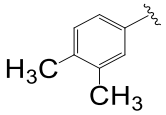	Cl	0.11 ± 0.02	S9-A13	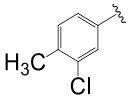	CH_3	0.09 ± 0.01
S9-A05	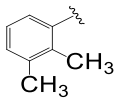	CH_3	>30	S9-A14	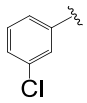	CH_2CH_3	>30
S9-A06	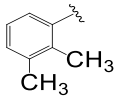	Cl	>30	S9-A15	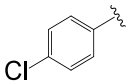	CH_2CH_3	>30
S9-A07	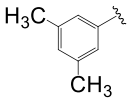	CH_3	0.58 ± 0.04	S9-A16	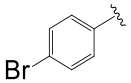	H	>30
S9-A08	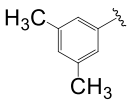	Cl	0.10 ± 0.02	S9-A17	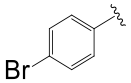	CH_2CH_3	>30
S9-A09	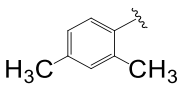	CH_3	>30	S9-A18	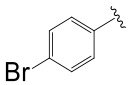	CH_3	0.26 ± 0.01

Potent inhibition of SLC26A9-mediated anion exchanges by S9-A13

The effects of S9-A13 on SLC26A9-mediated anion (Cl^-/I^- and Cl^-/SCN^-) exchange activities were measured in LN215-SLC26A9-YFP cells. S9-A13 potently inhibited SLC26A9-mediated Cl^-/I^- and Cl^-/SCN^- exchange activities with IC_{50} of 90.9 ± 13.4 nM and 171.5 ± 34.7 nM, respectively (Figure 6.3A-D). To determine whether S9-A13 affects cell viability, MTS assays were performed on Calu-3 cells endogenously expressing SLC26A9. Cells were treated with S9-A13 up to a concentration of 10 µM. No cytotoxicity was observed for S9-A13 even at high concentrations of the inhibitor (Figure 6.3E).

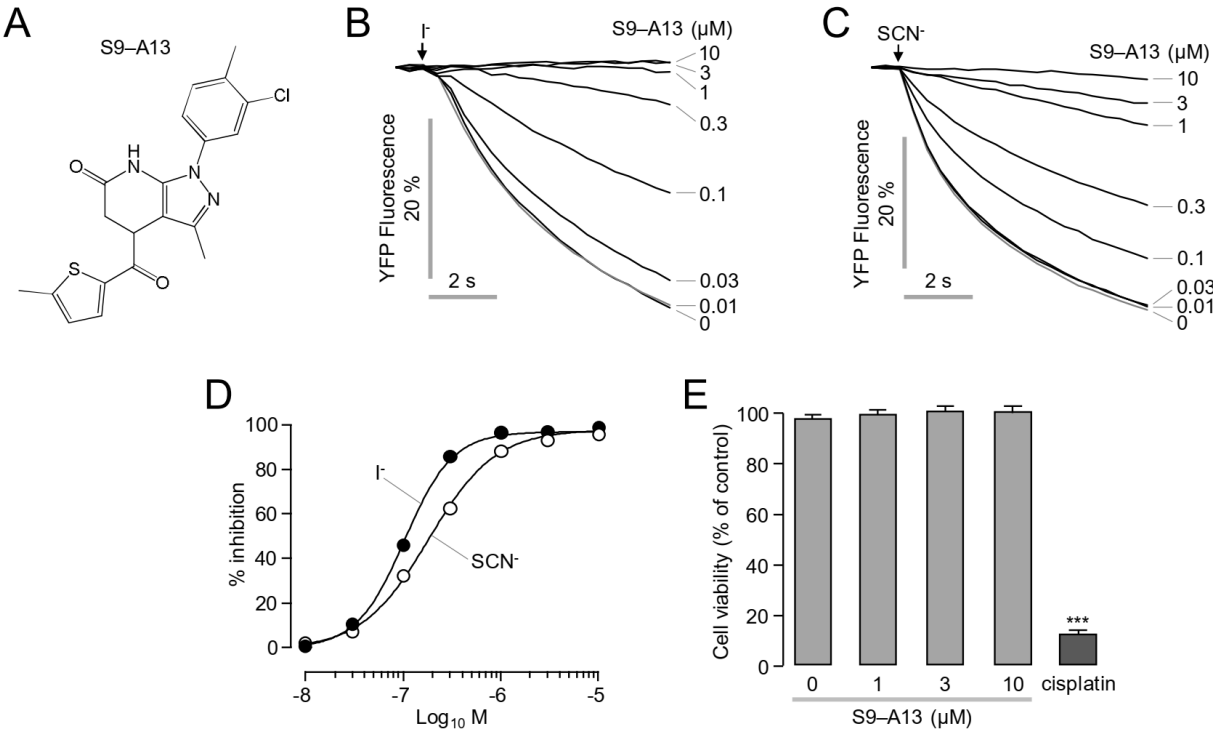

Figure 6.3 | *Effect of S9-A13 on SLC26A9-mediated Cl-/base exchange activity.*
A) Chemical structure of S9-A13. B,C) SLC26A9-mediated Cl^-/I^- and Cl^-/SCN^- exchange activities were measured in LN215-SLC26A9-YFP cells. Indicated concentrations of S9-A13 were pretreated for 10 minutes. D) S9-A13 dose-response for the inhibition of SLC26A9-mediated Cl^-/I^- and Cl^-/SCN^- exchange activity. Mean ± SEM (n=5). *significant activation by IF ($p<0.05$; paired t-test). E) Effect of S9-A13 on cell viability in Calu-3 cells. Cells were treated with S9-A13 for 24 h and then cell viability was determined by MTS colorimetric assay. Mean ± SEM (n=6).

Selective inhibition of SLC26A9 by S9-A13

We examined potential effects of S9-A13 on other anion exchangers (SLC26A3, SLC26A4, SLC26A6), and chloride channels (CFTR, ANO1 and VRAC). However, even a high

concentration (10 µM) S9-A13 did not affect the Cl^-/I^- exchange activity of SLC26A3 and SLC26A4 or Cl^-/SCN^- exchange activity of SLC26A6. 10 µM of S9-A13 did also not alter chloride transport by CFTR, ANO1 and VRAC. In contrast, the Cl^-/I^- exchange activities of SLC26A3, SLC26A4 and SLC26A6 were significantly inhibited by DRAinh-A250, YS-01 and niflumic acid, while Cl^- transport by CFTR, ANO1 and VRAC was completely blocked by CFTRinh-172, Ani9-5f and DCPIB, respectively (Figure 6.4A-G).

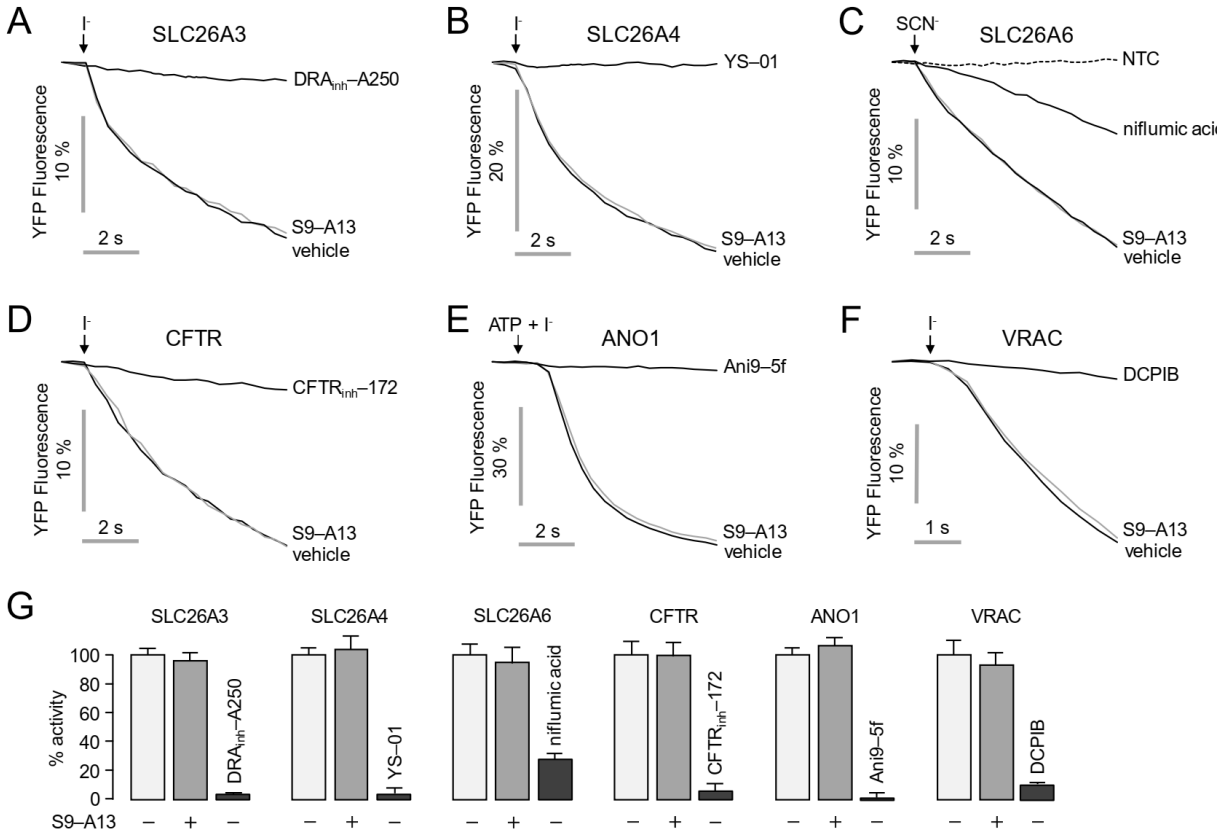

Figure 6.4 | *Effect of S9-A13 does not inhibit other SLC26 family members or chloride channels.*
A-C) Effects of S9-A13 on Cl^-/I^- exchange activities by SLC26A3, SLC26A4 and SLC26A6 were measured using YFP fluorescence quenching assay. Cells were treated with 10 µM of S9-A13 (gray line) for 10 min. SLC26A3, SLC26A4 and SLC26A6 were inhibited by DRAinh-A250 (10 µM), YS-01 (10 µM) and niflumic acid (500 µM), respectively. D-F) Effects of S9-A13 on CFTR, ANO1 and VRAC measured by YFP quenching in FTR-CFTR-YFP, FTR-ANO1-YFP, and LN215-YFP cells. For activation of CFTR, cells were pretreated with 10 µM forskolin. ANO1 was activated by 100 µM ATP. CFTR and ANO1 were inhibited by CFTRinh-172 (10 µM) and Ani9-5f (10 µM), respectively. VRAC was activated by a hypotonic challenge and was inhibited by 30 µM DCPIB. G) Summary of the results obtained in (A-F). Mean ± SEM (n=4-5).

S9-A13 inhibits SLC26A9 but shows little effects on CFTR currents in HEK293 cells

HEK293 cells were transfected with SLC26A9-cDNA, which induced strong expression of SLC26A9 protein (Figure 6.5A,B). Partially membrane-localized SLC26A9 caused robust constitutive whole cell currents as detected by whole cell patch clamping, which were inhibited by S9-A13 in a dose-dependent manner (Figure 6.5C-F). Currents in mock-transfected cells were not affected by S9-A13. Moreover, CFTR currents were only marginally inhibited at the highest concentration of S9-A13 (5 µM), and only at strongly depolarized clamp voltages (Figure 6.5G,H). Notably, SLC26A9 currents were not further stimulated by increase in intracellular cAMP using IBMX/forskolin (Figure 6.5I).

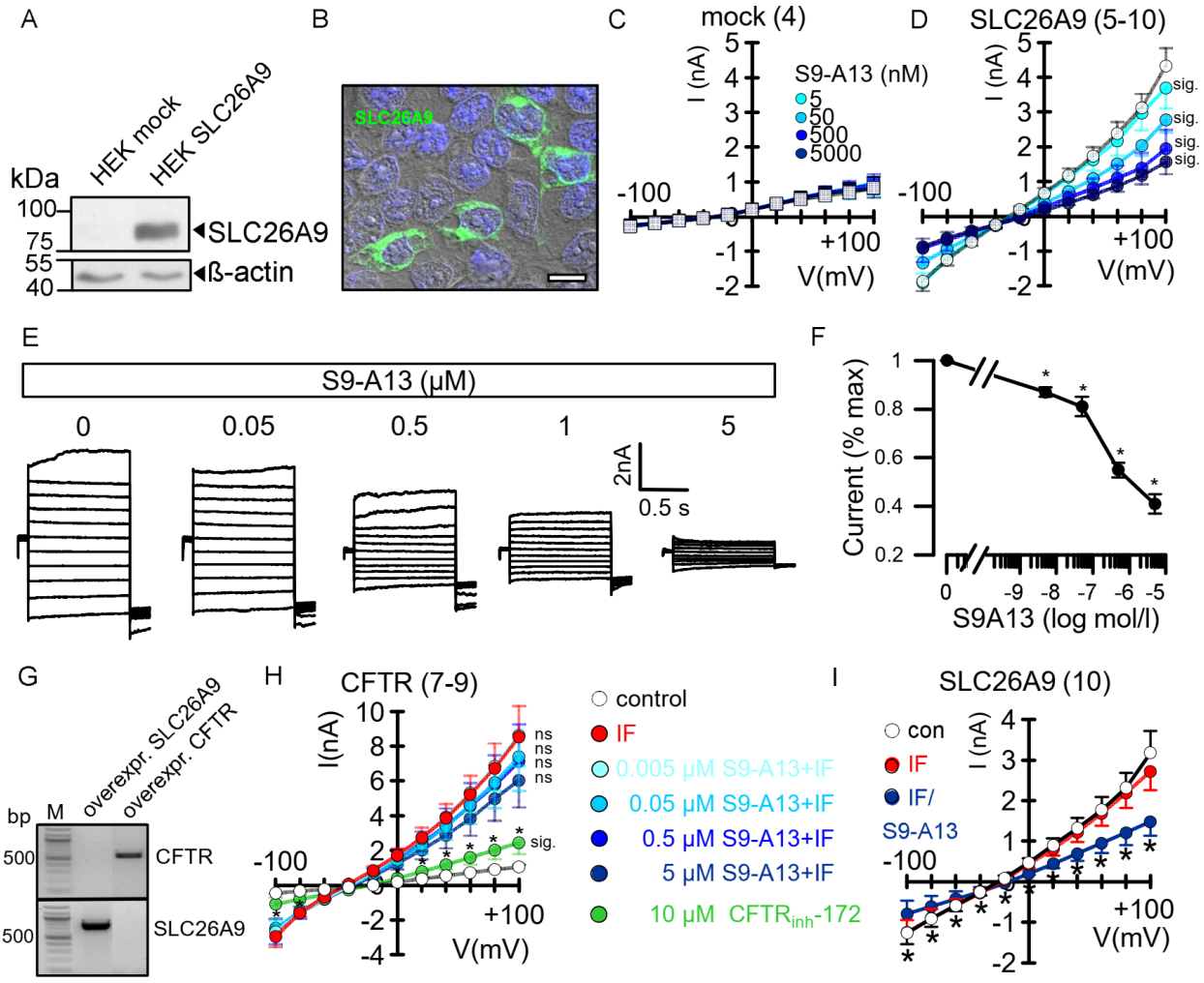

Figure 6.5 | *S9-A13 inhibits SLC26A9 currents in HEK293 cells.*

A,B) Western blot and immunolabelling of SLC26A9 expressed in HEK293 cells demonstrating only partial membrane expression of SLC26A9. Bar = 20 µm. C) Current/voltage relationships for whole cell currents obtained in mock-transfected HEK293 cells, demonstrating absence of basal currents and lack

of S9-A13 effects. D) Enhanced basal ion currents in cells expressing SLC26A9, which are inhibited dose-dependently by S9-A13. E) Overlays of SLC26A9 currents showing inhibition by S9-A13. F) Corresponding concentration-response curve. G) RT-PCR showing overexpression of SLC26A9 and CFTR in HEK293 cells. H) Lack of inhibition of CFTR whole cell currents (IBMX and forskolin, IF; 100 µM and 2 µM) by S9-A13. Only the highest concentration of S9-A13 (5 µM) inhibited currents at +100 mV clamp voltages, while CFTRinh-172 (10 µM) strongly inhibits CFTR currents. I) Inhibition of SLC26A9 by S9-A13 and lack of further activation of SLC26A9 by IF. Mean ± SEM (number of cells). *significant inhibition by S9-A13 and CFinh172 (10 µM) ($p<0.05$; paired t-test).

S9-A13 has a minor effect on ion transport in human airway epithelial cells

We analysed the effects of S9-A13 in BCi-NS1 human airway epithelial cells, which strongly express CFTR[191]. These cells express endogenously a number of SLC26A9 splice variants, leading to isoforms a (87 kDa; NM_052934.4), b (97,3 kDa; NM_134325.3), x1 (77 kDa; XM_011509121.2), x2 (68,9 kDa; XM_011509122.2), and x3 (51 kDa; XM_011509124.2)[163] (Figure 6.6A, Supplementary Figure 6.1). The same pattern for SLC26A9 splice variants was detected in other human airway epithelial cell lines, such as Calu3 or CFBE14o- (not shown). The larger band size for SLC26A9 in airways of about 120 kDa is most likely due to glycosylation[159], while overexpression of SLC26A9 in HEK293 cells produced a band at only around 90 kDa (Figure 6.5A). Immunostaining of SLC26A9 in plastic grown BCi-NS1 cells demonstrated intracellular and plasma membrane localization (Figure 6.6B). Surprisingly, S9-A13-inhibitable Cl^- currents were not detected, suggesting no Cl^- transport by SLC26A9 in normal airways (Figure 6.6C).

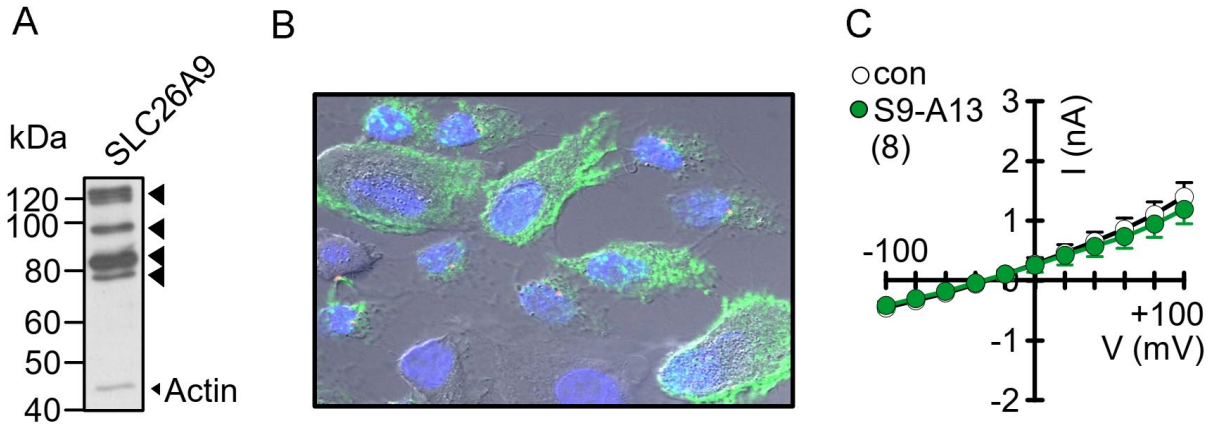

Figure 6.6 | *Endogenous SLC26A9 in BCi-NS1 human airway epithelial cells does not produce a Cl^- current.*

A) Western blot indicates expression of various isoforms of SLC26A9. B) Immunocytochemistry of SLC26A9 in non-polarized BCi-NS1 cells. C) Current/voltage relationships showing no effect S9-A13 (5 µM) on constitutive currents. Mean ± SEM (number of cells).

BCi-NS1 cells were grown on permeable supports in PneumaCult™ differentiation medium under ALI. BCi-NS1 formed a well differentiated epithelium with mostly ciliated epithelial cells (Figure 6.7A). The effects of S9-A13 on short circuit currents were examined in Ussing chamber recordings. We found a small albeit significant inhibition of basal Isc by increasing concentrations of S9-A13 (Figure 6.7B,C). However, when compared to the pronounced inhibition of IF-activated Isc by CFTRinh-172 (CFinh), inhibition of Isc by S9-A13 was negligible. In BCi-NS1 airway cells, CFTRinh-172 inhibited also basal Isc present under non-stimulated conditions (Supplementary Figure 6.4C-E). Essentially identical results were obtained in primary human airway epithelial cells (Supplementary Figure 6.4A,B). The results indicate that CFTR is in charge of both basal and stimulated Cl^- secretion in human airways.

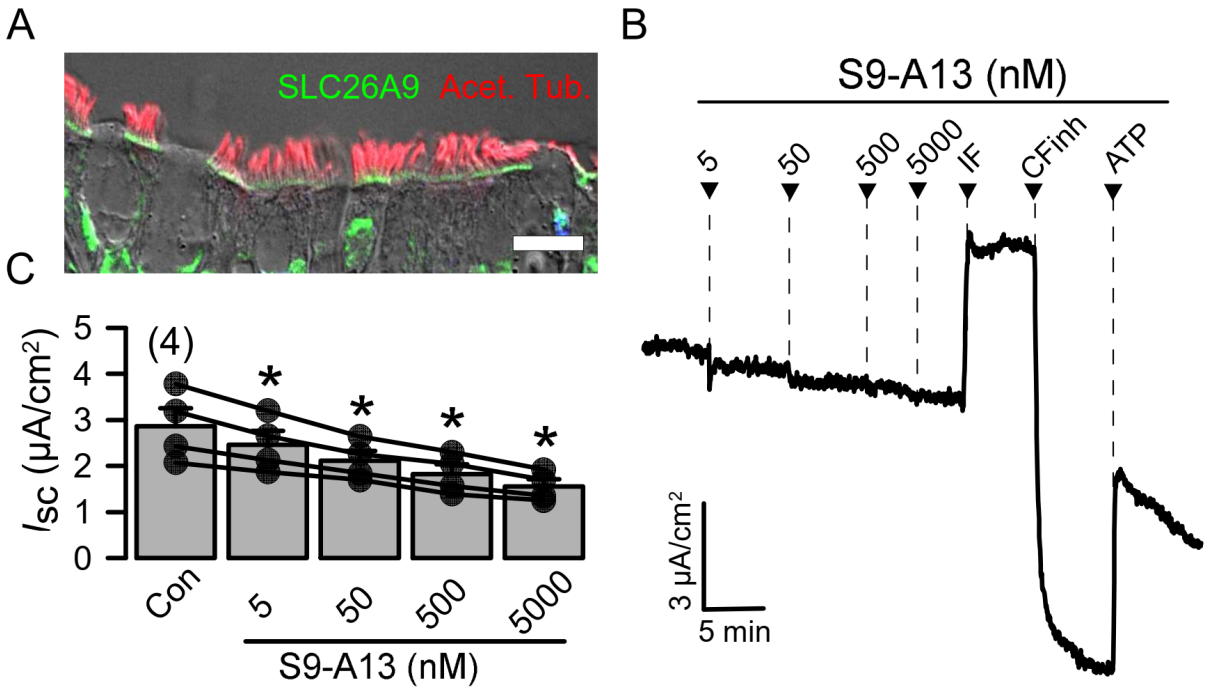

Figure 6.7 | *Minimal contribution of SLC26A9 to basal ion transport in differentiated BCi-NS1 airway epithelial cells.*

A) Pseudostratified ciliated airway epithelium formed by differentiated BCi-NS1 cells. Immunohistochemistry indicates apical expression of SLC26A9 in ciliated cells. Bar = 10 µm. C,D) Small but significant concentration-dependent inhibition of basal short circuit currents by S9-A13 (Isc; presence of amiloride). Increasing concentrations of S9-A13 were added subsequently to the chamber. Activation of CFTR by IF (100 µM/2 µM) and inhibition by CFTRinh-172 (CFinh; 20 µM) was dominating when compared to the effects of S9-A13. ATP was applied at 100 µM. Mean ± SEM (number of tissues). *significant inhibition of Isc ($p<0.05$; paired t-test).

Basal transport in mouse trachea is due to Cftr but not Slc26a9

We also examined expression of Slc26a9, constitutive transport (I'sc; measured under open circuit conditions) and inhibition by S9-A13 in freshly excised mouse tracheas. Immunohistochemistry demonstrated apical expression of Slc26a9 in ciliated cells of mouse airway epithelium, while non-ciliated cells such as club cells and goblet cells did not express Slc26a9 (Figure 6.8A). S9-A13 did not inhibit constitutive (basal) ion transport in mouse trachea (Figure 6.8B,C). In contrast, CFTRinh-172 dose-dependently blocked basal Isc, again demonstrating CFTR as the constitutive Cl^- conductance in airways (Figure 6.8D,E). In contrast to Ca^{2+}-dependent (Tmem16a) Cl^- secretion (ATP), cAMP-activated transport (Cftr; IF) was small, due to low expression of Cftr in mouse trachea[325]. The small activation of I'sc by IF in the presence of CFTRinh-172, is explained by activation of KCNQ1/KCNE3 K^+ channels[326].

SLC26A9 supports alkalization of ASL pH and H^+ secretion by gastric cells

Because we found little contribution of SLC26A9 to Cl^- transport, we examined if SLC26A9 has a different function in airways. In ASL pH measurements, fully differentiated nasal epithelial cells were exposed to S9-A13 or control solution. Online recordings of ASL pH under thin film conditions indeed showed a sustained decrease in ASL pH by S9-A13 (Figure 6.9A–D). Two hours after application of S9-A13, ASL pH dropped by 0.23 ± 0.11 units (n = 6). Subsequent stimulation of CFTR by forskolin caused only a small but not significant increase in ASL pH in airways exposed to S9-A13. These results strongly suggest a role of SLC26A9 for alkalization of ASL pH. As SLC26A9 was proposed as an apical Cl^- transporter relevant for HCl secretion by gastric parietal cells[302], we also examined the effect of S9-A13 on histamine-induced H^+ secretion by HGT-1 human gastric cells. Remarkably, S9-A13 significantly inhibited H^+ secretion by HGT-1 cells, supporting the concept of SLC26A9 being a Cl^- release channel in parietal cells[301,302,319] (Figure 6.9E).

Discussion

In the present study, we demonstrate S9-A13 as the first specific and highly potent inhibitor of SLC26A9. S9-A13 inhibits SLC26A9 in the low nanomolar range. It does not show cytotoxic effects, even at micromolar concentrations. The inhibitor was used to examine the potential role of SLC26A9 for ion transport in the airway epithelium. This is of particular interest in cystic fibrosis, as genome-wide association studies demonstrated SLC26A9 as an important modifier of CF lung and gastrointestinal disease: (i) SLC26A9 is expressed in the intestinal and airway epithelium as well as other CF-relevant tissues, (ii) single nucleotide polymorphisms

(cSNPs) of SLC26A9 were found to be associated with variable anion transport properties, and (iii) SLC26A9 was shown to modulate CF-related intestinal disease, diabetes and airway response to CFTR-therapeutics[167,327-330].

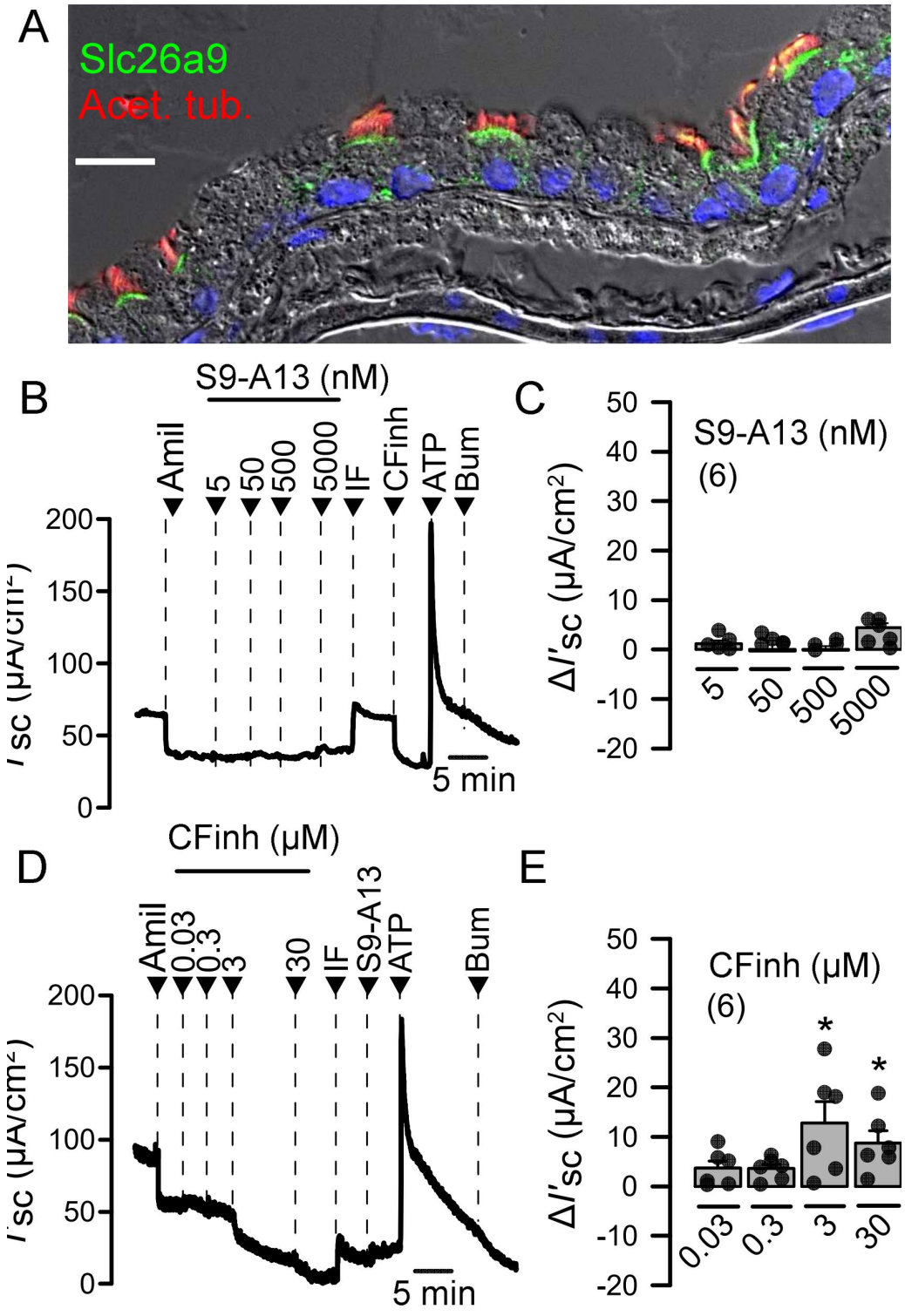

Figure 6.8 | *Basal ion transport in mouse trachea is due to CFTR but not SLC26A9.*

A) Airway epithelium from mouse trachea. Immunohistochemistry indicates apical expression of

SLC26A9 in ciliated airway epithelial cells. Bar = 20 µm. B,C) Constitutive equivalent short circuit current (I'sc) assessed in open circuit Ussing chamber recordings, were not inhibited by S9-A13. D,E) Concentration dependent inhibition of constitutive Isc by CFTRinh-172. Mean ± SEM (number of tracheas). *significant inhibition of Isc ($p<0.05$; paired t-test).

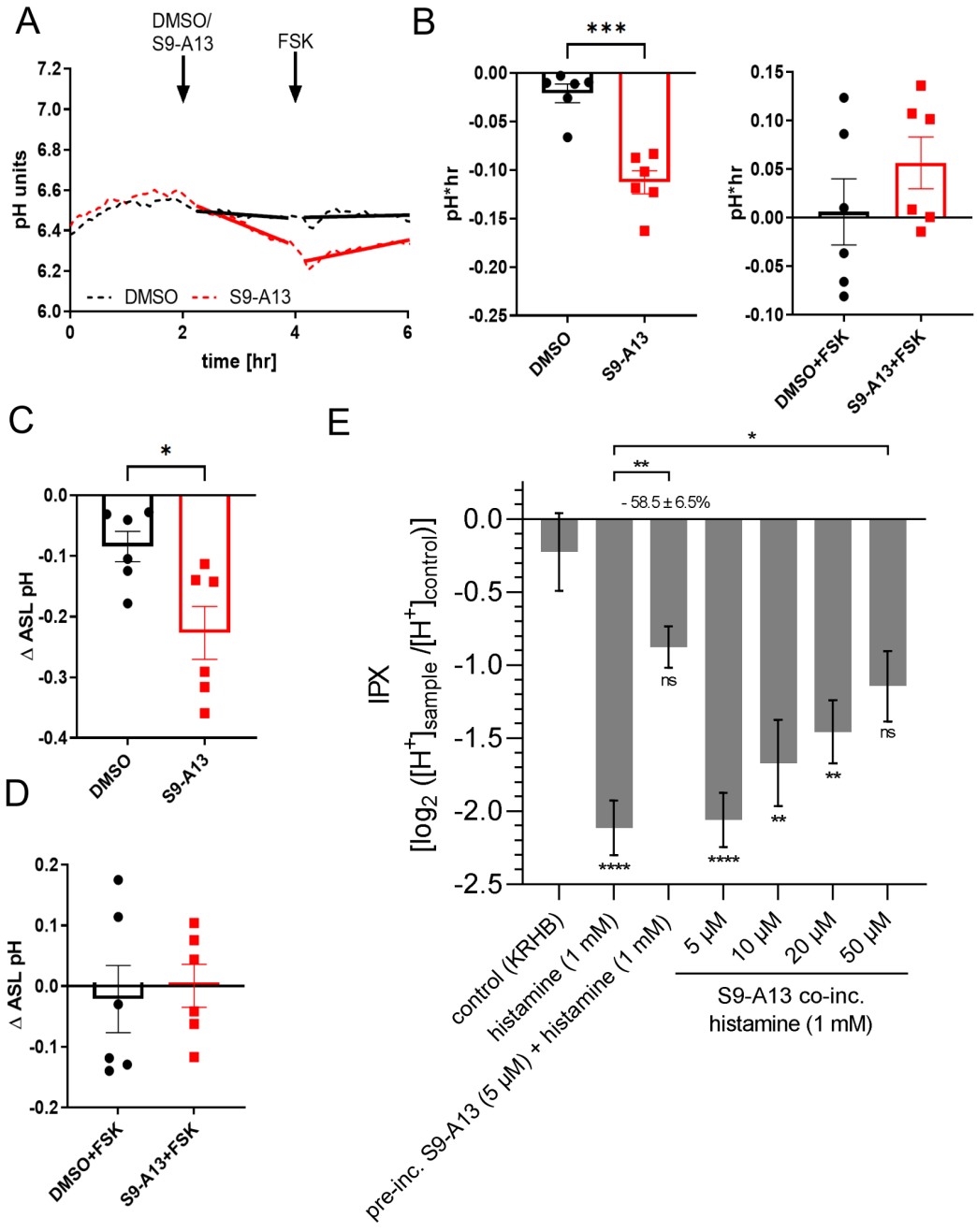

Figure 6.9 | *SLC26A9 supports alkalization of ASL pH and H⁺ secretion by gastric cells.*
A) Real-time ASL pH traces showing response to basolateral addition of S9-A13 (5 µM) or control (DMSO) and subsequent stimulation with forskolin (FSK; 10 µM). B) Rate of ASL pH change per hour after adding S9-A13 or control (left) and rate of pH change after adding FSK (right). C) Absolute change in ASL pH after adding S9-A13 or control. D) Absolute change in ASL pH after adding FSK. Mean ± SEM (n = 6).

*significant inhibition of Isc ($p<0.05$; paired t-test). E) Summary of the inhibitory effects of S9-A13 (30 min preincubation or 10 min coincubation) on proton secretion by HGT-1 human gastric cells stimulated with histamine (1 mM). Mean ± SEM (n = 4 – 6). *significant difference ($p < 0.05$ – 0.0001; one-way ANOVA & Holm-Šidák post hoc test).

A number of studies argue in favour of CFTR being responsible for constitutive (basal) anion secretion that is absent in CF airways[176,331-333]. Other reports provided evidence for the role of SLC26A9 in basal airway Cl^- transport[159,166,311,313,316]. So far it was difficult to discriminate between both conductances due to the lack of specific inhibitors for SLC26A9. SLC26A9 inhibitors used in earlier studies were not specific and inhibited also other Cl^- channels[159-161]. Moreover, expression and activity of both CFTR and SLC26A9 are functionally connected. Intracellular trafficking and constitutive activity of SLC26A9 are compromised in cystic fibrosis (CF) airway epithelia expressing the trafficking mutant F508del-CFTR[166,303,304]. In the presence of F508del-CFTR, binding of the PDZ-domain protein CAL inhibits the function of SLC26A9 due to enhanced endoplasmic reticulum-associated proteasomal degradation[310]. Vice-versa, SLC26A9 may support biogenesis and/or stabilization of CFTR[334].

Here we present evidence that SLC26A9 is located in the apical membrane of ciliated airway epithelial cells, but not in non-ciliated club or goblet cells. Overexpression of SLC26A9 induced a basal Cl^-- conductance in HEK293 cells, which was well inhibited by S9-A13. Unlike reported recently[313], SLC26A9 in HEK293 cells could not be further activated by increase in intracellular cAMP (Figure 6.5I). SLC26A9 is expressed endogenously in human airway epithelial cells such as CFBE, Calu3, and BCI-NS1, but Cl^- transport by SLC26A9 could not be detected in these cells using S9-A13. As airways express CFTR, we speculate regulation of SLC26A9-mediated HCO_3^- transport by CFTR.

Evidence for a role of SLC26A9 in HCO_3^- transport was presented earlier [158,162,301,302,319,335]. Other studies detected transport of Cl^- but not HCO_3^- by SLC26A9[159-161,165]. pH measurements in HEK293 cells expressing SLC26A9 did not provide conclusive evidence for SLC26A9-mediated HCO_3^- transport (Supplementary Figure 6.2). In CFTR-expressing BCi-NS1 cells, primary human airway epithelial cells, and mouse trachea, a substantial SLC26A9-mediated Cl^- transport could not be detected (Figures 6.6-6.8, Supplementary Figure 6.4). In contrast, airway surface liquid pH was significantly reduced by S9-A13, suggesting a role of SLC26A9 for HCO_3^- secretion (Figure 6.9A-D).

In cells that only express SLC26A9 but not CFTR, such as HEK293 cells or LN215 cells, Cl^-/HCO_3^- exchange by SLC26A9 could not be detected, while Cl^- transport by SLC26A9 is clearly present (Figures 6.1-6.3, 6.5, Supplementary Figure 6.3). Stomach mucosa expresses only low levels of CFTR[336], here, SLC26A9-mediated Cl^- transport may parallel H^+ secretion by the proton pump. This is supported by S9-A13-dependent inhibition of H^+ secretion in HGT-1

human gastric cells[301,302,319] (Figure 6.9). We speculate that depending on expression of CFTR, SLC26A9 may transport Cl^- or HCO_3^-[162]. While Cl^- secretion is due to CFTR, basal HCO_3^- secretion might be due to SLC26A9 (Figure 6.8, Supplementary Figure 6.4C,D). Immunofluorescence suggested pronounced expression in ciliated cells, while transcriptome analysis indicated SLC26A9 enriched in pulmonary neuroendocrine cells, where it could have sensory, neuroendocrine or other functions to protect airways from mucus obstruction. Interestingly, even in the presence of the inhibitor of adenylate cyclase type 1, ST034307, or in the presence of the adenosine A2B receptor inhibitor PSB603, basal Cl^- secretion by CFTR is still detectable (Supplementary Figure 6.4E). This suggests that CFTR does not need to be activated by cAMP/PKA to produce a basal Cl^- conductance, but may be activated by SLC26A9[334]. The novel SLC26A9 inhibitor S9-A13 may allow to further unravel functional relationships between CFTR and SLC26A9.

Acknowledgements

This research was supported by the UK Cystic Fibrosis Trust SRC013, German Research Foundation (DFG) KU756/14-1, Gilead Foundation, and National Research Foundation of Korea NRF2018R1A6A1A03023718/NRF2020R1C1C1008332). The technical assistance by Patricia Seeberger is greatly appreciated. We thank Prof. Dr. Nick Klymiuk and Dr. Florian Jaudas (Molecular Animal Breeding and Biotechnology, LMU Munich) for providing the piglet lung tissues.

Supplementary material

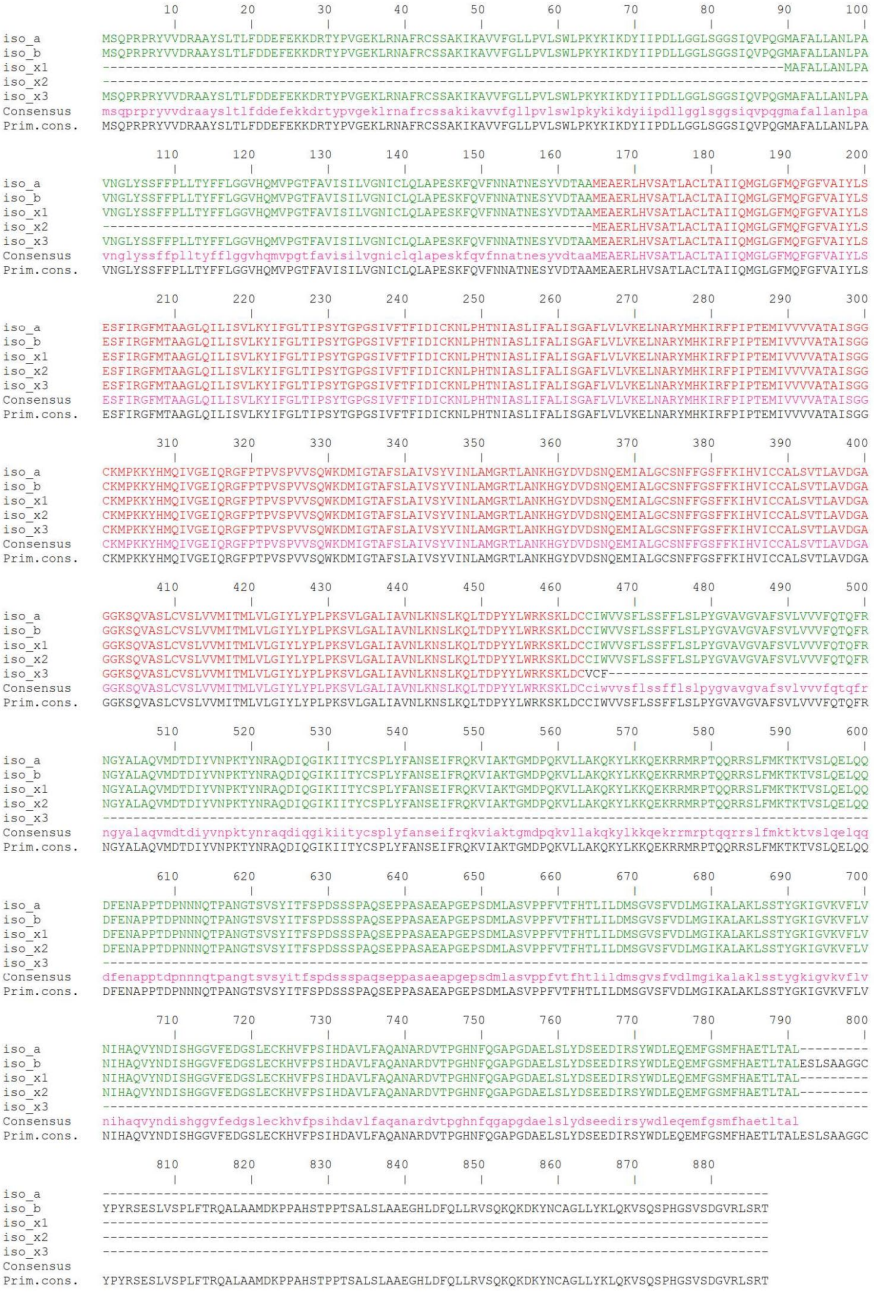

Supplementary Figure 6.1 | *Alignment of human SLC26A9 isoforms.*

NPS@: Network Protein Sequence Analysis TIBS 2000 March Vol. 25, No 3 [291]:147-150 Combet C., Blanchet C., Geourjon C., Deléage G.

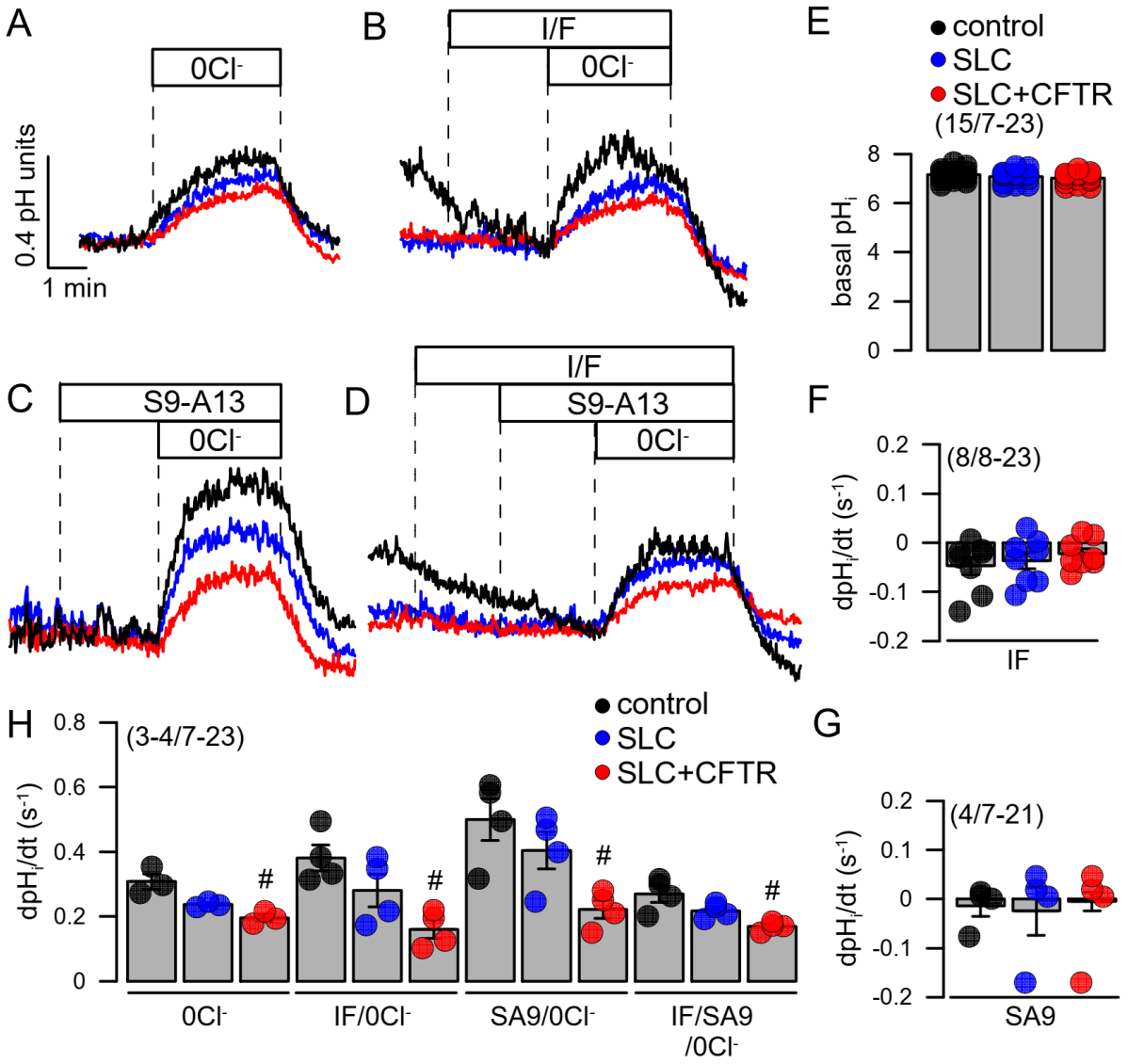

Supplementary Figure 6.2 | *No evidence for CFTR-regulated HCO_3^- transport of SLC26A9.*
A-D) Original recordings of intracellular pH (pH_i) using BCECF-fluorescence in HEK293 cells. Cells expressed SLC26A9 (blue), co-expressed SLC26A9+CFTR (red), or were mock transfected (black). $0Cl^-$ indicates removal of Cl^- from the extracellular bath solution. E-G) Summary of basal pH_i and changes (initial slope) induced by IBMX and forskolin (I/F; 100 µM/2 µM) or S9-A13 (SA9; 5 µM). H) Summary of changes induced by $0Cl^-$ (initial slope) under the various conditions. No evidence was found for HCO_3^- transport by expression of SLC26A9. Reduced alkalinization in the presence of CFTR may indicate release of HCO_3^- by CFTR. Mean ±SEM (number of coverslips/number of cells). #significant difference when compared to mock ($p<0.05$; unpaired t-test).

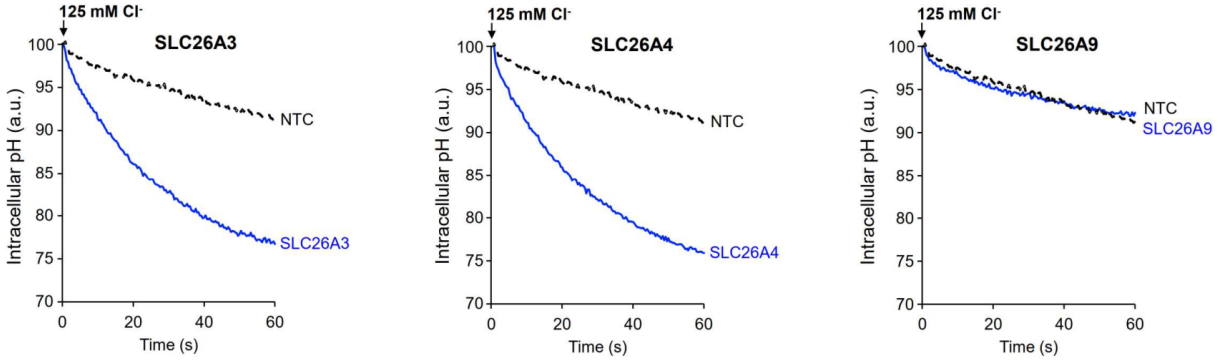

Supplementary Figure 6.3 | *No evidence for Cl^-/HCO_3^- exchange activity of SLC26A9.*
Cl^-/HCO_3^- exchange activities of SLC26A3, SLC26A4 and SLC26A9 were detected in LN215 cells by assessing changes in the intracellular pH. Replacement of extracellular Cl^- free bath solution (0 mM Cl^-, 25 mM HCO_3^-) by an extracellular bath solution with high chloride concentration (125 mM Cl^-, 25 mM HCO_3^-). A pronounced Cl^-/HCO_3^- exchange activity was found for SLC26A3 and SLC26A4 but was undetectable for SLC26A9. Intracellular pH traces show traces representative of three independent experiments.

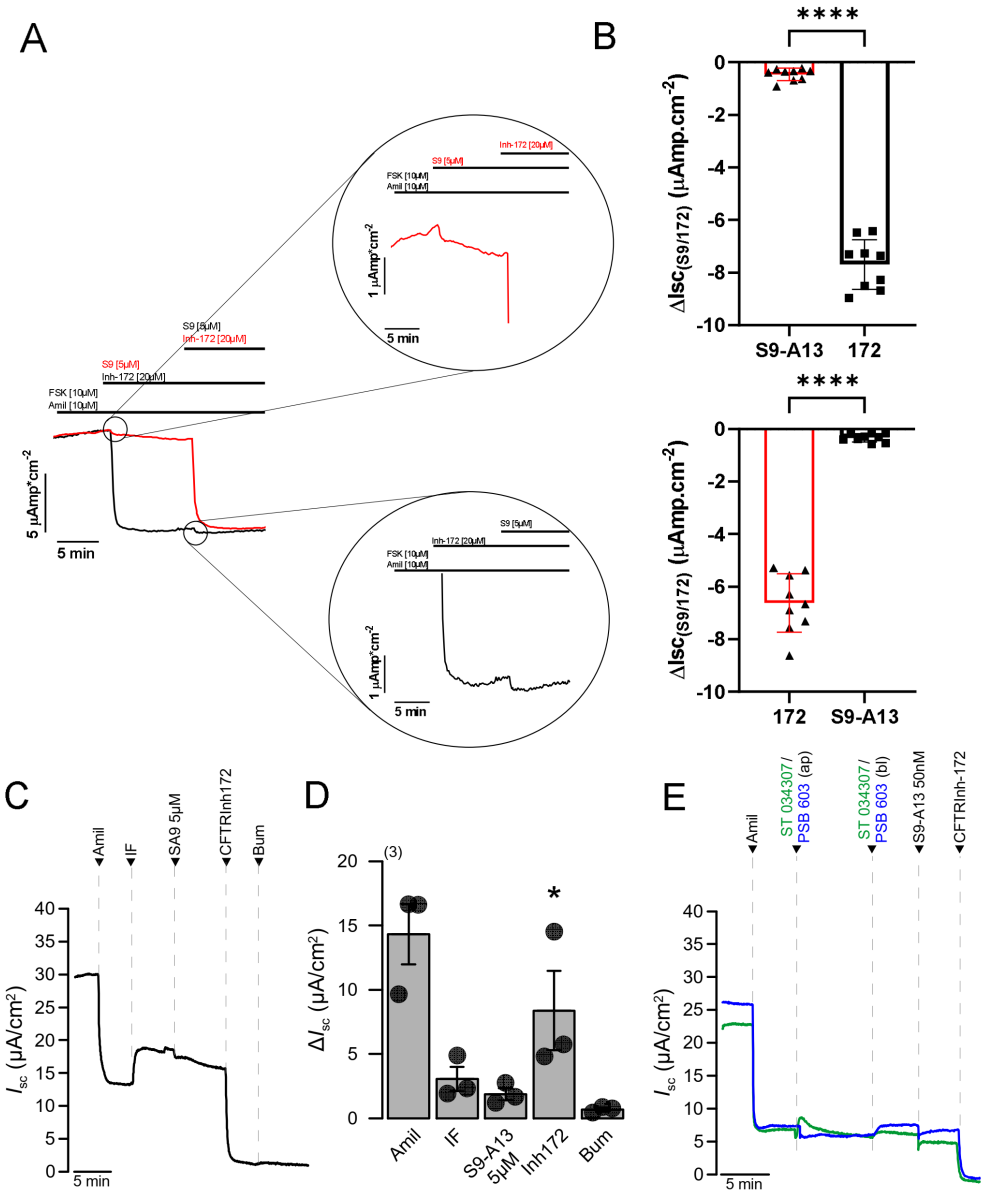

Supplementary Figure 6.4 | *Negligible Cl^- transport by SLC26A9 in human airway epithelia.*
A) Original Ussing chamber recordings of primary human airway epithelial cells grown under polarized conditions in an air-liquid interface (ALI). After inhibition of ENaC by amiloride (10 µM) and stimulation with forskolin (10 µM) the SLC26A9 inhibitor S9-A13 (S9; 5 µM) was applied before or after application of CFTRinh172 (Inh-172; 20 µM). Under both conditions SLC26A9 had very little contribution to electrogenic ion transport (short circuit current; Isc). B) Summaries for the inhibition of Isc by CFTRinh172 and S9-A13 (n=9; *p<0.001; unpaired t-test). C,D) Original recordings and summaries for Isc changes in polarized (ALI) BCi-NS1 human airway epithelial cells, demonstrating little effect of S9, but clear inhibition of Isc by CFTRinh172 (5 µM) after stimulation with IBMX/forskolin (100 µM/2 µM). Mean ± SEM. *indicates significant difference (p<0.05; unpaired t-test). E) Original Isc recordings from BCi-NS1 cells indicate that even in the presence of the inhibitor of the adenylate cyclase type 1, ST034307 (30 µM), or the adenosine A2B receptor inhibitor PSB603 (100 nM), basal Cl^- secretion is due to CFTR, as indicated by inhibition with CFTRinh172 (5 µM).

CHAPTER 7 | DISCUSSION

TMEM16A plays a more relevant role in airway mucus production/release and bronchoconstriction than in fluid secretion, particularly under inflammation

There is an ongoing debate as to whether TMEM16A should be activated or inhibited for the treatment of chronic airway inflammatory diseases. To this date, several TMEM16A activators have proceeded into clinical trials. Denufosol (INS37217), a metabolically stable $P2Y_2$-receptor dinucleotide agonist, was shown to mediate increases in intracellular Ca^{2+}, activate Ca^{2+}-activated Cl^- channel (CaCC) currents, enhance ciliary beating frequency (CBF), and, in parallel, to attenuate ENaC function, contributing to a transient increase in airway fluid volume and improved mucociliary clearance (MCC)[337,338]. However, in a phase III clinical trial where CF patients were treated via inhalation three times daily for 48 weeks, denufosol failed to show improvement in pulmonary function or reduce the incidence of pulmonary exacerbations[174]. This has been ascribed to the only transient activation profile of $P2Y_2$ receptors, that rapidly depletes intracellular Ca^{2+} stores and desensitizes the receptor, which may even negatively influence MCC in the long term[338]. On the other hand, denufosol-mediated stimulation of airway $P2Y_2$ receptors has also been shown to lead to acute mucin production/secretion that may counteract MCC improvement by increasing the mucus volume in the airway surface liquid (ASL)[337]. This might explain why the most common adverse effect observed in clinical trials involving denufosol was cough[339]. Moreover, lancovutide (duramycin; Moli1901), a bacterial-derived polycyclic peptide whose hypothesized mechanism of action is to induce increases in intracellular Ca^{2+} that lead to activation of CaCCs in CF epithelia at low concentrations of the drug (≤ 1 μM)[340,341], has recently also failed to show clinical benefit for CF patients in a phase II trial, showing in contrast an increased number of adverse events in the treated groups, with again the most observed unfavorable effect being cough[175]. This is in accordance with our data, where we show that Eact, a putative TMEM16A-activator[195], acutely induces mucus release and bronchoconstriction, when applied directly to the airways of asthmatic mice, via intratracheal (I.T.) instillation (Figure 2.2). In parallel, Eact has been shown to induce CF airway epithelial Cl^- secretion in a dose-dependent manner, particularly under inflamed conditions (IL-4 treatment)[195]. Furthermore, brevenal had originally been shown to improve tracheal mucus velocity at picomolar concentrations, by modulating sodium absorption in allergic sheep airways[202,342]. Later, it was reported by Silurian Pharmaceuticals to be an activator of CaCC[135]. Our data suggest that brevenal is an activator as well as a potentiator of TMEM16A (Figure 2.7), and that these effects are not driven by an increase in intracellular Ca^{2+} (Figure 2.8A-C). Brevenal therefore potentially modulates the Ca^{2+}-sensitivity of TMEM16A, allowing it to be activated at lower, basal Ca^{2+} levels. In parallel, acute administration of brevenal via I.T. instillation to mouse airways leads to mucus release and airway constriction

(Figure 2.8D-F). Ultimately, the balance between airway mucus production/release and Cl^-/fluid secretion by activation of TMEM16A seems to bend towards mucus accumulation in the airways, which, together with enhanced airway constriction, may worsen the pathology in inflamed airways. It is important to re-emphasize that TMEM16A is hardly expressed in fluid-secretory ciliated cells, yet shows a clear expression in mucus-secretory and airway smooth muscle (ASM) cells, which are hyper/metaplastic under airway inflammation[99,132,135,143]. Moreover, our staining data (Supplementary Figure 2.2) and previous reports[187,189] suggest that activation of upregulated TMEM16A in the pulmonary arterial (PA) endothelium and smooth muscle cells of asthma and CF patients may contribute to pulmonary artery remodeling, constriction, and PA hypertension, which further compromises lung function. This clearly asserts the importance of evaluating the effects of activators/potentiators and inhibitors of TMEM16A under inflammatory conditions.

It may be relevant to contemplate the physiological sense of having two distinct pathways driving airway fluid secretion. Others have reported that the concentrations of nucleotides and their metabolites within the ASL are major regulators of airway surface hydration[338]. It has been described that the mechanical stress suffered by the beating airway cilia varies with the viscoelasticity of the mucus layer, and that ciliated cells release ATP to the airway lumen accordingly, in order to regulate mucus hydration[338]. ATP-mediated activation of apical membrane $P2Y_2$ purinergic receptors stimulates both cAMP- and Ca^{2+}-induced fluid secretion via CFTR and CaCCs, as well as inhibition of fluid absorption via ENaC[338,343]. In parallel, extracellular ectonucleotidases hydrolyze secreted ATP to its ultimate breakdown product adenosine, which activates P1 purinoreceptors, such as the adenosine A2B receptor, that contribute to enhanced intracellular cAMP levels[343] (Figure 7.1).

Of note are the different channel characteristics of CFTR and CaCCs. In the case of CFTR, the cAMP-dependent activation of protein kinase A (PKA) leads to phosphorylation of CFTR's regulatory (R) domain, inducing disengagement of this domain from an initial inhibitory position. In parallel, intracellular ATP binding to CFTR's two nucleotide binding domains (NBD1/2) causes NBD dimerization and conformational changes that conclude in the opening of the channel pore[344]. CFTR channels show time- and voltage-independent gating behavior, meaning that, once opened, the channel conducts Cl^- at steady-state levels according to its electrochemical gradient until ATP hydrolysis disrupts the NBD dimer and closes the pore[344,345]. TMEM16A, the only recognized airway CaCC (with the exception of TMEM16F), shows a time- and voltage-dependent activation profile, and most importantly, also shows time-dependent deactivation kinetics[346]. Ca^{2+}-binding within a transmembrane domain of TMEM16A, in the vicinity of the channel pore, induces electrostatic and conformational changes that lead to pore dilation and allow the permeation of Cl^-[128] (see Figure 1.4).

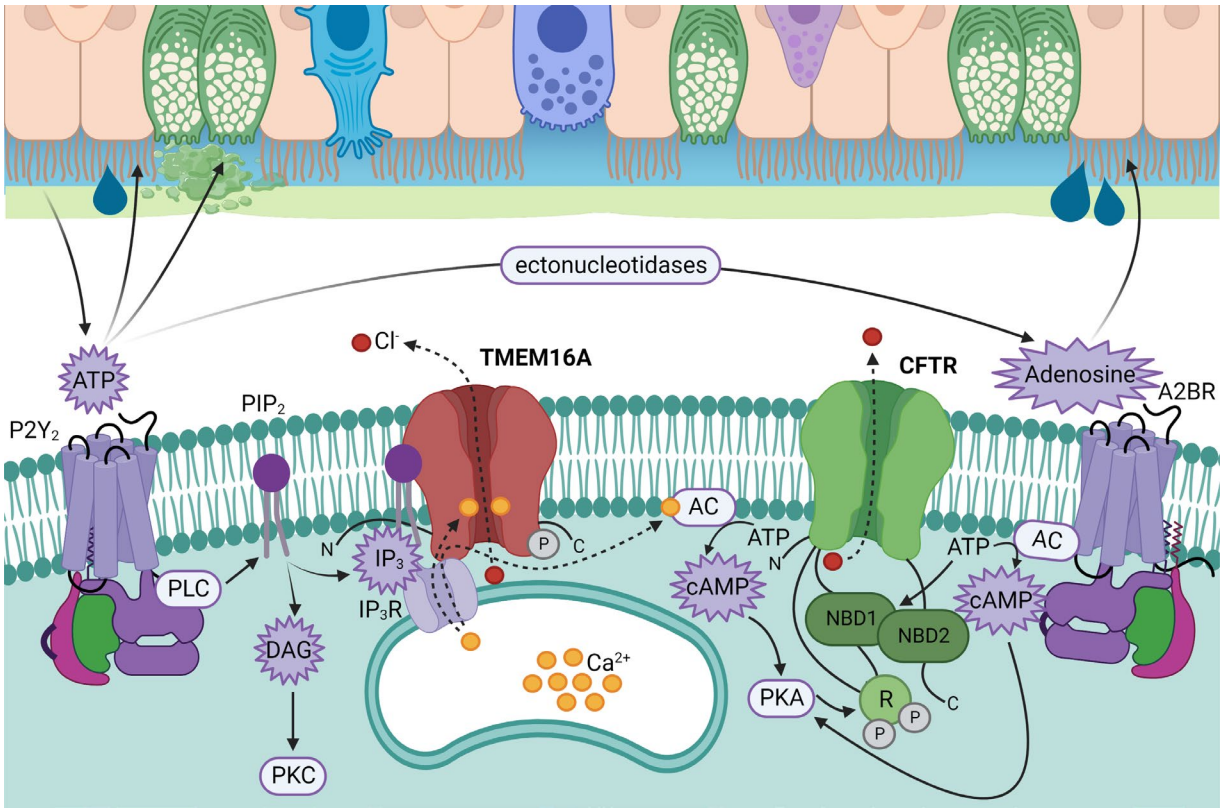

Figure 7.1 | *Model describing the local regulation of mechanical stress-induced Ca^{2+}- and cAMP-dependent signalling in the human airway epithelium.*

Ciliated cells (beige) release ATP into the airway lumen upon mechanical stress-sensing. ATP is broken down into adenosine by ectonucleotidases, ATP/adenosine-mediated activation of ciliated apical membrane $P2Y_2$ and A2B receptors stimulates both cAMP- and Ca^{2+}-induced secretion via CFTR and CaCCs (TMEM16A). ATP also stimulates mucin granule release by goblet cells (green). Ca^{2+}-dependent AC stimulation is necessary for full CFTR activation. Created with BioRender.com.

Notably, however, TMEM16A shows a fast and prominent rundown of its Cl^- conductance even in the continuous presence of Ca^{2+} ions, which is thought to be regulated at least partially by a TMEM16A-phosphorylation balance mediated by calcium/calmodulin-dependent protein kinase II (CaMKII) and protein phosphatases 1 and 2A (PP1/PP2A)[347]. Moreover, other reports have proposed a regulatory module within TMEM16A that interacts with the membrane phospholipid PIP_2, which helps to stabilize the open state of the channel by preventing the ion pore from collapsing and entering the desensitized state, thereby slowing down the Cl^- current decay[348,349]. On that note, most of the Ca^{2+}-activated Cl^- current detected in airways may be mediated by CFTR, via activation of Ca^{2+}-dependent adenylate cyclase (AC) enzymes that convert intracellular ATP into cAMP, which has been described as necessary for full CFTR activation[139,192] (Figure 7.1). Overall, in co-expression with CFTR, TMEM16A may work mostly as a transient signal transducer, translating the ATP/Ca^{2+} stimulus into more sustained and prolonged Cl^- and fluid secretion by CFTR, which may be required to maintain continuous sufficient hydration of the ASL. In parallel, ATP is also the main mucin secretagogue of the airway surface epithelium, this secretion being mediated by TMEM16A in mucus-

secretory goblet cells as shown by our current and previous data[145]. One could therefore additionally or alternatively propose that the physiological role of TMEM16A in the airways is to couple activated mucus release with a fast and robust yet short-timed TMEM16A-dependent fluid secretion. This may be necessary to avoid depleting the airways of fluid when a copious amount of mucus is swiftly released and adsorbs more than 100-fold its mass in water[31]. The ATP/ectonucleotidase secretory balance may very well be regulated by the airway epithelium to preferentially induce CFTR or TMEM16A activation, according to the mucus and fluid needs of the ASL.

This physiological mechanism may however be disturbed under inflammation, due to goblet cell hyper/metaplasia and TMEM16A upregulation in these cells. ATP-mediated activation of TMEM16A would then disproportionately induce copious mucus release without sufficient parallel fluid secretion, causing mucus obstruction. In this work, we show that the basolateral Ca^{2+}-activated K^+ channel KCNN4 is also upregulated during T_H2-mediated inflammation (Supplementary Figure 3.2). We also show in airway epithelial cells that ATP-stimulated KCNN4 activation, which induces basolateral K^+ secretion, hyperpolarizes the cell and prevents activation of voltage-dependent TMEM16A channels (Supplementary Figures 3.2-3.4). One could hypothesize that the parallel upregulation of TMEM16A and KCNN4 in airway goblet cells under inflammation might be a mechanism to protect the airways from excessive TMEM16A activation and mucus hypersecretion. Purinergic receptor desensitization, for e.g., happens physiologically to prevent the airways from flooding and mucus hyperrelease[338]. Ultimately, any strategy aimed at increasing TMEM16A-dependent fluid secretion in inflamed airways should target TMEM16A specifically in ciliated epithelial cells and, rather than interfering with intracellular Ca^{2+} levels, it would preferentially stabilize the active state of the channel, slowing the Cl^- current rundown, or enhance its Ca^{2+}-sensitivity.

Niclosamide and other reported TMEM16A inhibitors may work in a Ca^{2+}-mediated, TMEM16A-independent manner

Contrary to TMEM16A activators, TMEM16A inhibitors have consistently been overlooked when it comes to assessing their effects on airway muco-obstructive diseases in clinical trials. One reason for this is the hypothesis that these compounds do not directly inhibit the TMEM16A channel, but rather interfere with intracellular Ca^{2+} signaling, thereby dampening activation of TMEM16A but also other Ca^{2+}-dependent processes. This is of major relevance given that decreasing Ca^{2+} levels may strongly disturb airway ciliary beating and compromise MCC[350,351]. Moreover, this could also further compromise CFTR function in CF patients with residual activity, given that Ca^{2+}-dependent AC activity could be reduced. We have previously analyzed several TMEM16A inhibitors in different cell lines and confirmed that in fact most of

them consistently interfere with intracellular Ca^{2+} signals[196]. In particular, we concluded from the current (Figure 4.7) and previous work[196] that niclosamide alone induces an increase in intracellular Ca^{2+} by supporting ER Ca^{2+} store leakage via inhibition of Ca^{2+} reuptake by the SERCA pump, and, that in parallel, niclosamide also prevents store-operated Ca^{2+} entry (SOCE) via inhibition of extracellular Ca^{2+} influx channels. This leads to ER Ca^{2+} depletion and to a much lower Ca^{2+} release response after stimulation with ATP. Nevertheless, evidence that the effects of niclosamide on intracellular Ca^{2+} signaling may likewise be happening through direct interference with TMEM16A also exist. We found that in the presence of TMEM16A, niclosamide dampens the Ca^{2+} release stimulated by ATP, yet this effect is lost upon TMEM16A-knockdown[196]. Moreover, a conserved hydrophobic drug binding pocket has been identified in the TMEM16 family of proteins, where, in the particular case of TMEM16F, niclosamide was shown to bind[352]. This binding site shows a high degree of conservation in TMEM16A, and mutations of residues in the putative TMEM16A pocket did significantly affect niclosamide-mediated inhibition of TMEM16A, while in the absence of the antagonist these mutations showed no effect on TMEM16A-Cl^- currents[352]. It was speculated that binding of niclosamide to this TMEM16A pocket locks the ion conduction pore and the gating element in a closed configuration[352]. This supports our previous data showing that pre-incubation with niclosamide provides a much stronger inhibitory effect on activated TMEM16A-mediated Cl^- currents than acute application[196]. Altogether, the data suggest that niclosamide may be acting on TMEM16A inhibition via a direct pathway and/or an indirect, Ca^{2+}-signaling interfering pathway, depending on the cellular context. Furthermore, by directly interfering with the channel conductance, niclosamide may prevent TMEM16A-dependent Cl^- efflux-mediated cell depolarization, which supports activation of voltage-dependent ryanodine receptors (RyRs) and further ER Ca^{2+} store release. One other exotic possibility would be that niclosamide binding interferes with the conformation of TMEM16A in a way that affects its interaction with the IP_3R and ER tethering. This remains however to be explored.

Another major concern when it comes to currently identified TMEM16A inhibitors is their lack of specificity. The fact that this recently identified binding pocket for niclosamide is conserved within the TMEM16 family may explain why other members, such as TMEM16F, are also inhibited by niclosamide[150]. Moreover, given the highly lipophilic nature of all drugs identified to inhibit TMEM16A[135], we imagine that most of them probably bind a similar, if not the same, hydrophobic pocket in the structure of TMEM16s and perpetrate their inhibitory effect in the same manner as niclosamide. The same study showed one other molecule that has been shown to inhibit TMEM16A, 1PBC, binding the same conserved pocket in TMEM16F[352]. This might cause potential off-target effects given that different TMEM16 paralogs play different physiological functions in cells. One TMEM16A inhibitor that has inconsistently been shown to interfere with Ca^{2+}-signaling is ani9. Ani9 was described as a highly potent and selective TMEM16A inhibitor, showing an IC_{50} of 77 ± 1.1 nM, and was also reported as not affecting

intracellular Ca^{2+} levels[353]. We have observed that while ani9 consistently ablates TMEM16A-mediated Cl^- currents, the effects on Ca^{2+} vary between cell lines[196]. Nevertheless, when ani9 does dampen intracellular Ca^{2+} signals, it does so always to a fractional extent of what is observed for other inhibitors such as niclosamide and benzbromarone, even when ani9 is applied at a 10x higher concentration[196]. We speculate that these differences might be indicative of the different contributory effects of TMEM16A for intracellular Ca^{2+} levels. One could hypothesize that TMEM16A mostly supports enhanced Ca^{2+} signals via its interaction with the ER IP_3R, while the Cl^- efflux-mediated depolarization and activation of RyRs might play only a small additional role depending on the particular cellular context and RyR (subtype) expression. As ani9 is expected to be a specific channel pore blocker, this might explain why it inconsistently affects Ca^{2+} signals and why it does so in a limited magnitude. Consistently, ani9 has in our hands failed to show inhibitory effects on mucus production in differentiated human airway epithelial cells (data not shown) and it did also not affect TMEM16F-mediated Cl^- current magnitudes[196]. Others have also reported lack of bronchorelaxing activity for ani9 in freshly isolated human airways, while niclosamide was strongly effective[180]. Nonetheless, despite potential Ca^{2+}-interfering effects, one must not obliviate the fact that niclosamide as well as other TMEM16A inhibitors (e.g. benzbromarone) are FDA- and/or EMA-approved drugs that have passed tolerability and safety tests in clinical settings. Niclosamide is currently being evaluated for repurposing on a number of different conditions such as Parkinson's disease, viral and microbial infections, as well as several cancers[212,354]. While some of these diverse pharmacological activities are related to niclosamide's ability to modulate a selection of "off-target" signaling pathways implicated in different diseases, inhibition of TMEM16 paralogs may also be involved in particular scenarios such as cancer, where the role of TMEM16A has extensively been described[355,356]. Recently, in the wake of the global COVID-19 pandemic, a role for niclosamide in limiting severe acute respiratory syndrome coronavirus type 2 (SARS-CoV-2) viral lung infection was also reported. Niclosamide was shown to inhibit Ca^{2+}-activated TMEM16F-dependent fusion of the SARS-CoV-2 viral envelope and airway epithelial cell membranes, suppressing the viral entry process[357]. Additionally, it was also shown to prevent SARS-CoV-2-induced cell fusion and pathologic syncytia formation by infected pneumocytes, detected in the lungs of patients with severe COVID-19[249,250]. This is related to the lipid scramblase function of TMEM16F, that allows for bilayer lipid translocation and membrane disruption events[358].

CLCA1-dependent airway mucus production is mediated through TMEM16A

In asthma, T_H2 inflammation-mediated IL-13-dependent STAT6/SPDEF activation and mucous cell metaplasia has been shown to induce upregulation of several genes, of which the

secreted protein CLCA1 is one of the most strongly represented[106,107]. While the effects of CLCA1 on Ca^{2+}-activated Cl^- currents have long been described, it was only later elucidated that CLCA1 does not form a channel itself, but rather regulates CaCCs, such as TMEM16A[220,221]. An internal matrix-metalloprotease-like domain was shown to allow intracellular self-cleavage of CLCA1, necessary for the interaction of its N-terminal fragment with TMEM16A upon secretion[359]. More recently, it was clarified that this domain, called von Willebrand factor type A (VWA), is also used to extracellularly bind and stabilize TMEM16A at the plasma membrane, thereby potentiating CaCC currents[222,360]. This interaction seems to be independent of the proteolytic activity of VWA[359]. The requirement of CLCA1 for IL-13-mediated MUC5AC production in airway epithelial cells had been proposed earlier, as well as the sufficientness of CLCA1 to induce MUC5AC, independently of IL-13[108]. However, a role for TMEM16A in this pathway had not yet been described. In this work we applied N-CLCA1-conditioned media to non-polarized airway epithelial cells and confirmed a potentiation of ATP-stimulated whole cell currents (Supplementary Figure 3.4), as well as enhanced TMEM16A-plasma membrane expression, parallel to unaffected transcript expression (Figure 3.4). However, we observed that when applied to polarized airway epithelial cells, that partially differentiate into mucus-secretory cells, N-CLCA1 strongly enhances mucus production in a TMEM16A expression-dependent manner (Figure 3.6F-G). Notably, exposure of these cells to N-CLCA1 (data not shown) or IL-13, which powerfully induces CLCA1 expression, did not enhance CaCC currents. These results again question the contribution of TMEM16A for Cl^- and fluid secretion in differentiated airways, particularly given that TMEM16A expression in ciliated cells is minimal. When we further assessed N-CLCA1 potentiation of TMEM16A in naïve mouse airways by directly administering it via I.T. instillation, we obtained identical results – enhanced mucus production/secretion, particularly in pre-inflamed (asthmatic) airways (Figures 3.1-3.2), without concomitant enhancement of Cl^- currents (Figure 3.3). Once again, our data supports that broad activation/potentiation of TMEM16A in native airways might worsen an already inflamed phenotype.

One could speculate on the link between TMEM16A activation and MUC5AC expression. The IL-13-CLCA1 axis has been shown to require mitogen-activated protein kinase 13 (MAPK13) for induction of MUC5AC expression, with MAPK13 inhibitors dose-dependently ablating IL-13-mediated MUC5AC protein production[108]. At that time however, the identity of the putative receptor that translates the exogenous CLCA1 stimulus into a MAPK13-dependent signalling cascade was unknown. In parallel, work on the role of TMEM16A in cancer progression unravelled a role for MAPK signalling activation during TMEM16A-mediated cancer cell proliferation. The data indicate potent and specific phosphorylation of MAPK1/2 (originally called extracellular signal-regulated kinase (ERK)1/2) upon TMEM16A overexpression, which was reversed by shRNA against TMEM16A[231]. Moreover, both highly selective MAPK1/2 inhibitors or MAPK1/2 knockdown by siRNA were shown to completely abrogate TMEM16A-

mediated proliferation. Following channel mutational studies, it was proposed that MAPK activation by TMEM16A was positively dependent on its Cl^- conductance and hence modulation of intracellular Cl^- levels[231]. This activation could potentially be mediated by Cl^--sensitive with-no-lysine(K) kinases (WNKs)[361], since several members of this family have been shown to activate proteins within the MAPK signalling pathway[362-364]. Interestingly, TMEM16A-knockdown has also been shown in different studies to suppress phosphorylation of p38[365-367], consisting of MAPK11-14, which show a high degree of sequence similarity, common structural basis of activation, and selective cellular and tissue expression[368]. Therefore, MAPK13 (p38δ) induction by TMEM16A could very well be also in place (Figure 7.2). One could rather easily evaluate in airway epithelial cell models, whether extracellular N-CLCA1 stimulation-dependent phosphorylation of MAPK13 is mediated by TMEM16A by making use of overexpression and knockdown experiments. Additionally, to determine whether or not it is dependent on TMEM16A-mediated Cl^- secretion, one could make use of TMEM16A mutants that show impaired Cl^- conductance, such as the previously assessed TMEM16A-K610A[231]. This could potentially provide a definitive closure to the CLCA1-TMEM16A-MUC5AC axis and would further argue against even potentiation of TMEM16A in inflammatory muco-obstructive diseases, given that an increase in TMEM16A-dependent Cl^- secretion in airway goblet cells would not only support mucus secretion but also enhance mucus production.

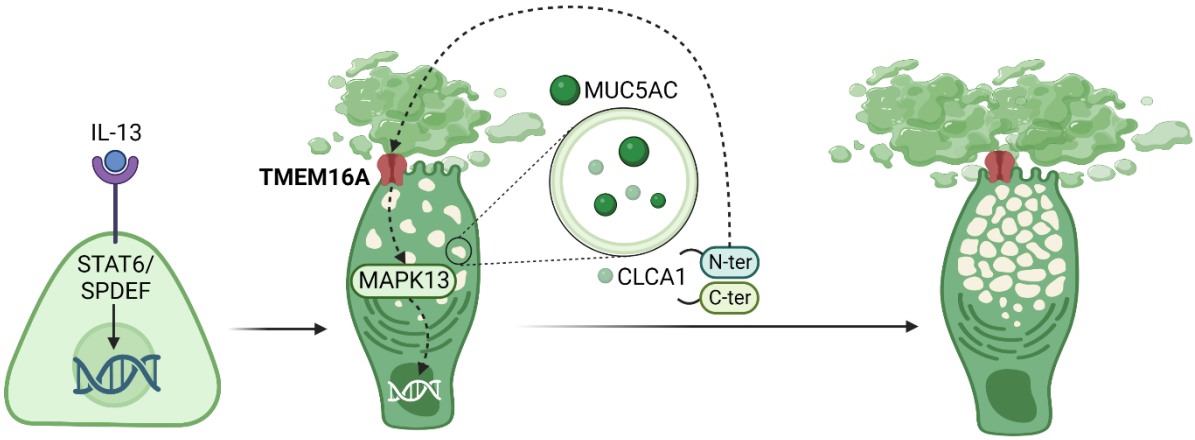

Figure 7.2 | *Model describing the putative pathway for IL-13-induced TMEM16A-dependent MUC5AC production in the airways.*

IL-13 binding to its receptor in non-goblet airway epithelial cells drives STAT6/SPDEF activation and translation of several goblet cell-specific genes, leading to goblet cell (trans)differentiation. CLCA1 is produced and stored in secretory vesicles, where it suffers self-cleavage in C-terminal and N-terminal fragments before secretion. Secreted N-terminal CLCA1 interacts with TMEM16A in an autocrine or paracrine fashion and induces the production of MUC5AC via MAPK13, enhancing the mucin granule content of goblet cells and the secreted mucus volume. Created with BioRender.com.

TMEM16A-dependent CLCA1 secretion contributes to airway inflammation

Further considerations when it comes to regulatory pathways connecting CLCA1 and TMEM16A relate to a proposed role for TMEM16A in general exocytic processes[145]. Our group has previously made use of a TMEM16A airway ciliated cell-specific knockout mouse model. We showed that these mice have a secretory defect that leads to spontaneous basal mucus accumulation in airway mucous cells[145]. It was hypothesized that TMEM16A in ciliated cells supports the release of exocytic vesicles involved in paracrine signalling, potentially carrying factors relevant for mucous cell emptying. ATP-induced airway mucus release was shown to be strongly compromised in these mice[145]. Interestingly, our group later showed that there is also co-accumulation of mouse CLCA1 (previously CLCA3) in these cells, which correlates to the observed localization of CLCA1 in airway mucin secretory granules[369]. In the current and in ongoing work (Figure 4.2 and data not shown) we also observed mucous cell intracellular retention of CLCA1 in mouse airways treated with niclosamide. As niclosamide was shown to dampen expression of SPDEF (Figure 3.5), we do not expect that our observations reflect an increase in CLCA1 protein production but rather a defect in secretion. This could potentially be a mechanism through which niclosamide and TMEM16A are further involved in the regulation of inflammation, as CLCA1 stimulation was shown to activate alveolar macrophages *in vitro* and induce the expression of several pro-inflammatory and leucotactic cytokines[370,371]. Global gene expression analyses of these macrophages also identified short palate lung and nasal epithelial clone 1 (SPLUNC1) as the most-prominently down-regulated gene upon CLCA1 stimulation[370]. SPLUNC1 has been described as an autocrine secreted negative regulator of ENaC, preventing Na^+ hyperabsorption and ASL dehydration in normal airways[372], and lower SPLUNC1 levels were recently correlated with increased episodes of clinical worsening (acute pulmonary exacerbations) in cystic fibrosis[373]. In parallel, CLCA1 protein has been shown to be profoundly upregulated in the bronchial mucosa of CF patients[374]. We have in fact consistently observed a tendency for, or a significant increase in ENaC-dependent, amiloride-sensitive currents in tissues treated with CLCA1 (Figure 3.3 and data not shown). Furthermore, a significant positive correlation between CLCA1 protein expression and mucus production, as well as a negative correlation between CLCA1 expression and lung function parameters, has also been found in smokers vs. non-smokers, and to an even stronger degree in COPD patients, all which typically show mostly non-T_H2 mediated inflammation[375,376]. Moreover, luminal administration of N-CLCA1 to mouse airways via I.T. instillation surprisingly strongly enhanced the expression of TMEM16A in the underlining ASM (data not shown), which may contribute to airway hyperresponsiveness. Taken together, the data suggest that inhibiting TMEM16A in the airways might contribute via inhibition of CLCA1 secretion to better clinical outcomes for asthma, COPD and CF patients.

Broad-spectrum effects of niclosamide for the treatment of inflammatory muco-obstructive airway diseases

Our group proposed niclosamide as a treatment for inflammatory muco-obstructive airway diseases[150]. Intraperitoneal application of niclosamide was shown to reduce mucus production and secretion, as well as cholinergic stimulus-activated bronchoconstriction in the airways of asthmatic mice. Moreover, immune cell infiltration measured by the cell marker CD45+ was also shown to be reduced under niclosamide treatment[150]. We have recently particularly detected a dampened eosinophilic infiltration in the same conditions (data not shown). Human airway epithelial cell cultures showed consistently an inhibitory effect on IL-13-mediated mucus overproduction by niclosamide, as well as a strongly attenuated inflammatory cytokine IL-8 release[150]. In the present work, we applied niclosamide directly to asthmatic mouse airways via intratracheal (I.T.) instillation and were able to reproduce the inhibitory effects on mucus production/secretion (Figure 2.3). Furthermore, we showed that three-day incubation of airway epithelial cells with niclosamide strongly downregulated the expression of the central inflammatory mediator SPDEF and of TMEM16A (Figure 2.6), which downregulated MUC5AC. While a direct link between SPDEF transcription factor activity and TMEM16A gene expression has not been established, several other pathways involving transcription factors STAT3, STAT6, NF-kB, and others, have been shown to lead to upregulation of TMEM16A gene expression[130]. As niclosamide has been identified as an inhibitor of the STAT3 signaling pathway[377], this might explain its inhibitory effects on TMEM16A expression upon longer-term incubations. Alternatively, niclosamide might directly inhibit STAT6 upstream of both TMEM16A and SPDEF, which would better explain inhibition of IL-13-mediated TMEM16A upregulation. Inhibition of SPDEF expression may very well also be one mechanism through which niclosamide exerts its inhibitory effects on goblet cell metaplasia (GCM) and mucus production in the airways, as SPDEF has been shown to be required for airway GCM[27,201]. We have previously shown upregulation of mucus production in airway epithelial cells under several pathway/signaling molecule stimulations, namely JAG-1, IL-8 and IL-13, which is always highly dependent on TMEM16A expression/function[191]. Besides its inhibitory effects on mucus production and secretion, the inhibition of CLCA1 secretion by niclosamide in the airways may play a role in dampening pro-inflammatory cytokine secretion, which we have consistently observed in previous[150] and ongoing work (data not shown). Moreover, we addressed the potential detrimental effects on MCC caused by interference of niclosamide with intracellular Ca^{2+} levels. Our analyses of ciliary stroke amplitude and frequency in isolated mouse tracheas where niclosamide was applied acutely (Supplementary Figure 2.3), as well as particle movement tracking in inflamed (asthmatic) tracheas treated with niclosamide for 5 days (Figure 4.3), revealed no negative effects of niclosamide on these MCC parameters. MCC in treated inflamed airways was rather increased almost back to control levels. This suggests that

whichever Ca^{2+}-dampening effects of niclosamide are present, these are outperformed by the inhibition of mucus production/secretion in asthmatic animals, supporting the administration of niclosamide as a therapy for airway muco-obstructive diseases. Nevertheless, administration of niclosamide and other TMEM16A-inhibitors should be directed to the airways, circumventing systemic side effects, and specifically at airway epithelial mucous cells and smooth muscle cells, given potential deleterious effects on ciliated cells, both on inhibition of TMEM16A-dependent fluid secretion as well as on ciliary beating.

In this work, we achieved the encapsulation of niclosamide in functionalized polyethylene-glycol (PEG) microspheres (4-45μm) and nanospheres (97-125nm). These particles were designed to grant a slow release of niclosamide[283], allowing to reduce the number of applications necessary to maintain an effective, steady-state level of niclosamide in the airways. While microspheres have an aerodynamic diameter that would allow them to better reach the deep lung with minimized particle losses when aerosolized[378], nanospheres have better chances at mucus layer penetration[22] and direct epithelial drug delivery. The hydrophilic, positively-charged polymer structure used was also formulated to ensure proper muco-adhesion and penetration, avoiding premature clearance and facilitating particle access to the underlying epithelial cell layer[286]. Ultimately, the inhibitory effects on airway mucus were comparable between free and encapsulated niclosamide when applied to asthmatic mouse airways (Figures 2.3, 4.1). This might have to do with the fact that, since via I.T. instillation it is difficult to assess how much of the instilled compound will be readily available on the airway surface, an incredibly high amount (30μM) was administered and may have masked differences in efficacy. Furthermore, the application of all three formulations of the drug was performed daily for 5 days, which did not allow for long-term analyses of the potential benefits of encapsulation. Forwardly, one would aim at conjugating these encapsulated formulations, particularly nanospheres, with goblet cell specific markers that would allow for particle docking and drug release in the proximity of the cell target, or even cell-specific internalization of the particle. Of note, our collaborators in this project have addressed the poor target cell specificity of nanoparticles in other biochemical application contexts, namely, they developed particles that can specifically identify and bind kidney mesangial cells in an influenza virus-like approach[379]. In brief, angiotensin-I (ang-I) is conjugated as a precursor ligand to the particle surface and allows for recognition by angiotensin-converting enzymes (ACEs) on the target cell. Following enzymatic processing by ACE, resulting angiotensin-II (ang-II) as a secondary/activated ligand binds a neighboring ang-II type-1 receptor (AT1R) on that same cell, that mediates particle internalization via endocytosis. This two-step mechanism allows for prevention of particle recognition or uptake by off-target cells that only express one of the two necessary surface proteins[379]. This strategy showed outstanding target-cell affinity with picomolar avidities and was able to selectively identify target cells in the presence of 90% off-target cells[379]. Currently, we are not aware of any set of ligands that would translate this

approach into an airway goblet-cell (GC) specific strategy. Nevertheless, given the high lipophilicity of niclosamide and readily passive lipid bilayer diffusion, conjugation of niclosamide-encapsulating particles with a ligand that binds a single GC-specific cell surface molecule or receptor could be enough of an alternative. A possible target for this would be the histamine receptor type 2 (H2R), as this subtype was identified to be involved in histamine-mediated airway goblet cell mucus secretion, while H1R and H3R were unrelated[380]. Histamine is elevated in the airways of asthmatic patients and is responsible for many of the pathophysiological features in allergic asthma, including enhanced mucus secretion and bronchoconstriction[381]. Many asthmatic patients take daily antihistaminic drugs that antagonize the H1R expressed in ASM cells and involved in airway hyperresponsiveness[382]. On that note, conjugation of locally deposited niclosamide-encapsulating nanoparticles with cimetidine, an H2R-specific antagonist, could allow for goblet-cell docking and directed niclosamide release, as well as a secondary, competitive binding, niclosamide-independent management of asthma.

SLC26A9 expression is coupled to CFTR in airway ciliated epithelial cells

The expression of most members of the SLC26 family of anion transporters has been localized to the luminal membrane of epithelial linings in particular organs, such as SLC26A3 in the colon[383] and pancreas[384], and SLC26A4 in the kidney[385] and thyroid[386], where they are involved in the regulation of the content and pH of the respective epithelial secretions. For several SLC26 members, a physical and functional interaction with CFTR has also been described, mediated by the regulatory (R) region of CFTR and the sulphate transporter and anti-sigma factor antagonist (STAS) domain common to all SLC26 proteins. This interaction is facilitated by PDZ-binding motifs expressed on the C-terminal region of both SLC26 proteins and CFTR[156,387] (Figure 7.3). PDZ domain adaptor proteins are known for recruiting several receptors, transporters, and ion channels together, forming multiprotein signalling complexes[388]. As SLC26A9 is highly expressed in the lungs and has been identified as a gene modifier of CF lung disease[158,167], potentially by supporting Cl^- and/or HCO_3^- secretion, one would expect a similar pattern of apical epithelial localization as obtained for other SLC26 members, as well as for SLC26A9 itself in the stomach[163]. However, no clear-cut immunolocalization of SLC26A9 in the airway epithelium had yet been achieved, with most current staining procedures suggesting mostly tight-junctional localization, which seemed incompatible with the mediation of transcellular secretion[303,304]. In our study, we detected a clear apical localization of SLC26A9 in normal superficial epithelium of native human, mouse and piglet airways, as well as cultured polarized human airway epithelia, while no submucosal gland staining was ever observed (Figures 5.1-5.4, 6.7-6.8).

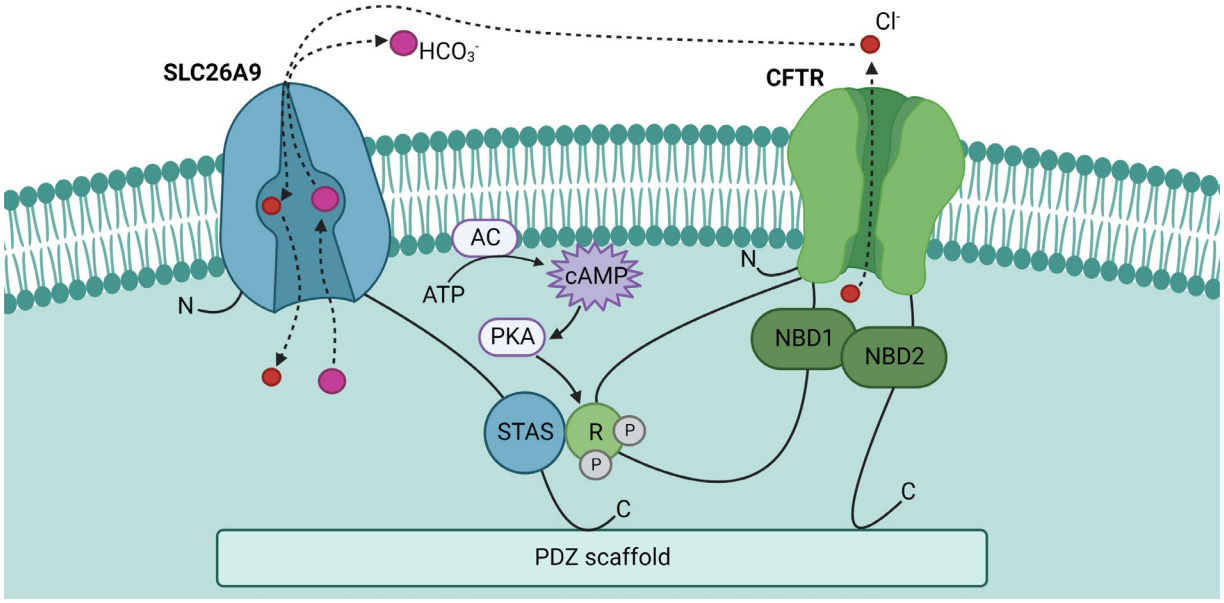

Figure 7.3 | *Schematic representation of the interaction between SLC26A9 and CFTR.*
SLC26A9 contains an SLC26 family-conserved cytoplasmic STAS domain, involved in protein-protein interactions and regulation, as well as a PDZ-binding motif at its C-terminal. The R domain of CFTR is known to interact with the SLC26A9-STAS pre- and more so post-phosphorylation (P). CFTR also contains a PDZ-binding motif at its C-terminal, which interacts with the same PDZ scaffold as SLC26A9. Created with BioRender.com.

Particularly, this staining seemed to be exclusively localized to ciliated epithelial cells, upon co-staining with cilia marker acetylated tubulin. CFTR expression has also been detected in airway ciliated cells[58,133]. For SLC26A9, PDZ scaffold-mediated interaction with CFTR has been previously described to affect its biogenesis. Positive regulation of SLC26A9 membrane expression by PDZ domain protein NHERF-1, and negative regulation by CAL, has been demonstrated in human bronchial cells, both these affinities being increased by co-expression with normal CFTR[166]. In the presence of the folding/trafficking mutant F508del-CFTR, however, only the interaction of SLC26A9 with the negative regulator CAL is increased, leading to intracellular retention and degradation of SLC26A9, as happens for F508del-CFTR itself[166]. This explains why we find a lack of apical staining in airways from F508del/F508del homozygous CF patients (Figure 5.3). Interestingly, airways from CFTR-knockout (CFTR-/-) piglets show normal apical staining of SLC26A9 (Figure 5.4), which suggests that its increased CAL affinity is specifically induced by F508del-CFTR interaction. This indicates that particularly in the airways of patients carrying severe mutations where no CFTR is produced at all, SLC26A9 may be normally expressed at the apical membrane of ciliated cells. Clearly, these patients still show a severe diseased airway phenotype, which would suggest that basal, independent SLC26A9 activity is not able to compensate for the lack of CFTR-mediated function. Nevertheless, developing molecules that interfere with the SLC26A9 interaction with F508del-CFTR and CAL for most CF cases, and/or stimulating SLC26A9 in CFTR-knockout

(KO)-like conditions, may be relevant strategies when it comes to SLC26A9 modulation in CF airways.

SLC26A9 does not contribute directly to the basal airway Cl^- conductance, but supports airway surface liquid pH regulation by mediating a Cl^-/HCO_3^- exchange

To date, several clashing observations regarding the transport mode and selectivity of SLC26A9 have been described. Particularly, observations that it may operate solely as an uncoupled Cl^- transporter or additionally as a Cl^-/HCO_3^- exchanger in the airways have been put forward[159-163]. Evidence for mixed modes of transport and selectivity have also been described for other SLC26 members, such as SLC26A3, which has been shown to mediate a Cl^-/HCO_3^- exchange but also an uncoupled HCO_3^- secretory function in the intestine, relevant for salt (NaCl) and fluid absorption as well as intestinal pH regulation[383,389,390]. The closely related SLC26A4 has also been shown to mediate a Cl^-/HCO_3^- exchange in particular cells of the kidney, being also involved in salt reabsorption[391]. For both SLC26A3 and SLC26A4, a positive regulatory interaction with CFTR has been described, with these channels showing cAMP-insensitive basal Cl^-/HCO_3^- exchange that gains cAMP-sensitivity (i.e., is stimulated by cAMP) upon co-expression of functional CFTR[392,393]. These transporters may support CFTR function by mediating the recycling (uptake) of Cl^- upon CFTR-mediated luminal secretion (Figure 7.3). In this work, we made use of the novel, highly potent and specific SLC26A9-inhibitor S9-A13, to decisively distinguish between SLC26A9- and CFTR-mediated currents in native airways and airway models, and further the knowledge into SLC26A9-mediated transport in the presence or absence of CFTR. Our data strongly suggest that in the absence of CFTR, SLC26A9 mediates an unstimulated uncoupled Cl^- transport and that this is cAMP-insensitive (Figure 6.5), as demonstrated for SLC26A3 and SLC26A4. Furthermore, in differentiated airway epithelial cell cultures, which express both CFTR and SLC26A9 (Figure 5.5), and clearly reproduce the native ciliated apical localization of SLC26A9, a basal SLC26A9-dependent Cl^- transport can hardly be detected (Figure 6.7). SLC26A9 may in these conditions be mostly mediating an electroneutral Cl^-/HCO_3^- exchange, or an electrogenic, low-turnover exchange that does not generate appreciable currents. By making use of CFTR inhibitor CFTRinh-172, we rather detected a mostly CFTR-dependent basal and cAMP-activated transepithelial current in this human airway model (Figure 6.7). These results were remarkably reproduced in primary human nasal epithelial cultures (Supplementary Figure 6.4) and mouse airways (Figure 6.8), showing species and model redundancy of this mechanism. On the other hand, we found no evidence for a Cl^-/HCO_3^- exchange activity of single overexpressed SLC26A9 (Supplementary Figure 6.3), while this was clear for SLC26A3 and SLC26A4. In parallel, however, airway surface liquid pH measurements of differentiated primary human nasal epithelial cultures

detected an acidification of the airway surface liquid (ASL) pH upon SLC26A9 inhibition, supporting a role for a Cl^-/HCO_3^- exchange in the presence of CFTR (Figure 6.9). Interestingly, we observed that the basal activity attributed to CFTR does not seem to be affected by inhibition of Ca^{2+}-dependent AC1 or adenosine A2B receptor activity, which proposes a cAMP-independent activation mode for CFTR (Supplementary Figure 6.4). This seems to require however a more native environment, given that, unlike SLC26A9, CFTR overexpression in heterologous systems does not generate a basal current, but requires cAMP-stimulation for Cl^- secretion (Figure 6.5). Evidence for CFTR activation in a cAMP/PKA-independent manner has been described earlier[394].

While CFTR-/- mice showed no cAMP-mediated airway Cl^- secretion[395], constitutive and cAMP-mediated Cl^- secretion did not differ between wild-type and SLC26A9-/- mice[168], arguing against a role for SLC26A9 in Cl^- secretion in native airways. Nevertheless, upon induction of T_H2-mediated inflammation via intratracheal instillation of IL-13, SLC26A9 appeared to contribute to basal Cl^- secretion, with treated SLC26A9-/- mice showing lower basal currents and significant airway mucus accumulation and obstruction[168]. However, this decreased basal transport could still be attributed to CFTR. While the lack of SLC26A9 expression does not seem to affect presumed basal transport by CFTR in physiological conditions – and one would hypothesize that KO of SLC26A9 does not prevent membrane expression of CFTR, as vice-versa – the need for a mutual CFTR/SLC26A9 interaction for enhanced secretion, as was demonstrated for SLC26A4 in the kidney, might only come into relevance in a pathological condition (i.e., airway inflammation). Now, lack of presumed SLC26A9-mediated Cl^- recycling would hinder CFTR-mediated Cl^- secretion. At the same time, HCO_3^- secretion would be severely compromised, which may strongly contribute to the mucus obstruction phenotype, as a copious mucus release under inflammation would require a parallel increase in HCO_3^- secretion for proper mucus expansion and clearance. Our data (Figures 3.1-3.2, 5.6 and data not shown) strongly suggest a T_H2-dependent increase in CFTR expression and function, which may be accompanied by a parallel increase in SLC26A9 membrane expression and function, as the trafficking and activity of both proteins is tightly connected. This may further be supported by a TMEM16A-dependent mechanism (schematized on Figure 5.7). Direct stimulation of CFTR function via STAS-R interaction, Cl^- recycling, and HCO_3^- secretion, rather than a direct contribution to Cl^- efflux, could still explain why certain SLC26A9 variants are modifiers of lung function in CF and of the response to CFTR-modulator therapies. Furthermore, evidence that SLC26A9 expression facilitates biogenesis and membrane insertion of CFTR has also been demonstrated[304,334].

Mode of transport by SLC26A9 may be defined by CFTR interaction

Physiologically, change of the transport mode for SLC26A9 from uncoupled Cl^- secretion to Cl^-/HCO_3^- exchange in the presence of CFTR would make sense, given that Cl^- secretion is more effective through CFTR, which as a true channel shows a much larger Cl^- conductance than SLC26A9[162,396]. Furthermore, under inflammation, maintenance of a robust HCO_3^- secretion might be of relevance for mucus expansion. At physiological conditions, CFTR shows an extremely low HCO_3^-:Cl^- current ratio, with direct CFTR-mediated HCO_3^- transport shown as not sufficient to account for the HCO_3^- efflux that goes on in several CFTR-expressing epithelia[155]. Increase in intracellular Ca^{2+} has also been shown to block uncoupled SLC26A9-Cl^- currents, with no present assessment of its effect on the Cl^-/HCO_3^- exchange activity[161]. One could hypothesize that this exchange would remain significantly unaffected, as this could be an additional mechanism to guarantee HCO_3^- secretion upon Ca^{2+}-induced mucus release.

The preeminent question would then be: How can CFTR interaction modulate the transport mode of SLC26A9? The mutual stimulatory activation of CFTR and Cl^-/HCO_3^- exchange described for other SLC26 protein members may be facilitated in three steps: 1) tethering of both proteins in close proximity by their PDZ-adaptor scaffold; 2) direct interaction of the SLC26-STAS domain and the regulatory domain on CFTR (R) pre- and more so post-cAMP/PKA-mediated R phosphorylation; and 3) SLC26-mediated recycling of the CFTR-secreted Cl^-. Earlier reports have shown that deletion of the STAS domain in SLC26A9 dramatically reduces the uncoupled Cl^- currents to about 10%, with a more modest effect on the Cl^-/HCO_3^- exchange activity (30% residual function)[397], which suggests that the presence/conformation of the STAS domain may be determining the HCO_3^- affinity and transport mode of SLC26A9. When SLC26A9 is expressed on its own, a large fraction of its turnovers potentially results in uncoupled Cl^- flux, while CFTR co-expression and STAS-R interaction may alter STAS conformation and shift the turnovers into a coupled Cl^-/HCO_3^- exchange. Interestingly, pull-down experiments revealed that the purified CFTR R domain interacts mainly with the purified monomeric SLC26A9-STAS, while interaction with the dimerized form appeared to be weak to non-existent[397]. CFTR co-expression may interfere with SLC26A9 dimerization (see Figure 1.5), which may be required for the predominantly non-HCO_3^- permeable, uncoupled transport. A recent report has shown that nearly all interactions between dimerized SLC26A9 subunits are mediated by their STAS domains[165]. Surprisingly, co-expression of SLC26A9 and the purified nucleotide-binding domain 1 (NBD1)+R-CFTR in a heterologous system led to inhibition of both transport modes of SLC26A9[397]. In a more native environment, and upon CFTR activation which involves R domain phosphorylation and translocation, this interaction might lead to different results. This SLC26A9-STAS-R-CFTR binding interaction differs from the activatory mechanism previously described for SLC26A3 and SLC26A6[155,156]. Of note, interaction of NBD1+R-CFTR with chimeric SLC26A9 carrying the

SLC26A6-STAS tentatively stimulates the exchange function while not affecting the uncoupled transport[397], indicating that CFTR-mediated effects are SLC26 member-specific and have physiological relevance. Based on the hypothesis that the mode of transport for SLC26A9 is determined by CFTR, SLC26A9 may contribute with uncoupled Cl^- transport to the basal airway conductance detected in CFTR-/- mice[136,395]. Additionally, binding and regulation of endogenous SLC26A9-STAS by other proteins in a native environment may also contribute to the determination of its HCO_3^- affinity and dominant transport mode in a given epithelium. Ultimately, besides interfering with the retention and degradation of SLC26A9 in the most common CF cases of F508del-CFTR homozygosity and activating SLC26A9 in lack of CFTR membrane expression conditions to upregulate uncoupled apical Cl^- secretion, stimulation of SLC26A9 in the presence of several membrane localized CFTR mutants could still benefit CF patients by increasing HCO_3^- secretion into the ASL, improving MCC and innate antimicrobial defenses. On the other hand, given normal CFTR expression and R-STAS interaction but absent/strongly defective CFTR activity, this stimulated HCO_3^- secretion by SLC26A9 – in the form of a Cl^-/HCO_3^- exchange – could come at the expense of depleting the ASL of Cl^- ions and inducing further dehydration.

CHAPTER 8 | CONCLUSIONS AND FUTURE PERSPECTIVES

TMEM16A and SLC26A9 both play relevant roles in airway homeostasis under physiological conditions and may be involved in the development or prevention of airway pathology. Namely, we conclude that TMEM16A plays a more relevant role in airway mucus production and release, and bronchoconstriction, than in fluid secretion, which is critical under inflammation. The contribution of enhanced TMEM16A expression and function in inflamed airways – particularly in mucus-secretory and airway smooth muscle cells – may support the development of chronicity in airway disease, which has serious long-term deleterious effects in lung function. TMEM16A-inhibitors should be assessed in a clinical trial context, evaluating if the results obtained in mouse models and human epithelial cultures can be translated into the more complex human physiological background. Niclosamide, namely, despite its potential secondary TMEM16A-independent and off-target effects, as an FDA/EMA-approved medicine, should be seriously considered for repurposing as a treatment for inflammatory airway disease. Inhibition by niclosamide of CLCA1 secretion and potentially even production in the airways, via downregulation of SPDEF, may contribute to counteract several pro-inflammatory roles that are now described for CLCA1 – enhanced mucus production/secretion via TMEM16A, stimulation of cytokine release by immune cells, and SPLUNC1 downregulation which supports Na^+ hyperabsorption and airway dehydration. Further, the application of niclosamide should be directed at mucus-secretory cells in the airway epithelium, imaginably encapsulated in nanoparticles coupled to histamine receptor type 2 antagonists, aiming for a double-sided, niclosamide-dependent and -independent management of airway hyperresponsiveness, while circumventing the need for repetitive applications and potential systemic side effects of the drug. Nevertheless, in CF, and COPD cases where CFTR dysfunction is in place, the reduction of mucus content may be insufficient to restore proper mucociliary clearance, given that a defective HCO_3^- secretion would still play a significant role in mucus pathology. Here, a combined strategy with stimulation of SLC26A9 might come into play. Given its coupled expression to CFTR in airway ciliated cells and mutual regulatory interaction, SLC26A9 expression enhancers or potentiators may contribute to HCO_3^- release into the airway surface liquid, as well as facilitate CFTR membrane insertion and function. Nonetheless, a lot remains to be uncovered for SLC26A9, particularly whether in native conditions the interaction of R-CFTR with SLC26A9-STAS is responsible for altering its transport mode from uncoupled Cl^- transport to coupled Cl^-/HCO_3^- exchange. We propose this mechanism to explain the lack of SLC26A9-contribution to basal and stimulated Cl^- currents in models which expressed normal CFTR, detected by the herein described novel highly potent and selective SLC26A9 inhibitor S9-A13. To solve this, one could firstly make use of polarized primary human airway epithelial cells carrying distinct R-CFTR and other mutations, as a near physiological model to assess for differences in sensitivity of basal and stimulated currents to S9-A13.

ACKNOWLEDGEMENTS

First and foremost, I would like to thank my in-house PhD mentors, Prof. Dr. Karl Kunzelmann and Prof. Dr. Rainer Schreiber, for nearly 4 years of teachings, experience and expertise shared. Karl, my deepest thanks for all the times that a knock on your door and a “Do you have 5 minutes?” led to several hours of brainstorming and fruitful discussions. Rainer, thank you for every time my questions were met with a readily available Physiology lecture. There is really nothing like learning it “from the beginning”.

I am also extremely grateful for having had an unofficial, third in-house mentor, Dr. Jiraporn Ousingsawat. Ji, thank you for always making the time and always lending a hand in designing, performing, and discussing experiments.

Thank you to all the members of our UK Cystic Fibrosis Trust Strategic Research Centre (SRC013): Prof. Dr. Michael Gray, Prof. Dr. Margarida Amaral, and Prof. Dr. Jeffrey Beekman, who served as external mentors and provided much appreciated feedback and suggestions on countless progress reports during these 4 years; and Livia Delpiano, Violeta Railean and Lisa Rodenburg, for sharing our PhD journeys together.

A word of acknowledgment goes out to the funding sources that made this research possible: UK Cystic Fibrosis Trust, German Research Foundation and Gilead Foundation.

I also greatly appreciate the technical assistance of Ernestine Tartler (Tini), Patricia Seeberger and Helena Lowack, without whom this work would have taken double the time for completion.

Thank you, thank you, and thank you again, to all the colleagues and friends I was lucky enough to share a lab with. Maddie (Dr. Madalena Pinto), Robi (Dr. Roberta Benedetto) and Bustorffinha (Dr. Inês Cabrita), thank you for taking me in and showing me the way until I learned to walk it by myself (yet never alone). Kuka (Khaoula Talbi), thank you for all the singing, all the laughter, and all the discussions that made this journey lighter.

Um gigante obrigada aos meus amigos de sempre e aos mais recentes, por toda a paciência, apoio e compreensão, por respeitarem o meu amor à camisola e ainda assim não me deixarem esquecer de que a vida são dois dias e de que eu sou mais do que o que eu faço.

Agradeço à minha família: irmãos, primos, tios, tios-avós, avós; aos que estão mais perto e aos que estão mais longe, aos que ainda cá estão e aos que já partiram, por todo o apoio, confiança e motivação. Como é bom poder subir sem medo de cair, sabendo que nunca me vai faltar quem me ampare.

Esta tese, dedico-a aos meus pais. Mãe, obrigada pelos ouvidos incansáveis que suportaram as minhas frustrações e se alegraram pelas boas novas, pela companhia, pela força, pela ajuda a instalar-me numa vida nova e por me receberes sempre na vida velha com o que eu mais tenho saudades de comer. Pai, já lá vão nove anos e três capítulos desde que me deixaste na faculdade pela primeira vez e me disseste que ia tudo passar muito rápido.

Como tinhas razão! Estiveste sempre a meu lado em todas as etapas, suportaste comigo todas as dificuldades e celebraste comigo todas as vitórias. Não o quereria de nenhuma outra maneira. Obrigada por tudo aquilo a que meras palavras não fazem jus.

Vielen Dank an alle!
Many thanks to all!
Muito obrigada a todos!

ERKLÄRUNGEN

Hiermit erkläre ich, gem. § 6 Abs. 2, Nr. 6 der Promotionsordnung der Math.-Nat.-Fachbereiche zur Erlangung des Dr. rer. nat., dass ich die vorliegende Dissertation selbständig verfasst und mich keiner anderen als der angegebenen Hilfsmittel bedient habe.

Regensburg, den

RAQUEL MARTINS CENTEIO

Regensburg, Germany raquel.centeio@hotmail.com linkedin.com/in/raquelcenteio

Avid learner and proactive researcher with 5 years of experience in airway pathophysiology. Successfully supported the diagnosis, prognosis, and treatment combination indication for **25+ patients** with Cystic Fibrosis (CF) carrying common to very rare CFTR mutations, which contributed to **2 research papers** describing biomarkers and personalized medicine tools for CF. Moved on to successfully contribute to **10+ research papers** exploring TMEM16A and SLC26A9 as alternative non-CFTR protein targets for restoring airway function in CF, asthma, and other muco-obstructive lung diseases.

WORK AND EDUCATION

Jan 2019 — Feb 2023

PhD in Biomedicine, **Institute of Physiology, University of Regensburg, Germany**

Dissertation “Restoring airway function in muco-obstructive diseases by modulating TMEM16A and SLC26A9” under the supervision of Prof. Dr. Karl Kunzelmann.

Sep 2016 — Nov 2018

MSc in Medical Biochemistry, Faculty of Sciences, University of Lisbon, Portugal

Top 10%

Dissertation “Diagnosis, prognosis and personalized treatment of Cystic Fibrosis” under the supervision of Prof. Dr. Margarida Amaral.

Sep 2013 — Jul 2016

BSc in Biochemistry, Faculty of Sciences, University of Lisbon, Portugal

Top 10%

ADDITIONAL TRAINING

Jan 2019 — Jul 2019

FELASA-B, University Hospital Regensburg, Germany

AWARDS

Feb 2020 *(postponed to 2022)*

German Cystic Fibrosis Association travel grant for participation in the 2020 European Cystic Fibrosis Society Basic Science Conference in Albufeira, Portugal

CONFERENCES

Nov 2022

North American Cystic Fibrosis Conference, Philadelphia, PA, USA
Talk "The novel SLC26A9 inhibitor S9-A13 provides no evidence for a role of SLC26A9 in airway chloride secretion but suggests a contribution to the regulation of airway surface liquid pH"

Mar 2022 — Apr 2022

European Cystic Fibrosis Society Basic Science Conference, Albufeira, Portugal
Talk "Hydrogel-encapsulated Niclosamide for topical treatment of inflammatory airway diseases"

Sep 2021 — Oct 2021

German Physiological Society Meeting, Frankfurt am Main, Germany
Poster "Modulation of TMEM16A as a therapy for Cystic Fibrosis airway disease"

May 2021

UK Cystic Fibrosis Conference (online via Zoom)
Talk "Modulation of TMEM16A as a therapy for Cystic Fibrosis airway disease"

Sep 2019

UK Cystic Fibrosis Conference, London, UK
Poster "Pathophysiological properties of airways from newborn Cystic Fibrosis piglets"

LAB SKILLS

Animal Care (Mice): Handling and restrain, animal breeding, maintaining and evaluating animal records, intraperitoneal administration of injections, transcardial perfusion, bronchoalveolar lavage, intratracheal instillation, dissection/tissue collection, sample handling techniques.

Cell Culture: Primary cells (human/mouse/piglet), immortalized cell-lines, generation of 3D-airway and intestinal organoids from native tissue/cultures, transient transfection of mammalian cells (lipofectamine/electroporation), lentiviral transduction of mammalian cells.

(Electro)Physiology: Ussing chamber (short/open-circuit) measurements of human/mouse native tissue or cultured cells, measurements of intracellular pH, measurements of intracellular calcium levels, measurements of halide-mediated quenching of intracellular (YFP) fluorescence, organoid swelling/shrinking assays.

Histology: Embedding processes: paraffin; cryopreservation of tissues; use of a microtome for tissue slicing; histological staining processes (Alcian blue, PAS).

Immunostaining: Immunohisto/cytochemistry.

Microscopy: Light microscopy, fluorescence microscopy.

Molecular biology: DNA, RNA, and protein determinations, *in vitro* mutagenesis, preparation of competent cells, bacterial transformation, plasmid preparation, ELISA, TCA-precipitation of supernatant proteins, biotinylation experiments, western blot, flow cytometry.

Softwares: GraphPad Prism, Grapher, ImageJ, ZEN (Zeiss), Microsoft Office (Excel, Word, PowerPoint)

SOFT SKILLS

Creative thinking; Effective time management; Data processing and critical thinking; Problem solving; Adaptability; Teamwork; Supervising; Science communication.

LANGUAGES

English | Spanish | Portuguese

German | French

PUBLICATIONS

1. Rodenburg LW, Delpiano L, Railean V, **Centeio R**, Pinto MC, Smits SMA, Van der Windt IS, Van Hugten CFJ, Van Beuningen SFB, Rodenburg RNP, Van der Ent CK, Amaral MD, Kunzelmann K, Gray MA, Beekman JM, Amatngalim GD. Drug repurposing for Cystic Fibrosis: identification of drugs that induce CFTR-independent fluid secretion in nasal organoids. Int J Mol Sci. (**2022**); 23(20):12657.
2. Jo S*, **Centeio R***, Park J, Ousingsawat J, Jeon D-K, Talbi K, Schreiber R, Ryu K, Kahlenberg K, Somoza V, Delpiano L, Gray MA, Amaral MD, Railean V, Beekman JM, Rodenburg LW, Namkung W, Kunzelmann K. The SLC26A9 inhibitor S9-A13 provides no evidence for a role of SLC26A9 in airway chloride secretion but suggests a contribution to regulation of ASL pH and gastric proton secretion. FASEB J. (**2022**) 36(11):e22534. (*shared first authorship).
3. Ousingsawat J, **Centeio R**, Schreiber R, Kunzelmann K. Expression of SLC26A9 in Airways and Its Potential Role in Asthma. Int J Mol Sci. (**2022**); 23(6):2998.
4. Ousingsawat J, **Centeio R**, Cabrita I, Talbi K, Zimmer O, Graf M, Göpferich A, Schreiber R, Kunzelmann K. Airway Delivery of Hydrogel-Encapsulated Niclosamide for the Treatment of Inflammatory Airway Disease. Int J Mol Sci. (**2022**); 23(3):1085.

5. Talbi K, Ousingsawat J, **Centeio R**, Schreiber R, Kunzelmann K. Calmodulin-Dependent Regulation of Overexpressed but Not Endogenous TMEM16A Expressed in Airway Epithelial Cells. Membranes (**2021**); 11(9):723.
6. **Centeio R***, Ousingsawat J*, Cabrita I, Schreiber R, Talbi K, Benedetto R, Doušová T, Verbeken EK, De Boeck K, Cohen I, Kunzelmann K. Mucus Release and Airway Constriction by TMEM16A May Worsen Pathology in Inflammatory Lung Disease. Int J Mol Sci. (**2021**); 22(15):7852. (*shared first authorship).
7. **Centeio R***, Ousingsawat J*, Schreiber R, Kunzelmann K. CLCA1 Regulates Airway Mucus Production and Ion Secretion Through TMEM16A. Int J Mol Sci. (**2021**); 22(10): 5133. (*shared first authorship).
8. Silva IAL, Duarte A, Marson FAL, **Centeio R**, Doušová T, Kunzelmann K, Amaral MD. Assessment of Distinct Electrophysiological Parameters in Rectal Biopsies for the Choice of the Best Diagnosis/Prognosis Biomarkers for Cystic Fibrosis. Front. Physiol. (**2020**); 11:604580.
9. **Centeio R**, Ousingsawat J, Schreiber R, Kunzelmann K. Ca^{2+} Dependence of Volume-Regulated VRAC/LRRC8 and TMEM16A Cl^- Channels. Front Cell Dev Biol (**2020**); 8:596879.
10. Cabrita I, Benedetto R, Wanitchakool P, Lérias J, **Centeio R**, Ousingsawat J, Schreiber R, Kunzelmann K. TMEM16A Mediates Mucus Production in Human Airway Epithelial Cells. Am J Respir Cell Mol Biol (**2020**); 64(1):50-58.
11. Silva IAL, Doušová T, Ramalho S, **Centeio R**, Clarke LA, Railean V, Botelho HM, Holubová A, Valášková I, Yeh J-T, Hwang T-C, Farinha CM, Kunzelmann K, Amaral MD. Organoids as a personalized medicine tool for ultra-rare mutations in cystic fibrosis: The case of S955P and 1717-2A>G. Biochim Biophys Acta Mol Basis Dis (**2020**); 1866(11):165905.
12. Benedetto R*, **Centeio R***, Ousingsawat J, Schreiber R, Janda M, Kunzelmann K. Transport properties in CFTR-/- knockout piglets suggest normal airway surface liquid pH and enhanced amiloride-sensitive Na^+ absorption. Pflügers Arch (**2020**); 472(10):1507-1519. (*shared first authorship).
13. **Centeio R**, Cabrita I, Benedetto R, Talbi K, Ousingsawat J, Schreiber R, Sullivan JK, Kunzelmann K. Pharmacological Inhibition and Activation of the Ca^{2+} Activated Cl^- Channel TMEM16A. Int J Mol Sci (**2020**); 21(7):2557.
14. Kunzelmann K, **Centeio R**, Wanitchakool P, Cabrita I, Benedetto R, Saha T, Hoque KM, Schreiber R. Control of Ion Transport by Tmem16a Expressed in Murine Intestine. Front Physiol. (**2019**); 10:1262.

REFERENCE LIST

1. De Rose, V., Molloy, K., Gohy, S., Pilette, C. & Greene, C.M. Airway Epithelium Dysfunction in Cystic Fibrosis and COPD. *Mediators of inflammation* **2018**, 1309746 (2018).
2. Ganesan, S., Comstock, A.T. & Sajjan, U.S. Barrier function of airway tract epithelium. *Tissue barriers* **1**, e24997 (2013).
3. Livraghi, A. & Randell, S.H. Cystic fibrosis and other respiratory diseases of impaired mucus clearance. *Toxicologic pathology* **35**, 116-129 (2007).
4. Chen, E.Y., Yang, N., Quinton, P.M. & Chin, W.C. A new role for bicarbonate in mucus formation. *American journal of physiology. Lung cellular and molecular physiology* **299**, L542-549 (2010).
5. Poulsen, J.H., Fischer, H., Illek, B. & Machen, T.E. Bicarbonate conductance and pH regulatory capability of cystic fibrosis transmembrane conductance regulator. *Proc. Natl. Acad. Sci. USA* **91**, 5340-5344 (1994).
6. Choi, J.Y.*, et al.* Aberrant CFTR-dependent HCO3- transport in mutations associated with cystic fibrosis. *Nature* **410**, 94-97 (2001).
7. Coakley, R.D.*, et al.* Abnormal surface liquid pH regulation by cultured cystic fibrosis bronchial epithelium. *Proc. Natl. Acad. Sci. U. S. A* **100**, 16083-16088 (2003).
8. Hug, M.J., Tamada, T. & Bridges, R.J. CFTR and bicarbonate secretion by [correction of to] epithelial cells. *News Physiol Sci* **18**, 38-42 (2003).
9. Tang, L., Fatehi, M. & Linsdell, P. Mechanism of direct bicarbonate transport by the CFTR anion channel. *Journal of cystic fibrosis : official journal of the European Cystic Fibrosis Society* **8**, 115-121 (2009).
10. Garnett, J.P.*, et al.* Novel role for pendrin in orchestrating bicarbonate secretion in cystic fibrosis transmembrane conductance regulator (CFTR)-expressing airway serous cells. *The Journal of biological chemistry* **286**, 41069-41082 (2011).
11. Sha, Q., Truong-Tran, A.Q., Plitt, J.R., Beck, L.A. & Schleimer, R.P. Activation of airway epithelial cells by toll-like receptor agonists. *American journal of respiratory cell and molecular biology* **31**, 358-364 (2004).
12. Gandhi, V.D. & Vliagoftis, H. Airway epithelium interactions with aeroallergens: role of secreted cytokines and chemokines in innate immunity. *Frontiers in immunology* **6**, 147 (2015).
13. Noguchi, M., Furukawa, K.T. & Morimoto, M. Pulmonary neuroendocrine cells: physiology, tissue homeostasis and disease. *Disease models & mechanisms* **13**(2020).
14. Geitani, R., Moubareck, C.A., Xu, Z., Karam Sarkis, D. & Touqui, L. Expression and Roles of Antimicrobial Peptides in Innate Defense of Airway Mucosa: Potential Implication in Cystic Fibrosis. *Frontiers in immunology* **11**, 1198 (2020).
15. Twigg, M.S.*, et al.* The Role of Serine Proteases and Antiproteases in the Cystic Fibrosis Lung. *Mediators of inflammation* **2015**, 293053 (2015).
16. Meyer, M. & Jaspers, I. Respiratory protease/antiprotease balance determines susceptibility to viral infection and can be modified by nutritional antioxidants. *American journal of physiology. Lung cellular and molecular physiology* **308**, L1189-1201 (2015).
17. McKelvey, M.C.*, et al.* Proteases, Mucus, and Mucosal Immunity in Chronic Lung Disease. *International journal of molecular sciences* **22**(2021).
18. Laulajainen-Hongisto, A., Toppila-Salmi, S.K., Luukkainen, A. & Kern, R. Airway Epithelial Dynamics in Allergy and Related Chronic Inflammatory Airway Diseases. *Frontiers in cell and developmental biology* **8**, 204 (2020).
19. Davis, J.D. & Wypych, T.P. Cellular and functional heterogeneity of the airway epithelium. *Mucosal immunology* **14**, 978-990 (2021).
20. Wine, J.J. & Joo, N.S. Submucosal glands and airway defense. *Proceedings of the American Thoracic Society* **1**, 47-53 (2004).
21. Widdicombe, J.H. & Wine, J.J. Airway Gland Structure and Function. *Physiological reviews* **95**, 1241-1319 (2015).

22. Fahy, J.V. & Dickey, B.F. Airway mucus function and dysfunction. *N Engl J Med* **363**, 2233-2247 (2010).
23. Ma, J., Rubin, B.K. & Voynow, J.A. Mucins, Mucus, and Goblet Cells. *Chest* **154**, 169-176 (2018).
24. Thornton, D.J. & Sheehan, J.K. From mucins to mucus: toward a more coherent understanding of this essential barrier. *Proceedings of the American Thoracic Society* **1**, 54-61 (2004).
25. Evans, C.M. & Koo, J.S. Airway mucus: the good, the bad, the sticky. *Pharmacology & therapeutics* **121**, 332-348 (2009).
26. Bonser, L.R. & Erle, D.J. Airway Mucus and Asthma: The Role of MUC5AC and MUC5B. *Journal of clinical medicine* **6**(2017).
27. Chen, G.*, et al.* SPDEF is required for mouse pulmonary goblet cell differentiation and regulates a network of genes associated with mucus production. *The Journal of clinical investigation* **119**, 2914-2924 (2009).
28. Song, J.*, et al.* Targeted epigenetic editing of SPDEF reduces mucus production in lung epithelial cells. *American journal of physiology. Lung cellular and molecular physiology* **312**, L334-l347 (2017).
29. Thai, P., Loukoianov, A., Wachi, S. & Wu, R. Regulation of airway mucin gene expression. *Annual review of physiology* **70**, 405-429 (2008).
30. Williams, O.W., Sharafkhaneh, A., Kim, V., Dickey, B.F. & Evans, C.M. Airway mucus: From production to secretion. *American journal of respiratory cell and molecular biology* **34**, 527-536 (2006).
31. Adler, K.B., Tuvim, M.J. & Dickey, B.F. Regulated mucin secretion from airway epithelial cells. *Front Endocrinol. (Lausanne)* **4**, 129 (2013).
32. Davis, C.W. & Dickey, B.F. Regulated airway goblet cell mucin secretion. *Annual review of physiology* **70**, 487-512 (2008).
33. Gustafsson, J.K.*, et al.* Bicarbonate and functional CFTR channel are required for proper mucin secretion and link cystic fibrosis with its mucus phenotype. *The Journal of experimental medicine* **209**, 1263-1272 (2012).
34. Lee, R.E., Miller, S.M. & Randell, S.H. Adult Pulmonary Epithelial Stem Cells and Their Niches. in *Encyclopedia of Tissue Engineering and Regenerative Medicine* (ed. Reis, R.L.) 319-336 (Academic Press, Oxford, 2019).
35. Lam, M., Lamanna, E. & Bourke, J.E. Regulation of Airway Smooth Muscle Contraction in Health and Disease. *Advances in experimental medicine and biology* **1124**, 381-422 (2019).
36. Billington, C.K. & Penn, R.B. Signaling and regulation of G protein-coupled receptors in airway smooth muscle. *Respiratory research* **4**, 2 (2003).
37. Shigemura, M. & Sznajder, J.I. Elevated CO(2) modulates airway contractility. *Interface focus* **11**, 20200021 (2021).
38. Wessler, I. & Kirkpatrick, C.J. Acetylcholine beyond neurons: the non-neuronal cholinergic system in humans. *British journal of pharmacology* **154**, 1558-1571 (2008).
39. Pelaia, G.*, et al.* Molecular mechanisms underlying airway smooth muscle contraction and proliferation: implications for asthma. *Respiratory medicine* **102**, 1173-1181 (2008).
40. Ouedraogo, N. & Roux, E. Physiology of Airway Smooth Muscle Contraction: An Overview. *J Pulm Respir Med* **4**(2014).
41. Bai, Y. & Sanderson, M.J. Airway smooth muscle relaxation results from a reduction in the frequency of Ca2+ oscillations induced by a cAMP-mediated inhibition of the IP3 receptor. *Respiratory research* **7**, 34 (2006).
42. Dowell, M.L., Lavoie, T.L., Solway, J. & Krishnan, R. Airway smooth muscle: a potential target for asthma therapy. *Current opinion in pulmonary medicine* **20**, 66-72 (2014).
43. Tliba, O. & Panettieri, R.A., Jr. Noncontractile functions of airway smooth muscle cells in asthma. *Annual review of physiology* **71**, 509-535 (2009).
44. Lavoie, T.L.*, et al.* Disrupting actin-myosin-actin connectivity in airway smooth muscle as a treatment for asthma? *Proceedings of the American Thoracic Society* **6**, 295-300 (2009).
45. Aghasafari, P., George, U. & Pidaparti, R. A review of inflammatory mechanism in airway

diseases. *Inflammation research : official journal of the European Histamine Research Society ... [et al.]* **68**, 59-74 (2019).
46. Carlier, F.M., de Fays, C. & Pilette, C. Epithelial Barrier Dysfunction in Chronic Respiratory Diseases. *Frontiers in physiology* **12**, 691227 (2021).
47. World Health Organization. *Chronic obstructive pulmonary disease (COPD)*. (2022).
48. World Health Organization. *Asthma*. (2022).
49. Li, X., Cao, X., Guo, M., Xie, M. & Liu, X. Trends and risk factors of mortality and disability adjusted life years for chronic respiratory diseases from 1990 to 2017: systematic analysis for the Global Burden of Disease Study 2017. *BMJ* **368**, m234 (2020).
50. Boucher, R.C., Knowles, M.R., Stutts, M.J. & Gatzy, J.T. Epithelial dysfunction in cystic fibrosis lung disease. *Lung* **161**, 1-17 (1983).
51. Heijerman, H. Infection and inflammation in cystic fibrosis: a short review. *Journal of cystic fibrosis : official journal of the European Cystic Fibrosis Society* **4 Suppl 2**, 3-5 (2005).
52. Shaykhiev, R. Emerging biology of persistent mucous cell hyperplasia in COPD. *Thorax* **74**, 4-6 (2019).
53. Athanazio, R. Airway disease: similarities and differences between asthma, COPD and bronchiectasis. *Clinics (Sao Paulo, Brazil)* **67**, 1335-1343 (2012).
54. Cystic Fibrosis Mutation Database (CFTR1). CFTR Mutations List. (2011).
55. Clinical and Functional Translation of CFTR (CFTR2). CFTR2 Variant List History. (2022).
56. Sheppard, D.N. & Welsh, M.J. Structure and function of the CFTR chloride channel. *Physiol. Rev* **79**, S23-S45 (1999).
57. Lara-Reyna, S., Holbrook, J., Jarosz-Griffiths, H.H., Peckham, D. & McDermott, M.F. Dysregulated signalling pathways in innate immune cells with cystic fibrosis mutations. *Cellular and molecular life sciences : CMLS* **77**, 4485-4503 (2020).
58. Kreda, S.M.*, et al.* Characterization of wild-type and deltaF508 cystic fibrosis transmembrane regulator in human respiratory epithelia. *Mol Biol Cell* **16**, 2154-2167 (2005).
59. De Boeck, K. & Amaral, M.D. Progress in therapies for cystic fibrosis. *Lancet Respir Med* **4**, 662-674 (2016).
60. Noone, P.G. & Knowles, M.R. 'CFTR-opathies': disease phenotypes associated with cystic fibrosis transmembrane regulator gene mutations. *Respiratory research* **2**, 328-332 (2001).
61. Hirtz, S.*, et al.* CFTR Cl^- channel function in native human colon correlates with the genotype and the phenotype in cystic fibrosis. *Gastroenterology* 127, 1085-1095 (2004).
62. Taylor-Cousar, J.L.*, et al.* Clinical development of triple-combination CFTR modulators for cystic fibrosis patients with one or two F508del alleles. *ERJ open research* **5**(2019).
63. Kim, S.J. & Skach, W.R. Mechanisms of CFTR Folding at the Endoplasmic Reticulum. *Frontiers in pharmacology* **3**, 201 (2012).
64. Saint-Criq, V. & Gray, M.A. Role of CFTR in epithelial physiology. *Cellular and molecular life sciences : CMLS* **74**, 93-115 (2017).
65. Smith, J.J., Karp, P.H. & Welsh, M.J. Defective fluid transport by cystic fibrosis airway epithelia. *J. Clin. Invest* **93**, 1307-1311 (1994).
66. Boucher, R.C. Evidence for airway surface dehydration as the initiating event in CF airway disease. *J Intern. Med* **261**, 5-16 (2007).
67. Smith, J.J. & Welsh, M.J. cAMP stimulates bicarbonate secretion across normal, but not cystic fibrosis airway epithelia. *J. Clin. Invest* **89**, 1148-1153 (1992).
68. Borowitz, D. CFTR, bicarbonate, and the pathophysiology of cystic fibrosis. *Pediatric pulmonology* **50 Suppl 40**, S24-s30 (2015).
69. Mall, M.A. & Hartl, D. CFTR: cystic fibrosis and beyond. *The European respiratory journal* **44**, 1042-1054 (2014).
70. Weber, A.J., Soong, G., Bryan, R., Saba, S. & Prince, A. Activation of NF-kappaB in airway epithelial cells is dependent on CFTR trafficking and Cl- channel function. *American journal of physiology. Lung cellular and molecular physiology* **281**, L71-L78

(2001).
71. Courtney, J.M., Ennis, M. & Elborn, J.S. Cytokines and inflammatory mediators in cystic fibrosis. *Journal of cystic fibrosis : official journal of the European Cystic Fibrosis Society* **3**, 223-231 (2004).
72. Ratjen, F., Hartog, C.M., Paul, K., Wermelt, J. & Braun, J. Matrix metalloproteases in BAL fluid of patients with cystic fibrosis and their modulation by treatment with dornase alpha. *Thorax* **57**, 930-934 (2002).
73. Gramegna, A.*, et al.* Neutrophil elastase in bronchiectasis. *Respiratory research* **18**, 211 (2017).
74. Durieu, I.*, et al.* Subepithelial fibrosis and degradation of the bronchial extracellular matrix in cystic fibrosis. *American journal of respiratory and critical care medicine* **158**, 580-588 (1998).
75. Hartl, D.*, et al.* Cleavage of CXCR1 on neutrophils disables bacterial killing in cystic fibrosis lung disease. *Nature medicine* **13**, 1423-1430 (2007).
76. Voynow, J.A., Fischer, B.M. & Zheng, S. Proteases and cystic fibrosis. *The international journal of biochemistry & cell biology* **40**, 1238-1245 (2008).
77. Caldwell, R.A., Boucher, R.C. & Stutts, M.J. Neutrophil elastase activates near-silent epithelial Na+ channels and increases airway epithelial Na+ transport. *American journal of physiology. Lung cellular and molecular physiology* **288**, L813-819 (2005).
78. Harris, M., Firsov, D., Vuagniaux, G., Stutts, M.J. & Rossier, B.C. A novel neutrophil elastase inhibitor prevents elastase activation and surface cleavage of the epithelial sodium channel expressed in Xenopus laevis oocytes. *The Journal of biological chemistry* **282**, 58-64 (2007).
79. Le Gars, M.*, et al.* Neutrophil elastase degrades cystic fibrosis transmembrane conductance regulator via calpains and disables channel function in vitro and in vivo. *American journal of respiratory and critical care medicine* **187**, 170-179 (2013).
80. Vandivier, R.W.*, et al.* Elastase-mediated phosphatidylserine receptor cleavage impairs apoptotic cell clearance in cystic fibrosis and bronchiectasis. *The Journal of clinical investigation* **109**, 661-670 (2002).
81. Zhang, Y., Wang, L., Mutlu, G.M. & Cai, H. More to Explore: Further Definition of Risk Factors for COPD - Differential Gender Difference, Modest Elevation in PM(2).(5), and e-Cigarette Use. *Frontiers in physiology* **12**, 669152 (2021).
82. Brusselle, G.G., Joos, G.F. & Bracke, K.R. New insights into the immunology of chronic obstructive pulmonary disease. *Lancet (London, England)* **378**, 1015-1026 (2011).
83. Barnes, P.J. Small airway fibrosis in COPD. *The international journal of biochemistry & cell biology* **116**, 105598 (2019).
84. Tantucci, C. & Modina, D. Lung function decline in COPD. *International journal of chronic obstructive pulmonary disease* **7**, 95-99 (2012).
85. Vlahos, R. & Bozinovski, S. Role of alveolar macrophages in chronic obstructive pulmonary disease. *Frontiers in immunology* **5**, 435 (2014).
86. Cantin, A.M.*, et al.* Cystic fibrosis transmembrane conductance regulator function is suppressed in cigarette smokers. *American journal of respiratory and critical care medicine* **173**, 1139-1144 (2006).
87. Dransfield, M.T.*, et al.* Acquired cystic fibrosis transmembrane conductance regulator dysfunction in the lower airways in COPD. *Chest* **144**, 498-506 (2013).
88. Hassan, F.*, et al.* Accumulation of metals in GOLD4 COPD lungs is associated with decreased CFTR levels. *Respiratory research* **15**, 69 (2014).
89. Baby, M.K., Muthu, P.K., Johnson, P. & Kannan, S. Effect of cigarette smoking on nasal mucociliary clearance: A comparative analysis using saccharin test. *Lung India : official organ of Indian Chest Society* **31**, 39-42 (2014).
90. Gensch, E.*, et al.* Tobacco smoke control of mucin production in lung cells requires oxygen radicals AP-1 and JNK. *The Journal of biological chemistry* **279**, 39085-39093 (2004).
91. Bodas, M.*, et al.* Cigarette Smoke Activates NOTCH3 to Promote Goblet Cell Differentiation in Human Airway Epithelial Cells. *American journal of respiratory cell and molecular biology* **64**, 426-440 (2021).

92. Kuruvilla, M.E., Lee, F.E. & Lee, G.B. Understanding Asthma Phenotypes, Endotypes, and Mechanisms of Disease. *Clinical reviews in allergy & immunology* **56**, 219-233 (2019).
93. Toskala, E. & Kennedy, D.W. Asthma risk factors. *International forum of allergy & rhinology* **5 Suppl 1**, S11-16 (2015).
94. Fernández-Caldas, E., Puerta, L. & Caraballo, L. Mites and allergy. *Chemical immunology and allergy* **100**, 234-242 (2014).
95. Jeffery, P.K. Comparison of the structural and inflammatory features of COPD and asthma. Giles F. Filley Lecture. *Chest* **117**, 251s-260s (2000).
96. Locksley, R.M. Asthma and allergic inflammation. *Cell* **140**, 777-783 (2010).
97. Fahy, J.V. Type 2 inflammation in asthma--present in most, absent in many. *Nat Rev Immunol* **15**, 57-65 (2015).
98. Shamri, R., Xenakis, J.J. & Spencer, L.A. Eosinophils in innate immunity: an evolving story. *Cell and tissue research* **343**, 57-83 (2011).
99. Al-Muhsen, S., Johnson, J.R. & Hamid, Q. Remodeling in asthma. *The Journal of allergy and clinical immunology* **128**, 451-462; quiz 463-454 (2011).
100. Doeing, D.C. & Solway, J. Airway smooth muscle in the pathophysiology and treatment of asthma. *Journal of applied physiology (Bethesda, Md. : 1985)* **114**, 834-843 (2013).
101. Tliba, O.*, et al.* IL-13 enhances agonist-evoked calcium signals and contractile responses in airway smooth muscle. *British journal of pharmacology* **140**, 1159-1162 (2003).
102. Gour, N. & Wills-Karp, M. IL-4 and IL-13 signaling in allergic airway disease. *Cytokine* **75**, 68-78 (2015).
103. Yu, H., Li, Q., Kolosov, V.P., Perelman, J.M. & Zhou, X. Interleukin-13 induces mucin 5AC production involving STAT6/SPDEF in human airway epithelial cells. *Cell communication & adhesion* **17**, 83-92 (2010).
104. Mundhenk, L.*, et al.* Both cleavage products of the mCLCA3 protein are secreted soluble proteins. *The Journal of biological chemistry* **281**, 30072-30080 (2006).
105. Wisnewski, A.V., Liu, J. & Colangelo, C.M. Glutathione reaction products with a chemical allergen, methylene-diphenyl diisocyanate, stimulate alternative macrophage activation and eosinophilic airway inflammation. *Chemical research in toxicology* **28**, 729-737 (2015).
106. Wisnewski, A.V., Liu, J. & Redlich, C.A. Analysis of Lung Gene Expression Reveals a Role for Cl- channels in Diisocyanate Induced Airway Eosinophilia in a Mouse Model of Asthma Pathology. *American journal of respiratory cell and molecular biology* (2020).
107. Hoshino, M.*, et al.* Increased expression of the human Ca2+-activated Cl- channel 1 (CaCC1) gene in the asthmatic airway. *Am. J Respir. Crit Care Med* **165**, 1132-1136 (2002).
108. Alevy, Y.G.*, et al.* IL-13-induced airway mucus production is attenuated by MAPK13 inhibition. *J Clin. Invest* **122**, 4555-4568 (2012).
109. Liu, C.L. & Shi, G.P. Calcium-activated chloride channel regulator 1 (CLCA1): More than a regulator of chloride transport and mucus production. *World Allergy Organ J* **12**, 100077 (2019).
110. Dougherty, R.H. & Fahy, J.V. Acute exacerbations of asthma: epidemiology, biology and the exacerbation-prone phenotype. *Clinical and experimental allergy : journal of the British Society for Allergy and Clinical Immunology* **39**, 193-202 (2009).
111. Garth, J., Barnes, J.W. & Krick, S. Targeting Cytokines as Evolving Treatment Strategies in Chronic Inflammatory Airway Diseases. *International journal of molecular sciences* **19**(2018).
112. Boulet, L.P. Airway remodeling in asthma: update on mechanisms and therapeutic approaches. *Current opinion in pulmonary medicine* **24**, 56-62 (2018).
113. Virchow, J.C.*, et al.* Importance of inhaler devices in the management of airway disease. *Respiratory medicine* **102**, 10-19 (2008).
114. Barnes, P.J. Glucocorticosteroids. *Handbook of experimental pharmacology* **237**, 93-115 (2017).
115. Cazzola, M., Page, C.P., Calzetta, L. & Matera, M.G. Pharmacology and therapeutics

of bronchodilators. *Pharmacological reviews* **64**, 450-504 (2012).
116. Dahl, R. Systemic side effects of inhaled corticosteroids in patients with asthma. *Respiratory medicine* **100**, 1307-1317 (2006).
117. Barnes, P.J. & Adcock, I.M. Glucocorticoid resistance in inflammatory diseases. *Lancet (London, England)* **373**, 1905-1917 (2009).
118. Nino, G., Hu, A., Grunstein, J.S. & Grunstein, M.M. Mechanism regulating proasthmatic effects of prolonged homologous beta2-adrenergic receptor desensitization in airway smooth muscle. *American journal of physiology. Lung cellular and molecular physiology* **297**, L746-757 (2009).
119. Gupta, M.K.*, et al.* Defective Resensitization in Human Airway Smooth Muscle Cells Evokes β-Adrenergic Receptor Dysfunction in Severe Asthma. *PloS one* **10**, e0125803 (2015).
120. Hurt, K. & Bilton, D. Inhaled interventions in cystic fibrosis: mucoactive and antibiotic therapies. *Respiration; international review of thoracic diseases* **88**, 441-448 (2014).
121. Lopes-Pacheco, M. CFTR Modulators: The Changing Face of Cystic Fibrosis in the Era of Precision Medicine. *Frontiers in pharmacology* **10**, 1662 (2019).
122. Xia, S.*, et al.* Simvastatin promotes alveolar epithelial cell proliferation and attenuates cigarette smoke-induced emphysema in rats. *Molecular medicine reports* **12**, 5903-5910 (2015).
123. Hisata, S.*, et al.* Reversal of emphysema by restoration of pulmonary endothelial cells. *The Journal of experimental medicine* **218**(2021).
124. Jenkins, C. Drugs for chronic obstructive pulmonary disease. *Australian prescriber* **40**, 15-19 (2017).
125. Solomon, G.M., Fu, L., Rowe, S.M. & Collawn, J.F. The therapeutic potential of CFTR modulators for COPD and other airway diseases. *Current opinion in pharmacology* **34**, 132-139 (2017).
126. Courville, C.A.*, et al.* Recovery of Acquired Cystic Fibrosis Transmembrane Conductance Regulator Dysfunction after Smoking Cessation. *American journal of respiratory and critical care medicine* **192**, 1521-1524 (2015).
127. Quesada, R. & Dutzler, R. Alternative chloride transport pathways as pharmacological targets for the treatment of cystic fibrosis. *Journal of cystic fibrosis : official journal of the European Cystic Fibrosis Society* **19**, S37-S41 (2019).
128. Paulino, C., Kalienkova, V., Lam, A.K.M., Neldner, Y. & Dutzler, R. Activation mechanism of the calcium-activated chloride channel TMEM16A revealed by cryo-EM. *Nature* **552**, 421-425 (2017).
129. Pedemonte, N. & Galietta, L.J. Structure and Function of TMEM16 Proteins (Anoctamins). *Physiological reviews* **94**, 419-459 (2014).
130. Bai, W., Liu, M. & Xiao, Q. The diverse roles of TMEM16A Ca(2+)-activated Cl(-) channels in inflammation. *J Adv Res* **33**, 53-68 (2021).
131. Caputo, A.*, et al.* TMEM16A, A Membrane Protein Associated With Calcium-Dependent Chloride Channel Activity. *Science (New York, N.Y.)* **322**, 590-594 (2008).
132. Huang, F.*, et al.* Calcium-activated chloride channel TMEM16A modulates mucin secretion and airway smooth muscle contraction. *Proc. Natl. Acad. Sci U. S. A* **109**, 16354-16359 (2012).
133. Scudieri, P.*, et al.* Association of TMEM16A chloride channel overexpression with airway goblet cells metaplasia. *The Journal of physiology* **590**, 6141-6155 (2012).
134. Caci, E.*, et al.* Upregulation of TMEM16A Protein in Bronchial Epithelial Cells by Bacterial Pyocyanin. *PLoS. ONE* **10**, e0131775 (2015).
135. Kunzelmann, K.*, et al.* TMEM16A in Cystic Fibrosis: Activating or Inhibiting? *Frontiers in pharmacology* **29**, 10:13 (2019).
136. Clarke, L.L.*, et al.* Relationship of a non-cystic fibrosis transmembrane conductance regulator-mediated chloride conductance to organ-level didease in *cftr (-/-)* mice. *Proc. Natl. Acad. Sci. USA* **91**, 479-483 (1994).
137. Benedetto, R.*, et al.* Epithelial Chloride Transport by CFTR Requires TMEM16A. *Scientific Reports* **7**, 12397 (2017).
138. Park, J.H.*, et al.* TMEM16A deficiency: a potentially fatal neonatal disease resulting from

impaired chloride currents. *J Med Genet* **58**, 247-253 (2020).
139. Namkung, W., Finkbeiner, W.E. & Verkman, A.S. CFTR-Adenylyl Cyclase I Association Is Responsible for UTP Activation of CFTR in Well-Differentiated Primary Human Bronchial Cell Cultures. *Mol. Biol. Cell* **21**, 2639-2648 (2010).
140. Jin, X.*, et al.* Activation of the Cl- Channel ANO1 by Localized Calcium Signals in Nociceptive Sensory Neurons Requires Coupling with the IP3 Receptor. *Sci. Signal* **6**, ra73 (2013).
141. Cabrita, I.*, et al.* Differential effects of anoctamins on intracellular calcium signals. *Faseb j* **31**, 2123-2134 (2017).
142. Huang, F.*, et al.* Studies on expression and function of the TMEM16A calcium-activated chloride channel. *Proc. Natl. Acad. Sci. U. S. A* **106**, 21413-21418 (2009).
143. Zhang, C.H.*, et al.* The transmembrane protein 16A Ca(2+)-activated Cl- channel in airway smooth muscle contributes to airway hyperresponsiveness. *Am J Respir. Crit Care Med* **187**, 374-381 (2013).
144. Wang, P.*, et al.* Inflammatory mediators mediate airway smooth muscle contraction through a G protein-coupled receptor-transmembrane protein 16A-voltage-dependent Ca(2+) channel axis and contribute to bronchial hyperresponsiveness in asthma. *The Journal of allergy and clinical immunology* **141**, 1259-1268.e1211 (2018).
145. Benedetto, R., Cabrita, I., Schreiber, R. & Kunzelmann, K. TMEM16A is indispensable for basal mucus secretion in airways and intestine. *FASEB J* **33**, 4502-4512 (2019).
146. Fill, M. & Copello, J.A. Ryanodine receptor calcium release channels. *Physiological reviews* **82**, 893-922 (2002).
147. Miner, K.*, et al.* Drug Repurposing: The Anthelmintics Niclosamide and Nitazoxanide Are Potent TMEM16A Antagonists That Fully Bronchodilate Airways. *Frontiers in pharmacology* **14**, 10:51 (2019).
148. Danielsson, J.*, et al.* Antagonists of the TMEM16A Calcium-activated Chloride Channel Modulate Airway Smooth Muscle Tone and Intracellular Calcium. *Anesthesiology* **123**, 569-581 (2015).
149. Kondo, M.*, et al.* Chloride ion transport and overexpression of TMEM16A in a guinea pig asthma model. *Clinical and experimental allergy : journal of the British Society for Allergy and Clinical Immunology* **47**, 795-804 (2017).
150. Cabrita, I., Benedetto, R., Schreiber, R. & Kunzelmann, K. Niclosamide repurposed for the treatment of inflammatory airway disease. *JCI Insight* **8**, 128414 (2019).
151. Chi, X.*, et al.* Structural insights into the gating mechanism of human SLC26A9 mediated by its C-terminal sequence. *Cell discovery* **6**, 55 (2020).
152. Alper, S.L. & Sharma, A.K. The SLC26 gene family of anion transporters and channels. *Mol. Aspects Med* **34**, 494-515 (2013).
153. Mount, D.B. & Romero, M.F. The SLC26 gene family of multifunctional anion exchangers. *Pflugers Archiv : European journal of physiology* **447**, 710-721 (2004).
154. Shcheynikov, N.*, et al.* Coupling modes and stoichiometry of Cl-/HCO3- exchange by slc26a3 and slc26a6. *The Journal of general physiology* **127**, 511-524 (2006).
155. Ko, S.B.*, et al.* A molecular mechanism for aberrant CFTR-dependent HCO(3)(-) transport in cystic fibrosis. *EMBO J 2002 Nov. 1. ;21. (21.):5662. -72* **21**, 5662-5672 (2002).
156. Ko, S.B.*, et al.* Gating of CFTR by the STAS domain of SLC26 transporters. *Nat. Cell Biol* **6**, 343-350 (2004).
157. Gray, M.A. Bicarbonate secretion: it takes two to tango. *Nat. Cell Biol* **6**, 292-294 (2004).
158. Lohi, H.*, et al.* Functional characterization of three novel tissue-specific anion exchangers SLC26A7, -A8, and -A9. *The Journal of biological chemistry* **277**, 14246-14254 (2002).
159. Bertrand, C.A., Zhang, R., Pilewski, J.M. & Frizzell, R.A. SLC26A9 is a constitutively active, CFTR-regulated anion conductance in human bronchial epithelia. *J Gen. Physiol* **133**, 421-438 (2009).
160. Dorwart, M.R., Shcheynikov, N., Wang, Y., Stippec, S. & Muallem, S. SLC26A9 is a Cl(-) channel regulated by the WNK kinases. *The Journal of physiology* **584**, 333-345 (2007).
161. Loriol, C.*, et al.* Characterization of SLC26A9, facilitation of Cl(-) transport by

bicarbonate. *Cell Physiol Biochem* **22**, 15-30 (2008).
162. Chang, M.H.*, et al.* Slc26a9-Anion Exchanger, Channel and Na(+) Transporter. *J Membr. Biol* (2009).
163. Xu, J.*, et al.* SLC26A9 is expressed in gastric surface epithelial cells, mediates Cl-/HCO3- exchange, and is inhibited by NH4+. *American journal of physiology. Cell physiology* **289**, C493-505 (2005).
164. Ohana, E., Shcheynikov, N., Yang, D., So, I. & Muallem, S. Determinants of coupled transport and uncoupled current by the electrogenic SLC26 transporters. *The Journal of general physiology* **137**, 239-251 (2011).
165. Walter, J.D., Sawicka, M. & Dutzler, R. Cryo-EM structures and functional characterization of murine Slc26a9 reveal mechanism of uncoupled chloride transport. *Elife* **8**(2019).
166. Bertrand, C.A.*, et al.* The CFTR trafficking mutation F508del inhibits the constitutive activity of SLC26A9. *American journal of physiology. Lung cellular and molecular physiology* **312**, L912-l925 (2017).
167. Strug, L.J.*, et al.* Cystic fibrosis gene modifier SLC26A9 modulates airway response to CFTR-directed therapeutics. *Hum Mol Genet* **25**, 4590-4600 (2016).
168. Anagnostopoulou, P.*, et al.* SLC26A9-mediated chloride secretion prevents mucus obstruction in airway inflammation. *J. Clin. Invest* **122**, 3629-3634 (2012).
169. Danahay, H.L.*, et al.* TMEM16A Potentiation: A Novel Therapeutic Approach for the Treatment of Cystic Fibrosis. *American journal of respiratory and critical care medicine* (2020).
170. Knowles, M.R., Clarke, L.L. & Boucher, R.C. Activation by extracellular nucleotides of chloride secretion in the airway epithelia of patients with cystic fibrosis. *N. Engl. J Med* **325**, 533-538 (1991).
171. Mall, M.*, et al.* Modulation of Ca2+ activated Cl- secretion by basolateral K+ channels in human normal and cystic fibrosis airway epithelia. *Pediatric Research* **53**, 608-618 (2003).
172. Son, M.*, et al.* Apical and basolateral ATP-induced anion secretion in polarized human airway epithelia. *Am. J Respir. Cell Mol. Biol* **30**, 411-419 (2004).
173. Kunzelmann, K. & Mall, M. Pharmacotherapy of the ion transport defect in cystic fibrosis: role of purinergic receptor agonists and other potential therapeutics. *American Journal of Respiratory Medicine* **2**, 299-309 (2003).
174. Ratjen, F.*, et al.* Long term effects of denufosol tetrasodium in patients with cystic fibrosis. *Journal of cystic fibrosis : official journal of the European Cystic Fibrosis Society* **11**, 539-549 (2012).
175. Eber, E.*, et al.* Aerosolized lancovutide in adolescents (≥12 years) and adults with cystic fibrosis - a randomized trial. *Journal of cystic fibrosis : official journal of the European Cystic Fibrosis Society* (2020).
176. Benedetto, R.*, et al.* Transport properties in CFTR-/- knockout piglets suggest normal airway surface liquid pH and enhanced amiloride-sensitive Na(+) absorption. *Pflugers Archiv : European journal of physiology* **472**, 1507-1519 (2020).
177. Okada, S.F.*, et al.* Coupled nucleotide and mucin hypersecretion from goblet-cell metaplastic human airway epithelium. *American journal of respiratory cell and molecular biology* **45**, 253-260 (2011).
178. Olivier, K.N.*, et al.* Acute safety and effects on mucociliary clearance of aerosolized uridine 5'-triphosphate +/- amiloride in normal human adults. *Am J Respir Crit. Care Med* **154**, 217-223 (1996).
179. Bennett, W.D.*, et al.* Effect of uridine 5'-triphosphate plus amiloride on mucociliary clearance in adult cystic fibrosis. *American journal of respiratory and critical care medicine* **153**, 1796-1801 (1996).
180. Danahay, H.*, et al.* Potentiating TMEM16A does not stimulate airway mucus secretion or bronchial and pulmonary arterial smooth muscle contraction. *FASEB Bioadv* **2**, 464-477 (2020).
181. Lin, J.*, et al.* TMEM16A mediates the hypersecretion of mucus induced by Interleukin-13. *Exp. Cell Res* **334**, 260-269 (2015).

182. Danielsson, J.*, et al.* Agonism of the TMEM16A Calcium-Activated Chloride Channel Modulates Airway Smooth Muscle Tone. *American journal of physiology. Lung cellular and molecular physiology* (2020).
183. Kent, B.D.*, et al.* Asthma and cystic fibrosis: a tangled web. *Pediatric pulmonology* **49**, 205-213 (2014).
184. Sun, H., Xia, Y., Paudel, O., Yang, X.R. & Sham, J.S. Chronic hypoxia-induced upregulation of Ca2+-activated Cl- channel in pulmonary arterial myocytes: a mechanism contributing to enhanced vasoreactivity. *The Journal of physiology* **590**, 3507-3521 (2012).
185. Forrest, A.S.*, et al.* Increased TMEM16A-Encoded Calcium-Activated Chloride Channel Activity Is Associated With Pulmonary Hypertension. *Am. J Physiol Cell Physiol* **303**, C1229-C1243 (2012).
186. Allawzi, A.M.*, et al.* Activation of Anoctamin-1 Limits Pulmonary Endothelial Cell Proliferation via p38-MAPK-dependent Apoptosis. *American journal of respiratory cell and molecular biology* (2017).
187. Papp, R.*, et al.* Targeting TMEM16A to reverse vasoconstriction and remodelling in idiopathic PAH. *The European respiratory journal* (2019).
188. Wells, J.M.*, et al.* Pulmonary artery enlargement and cystic fibrosis pulmonary exacerbations: a cohort study. *Lancet Respir Med* **4**, 636-645 (2016).
189. Zouk, A.N.*, et al.* Pulmonary artery enlargement is associated with pulmonary hypertension and decreased survival in severe cystic fibrosis: A cohort study. *PloS one* **15**, e0229173 (2020).
190. Schreiber, R., Castrop, H. & Kunzelmann, K. Allergen induced airway hyperresponsiveness is absent in ecto-5´-nucleotidase (CD73) deficient mice. *Pflugers Archiv : European journal of physiology* **457**, 431-440 (2008).
191. Cabrita, I.*, et al.* TMEM16A Mediated Mucus Production in Human Airway Epithelial Cells. *American journal of respiratory cell and molecular biology* (2020).
192. Lerias, J.*, et al.* Compartmentalized crosstalk of CFTR and TMEM16A (ANO1) through EPAC1 and ADCY1. *Cell Signal* **44**, 10-19 (2018).
193. Martins, J.R.*, et al.* Anoctamin 6 is an essential component of the outwardly rectifying chloride channel. *Proc. Natl. Acad. Sci. U. S. A* **108**, 18168-18172 (2011).
194. Grynkiewicz, G., Poenie, M. & Tsien, R.Y. A new generation of Ca^{2+} indicators with greatly improved fluorescence properties. *The Journal of biological chemistry* **260**, 3440-3450 (1985).
195. Namkung, W., Yao, Z., Finkbeiner, W.E. & Verkman, A.S. Small-molecule activators of TMEM16A, a calcium-activated chloride channel, stimulate epithelial chloride secretion and intestinal contraction. *FASEB J* **25**, 4048-4062 (2011).
196. Centeio, R.*, et al.* Pharmacological Inhibition and Activation of the Ca(2+) Activated Cl(-) Channel TMEM16A. *International journal of molecular sciences* **21**, 2557 (2020).
197. Genovese, M.*, et al.* TRPV4 and purinergic receptor signalling pathways are separately linked in airway epithelia to CFTR and TMEM16A chloride channels. *The Journal of physiology* (2019).
198. Chua, R.L.*, et al.* COVID-19 severity correlates with airway epithelium-immune cell interactions identified by single-cell analysis. *Nat Biotechnol* **38**, 970-979 (2020).
199. Cabrita, I.*, et al.* Cyst growth in ADPKD is prevented by pharmacological and genetic inhibition of TMEM16A in vivo. *Nat Commun* **11**, 4320 (2020).
200. Rajavelu, P.*, et al.* Airway epithelial SPDEF integrates goblet cell differentiation and pulmonary Th2 inflammation. *The Journal of clinical investigation* **125**, 2021-2031 (2015).
201. Park, K.S.*, et al.* SPDEF regulates goblet cell hyperplasia in the airway epithelium. *The Journal of clinical investigation* **117**, 978-988 (2007).
202. Abraham, W.M.*, et al.* Airway responses to aerosolized brevetoxins in an animal model of asthma. *American journal of respiratory and critical care medicine* **171**, 26-34 (2005).
203. Fatima, N., Cohen, C. & Siddiqui, M.T. DOG1 utility in diagnosing gastrointestinal stromal tumors on fine-needle aspiration. *Cancer Cytopathol* **119**, 202-208 (2011).
204. Ballard, S.T., Fountain, J.D., Inglis, S.K., Corboz, M.R. & Taylor, A.E. Chloride secretion

across distal airway epithelium: relationship to submucosal gland distribution. *Am. J. Physiol* **268**, L526-L531 (1995).
205. Finkbeiner, W.E*., et al.* Cystic fibrosis and the relationship between mucin and chloride secretion by cultures of human airway gland mucous cells. *American journal of physiology. Lung cellular and molecular physiology* **301**, L402-414 (2011).
206. Matusovsky, O.S*., et al.* Contractile Properties of Intrapulmonary Airway Smooth Muscle in Cystic Fibrosis. *American journal of respiratory cell and molecular biology* **60**, 434-444 (2019).
207. McCuaig, S. & Martin, J.G. How the airway smooth muscle in cystic fibrosis reacts in proinflammatory conditions: implications for airway hyper-responsiveness and asthma in cystic fibrosis. *Lancet Respir Med* **1**, 137-147 (2013).
208. Duran, C., Thompson, C.H., Xiao, Q. & Hartzell, H.C. Chloride Channels: Often Enigmatic, Rarely Predictable. *Annu. Rev. Physiol* **17**, 95-121 (2010).
209. Keeler, D.M., Grandal, M.K. & McCall, J.R. Brevenal, a Marine Natural Product, is Anti-Inflammatory and an Immunomodulator of Macrophage and Lung Epithelial Cells. *Mar Drugs* **17**(2019).
210. Hammer, C*., et al.* A coding variant of ANO10, affecting volume regulation of macrophages, is associated with Borrelia seropositivity. *Mol. Med* **21**, 26-37 (2015).
211. Perez, F.J*., et al.* Niflumic Acid Reverses Airway Mucus Excess and Improves Survival in the Rat Model of Steroid-Induced Pneumocystis Pneumonia. *Front Microbiol* **10**, 1522 (2019).
212. Kunzelmann, K. Getting hands on a drug for Covid-19: Inhaled and Intranasal Niclosamide. *Lancet Reg Health Eur* **4**, 400094 (2021).
213. Galietta, L.J*., et al.* IL-4 Is a Potent Modulator of Ion Transport in the Human Bronchial Epithelium In Vitro. *J Immunol* **168**, 839-845 (2002).
214. Simoes, F.B*., et al.* TMEM16A chloride channel does not drive mucus production. *Life Sci Alliance* **2**(2019).
215. Billet, A. & Hanrahan, J.W. The secret life of CFTR as a calcium-activated chloride channel. *The Journal of physiology* **591**, 5273-5278 (2013).
216. Benedetto, R*., et al.* Plasma membrane localized TMEM16 Proteins are Indispensable for expression of CFTR. *J Mol Med* **97**, 711-722 (2019).
217. Patel, A.C., Brett, T.J. & Holtzman, M.J. The role of CLCA proteins in inflammatory airway disease. *Annu. Rev. Physiol* **71**, 425-449 (2009).
218. Zhou, Y*., et al.* Characterization of a calcium-activated chloride channel as a shared target of Th2 cytokine pathways and its potential involvement in asthma. *American journal of respiratory cell and molecular biology* **25**, 486-491 (2001).
219. Hauber, H.P., Lavigne, F., Hung, H.L., Levitt, R.C. & Hamid, Q. Effect of Th2 type cytokines on hCLCA1 and mucus expression in cystic fibrosis airways. *J Cyst. Fibros* **9**, 277-279 (2010).
220. Gibson, A*., et al.* hCLCA1 and mCLCA3 are secreted non-integral membrane proteins and therefore are not ion channels. *The Journal of biological chemistry* **280**, 27205-27212 (2005).
221. Sala-Rabanal, M., Yurtsever, Z., Nichols, C.G. & Brett, T.J. Secreted CLCA1 modulates TMEM16A to activate Ca(2+)-dependent chloride currents in human cells. *Elife* **4. doi**, 10 (2015).
222. Sala-Rabanal, M., Yurtsever, Z., Berry, K.N., Nichols, C.G. & Brett, T.J. Modulation of TMEM16A channel activity by the von Willebrand factor type A (VWA) domain of the calcium-activated chloride channel regulator 1 (CLCA1). *The Journal of biological chemistry* **292**, 9164-9174 (2017).
223. Patel, A.C*., et al.* Genetic segregation of airway disease traits despite redundancy of calcium-activated chloride channel family members. *Physiol Genomics* **25**, 502-513 (2006).
224. Mundhenk, L*., et al.* mCLCA3 does not contribute to calcium-activated chloride conductance in murine airways. *Am J Respir. Cell Mol. Biol* **47**, 87-93 (2012).
225. Schreiber, R*., et al.* Expression and Function of Epithelial Anoctamins. *J. Biol. Chem* **285**, 7838-7845 (2010).

226. Nyström, E.E.L.*, et al.* Calcium-activated Chloride Channel Regulator 1 (CLCA1) Controls Mucus Expansion in Colon by Proteolytic Activity. *EBioMedicine* **33**, 134-143 (2018).
227. Xiao, Q.*, et al.* Voltage- and calcium-dependent gating of TMEM16A/Ano1 chloride channels are physically coupled by the first intracellular loop. *Proc. Natl. Acad. Sci. U. S. A* **108**, 8891-8896 (2011).
228. Walters, M.S.*, et al.* Generation of a human airway epithelium derived basal cell line with multipotent differentiation capacity. *Respiratory research* **14**, 135 (2013).
229. Qin, Y.*, et al.* Interleukin-13 stimulates MUC5AC expression via a STAT6-TMEM16A-ERK1/2 pathway in human airway epithelial cells. *Int Immunopharmacol* **40**, 106-114 (2016).
230. Kang, J.W.*, et al.* Synergistic mucus secretion by histamine and IL-4 through TMEM16A in airway epithelium. *American journal of physiology. Lung cellular and molecular physiology*, ajplung.00103.02017 (2017).
231. Duvvuri, U.*, et al.* TMEM16A, induces MAPK and contributes directly to tumorigenesis and cancer progression. *Cancer Res* **72**, 3270-3281 (2012).
232. Ruiz, C.*, et al.* Enhanced Expression of ANO1 in Head and Neck Squamous Cell Carcinoma Causes Cell Migration and Correlates with Poor Prognosis. *PLoS. ONE* **7**, e43265 (2012).
233. Ousingsawat, J.*, et al.* Loss of TMEM16A causes a defect in epithelial Ca2+ dependent chloride transport. *The Journal of biological chemistry* **284**, 28698-28703 (2009).
234. Rock, J.R.*, et al.* Transmembrane protein 16A (TMEM16A) is a Ca2+ regulated Cl- -secretory channel in mouse airways. *The Journal of biological chemistry* **284**, 14875-14880 (2009).
235. Vega, G.*, et al.* Lack of Kcnn4 improves mucociliary clearance in muco-obstructive lung disease. *JCI Insight* **5**(2020).
236. Bernard, K., Bogliolo, S., Soriani, O. & Ehrenfeld, J. Modulation of calcium-dependent chloride secretion by basolateral SK4-like channels in a human bronchial cell line. *J Membr. Biol* **196**, 15-31 (2003).
237. Lee, R.J. & Foskett, J.K. Ca signaling and fluid secretion by secretory cells of the airway epithelium. *Cell Calcium* **55**, 325-336 (2014).
238. Lee, R.J. & Foskett, J.K. cAMP-activated Ca2+ signaling is required for CFTR-mediated serous cell fluid secretion in porcine and human airways. *J Clin. Invest* **120**, 3137-3148 (2010).
239. Devor, D.C.*, et al.* Bicarbonate and chloride secretion in Calu-3 human airway epithelial cells. *J Gen. Physiol* **113**, 743-760 (1999).
240. Lee, R.J., Harlow, J.M., Limberis, M.P., Wilson, J.M. & Foskett, J.K. HCO3(-) secretion by murine nasal submucosal gland serous acinar cells during Ca2+-stimulated fluid secretion. *The Journal of general physiology* **132**, 161-183 (2008).
241. Lee, R.J. & Foskett, J.K. Mechanisms of Ca2+-stimulated fluid secretion by porcine bronchial submucosal gland serous acinar cells. *Am. J. Physiol Lung Cell Mol. Physiol* **298**, L210-L231 (2009).
242. Truong, E.C.*, et al.* Substituted 2-Acylaminocycloalkylthiophene-3-carboxylic Acid Arylamides as Inhibitors of the Calcium-Activated Chloride Channel Transmembrane Protein 16A (TMEM16A). *J Med Chem* **60**, 4626-4635 (2017).
243. Nyström, E.E.L., Arike, L., Ehrencrona, E., Hansson, G.C. & Johansson, M.E.V. Calcium-activated chloride channel regulator 1 (CLCA1) forms non-covalent oligomers in colonic mucus and has mucin 2-processing properties. *The Journal of biological chemistry* **294**, 17075-17089 (2019).
244. Hamann, M.*, et al.* Human ClCa1 modulates anionic conduction of calcium-dependent chloride currents. *J. Physiol* **587**, 2255-2274 (2009).
245. Tian, Y.*, et al.* Control of TMEM16A by INO-4995 and other inositolphosphates. *Br. J Pharmacol* **168**, 253-265 (2013).
246. Centeio, R.*, et al.* Mucus Release and Airway Constriction by TMEM16A May Worsen Pathology in Inflammatory Lung Disease. *International journal of molecular sciences* **22**(2021).

247. Simoes, F.*, et al.* CFTR supports cell death through ROS-dependent activation of TMEM16F (anoctamin 6). *Pflugers Archiv : European journal of physiology* **470**, 305-314 (2018).
248. Ousingsawat, J., Schreiber, R., Gulbins, E., Kamler, M. & Kunzelmann, K. P. aeruginosa Induced Lipid Peroxidation Causes Ferroptotic Cell Death in Airways. *Cell Physiol Biochem* **55**, 590-604 (2021).
249. Braga, L.*, et al.* Drugs that inhibit TMEM16 proteins block SARS-CoV-2 Spike-induced syncytia. *Nature* (2021).
250. Rajah, M.M., Bernier, A., Buchrieser, J. & Schwartz, O. The Mechanism and Consequences of SARS-CoV-2 Spike-Mediated Fusion and Syncytia Formation. *J Mol Biol*, 167280 (2021).
251. Pearson, H.*, et al.* TMEM16A/ANO1 calcium-activated chloride channel as a novel target for the treatment of human respiratory syncytial virus infection. *Thorax* (2020).
252. Braga, C.L.*, et al.* Niclosamide attenuates lung vascular remodeling in experimental pulmonary arterial hypertension. *Eur J Pharmacol* **887**, 173438 (2020).
253. Wu, C.J.*, et al.* Inhibition of severe acute respiratory syndrome coronavirus replication by niclosamide. *Antimicrob Agents Chemother* **48**, 2693-2696 (2004).
254. Fonseca, B.D.*, et al.* Structure-activity analysis of niclosamide reveals potential role for cytoplasmic pH in control of mammalian target of rapamycin complex 1 (mTORC1) signaling. *The Journal of biological chemistry* **287**, 17530-17545 (2012).
255. Prabhakara, C.*, et al.* Strategies to target SARS-CoV-2 entry and infection using dual mechanisms of inhibition by acidification inhibitors. *PLoS Pathog* **17**, e1009706 (2021).
256. Gassen, N.C.*, et al.* SARS-CoV-2-mediated dysregulation of metabolism and autophagy uncovers host-targeting antivirals. *Nat Commun* **12**, 3818 (2021).
257. Jurgeit, A.*, et al.* Niclosamide is a proton carrier and targets acidic endosomes with broad antiviral effects. *PLoS Pathog* **8**, e1002976 (2012).
258. Kunzelmann, K.*, et al.* Modulating Ca2+signals: a common theme for TMEM16, Ist2, and TMC. *Pflugers Archiv : European journal of physiology* **468**, 475-490 (2016).
259. Chen, X., Cao, R. & Zhong, W. Host Calcium Channels and Pumps in Viral Infections. *Cells* **9**(2019).
260. Chang-Graham, A.L.*, et al.* Rotavirus Calcium Dysregulation Manifests as Dynamic Calcium Signaling in the Cytoplasm and Endoplasmic Reticulum. *Sci Rep* **9**, 10822 (2019).
261. Yang, Y.*, et al.* Inhibitory effect on SARS-CoV-2 infection of neferine by blocking Ca(2+) -dependent membrane fusion. *J Med Virol* (2021).
262. Backer, V.*, et al.* A randomized, double-blind, placebo-controlled phase 1 trial of inhaled and intranasal niclosamide: A broad spectrum antiviral candidate for treatment of COVID-19. *Lancet Reg Health Eur*, 100084 (2021).
263. Abdulamir, A.S.*, et al.* A randomised controlled trial of effectiveness and safety of Niclosamide as add on therapy to the standard of care measures in COVID-19 management. *Ann Med Surg (Lond)* **69**, 102779 (2021).
264. Rocco, P.R.M.*, et al.* Early use of nitazoxanide in mild Covid-19 disease: randomised, placebo-controlled trial. *The European respiratory journal* (2021).
265. Devarakonda, B., Hill, R.A., Liebenberg, W., Brits, M. & de Villiers, M.M. Comparison of the aqueous solubilization of practically insoluble niclosamide by polyamidoamine (PAMAM) dendrimers and cyclodextrins. *Int J Pharm* **304**, 193-209 (2005).
266. Hobson, J.J.*, et al.* Scalable nanoprecipitation of niclosamide and in vivo demonstration of long-acting delivery after intramuscular injection. *Nanoscale* **13**, 6410-6416 (2021).
267. Manca, M.L.*, et al.* Liposomes coated with chitosan-xanthan gum (chitosomes) as potential carriers for pulmonary delivery of rifampicin. *J Pharm Sci* **101**, 566-575 (2012).
268. Ziegler, C.E., Graf, M., Nagaoka, M., Lehr, H. & Goepferich, A.M. In Situ Forming iEDDA Hydrogels with Tunable Gelation Time Release High-Molecular Weight Proteins in a Controlled Manner over an Extended Time. *Biomacromolecules* **22**, 3223-3236 (2021).
269. Ye, Y., Zhang, X., Zhang, T., Wang, H. & Wu, B. Design and evaluation of injectable niclosamide nanocrystals prepared by wet media milling technique. *Drug Dev Ind Pharm* **41**, 1416-1424 (2015).

270. Hoyle, C.E. & Bowman, C.N. Thiol-ene click chemistry. *Angew Chem Int Ed Engl* **49**, 1540-1573 (2010).
271. Liu, Y*., et al.* Stable Polymer Nanoparticles with Exceptionally High Drug Loading by Sequential Nanoprecipitation. *Angewandte Chemie* **132**, 4750-4758 (2020).
272. Qian, H., Wohl, A.R., Crow, J.T., Macosko, C.W. & Hoye, T.R. A Strategy for Control of "Random" Copolymerization of Lactide and Glycolide: Application to Synthesis of PEG-b-PLGA Block Polymers Having Narrow Dispersity. *Macromolecules* **44**, 7132-7140 (2011).
273. Abstiens, K., Maslanka Figueroa, S., Gregoritza, M. & Goepferich, A.M. Interaction of functionalized nanoparticles with serum proteins and its impact on colloidal stability and cargo leaching. *Soft Matter* **15**, 709-720 (2019).
274. Schindelin, J*., et al.* Fiji: an open-source platform for biological-image analysis. *Nat Methods* **9**, 676-682 (2012).
275. Riley, R.S., Ben-Ezra, J.M., Massey, D., Slyter, R.L. & Romagnoli, G. Digital photography: a primer for pathologists. *J Clin Lab Anal* **18**, 91-128 (2004).
276. Song, E. & Iwasaki, A. Method for Measuring Mucociliary Clearance and Cilia-generated Flow in Mice by ex vivo Imaging. *Bio Protoc* **10**, e3554 (2020).
277. Loewen, M.E. & Forsyth, G.W. Structure and function of CLCA proteins. *Physiological reviews* **85**, 1061-1092 (2005).
278. Centeio, R., Ousingsawat, J., schreiber, R. & Kunzelmann, K. CLCA1 Regulates Airway Mucus Production and Ion Secretion Through TMEM16A *Int ernational journal of molecular sciences* **22**, 5133 (2021).
279. Winpenny, J.P., Marsey, L.L. & Sexton, D.W. The CLCA gene family: putative therapeutic target for respiratory diseases. *Inflamm Allergy Drug Targets* **8**, 146-160 (2009).
280. Brandl, F*., et al.* Hydrogel-based drug delivery systems: comparison of drug diffusivity and release kinetics. *J Control Release* **142**, 221-228 (2010).
281. Jain, N.K*., et al.* Niclosamide encapsulated polymeric nanocarriers for targeted cancer therapy. *RSC Adv.* **9**, 26572 (2019).
282. Zhang, X., Zhang, Y., Zhang, T., Zhang, J. & Wu, B. Significantly enhanced bioavailability of niclosamide through submicron lipid emulsions with or without PEG-lipid: a comparative study. *J Microencapsul* **32**, 496-502 (2015).
283. Graf, M., Ziegler, C.E., Gregoritza, M. & Goepferich, A.M. Hydrogel microspheres evading alveolar macrophages for sustained pulmonary protein delivery. *Int J Pharm* **566**, 652-661 (2019).
284. Apaolaza, P.S*., et al.* Hyaluronic acid coating of gold nanoparticles for intraocular drug delivery: Evaluation of the surface properties and effect on their distribution. *Exp Eye Res* **198**, 108151 (2020).
285. Almeida, A.P.B*., et al.* Mucopenetrating lipoplexes modified with PEG and hyaluronic acid for CD44-targeted local siRNA delivery to the lungs. *J Biomater Appl* **34**, 617-630 (2019).
286. Bandi, S.P., Bhatnagar, S. & Venuganti, V.V.K. Advanced materials for drug delivery across mucosal barriers. *Acta Biomater* (2020).
287. Wu, K*., et al.* Short-term intratracheal use of PEG-modified IL-2 and glucocorticoid persistently alleviates asthma in a mouse model. *Sci Rep* **6**, 31562 (2016).
288. Kenyon, N.J*., et al.* Self-assembling nanoparticles containing dexamethasone as a novel therapy in allergic airways inflammation. *PloS one* **8**, e77730 (2013).
289. Lackie, P.M., Baker, J.E., Günthert, U. & Holgate, S.T. Expression of CD44 isoforms is increased in the airway epithelium of asthmatic subjects. *American journal of respiratory cell and molecular biology* **16**, 14-22 (1997).
290. Hoffmann, M*., et al.* SARS-CoV-2 Cell Entry Depends on ACE2 and TMPRSS2 and Is Blocked by a Clinically Proven Protease Inhibitor. *Cell* **181**, 271-280.e278 (2020).
291. Jose, R.J. & Manuel, A. COVID-19 cytokine storm: the interplay between inflammation and coagulation. *Lancet Respir Med* **8**, e46-e47 (2020).
292. Yang, H*., et al.* TMEM16F Forms a Ca(2+)-Activated Cation Channel Required for Lipid Scrambling in Platelets during Blood Coagulation. *Cell* **151**, 111-122 (2012).

293. Mattheij, N.J.*, et al.* Survival protein anoctamin-6 controls multiple platelet responses including phospholipid scrambling, swelling, and protein cleavage. *FASEB J* **30**, 727-737 (2015).
294. Sommer, A.*, et al.* Phosphatidylserine exposure is required for ADAM17 sheddase function. *Nat Commun* **7**, 11523 (2016).
295. Ousingsawat, J.*, et al.* Anoctamin 6 mediates effects essential for innate immunity downstream of P2X7-receptors in macrophages. *Nat. Commun* **6**, 6245- (2015).
296. Ousingsawat, J., Schreiber, R. & Kunzelmann, K. TMEM16F/Anoctamin 6 in Ferroptotic Cell Death. *Cancers (Basel)* **11**, pii: E625 (2019).
297. Pereira, S.V.N., Ribeiro, J.D., Bertuzzo, C.S. & Marson, F.A.L. Interaction among variants in the SLC gene family (SLC6A14, SLC26A9, SLC11A1, and SLC9A3) and CFTR mutations with clinical markers of cystic fibrosis. *Pediatric pulmonology* **53**, 888-900 (2018).
298. Ohana, E., Yang, D., Shcheynikov, N. & Muallem, S. Diverse transport modes by the Solute Carrier 26 family of anion transporters. *The Journal of physiology* **587**, 2179-2185 (2009).
299. Dallos, P. & Fakler, B. Prestin, a new type of motor protein. *Nat Rev Mol Cell Biol* **3**, 104-111 (2002).
300. El Khouri, E. & Toure, A. Functional interaction of the cystic fibrosis transmembrane conductance regulator with members of the SLC26 family of anion transporters (SLC26A8 and SLC26A9): physiological and pathophysiological relevance. *The international journal of biochemistry & cell biology* **52**, 58-67 (2014).
301. Liu, X.*, et al.* Loss of Slc26a9 anion transporter alters intestinal electrolyte and HCO3(-) transport and reduces survival in CFTR-deficient mice. *Pflugers Archiv : European journal of physiology* **467**, 1261-1275 (2015).
302. Xu, J.*, et al.* Deletion of the chloride transporter Slc26a9 causes loss of tubulovesicles in parietal cells and impairs acid secretion in the stomach. *Proc. Natl. Acad. Sci. U. S. A* **105**, 17955-17960 (2008).
303. Sato, Y., Thomas, D.Y. & Hanrahan, J.W. The anion transporter SLC26A9 localizes to tight junctions and is degraded by the proteasome when co-expressed with F508del-CFTR. *The Journal of biological chemistry* **294**, 18269-18284 (2019).
304. Pinto, M.C.*, et al.* Synergy in Cystic Fibrosis Therapies: Targeting SLC26A9. *International journal of molecular sciences* **22**(2021).
305. Amlal, H., Xu, J., Barone, S., Zahedi, K. & Soleimani, M. The chloride channel/transporter Slc26a9 regulates the systemic arterial pressure and renal chloride excretion. *J Mol Med (Berl)* **91**, 561-572 (2013).
306. Seidler, U. & Nikolovska, K. Slc26 Family of Anion Transporters in the Gastrointestinal Tract: Expression, Function, Regulation, and Role in Disease. *Compr Physiol* **9**, 839-872 (2019).
307. Klymiuk, N.*, et al.* Sequential targeting of CFTR by BAC vectors generates a novel pig model of cystic fibrosis. *J Mol Med (Berl)* **90**, 597-608 (2012).
308. Bebok, Z.*, et al.* Failure of cAMP agonists to activate rescued deltaF508 CFTR in CFBE41o- airway epithelial monolayers. *The Journal of physiology* **569**, 601-615 (2005).
309. Botelho, H.M.*, et al.* Protein traffic disorders: an effective high-throughput fluorescence microscopy pipeline for drug discovery. *Sci Rep* **5**, 9038 (2015).
310. Needham, P.G.*, et al.* SLC26A9 is selected for endoplasmic reticulum associated degradation (ERAD) via Hsp70-dependent targeting of the soluble STAS domain. *Biochem J* (2021).
311. Ousingsawat, J., Schreiber, R. & Kunzelmann, K. Differential contribution of SLC26A9 to Cl(-) conductance in polarized and non-polarized epithelial cells. *J Cell Physiol* **227**, 2323-2329 (2011).
312. Seo, Y.*, et al.* Synthesis and biological evaluation of novel Ani9 derivatives as potent and selective ANO1 inhibitors. *Eur J Med Chem* **160**, 245-255 (2018).
313. Salomon, J.J.*, et al.* Generation and functional characterization of epithelial cells with stable expression of SLC26A9 Cl- channels. *American journal of physiology. Lung cellular and molecular physiology* **310**, L593-602 (2016).

314. Rakonczay, Z., Jr.*, et al.* CFTR gene transfer to human cystic fibrosis pancreatic duct cells using a Sendai virus vector. *J Cell Physiol* **214**, 442-455 (2008).
315. Rode, B.*, et al.* The testis anion transporter TAT1 (SLC26A8) physically and functionally interacts with the cystic fibrosis transmembrane conductance regulator channel: a potential role during sperm capacitation. *Hum Mol Genet* **21**, 1287-1298 (2012).
316. Larsen, M.B.*, et al.* Separating the contributions of SLC26A9 and CFTR to anion secretion in primary human bronchial epithelia (HBE). *American journal of physiology. Lung cellular and molecular physiology* (2021).
317. Ballard, S.T. & Taylor, A.E. Bioelectric properties of proximal bronchiolar epithelium. *Am J Physiol* **267**, L79-84 (1994).
318. Al-Bazzaz, F.J. Regulation of Na and Cl transport in sheep distal airways. *Am J Physiol* **267**, L193-198 (1994).
319. Demitrack, E.S., Soleimani, M. & Montrose, M.H. Damage to the gastric epithelium activates cellular bicarbonate secretion via SLC26A9 Cl(-)/HCO(3)(-). *American journal of physiology. Gastrointestinal and liver physiology* **299**, G255-264 (2010).
320. Park, J.*, et al.* Novel pendrin inhibitor attenuates airway hyperresponsiveness and mucin expression in experimental murine asthma. *The Journal of allergy and clinical immunology* **144**, 1425-1428.e1412 (2019).
321. Besteman, S.B.*, et al.* Recurrent Respiratory Syncytial Virus Infection in a CD14-Deficient Patient. *The Journal of infectious diseases* **226**, 258-269 (2022).
322. Holik, A.K.*, et al.* Gastric Serotonin Biosynthesis and Its Functional Role in L-Arginine-Induced Gastric Proton Secretion. *International journal of molecular sciences* **22**(2021).
323. Ousingsawat, J., Centeio, R., Schreiber, R. & Kunzelmann, K. Expression of SLC26A9 in Airways and Its Potential Role in Asthma. *International journal of molecular sciences* **23**(2022).
324. Saint-Criq, V.*, et al.* Real-Time, Semi-Automated Fluorescent Measurement of the Airway Surface Liquid pH of Primary Human Airway Epithelial Cells. *J Vis Exp* (2019).
325. Rochelle, L.G.*, et al.* Distribution of ion transport mRNAs throughout murine nose and lung. *Am J Physiol* **279**, L14-L24 (2000).
326. Preston, P.*, et al.* Disruption of the K+ channel beta-subunit KCNE3 reveals an important role in intestinal and tracheal Cl- transport. *J. Biol. Chem* **285**, 7165-7175 (2010).
327. Chen, A.P., Chang, M.H. & Romero, M.F. Functional analysis of nonsynonymous single nucleotide polymorphisms in human SLC26A9. *Hum Mutat* **33**, 1275-1284 (2012).
328. Sun, L.*, et al.* Multiple apical plasma membrane constituents are associated with susceptibility to meconium ileus in individuals with cystic fibrosis. *Nat. Genet* **44**, 562-569 (2012).
329. Miller, M.R.*, et al.* Variants in Solute Carrier SLC26A9 Modify Prenatal Exocrine Pancreatic Damage in Cystic Fibrosis. *J Pediatr* **166**, 1152-1157.e1156 (2015).
330. Lam, A.N.*, et al.* Increased expression of anion transporter SLC26A9 delays diabetes onset in cystic fibrosis. *The Journal of clinical investigation* **130**, 272-286 (2020).
331. Ishibashi, K., Okamura, K. & Yamazaki, J. Involvement of apical P2Y2 receptor-regulated CFTR activity in muscarinic stimulation of Cl(-) reabsorption in rat submandibular gland. *Am J Physiol Regul. Integr. Comp Physiol* **294**, R1729-R1736 (2008).
332. Wang, X., Lytle, C. & Quinton, P.M. Predominant constitutive CFTR conductance in small airways. *Respir. Res* **6**, 7 (2005).
333. Song, Y., Salinas, D., Nielson, D.W. & Verkman, A.S. Hyperacidity of secreted fluid from submucosal glands in early cystic fibrosis. *American journal of physiology. Cell physiology* **290**, C741-C749 (2006).
334. Avella, M., Loriol, C., Boulukos, K., Borgese, F. & Ehrenfeld, J. SLC26A9 stimulates CFTR expression and function in human bronchial cell lines. *J Cell Physiol* **226**, 212-223 (2011).
335. Simão, S., Gomes, P., Pinho, M.J. & Soares-da-Silva, P. Identification of SLC26A transporters involved in the Cl^-/HCO_3^- exchange in proximal tubular cells from WKY and SHR. *Life Sci* **93**, 435-440 (2013).

336. Strong, T.V., Boehm, K. & Collins, F.S. Localization of cystic fibrosis transmembrane conductance regulator mRNA in the human gastrointestinal tract by in situ hybridization. *J Clin. Invest* **93**, 347-354 (1994).
337. Yerxa, B.R.*, et al.* Pharmacology of INS37217 [P(1)-(uridine 5')-P(4)- (2'-deoxycytidine 5')tetraphosphate, tetrasodium salt], a next-generation P2Y(2) receptor agonist for the treatment of cystic fibrosis. *J Pharmacol. Exp. Ther. 2002 Sep. ;302. (3.):871. -80* **302**, 871-880 (2002).
338. Button, B., Okada, S.F., Frederick, C.B., Thelin, W.R. & Boucher, R.C. Mechanosensitive ATP release maintains proper mucus hydration of airways. *Science signaling* **6**, ra46 (2013).
339. Kellerman, D.*, et al.* Denufosol: a review of studies with inhaled P2Y(2) agonists that led to Phase 3. *Pulmonary pharmacology & therapeutics* **21**, 600-607 (2008).
340. Cloutier, M.M., Guernsey, L. & Sha'afi, R.I. Duramycin increases intracellular calcium in airway epithelium. *Membrane biochemistry* **10**, 107-118 (1993).
341. Oliynyk, I., Varelogianni, G., Roomans, G.M. & Johannesson, M. Effect of duramycin on chloride transport and intracellular calcium concentration in cystic fibrosis and non-cystic fibrosis epithelia. *Apmis* **118**, 982-990 (2010).
342. Gold, E.P., Jacocks, H.M., Bourdelais, A.J. & Baden, D.G. Brevenal, a brevetoxin antagonist from Karenia brevis, binds to a previously unreported site on mammalian sodium channels. *Harmful algae* **26**, 12-19 (2013).
343. Thompson, R.J., Sayers, I., Kuokkanen, K. & Hall, I.P. Purinergic Receptors in the Airways: Potential Therapeutic Targets for Asthma? *Frontiers in allergy* **2**, 677677 (2021).
344. Zhang, Z., Liu, F. & Chen, J. Conformational Changes of CFTR upon Phosphorylation and ATP Binding. *Cell* **170**, 483-491.e488 (2017).
345. Cai, Z., Sohma, Y., Bompadre, S.G., Sheppard, D.N. & Hwang, T.C. Application of high-resolution single-channel recording to functional studies of cystic fibrosis mutants. *Methods in molecular biology (Clifton, N.J.)* **741**, 419-441 (2011).
346. Le, S.C., Liang, P., Lowry, A.J. & Yang, H. Gating and Regulatory Mechanisms of TMEM16 Ion Channels and Scramblases. *Frontiers in physiology* **12**, 787773 (2021).
347. Ayon, R.J.*, et al.* Molecular Mechanism of TMEM16A Regulation: Role of CaMKII and PP1/PP2A. *American journal of physiology. Cell physiology* (2019).
348. Tembo, M., Wozniak, K.L., Bainbridge, R.E. & Carlson, A.E. Phosphatidylinositol 4,5-bisphosphate (PIP2) and Ca(2+) are both required to open the Cl(-) channel TMEM16A. *The Journal of biological chemistry* (2019).
349. Jia, Z. & Chen, J. Specific PIP(2) binding promotes calcium activation of TMEM16A chloride channels. *Commun Biol* **4**, 259 (2021).
350. Schmid, A. & Salathe, M. Ciliary beat co-ordination by calcium. *Biology of the cell* **103**, 159-169 (2011).
351. Braiman, A. & Priel, Z. Efficient mucociliary transport relies on efficient regulation of ciliary beating. *Respiratory physiology & neurobiology* **163**, 202-207 (2008).
352. Cheng, Y.*, et al.* Identification of a conserved drug binding pocket in TMEM16 proteins. *Res Sq* (2022).
353. Seo, Y.*, et al.* Ani9, A Novel Potent Small-Molecule ANO1 Inhibitor with Negligible Effect on ANO2. *PloS one* **11**, e0155771 (2016).
354. Kadri, H., Lambourne, O.A. & Mehellou, Y. Niclosamide, a Drug with Many (Re)purposes. *ChemMedChem* **13**, 1088-1091 (2018).
355. Crottes, D. & Jan, L.Y. The multifaceted role of TMEM16A in cancer. *Cell Calcium* **82**, 102050 (2019).
356. Kunzelmann, K., Ousingsawat, J., Benedetto, R., Cabrita, I. & Schreiber, R. Contribution of Anoctamins to Cell Survival and Cell Death. *Cancers* **19**, E382 (2019).
357. Sim, J.R.*, et al.* Amelioration of SARS-CoV-2 infection by ANO6 phospholipid scramblase inhibition. *Cell reports* **40**, 111117 (2022).
358. Schreiber, R.*, et al.* Regulation of TMEM16A/ANO1 and TMEM16F/ANO6 ion currents and phospholipid scrambling by Ca2+ and plasma membrane lipid *J Physiology (London)* **596**, 217-229 (2018).

359. Yurtsever, Z.*, et al.* Self-cleavage of human CLCA1 protein by a novel internal metalloprotease domain controls calcium-activated chloride channel activation. *The Journal of biological chemistry* **287**, 42138-42149 (2012).
360. Berry, K.N. & Brett, T.J. Structural and Biophysical Analysis of the CLCA1 VWA Domain Suggests Mode of TMEM16A Engagement. *Cell reports* **30**, 1141-1151.e1143 (2020).
361. Piala, A.T.*, et al.* Chloride sensing by WNK1 involves inhibition of autophosphorylation. *Science signaling* **7**, ra41 (2014).
362. Zhou, B.*, et al.* WNK4 inhibits NCC protein expression through MAPK ERK1/2 signaling pathway. *American journal of physiology. Renal physiology* **302**, F533-539 (2012).
363. Xu, B.E.*, et al.* WNK1 activates ERK5 by an MEKK2/3-dependent mechanism. *The Journal of biological chemistry* **279**, 7826-7831 (2004).
364. Moniz, S.*, et al.* Protein kinase WNK2 inhibits cell proliferation by negatively modulating the activation of MEK1/ERK1/2. *Oncogene* **26**, 6071-6081 (2007).
365. Deng, L.*, et al.* Knockdown of TMEM16A suppressed MAPK and inhibited cell proliferation and migration in hepatocellular carcinoma. *Onco. Targets. Ther* **9**, 325-333 (2016).
366. Lian, H., Cheng, Y. & Wu, X. TMEM16A exacerbates renal injury by activating P38/JNK signaling pathway to promote podocyte apoptosis in diabetic nephropathy mice. *Biochemical and biophysical research communications* (2017).
367. Liu, D.*, et al.* TMEM16A Regulates Pulmonary Arterial Smooth Muscle Cells Proliferation via p38MAPK/ERK Pathway in High Pulmonary Blood Flow-Induced Pulmonary Arterial Hypertension. *J Vasc Res* **58**, 27-37 (2020).
368. Yurtsever, Z., Scheaffer, S.M., Romero, A.G., Holtzman, M.J. & Brett, T.J. The crystal structure of phosphorylated MAPK13 reveals common structural features and differences in p38 MAPK family activation. *Acta crystallographica. Section D, Biological crystallography* **71**, 790-799 (2015).
369. Leverkoehne, I. & Gruber, A.D. The murine mCLCA3 (alias gob-5) protein is located in the mucin granule membranes of intestinal, respiratory, and uterine goblet cells. *The journal of histochemistry and cytochemistry : official journal of the Histochemistry Society* **50**, 829-838 (2002).
370. Erickson, N.A.*, et al.* Soluble mucus component CLCA1 modulates expression of leukotactic cytokines and BPIFA1 in murine alveolar macrophages but not in bone marrow-derived macrophages. *Histochemistry and cell biology* **149**, 619-633 (2018).
371. Ching, J.C., Lobanova, L. & Loewen, M.E. Secreted hCLCA1 is a signaling molecule that activates airway macrophages. *PloS one* **8**, e83130 (2013).
372. Hobbs, C.A.*, et al.* Identification of the SPLUNC1 ENaC-inhibitory domain yields novel strategies to treat sodium hyperabsorption in cystic fibrosis airway epithelial cultures. *American journal of physiology. Lung cellular and molecular physiology* **305**, L990-l1001 (2013).
373. Khanal, S.*, et al.* SPLUNC1: a novel marker of cystic fibrosis exacerbations. *The European respiratory journal* **58**(2021).
374. Hauber, H.P.*, et al.* Expression of HCLCA1 in cystic fibrosis lungs is associated with mucus overproduction. *The European respiratory journal* **23**, 846-850 (2004).
375. Iwashita, H., Fujimoto, K., Morita, S., Nakanishi, A. & Kubo, K. Increased human Ca(2)(+)-activated Cl(-) channel 1 expression and mucus overproduction in airway epithelia of smokers and chronic obstructive pulmonary disease patients. *Respir. Res* **13**, 55-13 (2012).
376. Karakioulaki, M., Papakonstantinou, E., Goulas, A. & Stolz, D. The Role of Atopy in COPD and Asthma. *Frontiers in medicine* **8**, 674742 (2021).
377. Ren, X.*, et al.* Identification of Niclosamide as a New Small-Molecule Inhibitor of the STAT3 Signaling Pathway. *ACS Med Chem Lett* **1**, 454-459 (2010).
378. Cryan, S.A. Carrier-based strategies for targeting protein and peptide drugs to the lungs. *The AAPS journal* **7**, E20-41 (2005).
379. Maslanka Figueroa, S.*, et al.* Influenza A virus mimetic nanoparticles trigger selective cell uptake. *Proceedings of the National Academy of Sciences of the United States of America* **116**, 9831-9836 (2019).

380. Tamaoki, J., Nakata, J., Takeyama, K., Chiyotani, A. & Konno, K. Histamine H2 receptor-mediated airway goblet cell secretion and its modulation by histamine-degrading enzymes. *The Journal of allergy and clinical immunology* **99**, 233-238 (1997).
381. Wilson, A.M. The role of antihistamines in asthma management. *Treatments in respiratory medicine* **5**, 149-158 (2006).
382. Yamauchi, K. & Ogasawara, M. The Role of Histamine in the Pathophysiology of Asthma and the Clinical Efficacy of Antihistamines in Asthma Therapy. in *International journal of molecular sciences*, Vol. 20 (2019).
383. Talbot, C. & Lytle, C. Segregation of Na/H exchanger-3 and Cl/HCO3 exchanger SLC26A3 (DRA) in rodent cecum and colon. *American journal of physiology. Gastrointestinal and liver physiology* **299**, G358-367 (2010).
384. Greeley, T., Shumaker, H., Wang, Z., Schweinfest, C.W. & Soleimani, M. Downregulated in adenoma and putative anion transporter are regulated by CFTR in cultured pancreatic duct cells. *Am J Physiol* **281**, G1301-G1308 (2001).
385. Royaux, I.E.*, et al.* Pendrin, encoded by the Pendred syndrome gene, resides in the apical region of renal intercalated cells and mediates bicarbonate secretion. *Proceedings of the National Academy of Sciences of the United States of America* **98**, 4221-4226 (2001).
386. Bidart, J.M.*, et al.* Expression of pendrin and the Pendred syndrome (PDS) gene in human thyroid tissues. *The Journal of clinical endocrinology and metabolism* **85**, 2028-2033 (2000).
387. Shcheynikov, N.*, et al.* Regulatory interaction between CFTR and the SLC26 transporters. *Novartis Foundation symposium* **273**, 177-186; discussion 186-192, 261-174 (2006).
388. Lee, H.J. & Zheng, J.J. PDZ domains and their binding partners: structure, specificity, and modification. *Cell communication and signaling : CCS* **8**, 8 (2010).
389. Xia, W.*, et al.* The distinct roles of anion transporters Slc26a3 (DRA) and Slc26a6 (PAT-1) in fluid and electrolyte absorption in the murine small intestine. *Pflugers Archiv : European journal of physiology* **466**, 1541-1556 (2014).
390. Kini, A.*, et al.* Slc26a3 deletion alters pH-microclimate, mucin biosynthesis, microbiome composition and increases the TNFα expression in murine colon. *Acta physiologica (Oxford, England)* **230**, e13498 (2020).
391. Soleimani, M. The multiple roles of pendrin in the kidney. *Nephrology, dialysis, transplantation : official publication of the European Dialysis and Transplant Association - European Renal Association* **30**, 1257-1266 (2015).
392. Chernova, M.N.*, et al.* Acute regulation of the SLC26A3 congenital chloride diarrhoea anion exchanger (DRA) expressed in Xenopus oocytes. *The Journal of physiology* **549**, 3-19 (2003).
393. Berg, P.*, et al.* Impaired Renal HCO(3) (-) Excretion in Cystic Fibrosis. *J Am Soc Nephrol* **31**, 1711-1727 (2020).
394. Illek, B.*, et al.* cAMP-independent activation of CFTR Cl^- channels by the tyrosine kinase inhibitor genistein. *Am. J. Physiol* **268**, C886-C893 (1995).
395. Clarke, L.L.*, et al.* Defective epithelial chloride transport in a gene-targeted mouse model of cystic fibrosis. *Science (New York, N.Y.)* **257**, 11251128-11251128 (1992).
396. Tilly, B.C.*, et al.* Cyclic AMP-dependent protein kinase activation of cystic fibrosis transmembrane conductance regulator chloride channels in planar lipid bilayers. *J. Biol. Chem* **267**, 9470-9473 (1992).
397. Chang, M.H.*, et al.* Slc26a9 is inhibited by the R-region of CFTR via the STAS domain. *The Journal of biological chemistry* **284**, 28306-28318 (2009).